Response of orogenic crust to indentation by Adriatic continental lithosphere – Tauern Window, Eastern Alps (Austria)

Kumulative Dissertation
Von

Silvia Favaro

Zur

Erlangung des Doktorgrades der Naturwissenschaften
im Fachbereich Geowissenschaften

an der

Freien Universität Berlin

Berlin, Februar 2016

Diese Arbeit wurde von dem Promotionsausschuss des Fachbereiches Geowissenschaften am

16.Februar 2015 genehmigt.
………………………………………………………………………………………………

Prof. Dr. Mark R. Handy
Freie Universität Berlin

Dr. Ralf Schuster
Geologische Bundesanstalt (Wien)

Date of defense: 06/06/2016

ERKLÄRUNG

Hiermit erkläre ich, Silvia Favaro, dass diese Arbeit ausschließlich auf Grundlage der angegebenen Hilfsmittel und Hilfen selbstständig von mir verfasst wurde. Diese Arbeit wurde nicht in einem früheren Promotionsverfahren eingereicht.

Berlin, den 2. Februar 2016

Silvia Favaro

ZUSAMMENFASSUNG

Miozäne Indentation der orogenen Lithosphäre durch das Einkeilen der adriatischen Mikroplatte in den Ostalpen führte zu schneller Exhumierung durch Aufdomung, Abschiebung und Erosion im Bereich des Tauernfensters. Dieses tektonische Fenster ist das grösste der Alpen und legt den Kern des alpinen Orogens frei, den paläogenen Deckenstapel der europäischen Platte. Die Abkühlentwicklung des Tauernfensters variiert entlang seines Streichens [*Favaro et al.*, 2015]. So zeigen geologische Strukturen die frühesten Effekte einer raschen Abkühlung schon vor 24 Ma (Sonnblick Subdome) im östlichen Tauernfenster (ETD, Eastern Tauern Dome), im Gegensatz zu Abkühlaltern von 20-18 Ma in den Domstrukturen des westlichen Tauernfensters (WTD, Western Tauern Dome). Dementsprechend begann die schnelle Exhumierung im Liegenden der Brenner Scherzone später Fault [20 Ma, *Fügenschuh et al.*, 1997] als im Liegenden der Katschberg Abschiebung Fault [23 Ma, *Scharf et al.*, 2013a]. Trotz dieser Unterschiede entlang des Streichens fallen Exhumierung und Abkühlung mit sinistraler Transpression entlang der Giudicarie Linie zeitlich zusammen; diese begann vor etwas 23-21 Ma, wie durch Spaltspurdatierung an Zirkonen [*Pomella et al.*, 2011, 2012] und stratigraphische Analyse festgestellt wurde [*Luciani & Silvestrini*, 1996; *Luciani*, 1989].

Wir stellen eine tektonische Rekonstruktion der post-eozänen Krustenbewegungen in den Ostalpen vor. Während der Indentation fand in der orgenen Kruste eine Wanderung von Aufdomung und Exhumierung sowohl entlang und wie auch weg von der Indenterfront verursachte. Dies wird durch die Muster der Abkühlalter unterstützt, eingeschließlich unsere neuen radiometrischen ^{147}Sm/^{144}Nd Alter und ^{87}Rb/^{87}Sr Biotit- und Hellglimmer-Alter, die eine fortschreitende Verjüngung von Aufdomung und schneller Abkühlung vom Zentrum zu den westlichen und östlichen Rändern des Tauernfensters dokumentieren. Dieses Abkühlungsmuster interpretieren wir als Folge einer Fragmentierung des Austroalpins an der Spitze des Adriatischen Indenters (Southern Alps) während seiner Nordwärtsbewegung.

ABSTRACT

Indentation of orogenic lithosphere in the Eastern Alps by the impinging Adriatic microplate triggered rapid exhumation by doming, normal faulting and erosion focussed in the Tauern Window. This window is the most prominent tectonic window in the Alps and exposes the core of the Alpine orogen, a Paleogene nappe stack derived from the European plate. The cooling history of the Tauern Window varies along its strike [*Favaro et al.*, 2015], with rapid cooling affecting some structures as early as 24 Ma (Sonnblick Subdome) in the eastern Tauern Window (ETD, Eastern Tauern Dome) compared to 20-18 Ma for domed units in the western part (WTD, Western Tauern Dome). Likewise, the onset of rapid exhumation was somewhat older in the foowall of the Katschberg Normal Fault [23 Ma, *Scharf et al.*, 2013a] than in the footwall of the Brenner Shear Zone [20 Ma, *Fügenschuh et al.*, 1997]. Despite these along-strike differences, both exhumation and cooling coincided broadly with sinistral transpression along the Giudicarie Belt, beginning at c. 23-21 Ma, as constrained by zircon fission track data [*Pomella et al.*, 2011, 2012] and biostratigraphic criteria [*Luciani & Silvestrini*, 1996; *Luciani*, 1989].

We propose a map-view reconstruction of post-Eocene crustal motion in the Eastern Alps, in which folding in front of the Adriatic indenter induced a migration in doming and exhumation, both away from and and parallel to the indenter front. This is supported by cooling age patterns, including our new ^{147}Sm/^{144}Nd isochron age and ^{87}Rb/^{87}Sr biotite and white micas ages, that document progressive younging of doming and rapid cooling from the center to the eastern and western ends of the Tauern Window. We attribute this pattern to fragmentation of triangular-shaped Austroalpine blocks forming the leading edge of the Adriatic Indenter (Southern Alps) as this indenter advanced to the north.

ORGANIZATION

This thesis comprises 7 chapters, two of which are manuscripts and two are mapping reports compiled for the Geological Survey of Austria. At this writing, one of the manuscripts (Chapter 3) has just been published in Tectonophysics, one is accepted in Tectonophysics and the one is ready for submission to Tectonics (Chapter 2). The two mapping reports (Chapters 4 and 5) are published in the "Jahrbuch der Geologischebundesanstalt, Wien" (Geological Survey of Austria in Vienna). In Chapter 6, Andreas Scharf is the first author. An outline of all chapters follows below.

Chapter 1: Introduction

This is a brief introduction of the study area, the aim of the thesis and the analytical methods used.

Chapter 2: Changing patterns of exhumation in front of a crustal indenter – the kinematics of the Tauern Window (Eastern Alps)

Silvia Favaro, Mark R. Handy, Andreas Scharf, Ralf Schuster

In preparation for submission to Tectonics.

New structural and kinematic data are presented showing that folding was transitional to extensional shearing, both laterally (orogen-parallel) and temporally. The first author (Silvia Favaro) carried out almost all of the fieldwork underlying the structural and kinematic analyses and performed paleo-strain studies of brittle faults bordering the leading edge of the Adriatic indenter. An immediate result is that low-angle normal faulting related to Miocene orogenic extension continued to beneath the viscous-to-frictional transition and overprinted steep faults that formed during earlier stages of indentation and exhumation. A synthesis of structural and thermochronological data for the entire Tauern Window was the effort of the first author (Favaro) culminating in a map-view reconstruction of post-Eocene crustal motion in the Eastern Alps. This model yields fresh insight into the behavior of orogenic crust during indentation, and sheds new light on debate regarding the relative roles of tectonic and erosional denudation in the Eastern Alps. The second and last authors, (Mark Handy, Ralf Schuster) helped lead the discussion and write this manuscript. The first (Silvia Favaro) and third authors (Andreas Scharf) drew all the figures; Scharf was the other doctoral candidate in this project.

Chapter 3: Transition from orogen-perpendicular to orogen-parallel exhumation and cooling during crustal indentation – key constraints from ^{147}Sm/^{144}Nd and ^{87}Rb/^{87}Sr geochronology (Tauern Window, Alps)

Silvia Favaro, Ralf Schuster, Mark R. Handy, Andreas Scharf, Gerhard Pestal

This chapter was published on 8 December 2015 to: **Tectonophysics, Volume 665, pp. 1–16**
DOI: 10.1016/j.tecto.2015.08.037
Link: http://dx.doi.org/10.1016/j.tecto.2015.08.037

This chapter provides new thermochronological constraints on the timing of cooling related to the exhumation of orogenic crust in front of the Adriatic Indenter. These ages include a new ^{147}Sm/^{144}Nd isochron age of 25.7±0.9 Ma on a garnet-bearing assemblage from the lowest nappe in the core of the eastern part of the Tauern Window and 18 new ^{87}Rb/^{87}Sr biotite and white mica cooling ages from this same complex. This data, combined with previously published ^{87}Rb/^{87}Sr white mica ages, suggest that doming and exhumation began no later than 28 Ma immediately in front of the indenting Austro-alpine crustal blocks, then migrated laterally to the ESE during rapid exhumation and orogen-parallel stretching beginning at about 23 Ma. The first author (Silvia Favaro) with the help of the second author (Ralf Schuster) compiled a new tectonic and stratigraphic map of the study area which formed the basis for collecting the samples that were subsequently prepared and analyzed at the Geological Survey of Austria. The first author wrote the first version of this manuscript and drew all figures and tables. The second, third and fourth authors (Schuster, Handy, Scharf) significantly improved the text, the figures and the discussion section. Gerhard Pestal, an expert mapper in the area, contributed countless tips for fieldwork and contributed samples analyzed in this study, only one of which was actually analysed for the ^{147}Sm/^{144}Nd isochron age.

Chapter 4: Bericht 2012 über geologische Aufnahmen auf den Blättern 154 "Rauris, 155 "Bad Hofgastein" und 181 "Obervellach"

Silvia Favaro, Ralf Schuster

Published in the "Jahrbuch der Geologische Bundesanstalt, Wien", 2012. Bericht 2012 über geologische Aufnahmenauf den Blättern 154 Rauris, 155 Bad Hofgastein, 181 Obervellach, 152/1-4, pp. 268-272.

This report summarizes geological mapping in the Sonnblick area near Kolm-Saigurn (Austrian Map, Sheet ÖK154 "Rauris"), from the Tauern Valley to Mallnitz (Austrian Map, Sheet ÖK 155,"Bad Hofgastein") and from the southwestern slopes of the Mölltal to Obervellach (Austrian Map, Sheet ÖK 181, "Obervellach"). Mapping was conducted on the 1:10.000 scale and summarized in the above sheets on the 1:50.000 scale. This mapping also helped improve the official written guide for Sheet ÖK 154 "Rauris" of the Geological Map of Austria [*Pestal*, 2011] as well as the southwestern part of Sheet ÖK 155 "Bad Hofgastein".

Chapter 5: Bericht 2012 über geologische Aufnahmen auf den Blättern 154 “Rauris” und 181 “Obervellach”

Silvia Favaro

Published in the “Jahrbuch der Geologische Bundesanstalt, Wien”, 2012. Bericht 2012 über geologische Aufnahmen auf den Blättern 154 Rauris, 181 Obervellach, 152/1-4, pp.265-268

This report describes the structure of the Mallnitz Synform along three cross sections. Two are located in the Sonnblick area near Kolm- Saigurn (Sheet 154 "Rauris") and the third is situated near Obervellach (Sheet 181 "Obervellach"). Mapping on the 1:10.000 scale involved structural investigations (Silvia Favaro) that complimented geological mapping of a larger area by staff of the Geological Survey of Austria.

Chapter 6: Grain-size effects on the closure temperature of white mica in a crustal-scale extensional shear zone – implications of in-situ ^{40}Ar/^{39}Ar laser-ablation of white mica for dating shearing and cooling (Tauern Window, Eastern Alps)

Andreas Scharf, Mark R. Handy, Stefan M. Schmid, Silvia Favaro, Masafumi Sudo, Ralf Schuster, Konrad Hammerschmidt

This chapter was published on 2 April 2016 to: **Tectonophysics, Volume 674, pp. 210–226**
DOI: 10.1016/j.tecto.2016.02.014
Link: http://www.sciencedirect.com/science/article/pii/S0040195116001116

This chapter describes Ar/Ar laser ablation dating on white micas with respect with their microstructure at the northeastern end of the Eastern Tauern Dome. The first author (Andreas Scharf) analysed all samples in Ar/Ar laboratory at the Universitaet Potsdam and was introduced and supervised by the fith author (Masafumi Sudo). This author helped writing the section about the Ar/Ar laser ablation method. The second and the sixth authors (Favaro and Schuster) provided and analysed the samples for the Rb/Sr method. The first author (Andreas Scharf) wrote a first version of this manuscript and drew all figures and tables. All authors revised the manuscript and substantially improved it.

Chapter 7: Conclusion and future work

This chapter summarizes the main results and conclusions of the entire thesis.

TABLE OF CONTENTS

Chapter 1: Introduction

Chapter 2: Changing patterns of exhumation in front of a crustal indenter – the kinematics of the Tauern Window (Eastern Alps)

Chapter 3: Transition from orogen-perpendicular to orogen-parallel exhumation and cooling during crustal indentation – key constraints from ^{147}Sm/^{144}Nd and ^{87}Rb/^{87}Sr geochronology (Tauern Window, Alps)

Chapter 4: Bericht 2012 über geologische Aufnahmen auf den Blättern 154 "Rauris", 155 "Bad Hofgastein" und 181 "Obervellach"

Chapter 5: Bericht 2012 über geologische Aufnahmen auf den Blättern 154 “Rauris” und 181 “Obervellach”

Chapter 6: Grain-size effects on the closure temperature of white mica in a crustal-scale extensional shear zone – implications of in-situ ^{40}Ar/^{39}Ar laser-ablation of white mica for dating shearing and cooling (Tauern Window, Eastern Alps)

Chapter 7: Conclusion and future work

LIST OF FIGURES, TABLES AND PLATES

Chapter 1: Introduction

1.1 GEOLOGICAL FRAMEWORK

Alpine-Himalayan-type mountains belts rarely preserve their original structure from the time of suturing and collision, having in most cases been modified by indentation. The indentation of orogenic lithosphere by an impinging tectonic plate changes the dynamic and kinematic boundary conditions of the orogenic wedge, triggering rapid exhumation by doming, normal faulting and erosion, and in some cases, inducing lateral escape.

In the Alpine chain, highly metamorphosed orogenic crust derived primarily from the downgoing European plate was indented by the leading edge of the Adriatic microplate beginning in Oligocene time. This leading edge, termed the Adriatic Indenter, corresponds at the surface to the Periadriatic Fault and the Southern Alpine units to the south of this fault (Fig. 1.1); these units show brittle, predominantly south-vergent, thin-skinned thrusts and folds. The structures associated with indentation change along strike of the Alpine orogen: to the west of the Giudicarie Belt (Fig. 1.1), indentation involved backthrusting and backfolding [e.g., *Argand,* 1924; *Dal Piaz,* 1999], whereas to the east in the eastern Alps, it involved doming, extensional exhumation, and eastward lateral escape of the orogenic crust towards the Pannonian Basin [e.g., *Selverstone*, 2004; *Horvàth et al.*, 2006, *Scharf et al.,* 2013a]. This along differences correspond to the subdivision of the Adriatic Indenter into eastern and western parts, separated by the Giudicarie Belt, a large transpressional crustal-scale structure [*Müller et al.*, 2001; *Viola et al.*, 2001; *Pomella et al.*, 2011, 2012]. This thesis focuses on the role of the eastern part of this indenter in exhuming large tarcts of orogenic crust exposed in the Tauern Window (Fig. 1.1). The western Adriatic indenter is not considered any further in this thesis because it followed a separate evolution after early Miocene time.

The timing of the northward motion of the Adriatic Indenter in the eastern Alps is controversial: Zircon fission track and biostratigraphic ages from units along the Giudicarie Belt indicate that motion began in late Oligocene–Early Miocene time [*Pomella et al.*, 2012; *Luciani and Silvestrini*, 1996], whereas geochronological constraints suggest that exhumation of orogenic crust directly in front of the indenter started somewhat earlier [*Scharf et al.,* 2013a], certainly no later than 20 Ma according thermal modeling [*Fügenschuh et al.*, 1997]. Yet indentation and exhumation were kinematically linked in space, raising the question of the exact timing: was indentation diachronous in Oligocene and Miocene time or was the response of orogenic crust to indentation delayed?

My thesis deals with the kinematic, cooling and exhumation history of the eastern part of the Tauern Window (Plate 1, 2) where excellent 3-D exposure allows us to study the relationship between the indented orogenic units of the European crust and the leading edge of the indenter itself, represented by Austroalpine units immediately north of the Periadriatic Fault. My work focuses on key exhumation and escape structures, the Sonnblick and Hochalm domes, the Mölltal Fault and the Katschberg Normal Fault, a low-angle normal shear zone at the eastern end of the Tauern Window.

The overriding aim is to understand the relative contributions of folding, tectonic unroofing and lateral escape mechanisms to late- to post-collisional exhumation.

This thesis was conducted as part of an interdisciplinary research project supervised and initiated by Mark Handy and Claudio Rosenberg at the Freie Universitaet Berlin (the latter since moved to Université Pierre and Marie Curie, Paris) and developed by four PhD students; in addition to myself, these included Andreas Scharf (structural investigation, high-temperature thermochronology on the KNF, eastern Tauern Window), Audrey Bertrand (brittle structures, zircon fission tracks and thermal modeling of the Tauern Window) and Susanne Schneider (structural investigation and high-temperature termochronology of the western and central Tauern Window).

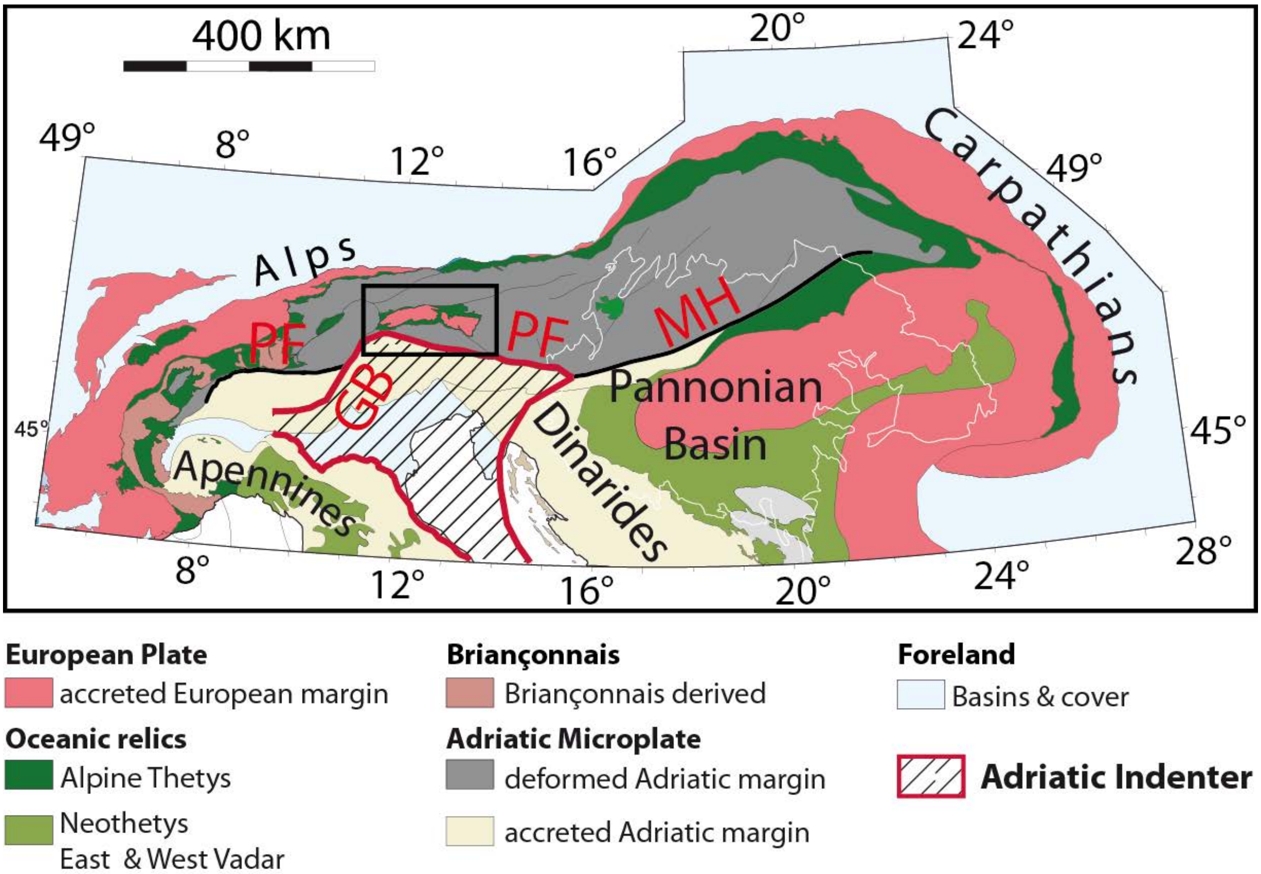

Figure 1.1: Tectonic Map of the Alps and Carpathians (modified after Schmid, 2008). GB - Giudicarie Belt; PF - Periadriatic Fault; MH - Midhungarian Fault. The black box contains the Tauern Window

1.2 METHODS

The following methods were used to address the main questions in this thesis, in particular pertaining to the relationship between indentation, exhumation and rapid cooling in the Tauern Window.

1) Structural mapping: A new tectonic and lithological map was constructed using ArcGIG (Plate 1, 2 and 3). Brittle and ductile structures were investigated along the southern boundary of the Hochalm and Sonnblick domes as well as along the Mallnitz Synform, where samples were collected for Rb/Sr and Sm/Nd analysis and thin section investigation.

2) Paleostrain analysis: Four outcrops (128 measurements) were chosen for a application of the P-T-B method (P pressure-, T tension- and B intermediate axes) with the software Win Tensor 3.0.0 [*Delvaux* and *Sperner*, 2003]: two in Austro-alpine units exposed along the railway line and two within Tauern Window near its southeastern border. The Mölltal Fault bounds the SE side of the Tauern Window and is one of the major faults in the area.

3) ^{87}Rb/^{87}Sr analysis of white mica and biotite: Biotite and whole rock from fifteen samples were analyzed and two of these samples were also analyzed for white mica. All samples come from the southern rim of the eastern Tauern Window and help us to understand how the age of rapid cooling varied along strike of the dome. The samples were prepared mechanically at the Geological Survey of Austria (Vienna). Rb ratios were measured at the Department of Geological Sciences, University of Vienna with a Finnigan® MAT 262, whereas Sr, Sm and Nd ratios were analyzed with a ThermoFinnigan® Triton TI TIMS.

4) ^{147}Sm/^{144}Nd garnet ages: Sample 155-6-2011 is ideally suited to place an upper age limit on the Barrow-type, amphibolite-facies metamorphism (Tauernkristallisation) because it contains both garnet and chloritoid that overgrow the folded duplex foliation formed during collision and crust thickening in the Venediger Nappe System. Mechanical and chemical preparation for the ^{147}Sm/^{144}Nd isotope analyses was performed at the Geological Survey of Austria in Vienna and at the Department of Lithospheric Research at the University of Vienna.

(5) Map-view reconstruction of post-Eocene crustal motion in the Eastern Alps: The indentation kinematics of the Eastern Alps was reconstructed back in time, first to the onset of Adriatic indentation of the Eastern Alps at 21 Ma, then to the beginning of exhumation of the Alpine orogenic wedge following break-off of the European slab beneath the Alps (30 Ma). Some simplifying assumptions were made regarding conservation of crustal volume and mass during indentation: The orogenic indenter and the Austroalpine crustal units are assumed to be rigid throughout indentation.

Chapter 2: Changing patterns of exhumation and denudation in front of an advancing crustal indenter, Tauern Window (Eastern Alps)

Favaro S. [1, *], Scharf A. [1, 3], Schuster R. [2], Handy M.R. [1]

[1] Department of Earth Sciences, Freie Universität Berlin, Malteserstrasse 74-100, 12249 Berlin, Germany

[2] Geologische Bundesanstalt, Neulinggasse 38, A-1030, Vienna, Austria

[3] Now at Department of Earth Science, Sultan Qaboos University, P.O. Box 36, Al-Khoudh, P.C. 123, Muscat, Sultanate of Oman

*Corresponding E-Mail: silvia.favaro@fu-berlin.de, Telephone: (+49 03) 838-70190

ABSTRACT

The migration of Miocene doming and orogen-parallel extension of orogenic crust in the Tauern Window reflects the changing shape of crustal indenters during northward motion of the Adriatic Microplate. New structural and kinematic data indicate that shortening of the Penninic nappes pile in the Tauern Window was transitional to east-west extension accommodated by first by upright folding and strike-slip faulting, then increasingly also by normal faulting at both ends of the window. Retrodeforming these post-nappe structures in map view yields a 2D reconstruction of the orogenic crust back to 30 Ma, including the onset of oblique indentation at 23-21 Ma. This model supports the notion that indentation involved approximately equal amounts of north-south shortening and orogen-parallel stretching as measured from the indenter tip. Upright folding accommodated less than half of this north-south shortening, due to eastward stretching and extrusion toward the Pannonian Basin. Comparison of areal denudation in maps for crustal configurations before (30 Ma) and after indentation (Present) indicate that erosion associated with upright folding was the primary agent of denudation, whereas extensional unroofing along normal faults at the eastern and western end of the Tauern Window accounted for only about a third of the total denudation.

2.1 INTRODUCTION

Indentation of orogenic lithosphere by an impinging tectonic plate changes the dynamic and kinematic boundary condition of the orogenic wedge, triggering rapid exhumation by doming, normal faulting and erosion [*Johnson*, 2002], and in some cases, inducing lateral, orogen-parallel escape [e.g., *Taponnier et al.*, 1986]. In the Alpine chain, the leading edge of the Adriatic Microplate (Southern Alpine crust) is divided into western and eastern blocks by the Giudicarie Belt. Thus, the response of the thickened European lithosphere to indentation varies along strike of the Alpine orogen: in the Western Alps, i.e., west of the Giudicarie Belt and the Brenner Shear Zone System (Fig. 2.1), indentation triggered backfolding and thrusting of the European crust [e.g., *Argand,* 1924; *Dal Piaz,* 1999] above a long, thin wedge of Adriatic lower crust [e.g., *Schmid et al.*, 2004, *Rosenberg &*

Kissling, 2013], whereas in the Eastern Alps, it involved doming, extensional exhumation, and eastward lateral escape of the orogenic crust exposed in the Tauern Window towards the Pannonian Basin [Fig. 2.1, e.g., *Selverstone*, 2004; *Horvàth et al*., 2006, *Scharf et al.,* 2013a].

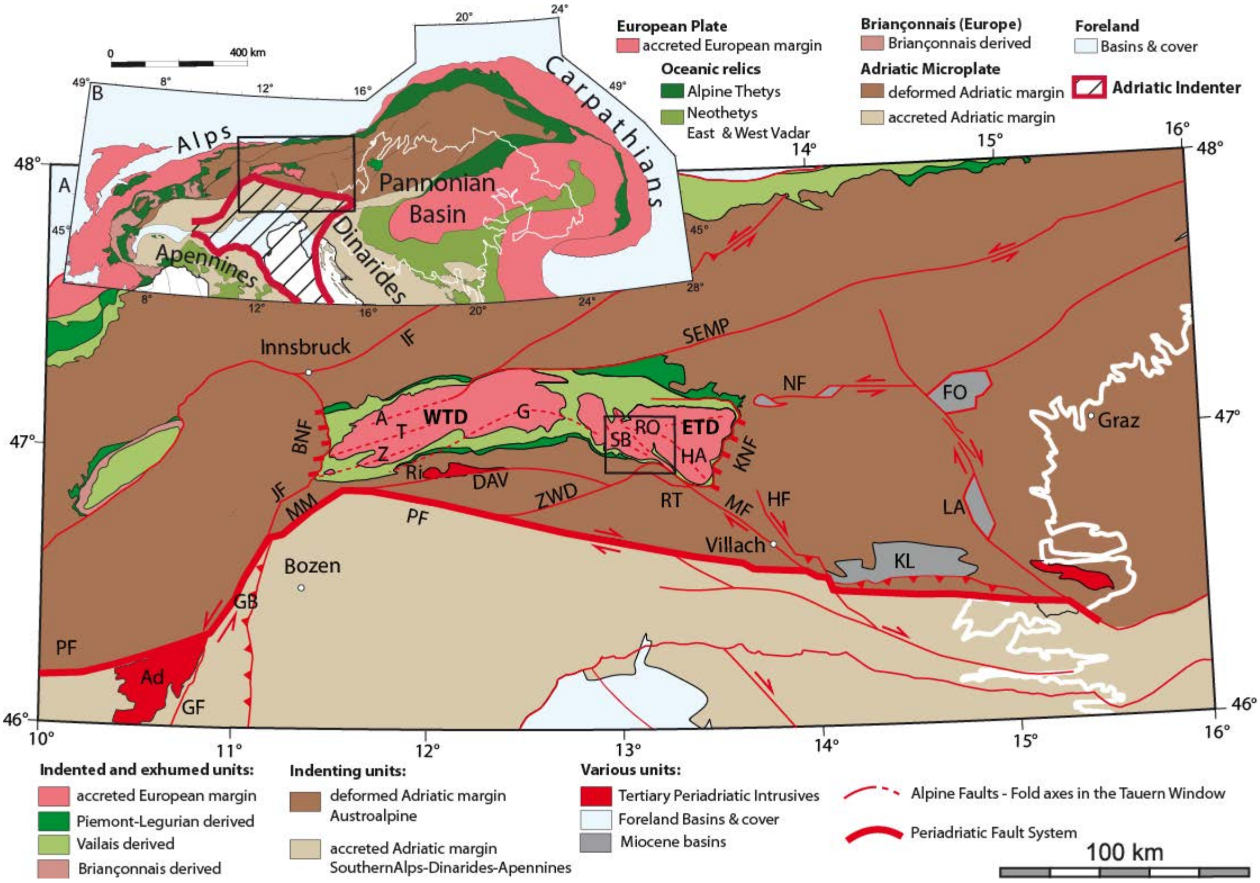

Figure 2.1: Tectonic Map of the Eastern Alps showing units of indenting Adriatic Plate (brown colours) and European plate (pink colour) with intervening oceanic units of Alpine Tethys (green colours) as modified from *Scharf et al*. [2013a]. Box indicates area in Fig. 2.2. Faults and shear zones: BSZS - Brenner Shear Zone System; DAV – Defereggen Anterselva Valles Fault; GB - Giudicarie Belt (includes Giudicarie Fault, GF); HF - Hochstuhl Fault; IF - Inntal Fault; JF – Jaufen Fault; KSZS - Katschberg Shear Zone System; MF - Mölltal Fault; MM - Meran Mauls Fault; NF - Niedere Tauern Southern Fault; PF - Periadriatic Fault; RT – Ragga-Teuchel Fault; SEMP - Salzach-Ennstal-Mariazell-Puchberg Fault; ZWD - Zwischenbergen-Wöllatratten-Drau Fault. Domes and thrust-belt: A - Ahorn; G - Granatspitz; HA – Hochalm; RO - Romate; SB - Sonnblick; T - Tux; Z - Zillertal. Neogene basins: FO - Fohnsdorf; KL - Klagenfurt; LA - Lavanttal; ETD - Eastern Tauern Subdome; WTD – Western Tauern Subdome. Periadriatic plutons: Ad - Adamello; Ri - Rieserferner. The white line delimits the western margin of the Pannonian Basin. Inset map shows major units of Alps and Carpathians, and the major continents and oceans involved in collision (Europe, Adria).

The Tauern Window in the Eastern Alps (Fig. 2.1) is well suited to study patterns of exhumation and denudation during indentation due to the three-dimensional exposure of deeply subducted and exhumed European crust in front of the Adriatic indenter. Denudation, i.e., the removal of rock from above exhuming crust [*England and Molnar*, 1990], can be broken down into contributions from erosion and tectonic unroofing; the latter involves normal faults which displace crust laterally in their hangingwalls while exhuming orogenic crust in their footwalls [e.g., the Brenner and Katschberg Normal Faults in Fig. 2.1, *Behrmann*, 1988; *Selverstone*, 1988; *Genser & Neubauer,* 1989; *Scharf et al.,* 2013a]. The mechanisms of exhumation vary along strike of the Tauern Window: the central part shows little or no orogen-parallel extension and preserves subduction-related fabrics, whereas the eastern and western ends of the window display km-scale upright folds and extensional shear zones that deform all accretionary structures, and overprint Oligocene Barrovian-type amphibolite-facies metamorphism [*Kurz et al.* 1998; *Scharf et al.* 2013a] of the so-called "Tauernkristallisation" [*Sander*, 1911]. Interestingly, the distribution of cooling ages in the Tauern Window indicates that rapid exhumation and subsequent cooling in Miocene time may have began earlier in the eastern than the western part [*Luth and Willingshofer*, 2008; *Scharf et al*., 2013a]. If so, rapid exhumation varied in time as well as in space in front of the Adriatic indenter. The pattern of exhumation and cooling through time is crucial in the light of an ongoing controversy in the Eastern Alps of whether denudation involved primarily upright-folding and erosion [*Rosenberg et al*., 2007], or whether tectonic unroofing in the footwalls of normal faults at either end of the Tauern Window [*Frisch et al*., 1998, 2000; *Linzer et al*., 2002] were responsible for the exposure of subducted European crust in the Tauern Window.

This paper demonstrates that orogen-normal shortening in front of the Adriatic indenter overlapped with the onset of crustal-scale extension and lateral escape of the Alpine orogenic edifice. New structural and kinematic data are presented showing that folding was transitional to extensional shearing both laterally (along strike) and temporally. Paleo-strain analysis of brittle faults bordering a crustal block along the leading edge of the Adriatic indenter indicates that low-angle normal faulting related to orogenic extension continued beneath the viscous-to-frictional transition and overprinted steep faults that formed during earlier stages of indentation and exhumation. Finally, structural and thermochronological data are synthesized for the entire Tauern Window to arrive at a map-view reconstruction of post-Eocene crustal motion in the Eastern Alps. This model yields new insight into the behavior of orogenic crust during indentation, particularly on the debate regarding the relative roles of tectonic and erosional denudation in the Eastern Alps.

2.2 GEOLOGICAL SETTING

The Tauern Window exposes accreted basement and cover of the originally down-going European crust, including remnants of Alpine Tethys. These accreted and exhumed units are exposed beneath remains of the upper Adriatic plate which frame the Tauern Window (Austroalpine units in Fig. 2.1). The Austro-alpine units exposed just south of the Tauern Window formed indenting blocks [Rieserferner and Drau-Möll, *Scharf et al.*, 2013a; *Favaro et al.*, 2015] and are separated from the Southern Alps by the Periadriatic Fault. The Southern Alps form the leading edge of the Adriatic Indenter, i.e., that part of the Adriatic Microplate which indented the orogenic crust.

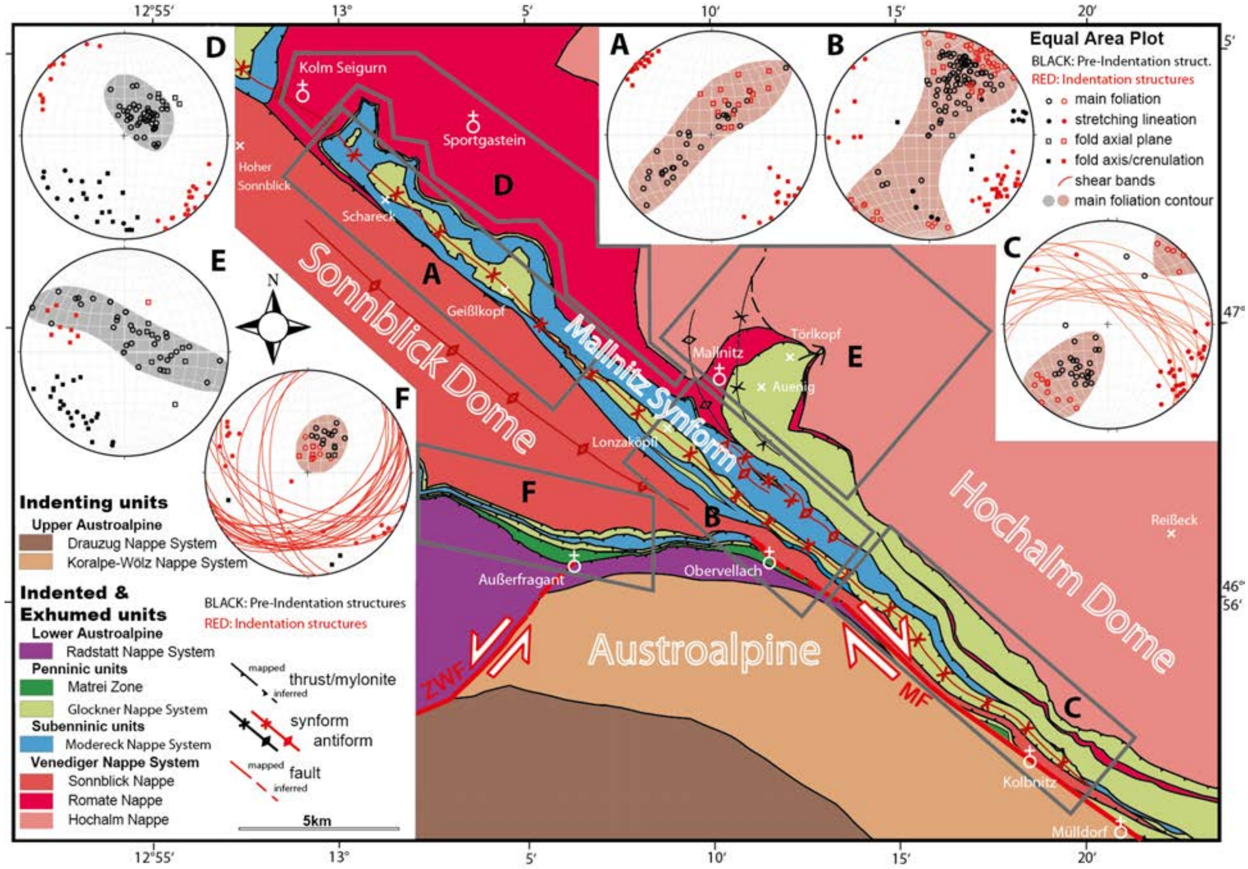

Figure 2.2: Map of the eastern Tauern Window showing indenting units of the upper plate (brown) and indented and exhumed units of the lower plate (all other colors). Structural domains A-F with equal-area plots showing orientations of the pre-indentational (black) and indentational structures (red). Brittle faults delimiting the Drau-Möll Block: MF – Mölltal Fault, ZWF – Zwischenberg-Wöllatratten Fault. See legend and text for explanation. Colors for units taken from *Schmid et al.* [2013].

During Adria-Europe convergence, the lower-plate units in the Tauern Window experienced deformation and metamorphism associated with accretion and subduction (D1), exhumation (D2, D3), collision (D4) and indentation (D5). The use of D followed by a number merely indicates the relative age of structures (1 oldest to 5 youngest) as constrained by overprinting relations and does not mean that these structures formed during distinct events at the scale of the orogen; in fact, they probably developed more or less continuously from Late Cretaceous to Miocene time [*Schmid et al.*, 2013]. The age of D5 structures related to exhumation varies across and along the Tauern Window, creating a pattern which we show below can be related to the progressive changes in the shape and kinematics of the indenting blocks.

The ends of the Tauern Window comprise two thermal and structural domes (D5), the Eastern and Western Tauern domes (ETD, WTD), which expose the deepest structural units. These domes are doubly plunging, upright antiforms that overprint duplex structures formed during north-directed collisional nappe stacking (D4). In the ETD, a roof thrust separates thin basement slices below (D4, Venediger Nappe System) from an isoclinally D3-folded thrust (D2) above. This folded thrust is the oldest structure in the area and emplaced Alpine Tethyan ophiolites (Glockner Nappe System) onto a distal unit of the European margin [Modereck Nappe System, *Schmid et al.*, 2013]. The units above the roof thrust have a composite S2-3 foliation that is locally overprinted by upright folds and shear zones related to indentation (D5). All pre-indentational structures (pre-D5) are overprinted by a thermal event, known locally as the Tauernkristallisation [*Sander*, 1911; *Hoinkes et al.*, 1999], that is marked by concentric isograds and iso-temperatures lines [*Oberhänsli et al.*, 2004; *Scharf et al.*, 2013b] culminates with amphibolite-facies conditions in the core of the ETD. When combined with thermochronology discussed below, these overprinting relationships place important constraints on the pattern of exhumation of accreted units during indentation.

2.3 STRUCTURES & KINEMATICS RELATED TO INDENTATION IN THE EASTERN TAUERN DOME

A NW-SE striking synform (the Mallnitz Synform) divides the ETD into two subdomes, the Sonnblick and Hochalm subdomes (Fig. 2.2). This synform contains the infolded remains of the D4 roof thrust mentioned above. The Sonnblick Subdome thins drastically at its southeastern end, forming an elongate gneiss lamellae only 50-70 m thick in map view [Fig. 2.2, "Sonnblick Walze" of *Exner*, 1948 or "Sonnblick Lamellae" of *Exner*, 1964]. The Hochalm Subdome is also thinned and truncated along its eastern margin by a top-SE, crustal-scale normal fault [the Katschberg Normal Fault, KNF, *Genser and Neubauer*, 1989] which, together with its steep northern and southern mylonitic branches [*Scharf et al.*, 2013a], accommodated E to SE-directed orogen-parallel extension (Fig. 2.1).

Figure 2.2 shows that structures related to nappe stacking and isoclinal folding (D_2-D_4 in black) are modified by post-nappe folding and shearing (D_5 structures in red). The intensity of D_5 overprinting increases from NW to SE parallel to the trace of the Mallnitz Synform, as marked by its progressive tightening, from isoclinal with a moderately SW-dipping axial plane (Fig. 2.3, sections a-c) to tight (section d) and isoclinal with a subvertical axial plane (Fig. 2.3, sections e-f). This tightening is accompanied by the development of an axial plane schistosity (Fig. 2.2, domain A) which varies from a spaced schistosity (Fig. 2.2, domain A; Fig. 2.3, cross sections a-c) to a penetrative mylonitic foliation (Fig. 2.2, domains B and C; Fig. 2.3, sections d-f) with a subhorizontal to gently SE-plunging stretching lineation (Fig. 2.2, domains A-C) and moderately dipping shear bands (Fig. 2.2, domain C). The counterclockwise curvature of older D_4 foliations and stretching lineations [*Exner*, 1964, his Plate 3; domains D, E in Fig. 2.2] into concordance with the D_5 shearing plane, as well as small-scale kinematic indicators (Fig. 2.4c) are consistent with transpressive sinistral shearing in map view combined with NE-side up exhumation of the Hochalm Subdome. This mylonite belt bends around the southeastern end of the D_5 Hochalm Subdome to become the Katschberg Normal Fault (KNF, Fig. 2.1). The coincidence of tectonic omission of footwall units along the KNF (26 km) with the axial culmination of the Hochalm Subdome indicates that D5 folding and top-E to -SE extensional shearing along the KNF were coeval [*Scharf et al.*, 2013a].

The Sonnblick Subdome folds a composite S_{4-5} foliation with a pronounced stretching lineation trending parallel to the antiformal axis. Within the subdome, some moderately inclined shear bands with both NW- and SE-plunging lineations indicate subvertical flattening beneath the Austroalpine units (domain F in Fig. 2.2). The southern end of the Sonnblick Subdome shows S- to SE-dipping shear bands indicating extensional exhumation of all Penninic units both above and below the D4 roof thrust (domain F in Fig. 2.2, Fig. 2.4a). The Penninic units in the footwall of this extensional shear zone are severely thinned, such that the previously thrusted and folded Glockner and Modereck Nappe Systems are reduced to only about 500 m of their original ~ 4 km thickness. A second, later set of shear bands along the S-margin of the Sonnblick Subdome near the Sonnblick Lamellae accommodated sinistral shearing in map view [*Kurz et al.*, 1996, Fig. 2.4c]. Although the shearing directions of these two sets of shear bands differ (see equal-area plot for domain F in Fig. 2.2), we interpret them to represent a progressive evolution from top-S to –SE extensional shearing to tightening of the Sonnblick Subdome during continuous northward motion of the indenting Drau-Möll Block (see section 2.5).

Locally, especially in fabric domain A (Fig. 2.2), relics of pre-indentational structures are still preserved, despite the strong D5 overprint. D4 fold axes and stretching lineations are preserved only in the late Paleozoic-Mesozoic cover of the Venediger nappe system and usually plunge to the S and SW. D4 folds are clearly recognizable because their axial planes strike perpendicular to the D5 structures and because they face to the NNW, i.e., in the direction of thrusting and nappe stacking (Fig 2.5a). The main foliation is mylonitic and contains shear bands indicating to top-N nappe stacking direction (Fig. 2.5b).

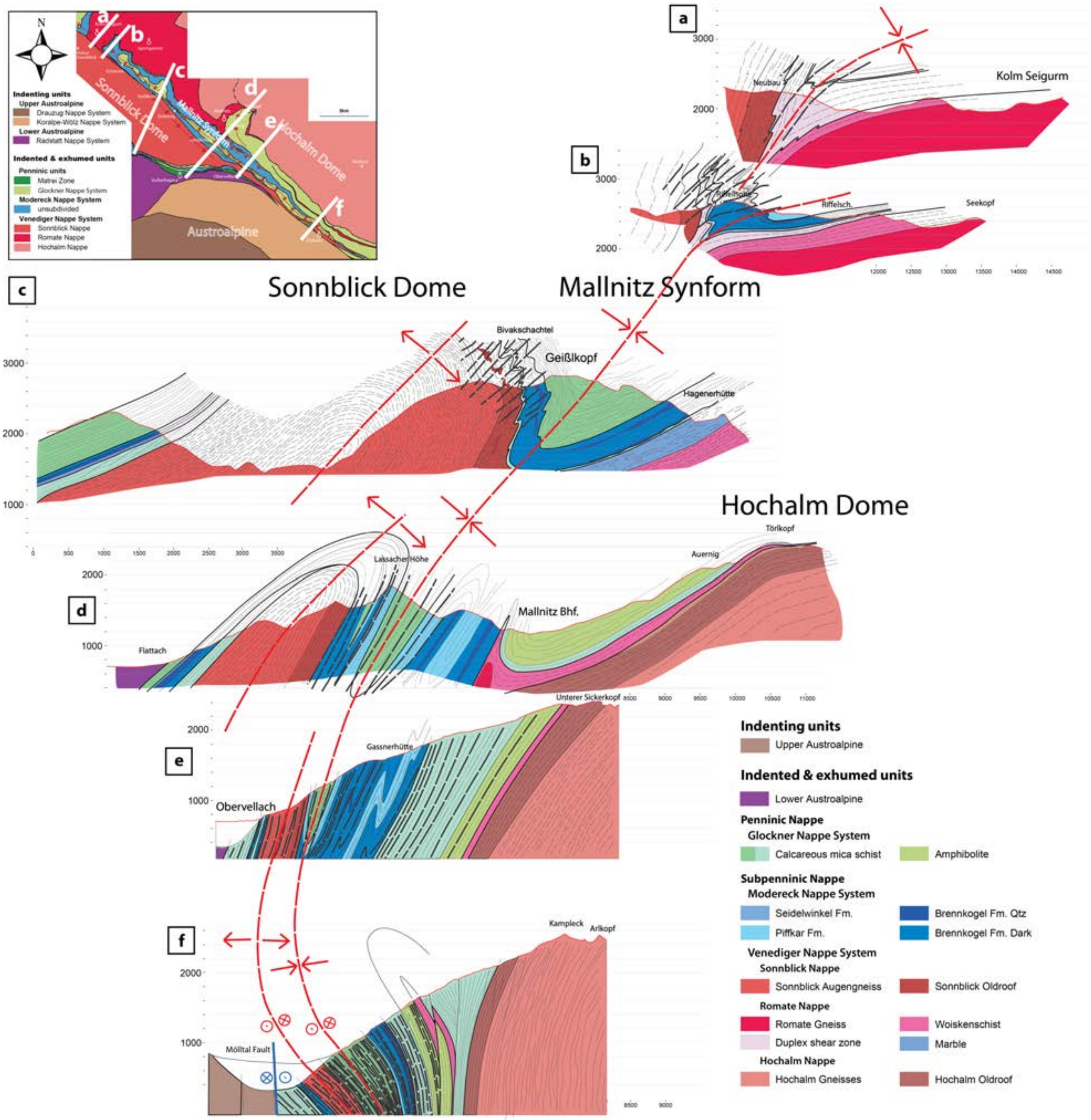

Figure 2.3: Cross sections of the Mallnitz Synform and adjacent Sonnblick and Hochalm subdomes: (a, b) “Rauris Valley” sections; (c) “Hagener” section; (d) “Mallnitz” section; (e) “Kaponig” section; (f) “Kolbnitz” section. Red dashed lines represents trace of the F5 axial planes; black dashed lines indicate main S5 foliation. Older foliations indicated with grey lines. Inset shows map of area as in Figure 2.2. Note in (f) the opposite shear senses of indenting Austroalpine crust along the Mölltal Fault (dextral, blue circles) and of indented orogenic crust along the steep southern branch of the Katchberg Normal Fault (sinistral, red circles) described in the text.

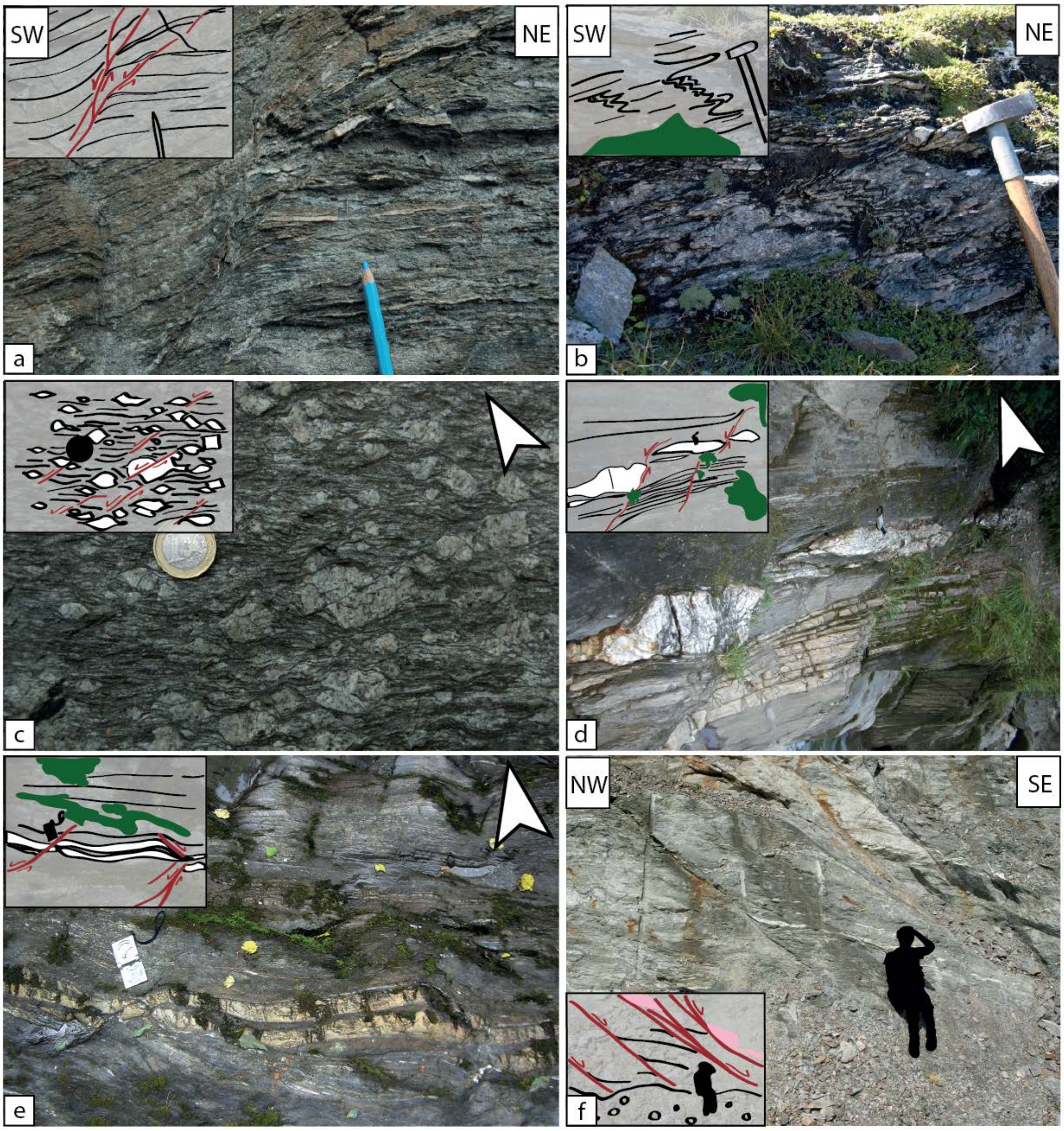

Figure 2.4: Key structures related to indentation as depicted in domains A-F in Figure 2.2: (a) top-down-to-SE ductile-brittle shear bands near Außerfragant at the southeastern end of Sonnblick Subdome, domain F; (b) isoclinal D5 folds deform $S_{2\text{-}3}$ in domain A (between Kolm Seigurm and Schareck); (c) augengneiss of the Sonnblick Lamellae in map view showing sinistral shear bands offsetting feldspar clasts in domain C (near Kolbnitz); (d) sinistral shear band offsetting quartz vein in map view near Obervellach, domain B; (e) sinistral and dextral shear bands in map view at SE end of Sonnblick Subdome near Obervellach, domain F, indicating flattening; (f) Mölltal Fault with older fault system (indicated in pink) in Austroalpine gneiss oriented parallel to the outcrop surface and offset by top-SSE faults marked in red. Younger faults show top-down-SE drag (Mülldorf, location in figure 2.1, first author for scale).

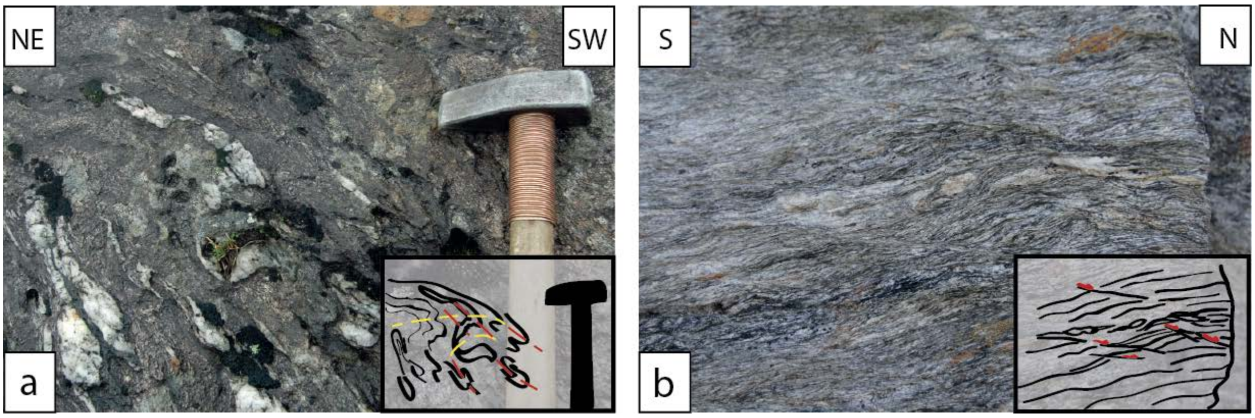

Figure 2.5: Pictures and sketches of collisional structures (D4) beneath the roof thrust in the ETD: (a) F5 folds (red axial plane) deform main foliation (presumably S4) and previously folded quartz veins (yellow F4 axial planes) in late Paleozoic cover of the Sonnblick thrust sheet in fabric domain A; (b) top-N shear bands in late Paleozoic granitoid at the base of the Romate thrust sheet.in fabric domain D.

2.4 KINEMATICS & PALEOSTRAIN ANALYSIS OF THE MÖLLTAL FAULT

The Mölltal Fault bounds the NE side of the Drau-Möll block (Fig. 2.2, inset). Detailed mapping shows that the best outcrops of cataclasites along the new Tauern railway line occur only within Austro-alpine units and do not coincide with the contact between Austro-alpine and Penninic units, at least at this locality. This contact is unfortunately buried beneath Plio-Pleistocene colluvium of the Möll Valley. The lack of coincidence of the Austro-alpine-Penninic contact with the best-exposed cataclasites suggests that brittle deformation post-dated the juxtaposition of Austro-alpine and Penninic units, which must have occurred already during Late Cretaceous nappe stacking [e.g., *Kurz et al.*, 2008; *Schmid et al.*, 2013].

Investigation of cataclasites at several fresh exposures along the new Tauern railroad line in the Möll Valley between Obervellach and Spittal a.d. Drau reveals two generations of fault surfaces (Fig. 2.4f): Surfaces aligned subparallel to the valley that carry subhorizontal striations (type 1) are cut by moderately SE-dipping surfaces (type 2) that rarely have striations.

The sense of motion on type 1 surfaces is usually sinistral as indicated by tension gashes and more rarely, hematite-bearing slickenfibers exposed along the railway line [criteria of *Petit*, 1987]. However, some dextral motion indicators are also present. Type 1 surfaces in the Penninic units along the northwestern side of the Möll Valley, e.g., within the Sonnblick Lamellae, display calcite-bearing slickenfibres consistent with dextral strike-slip motion. Thus, there is no clear picture of the sense of shear on the type 1 surfaces; both sinistral and dextral motions are recorded. Unfortunately, there are no overprinting relationships to indicate the relative age of these opposite motion senses. However, dextral motion is consistent with the map-view displacement of Austro-alpine nappe contacts by some 26 km [*Linzer et al.*, 2002]. Due to the shallow dip of these contacts, the actual displacement is much less, as discussed in subchapter 5.3. The sense of motion along the moderately dipping type 2, only exposed along the railway line, is more consistent; in both measured outcrops (stars E and F in Fig. 2.6), Riedel shears and dragged schistosity planes indicate that the southeastern block was downthrown with respect to the northwestern block. This is consistent with the sense of motion on the Katchberg Normal Fault.

Four outcrops with a total of 129 measurements were chosen for a paleostrain analysis with the so-called P-T-B method (P pressure-, T tension- and B intermediate axes): two in Austro-alpine units exposed along the railway line (stars CEG and DFH in Fig. 2.6), one in the Sonnblick Lamellae along the road connecting Obervellach and Mallnitz (star A in Fig. 2.6), and one in the Glockner Nappe System in a creek north of Kolbnitz (star B in Fig. 2.6). In order to perform such an analysis on these fault surfaces, the quality of slip-sense indicators was classified to weight the data (see Table 2.1.A in the Supplementary material 2.8 for a fully classified list of the data).

Cluster	n_t	n	e_1	e_2	e_3	R’	α_w	QR_t	Sh_{max}
a	17	14	13/180	70/049	14/273	1,5 (SS)	15,74	*C*	1±14,7
b	19	15	10/205	46/104	42/304	1,59 (TS)	18,64	*B*	27±13,8
c	6	6	08/020	81/184	02/290	1,56 (SS)	27,17	*D*	020±23,1
d	7	5	09/350	78/130	08/258	1,36 (SS)	28,01	*E*	168±19,7
e	12	10	28/294	62/105	04/202	1,5 (SS)	16,55	*C*	112±20,3
f	32	24	12/267	76/118	07/358	1,5 (SS)	15,01	*C*	87±19,9
g	16	15	69/136	07/028	20/296	0,48 (NF)	11,06	*E*	23±19,5
h	20	15	84/176	05/036	04/306	0,38 (NF)	20,63	*C*	36±23

Table 2.1: Results of paleostrain analysis; “Cluster” in the left-hand column refers to a group of measurements at a specific location in the four outcrops (stars in Figs. 2.1 and 2.2). n_t – total number of measurement, n – number of measurements used, e1, e2, e3 – principle finite strain axes, R’ - numerical value of the fault type (0-0.5 = normal fault, 0.5-1.5 = strike-slip, > 1.5 = thrust) with end-member fault category in parenthesis (SS – strike-slip, NF – normal fault, TS – thrust), QR - Quality Rank ranging from *A* (very good) to *E* (very poor) [*Delvaux* and *Sperner*, 2003] depending on the number of measurements, the average slip deviation angle, the confidence level of the field observation (1, poor to 5, excellent) and the variation of strike orientations within a cluster of measurements., α_w - deviation between observed and theoretical slip directions. Sh_{max} - average strain ratio, i.e., the shape of the finite strain ellipsoid. See Figure 2.6 for a graphical representation of these results.

The P - T - B method is based on the premise that slip vector and the normal to the fault plane define a plane that contains the maximum and minimum stress axes, $\sigma1$ and $\sigma3$. The P T and B axes coincide with $\sigma1$, $\sigma2$ or $\sigma3$ and are defined for each measured plane [*Marrett and Allmendinger*, 1990]. These axes are then calculated for all faults and plotted in an equal-area (Schmidt) net where the average directions of these axes are considered to be representative of the orientations of the principal stress axes. For small increments of strain (i.e., minor slip motions on the fault planes), the P - T - B axes coincide exactly with the principal stresses axes. However, measurable displacements are no longer incremental, so that the P-T-B axes often reflect finite strain rather than the principal axes of the paleostress tensor. For this reason, Table 1 lists the results in terms of the principle finite strain axes. Only fault surfaces with clearly defined dip azimuths and angles, and with striations having unequivocal shear sense indicators were used for P-T-B analysis with the software Win Tensor 3.0.0 [*Delvaux* and *Sperner*, 2003]. Type 2 fault surfaces were analyzed separately from type 1 surfaces in accordance with the overprinting relationship between these types in all outcrops. In addition, type 1 surfaces that indicate dextral motion were analyzed separately from those with sinistral motion in order to obtain a meaningful result.

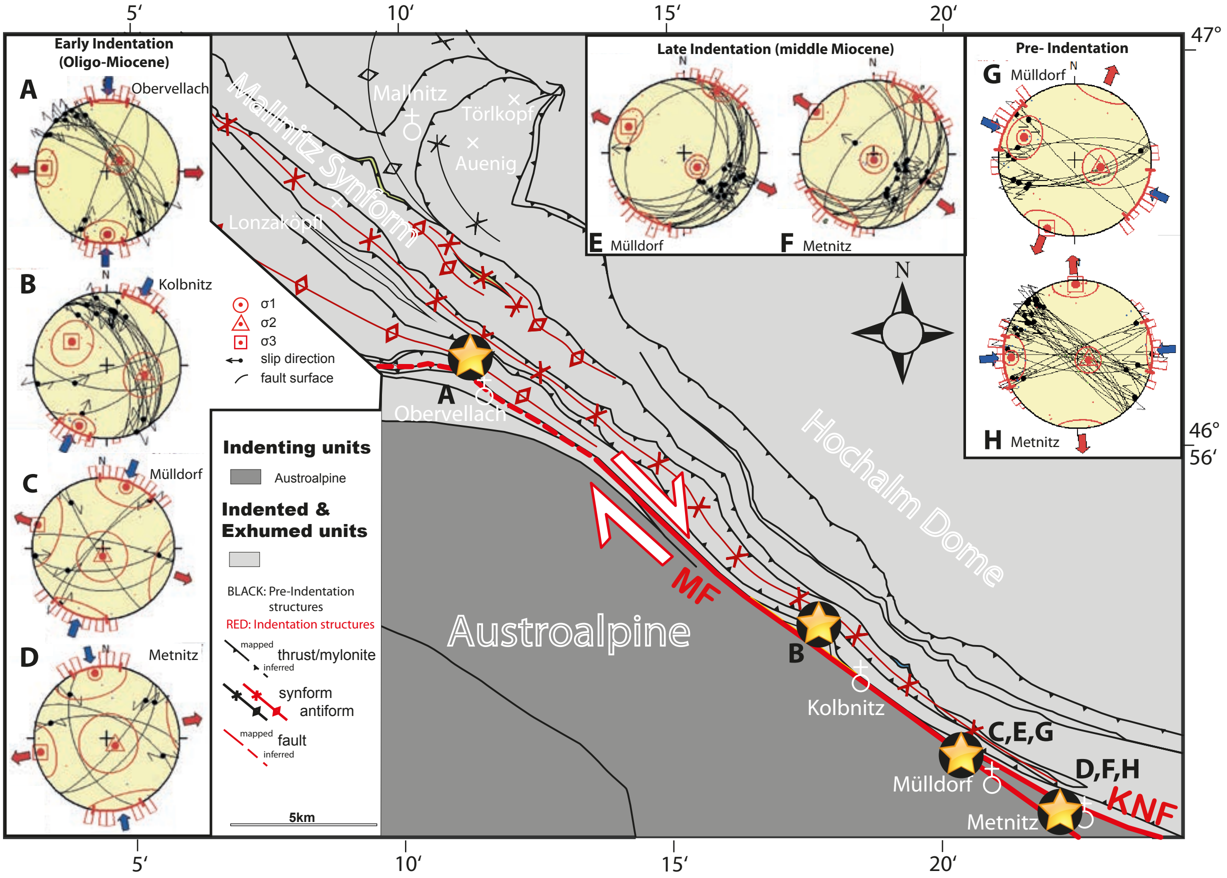

Figure 2.6: P-T-B paleostrain analysis of cataclasites along the Mölltal Fault that overprint mylonite of the southern branch of the KNF. (a) Brittle deformation of Sonnblick Lamellae near Obervellach, (b) brittle deformation in the Glockner Nappe System near Kolbnitz, (c, e, g) cataclasites in lower Australpine Unit, railroad near Mülldorf, (d, f, h) cataclasites in lower Australpine Unit, railroad cut near Metnitz.

The P-T-B analysis reveals that type 1 surfaces with dextral motion in the Penninic units accommodated N-S shortening and E-W extension (Fig. 2.6, a-d), which is consistent with dextral shear parallel to the trace of the Mölltal Fault as already proposed by several authors [*Kurz and Neubauer*, 1996; *Linzer et al.*, 2002; *Rosenberg*, 2007]. However, it is opposite to the ductile sinistral shear indicators in the southern mylonitic branch of the KNF bordering the Hochalm Subdome [*Scharf et al.*, 2013a], as discussed below. Most type 1 faults in the Austro-alpine units show E-W shortening and N-S extension, and only a few accommodated N-S shortening and E-W extension (Fig. 2.6c-d, g-h). In contrast, the moderately dipping type 2 surfaces accommodated NE-SW shortening and NW-SE extension (Fig. 2.6e, f). Again, this matches the pattern of E- to SE-directed extension along the KNF.

The dextral type 1 surfaces confirm the overall dextral displacement along the Mölltal Fault as inferred from the map-view offset of Austro-alpine units with similar Eo-Alpine histories [e.g, offset of the Koralpe-Wölz unit; *Linzer et al.*, 2002; *Schuster et al.*, 2004; *Schmid et al.*, 2013]. This dextral motion records the northward motion of the indenting Drau-Möll block (Fig. 2.2c), whereas the sinistral motion along the adjacent southwestern mylonitic margin of the Hochalm Subdome (Fig. 2.3f) is interpreted as the ductile response of the orgenic crust as it extended laterally to the southeast in front of the advancing indenter (Fig. 2.7b).

The sinistral type 1 surfaces indicate shortening and extension directions that do not fit with N-S directed indentation in Miocene time, nor indeed with any other recognizable strain pattern in the area. We therefore suspect that sinistral motion on such surfaces reflect local adjustments along the leading edge of the indenting Drau-Möll block that are superposed on the overall dextral motion. The type 2 fault surfaces whose motion sense coincides with the extensional direction of the KNF are interpreted to have formed during a late stage of lateral orogenic escape, most likely during or after activity along the KNF, as discussed below.

2.5. KINEMATIC MODEL of INDENTATION and TAUERN EXHUMATION

We now return to the main question posed in the introduction of how indentation was related to the shortening and lateral orogenic escape recorded in the sections above, and in turn, how these bear on both tectonic and erosional denudation. To do this, we reconstructed the kinematics of indentation of the Eastern Alps (Fig. 2.7) back in time, first to the onset of Adriatic indentation of the Eastern Alps at 21 Ma (Fig. 2.7b), then to the beginning of exhumation of the Alpine orogenic wedge at about 30 Ma (Fig. 2.7a) following break-off of the European slab beneath the Alps [*Davies and von Blanckenburg*, 1995; *Handy et al.*, 2015]. The reader is referred to the Supplementary material 2.7 for a detailed description of the displacements along faults in the Austroalpine units and Tauern Window that form the basis for this recosntruction.

2.5.1 Boundary conditions and assumptions

As usual in kinematic modeling, simplifying assumptions were made regarding the initial and final configurations of the crust and the conservation of crustal volume and mass during indentation. The leading edge of the eastern block of the indenting Adriatic Microplate comprises the eastern Southern Alps, i.e., the part of the Alps bounded by the Periadriatic Fault to the north and the Giudicarie Belt to the west (Fig. 2.1). This block is assumed to be rigid throughout indentation, as Miocene thrusts and folds in the eastern Southern Alps accommodated only modest shortening [minimum 50 km, *Schönborn*, 1999] compared to the overall amount of north-south Miocene shortening of the Alpine edifice north of the Periadriatic Fault in the Eastern Alps [109-124 km, *Rosenberg and Berger*, 2009]. Other units assumed to behave rigidly include the Austroalpine crustal units (shades of grey in Fig. 2.7) because in Tertiary time their temperature were below 300°C [*Handy and Oberhänsli*, 2004;

Oberhänsli et al., 2004; *Schuster et al.*, 2004] marking the transition from viscous to brittle behavior in quartz-rich rocks [*Handy et al.*, 1999; *Stipp et al.*, 2002]. Units in the Tauern Window (Penninic and Lower Austroalpine, Fig. 2.1) experienced temperatures greater than 300°C during indentation [*Luth and Willingshofer*, 2008] and were therefore ductile (red shades), as reflected by their changing shapes and areas in map view in Figure 2.7.

The blocks in Figures 2.7a and b are separated by zones of deformation which accommodated most of the relative motion of these blocks. White areas between blocks signify gaps which correspond to areas of shortening (i.e., folding and shearing) when going forward in time. Conversely, overlaps correspond to areas of extension and/or erosional denudation going forward in time. The size of these gaps and overlaps, as well as the amount of displacement along intervening faults is constrained by the age and displacement along these faults, as well as the thermal history of the area, as summarized in Fig. 2.8 and discussed below. Of course, kinematic reconstructions strive to maintain compatibility by minimizing gaps and overlaps, but in practice, perfect compatibility is almost never realized due to the assumption that all crustal blocks are rigid.

All crustal motions in Figure 2.7 are with respect to the top (northern) and left (western) sides of the grid which underlies the map. The only geological structure in Figure 2.7 that remains fixed with respect to this reference frame is the Giudicarie Fault. This fault and its related thrust belt accommodated sinistral motion of the eastern Adriatic Indenter from about 23 to 7 Ma [e.g., *Pomella et al.*, 2012; *Handy et al.*, 2015 and references therein]. The present location of the leading edge of the Adriatic Indenter is marked in blue for additional reference in Figures 2.7a-c.

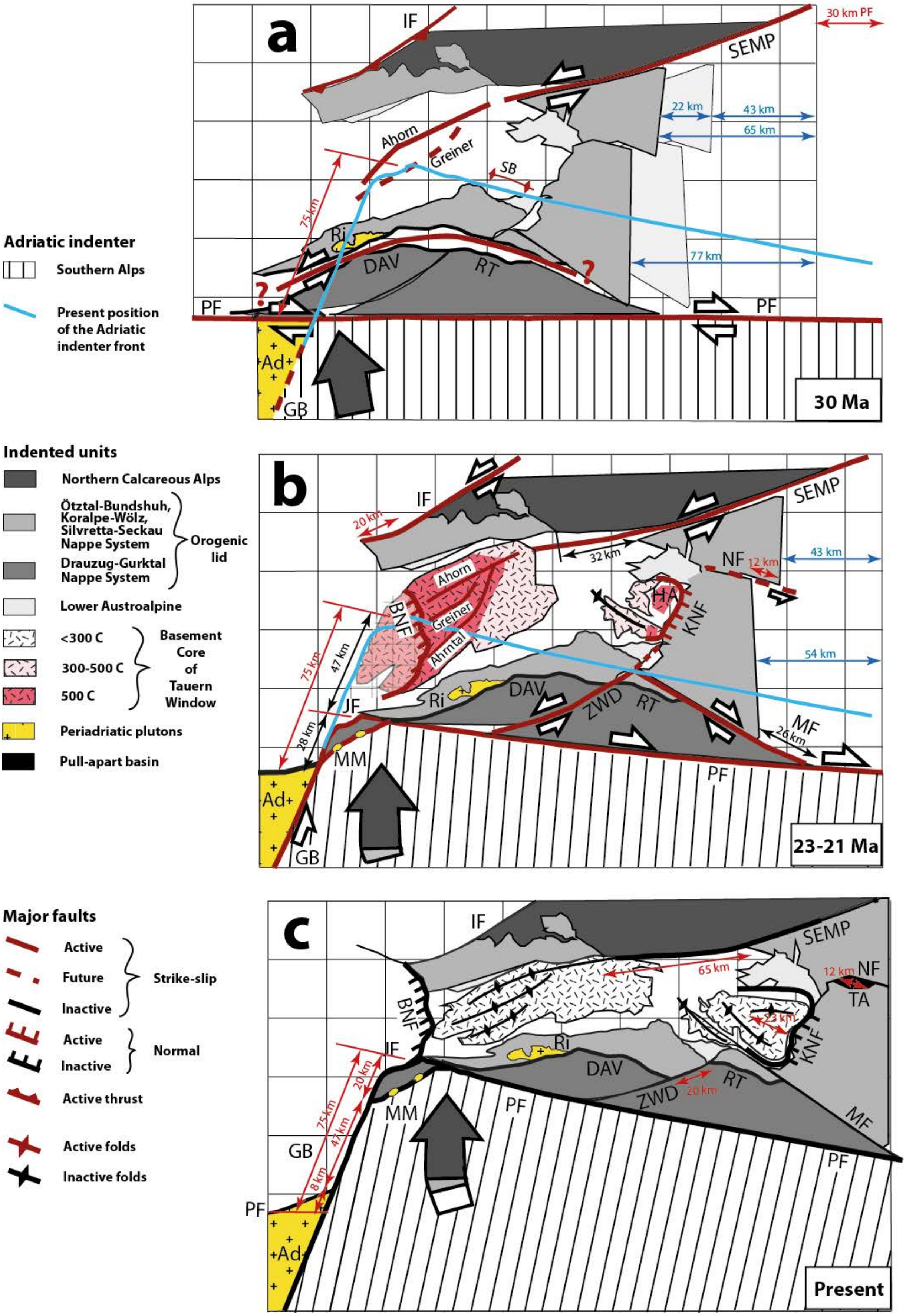

Figure 2.7: Map reconstructions of Adriatic indentation of the Eastern Alps in the Tauern Window area: (a) Initial exhumation during Periadriatic dextral strike-slip transpression and magmatism at 30 Ma; (b) Onset of

indentation along the Giudicarie Belt at 21 Ma, initiation of rapid exhumation (doming and extensional unroofing) of Penninic units in the western Tauern Window, ongoing exhumation in the eastern Tauern Window due to northward motion of Austro-alpine subindenters; (c) Present configuration as modified from map of *Schmid et al.* [2013]. Note that structures in the Tauern Window in (a) and (b) were buried at 30 Ma and 23 Ma, respectively, and are shown as projected to the surface at those times. Color shades indicate approximate temperature of buried crustal units: Red - 500°C, Pink - 300°C, Grey < 300°C. Folds and Domes: HA Hochalm, SB Sonnblick, Faults: BNF Brenner Normal Fault, DAV Defferegen-Antholz-Vals Fault, GB Giudicarie Belt, IF Inntal Fault, JF Jaufen Fault, KNF Katschberg Normal Fault, MF Mölltal Fault, MM Meran-Mauls Fault, NF Niedere Tauern Southern Fault, PF Periadriatic Fault, RT Ragga-Teuchel Fault, SEMP Salzach-Ennstal-Mariazell-Puchberg Fault, ZWD Zwischenbergen-Wöllatratten and Drautal Faults. Shear Zones: Ahorn, Greiner and Ahrntal in (a) and (b) mapped and dated by *Reicherter et al.* [1993], *Steffen et al.* [2001] and *Schneider et al.* [2013]. Periadriatic intrusive bodies: Ad Adamello, Ri Rieserferner. Arrows show lateral displacements: Red – displacement constrained by offset markers; Black – displacements obtained from rigid block motions and compatibility requirements; Blue – Amount of lateral escape resulting from displacements and block motions in the reconstructions.

2.5.2 Time slices of map-view restoration

Two main geologic considerations underlie our stepwise restoration of the Austroalpine subindenters and Tauern Window in Figure 2.7: The first concerns the shape of, the Periadriatic Fault prior to indentation, which in this part of the Alps must have been more-or-less straight up to 30 Ma (Fig. 2.7a) in order to accommodate an estimated 150 km of Paleogene dextral strike-slip motion between the warm Alpine orogenic edifice and the indenting Southern Alpine crust along the leading edge of the Adriatic Microplate [*Bögel*, 1975; *Laubscher*, 1988; *Schmid et al.*, 1989; *Handy et al.*, 2015]. The age of this motion is constrained by Oligocene syntectonic granitoids [c. 32 Ma, Figs. 2.1, 2.7, *Rosenberg*, *2004* and sources therein] as well as by 30-23 Ma cooling ages in Penninic nappes adjacent to the Periadriatic Fault in the Central Alps [*Hurford et al.*, 1986], where exhumation related to backfolding and –thrusting was broadly coeval with dextral Periadriatic motion [*Schmid et al.*, 1987, 1989]. Of the total 150 km of this dextral motion, about 30 km was accommodated by transpression on the Meran-Mauls Fault between 30 and 21 Ma, as shown in Figures 2.7a and b [*Ahrendt*, 1980; *Picotti et al.*, 1995; *Prosser*, 1998; 2000].

The second consideration concerns the amount and age of indentation along the sinistrally transpressive Giudicarie Belt. Total indentation is taken to be 75 km [Fig. 2.7c, *Laubscher, 1988; Ratschbacher et al., 1991b; Werling, 1992*] based on cumulative offsets of the formerly straight Periadriatic Fault [~50 km, *Castellarin et al.*, 2006] and the dextrally transpressive Meran-Mauls Fault [28 km, *Pomella et al.*, 2012]. The age of this indentation is constrained by the main activity of the Giudicarie Belt (Fig. 2.8), beginning at about 23-21 Ma (biostratigraphic dating of sediments beneath thrusts; *Scharf et al.*, 2013a; *Schmid et al.*, 2013] and ending no later than 7 Ma [Messinian unconformity sealing thrusts, *Pieri and Groppi*, 1981; see *Handy et al.*, 2015]. Earlier minor indentation probably initiated somewhat before 21 Ma along the Oligo-Miocene Meran-Mauls Fault

[Fig. 2.8, *Müller et al.*, 2001; *Prosser*, 1998], which together with the Jaufen Fault (Fig. 2.8), are interpreted to have formed a transpressional jog in the Periadriatic Fault by 21 Ma (Fig. 2.7b).

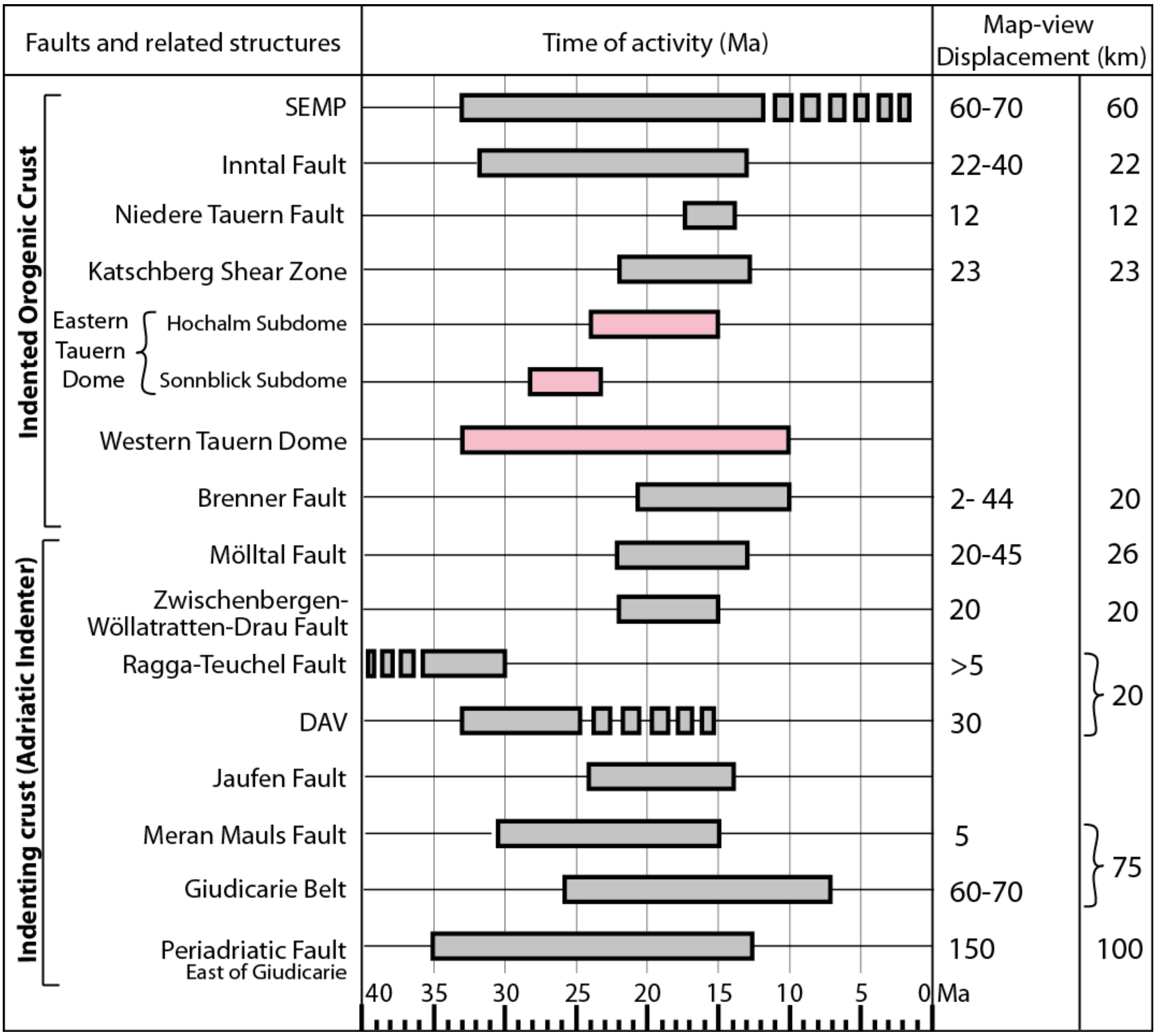

Figure 2.8: Age and displacement along main mylonitic (pink) and cataclastic (grey) faults involved in indentation. Bars and boxed dashes indicate probable and possible durations of fault activity, respectively. **SEMP** [*Ratschbacher et al.*, 1991a, b; *Frank*, 1987; *Peresson and Decker*, 1997; *Frisch et al.*, 1998; *Urbanek et al.*, 2002; *Linzer et al.*, 2002; *Glodny et al.*, 2008; *Schneider et al.*, 2013]; **Inntal Fault** [*Ortner and Sachsenhofer*, 1996, *Ortner et al.*, 2003b, 2006; *Linzer et al.*, 2002]; **Niedere Tauern Fault** [*Zeilinger*, 1997]; **Katschberg Shear Zone** [*Liu et al.*, 2001; *Dunkl et al.*, 2003; *Scharf et al.*, 2013a] **Hochalm Subdome** [*Cliff et al.*, 1985; *Bertrand et al.*, 2013; *Scharf et al.*, 2013a; *Favaro et al.*, 2015]; **Sonnblick Subdome** [*Inger and Cliff*, 1994; *Cliff et al.*, 1998, 2015; *Reddy et al.*, 1993; *Cliff and Meffan-Main*, 2003; *Favaro et al.*, 2015]; **Western Tauern Dome** [*Satir*, 1975; *Thöni*, 1980; *von Blanckenburg et al.*, 1989; *Glodny et al.*, 2008*; Luth and Willingshofer*, 2008; *Schneider and Hammerschmidt*, 2009; *Kitzig*, 2010; *Pollington and Baxter*, 2010; *Rosenberg and Garcia*, 2011; *Schneider et al.*, 2013]; **Brenner Fault** [*Fügenschuh et al.*, 1997; *Frisch et al.*, 1998; *Glodny et al.*, 2008; *Rosenberg and Garcia*, 2011]; **Mölltal Fault** [*Linzer*, 2002; *Scharf et al.*, 2013a]; **Zwischenbergen-Wöllatratten-Drau Fault** [*Scharf et al.*, 2013a]**;** **Ragga-Teuchel Fault** [*Deutsch*, 1984;

Hoke, 1990]; **DAV** [*Borsi et al.*, 1979; *Schulz*, 1990; *Müller et al.*, 2000, 2001; *Mancktelow et al.*, 2001; *Most*, 2003; *Romer and Siegesmund*, 2003; *Handy et al.*, 2005]; **Jaufen Fault** [*Müller et al.*, 1998, 2001; *Viola et al.*, 2001; *Pomella et al.*, 2010]; **Meran-Mauls Fault** [*Müller et al.*, 1998, 2001; *Prosser*, 1998; *Pomella et al.*, 2011, 2012]; **Giudicarie Belt** [*Luciani*, 1989; *Elias*, 1998; *Müller et al.*, 2001; *Viola et al.*, 2001; *Pomella et al.*, 2011, 2012]; **Periadriatic Fault** [*Bögel*, 1975; *Scharbart*, 1975; *Laubscher et al.*, 1988; *Läufer at al.*, 1997; *Frisch et al.*, 1998; *Müller et al.*, 1998, 2001; *Viola et al.*, 2000; *Mancktelow et al.*, 2001; *Stipp et al.*, 2004; *Handy et al.*, 2015].

2.5.3 Quantifying indentation, orogenic shortening and lateral escape

A notable result of our reconstruction is that the amounts of indentation and lateral escape are roughly the same, within error. Initial north-south shortening (28 km) accommodated chiefly by the Meran-Mauls Fault resulted in about 22 km of eastward lateral escape by 21 Ma (Figs. 2.7a and b). Continued indentation of some 47 km during main activity of the sinistrally transpressive Giudicarie Belt between 21 Ma and the Present induced about 43-54 km of lateral escape (Figs. 2.7b and c). Most of the total 71 km of lateral escape of the orogenic edifice was accommodated by strike-slip faulting along the sinistral SEMP and the dextral Periadriatic Fault (Fig. 2.7a); another 23 km of E-W extension was taken up along the Katschberg Normal Fault [*Scharf et al.*, 2013a]. The Brenner Normal Fault is kinematically linked to the Western Tauern Dome in its footwall and along strike to the sinistral SEMP. Together, the BNF and WTD acted as a bridge structure that transferred north-south motion on the Giudicarie Belt to east-west escape [*Scharf et al.*, 2013a, Figs. 2.1, 2.7b].

The style of deformation in the indented crust reflects its temperature and rheology during indentation; in the relatively cold (< 300°C) Austroalpine units just north of the Periadriatic Fault, indentation lead to the individuation of two triangular sub-indenters that deformed by a complex system of oblique-slip faults [*Linzer et al.*, 2002, *Scharf et al.*, 2013a], whereas in the warm Tauern Window (300-600°C), a system of upright folds and shear zones accommodated both vertical and lateral motions [*Scharf et al.*, 2013a; *Schmid et al.*, 2013; *Schneider et al.*, 2013]. Shortening in the Tauern Window itself is not homogeneous, with more north-south shortening in the west (WTD, 25-30 km) than in the east (ETD, 11 km). We note that our estimate of north-south shortening from the reconstruction in Figure 2.7 is somewhat less than the 32 km estimate obtained for the WDT by *Schmid et al.* [2013], and far less than the 49 km of *Rosenberg and Berger* [2009]. This is partly due to the different location of cross sections and fold profiles used in their estimates, and partly to their use of line-balancing which yields an upper limit of shortening in flexural-slip folds like those in the Tauern Window.

2.5.4 Assessing the relative roles of erosion and extensional unroofing

Comparing the areas of the Penninic units in the reconstruction (blue areas in Figure 2.9) allows us to estimate denudation in the Tauern Window due to erosion and orogen-parallel extension since 30 Ma and especially since pronounced indentation of the Eastern Alps beginning at c. 21 Ma. The blue area in Figure 2.9a (~ 3125 km^2) represents the total denuded area prior to the onset of lateral escape and orogen-parallel extensional faulting. This denudational area is therefore attributed solely to erosion, mostly due to upright folding and thickening which had been ongoing since the onset of Adria-Europe collision at c. 35 Ma [e.g., *Handy et al.*, 2010; *Schmid et al.*, 2013].

The component of denudation due to extensional unroofing is estimated by subtracting the blue area described above (~ 3125 km^2) and shown in Figure 2.9a from the blue area in the map for the Present in Figure 2.9c (~ 4375 km^2, ~5000 km^2 comprising the lower Austroalpine units). This latter area is in the footwalls of the oppositely dipping BNF and KNF and therefore represents Penninic crust removed by a combination of extensional unroofing and erosion since 30 Ma. The difference in areas (~ 1250 km^2) is therefore the denudational area associated with extensional exhumation and unroofing. Thus, about two thirds of the denuded area is attributable to erosion during north-south thickening and folding of the crust; only about a third of the total areal denudation is due to tectonic unroofing in the footwalls of the BNF and KNF.

Converting denuded area into denuded crustal volume requires making assumptions about the thickness of the crustal lid above the Tauern area. Geobarometry yields peak pressures of 10-11 kbar [*Franz et al.*, 1991; *Kurz et al.*, 1998, and references therein] and 7.5-8 kbar [*Dachs*, 1990; *Reddy*, 1990] for post-nappe Barrow-type metamorphism, respectively, in the Western and Eastern Tauern domes. This event, the "Tauernkristallisation", ranges in age from 30-25 Ma [*Oberhänsli et al.*, 2004; *Pollington and Baxter*, 2010; *Favaro et al.*, 2015] and preceded the onset of rapid exhumation in the eastern Tauern Window at about 23 Ma in the east [*Scharf et al.*, 2013a] and 20 Ma in the west [*Fügenschuh et al.*, 1997]. Thus, the peak pressures pertain to the thickened Tauern crust in Figure 2.9a prior to upright folding and extensional unroofing. For an average crustal density of 2.8 g/cm3, the pressures place an upper bound of 38 km on the thickness of the denuded lid above the western part of the Tauern Window, corresponding to a volume of c. 120.000 km^3 denuded since 30 Ma. A lower bound of about 28 km thickness and 87,000 km^3 denuded crust is obtained in a like manner for the eastern part of the Tauern Window, where post-nappe upright folds have lower amplitudes [cross sections in *Schmid et al.*, 2013].

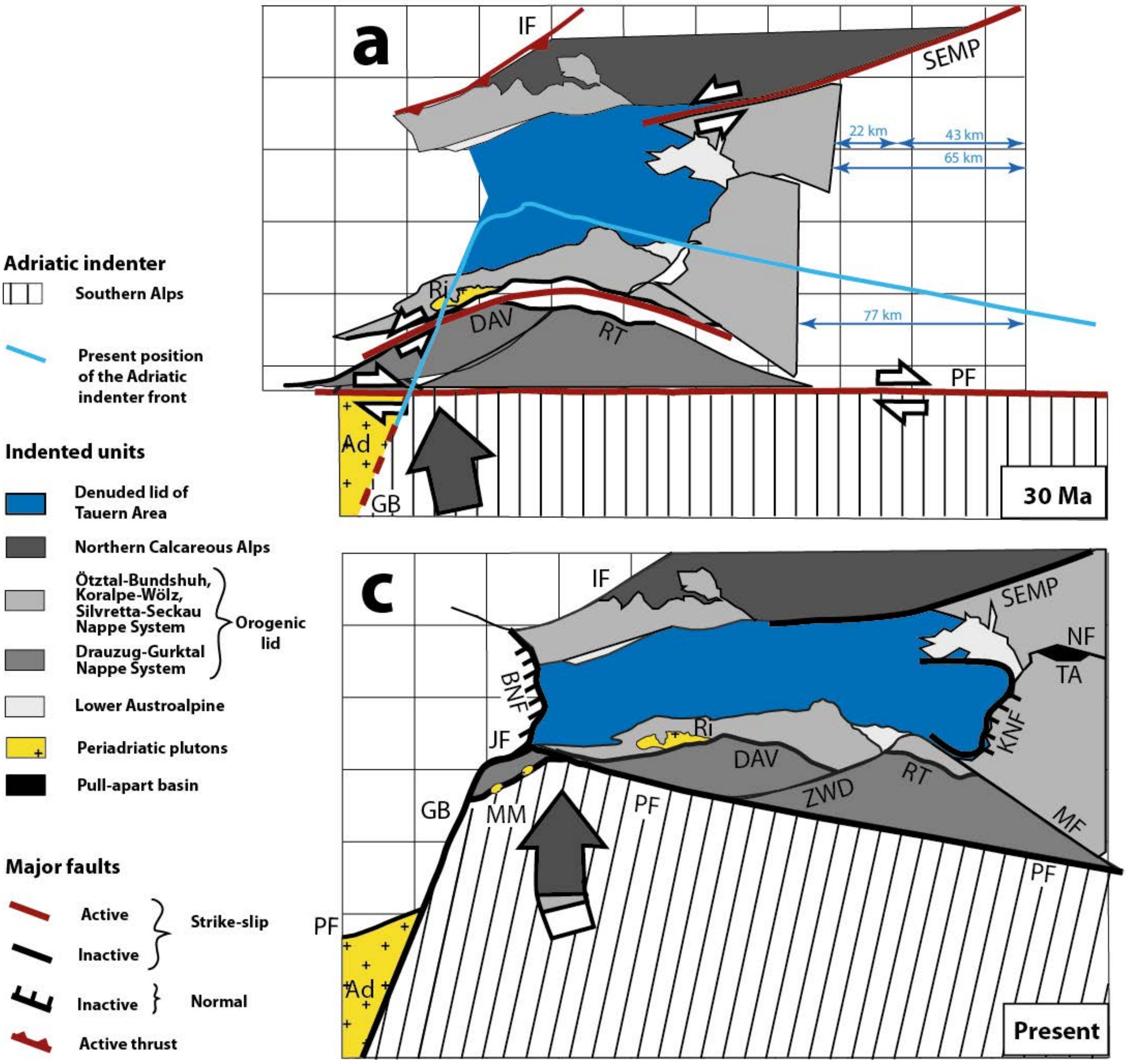

Figure 2.9: Map reconstructions of Adriatic indentation of the Eastern Alps with blue areas showing denuded Penninic crust in the Tauern Window at 30 Ma and Present, corresponding to maps in Figure 2.7a and c. Blue line in (a) indicates Present front of the indenting Southern Alpine crust.

The denuded crust from the Tauern area comprised Austroalpine crust as well as the upper part of the Penninic nappe pile. Detrital deposits with Tauern components are exposed today in Oligo-Miocene clastics of the Inntal Basin [the so-called “Inntal Tertiary”, *Frisch et al.*, 2001] and the related northern Alpine Molasse Basin. After about 22 Ma, deposition shifted progressively to the east in the Pannonian Basin, as drainage was channeled by the Miocene strike-slip faults that accommodated crustal block rotation and lateral eastward extrusion [*Frisch et al.*, 1998].

Our estimates of denudational volume of the Tauern source area (87,000-120,000 km3) are somewhat greater than the values (80,000 km3) estimated indirectly by *Kuhlemann* [2001] from an analysis of Miocene sediment bodies in the northern Alpine Molasse Basin. This discrepancy in the estimated source and sink volumes may be partly real, but more likely reflects *Kuhlemann*'s [2001] use of a smaller denudational thickness for the Tauern area (16 km) distributed over a larger area (5,000 km2) as derived from the reconstruction of *Frisch et al.* [1998]. Compared to our reconstruction in Figure 2.7, the *Frisch et al.*. [1998] model assumes that the Austroalpine units on the eastwen and western sides of the Tauern Window were contiguous before the onset of Miocene indentation, resulting in a much smaller proportion of fold-induced denudation [15,000 km3 of the aforementioned total of 80,000 km3, *Kuhlemann*, 2001].

2.6 CONCLUSIONS

The structure evolution of fault-bounded blocks of Austroalpine crust along the front of the Adriatic Indenter had a major effect on the pattern of shortening and lateral escape of the orogenic crust in the Tauern Window. In the eastern part of the window, initial indentation at c. 23 Ma involved post-nappe upright folding that propagated away from the indenter front as indicated by the northeastward younging of mica cooling ages in the Venediger Nappe System [*Favaro et al.*, 2015]. Ongoing indentation from c. 21 to 17 Ma lead to fragmentation of the Austroalpine subindenter, which was accommodated in the orogenic crust by a combination of continued upright folding and extensional exhumation in the footwall of the laterally migrating Katschberg Normal Fault. The contrast in rheology of the cold indenting block and hot orogenic crust is expressed by opposite shear senses in cataclasite along the indenter front (Mölltal Fault, dextral type 1 cataclasites) and in mylonite along the adjacent margin of the eastwardly stretching and exhuming Eastern Tauern Dome [sinistral southern branch of the Katschberg Normal Fault, see also *Scharf et al.*, 2013a]. By 17 Ma, the orogenic crust had cooled to below 300°C [*Dunkl et al.*, 2003; *Bertrand et al.*, 2013], resulting in brittle top-SE extension as recorded by shear surfaces in both the Austroalpine and Penninic units (cataclasites of the KNF and type 2 cataclasites of the Mölltal Fault).

Similar patterns of indentation, folding and orogen-parallel stretching are observed in the Western Tauern Window where, however, shortening was much greater and kinematically linked to lateral escape along the sinistral SEMP Fault via a transpressional bridge structure in the Western Tauern Dome [Fig. 2.7b, c; *Scharf et al.*, 2013a]. This bridge structure, which after 21 Ma included the Brenner Normal Fault [*Fügenschuh et al.*, 1997], accommodated some 70 km of E-W extension.

Retrodeforming the post-nappe fold and fault systems of the Tauern Window in map view yields a reconstruction of the orogenic crust reaching back to 30 Ma, including the onset of indentation at c. 23 Ma (Fig. 2.7). This 2-D model supports the notion that indentation lead to roughly equal amounts of north-south shortening (75 km) and east-west orogen-parallel stretching (71 km) of the orogenic crust in the Tauern Window. Estimates of the areas of denudation prior to and after the onset of indentation indicate that erosion associated with upright folding and thickening was the primary agent of denudation, whereas extensional unroofing accounted for only about a third of the total denudation and affected only the eastern and western ends of the Tauern Window in the footwalls of the Katschberg and Brenner Normal Faults.

Previous models of lateral escape and denudation in the Eastern Alps have tended either to emphasize the role of post-nappe, upright folding in the Tauern Window with only a small contribution of orogen-parallel extension [*Laubscher*, 1988; *Lammerer*, 1988; *Behrmann*, 1988; *Rosenberg et al.*, 2004, 2007; *Rosenberg and Garcia*, 2011, 2012] or, on the contrary, to assume orogen-parallel extension and unroofing to the virtual exclusion of doming [*Genser and Neubauer*, 1989; *Frisch et al.*, 2000; *Linzer et al.*, 2002]. We follow *Fügenschuh et al.* [1997] in proposing a mix of coeval doming and orogen-parallel stretching of the Tauern Window in Miocene time, but emphasize that the eastern and western parts of this window experienced different patterns of shortening and stretching: in the east, doming initiated before stretching and then migrated from SW to NE away from the indenter front [*Favaro et al.*, 2015]., whereas in the west, strike-slip shearing preceded upright folding and this folding progressed from NW to SE towards the indenter [*Schneider et al.*, 2013].

These contrasting strain patterns may reflect varied structure of the interface between indenting and indented crust along strike of the Tauern Window. Gravimetry reveals significant mass deficit in the vicinity of the western Tauern Window [*Ebbing et al.*, 2006], suggesting the existence of an anomalously dense body (c. 2.9 g/cm) in the underlying crust. A recent Moho study based on inverting the results of four independent geophysical methods (controlled-source seismology, ambient noise and local earthquake tomographies, receiver functions) indicates that the Moho beneath the eastern half of the Tauern Window is poorly defined or even absent [*Spada et al.*, 2013]. Resolution of this problem is contingent on higher resolution studies of the substructure along the front of the Adriatic Indenter.

2.7 SUPPLEMENTARY MATERIAL TO CHAPTER 2: 1

Reconstructing the orogenic crust in the Tauern Window area during Indentation (Fig. 2.7)

The starting point for the reconstruction in Figure 2.7 is the present-day surface geology (Fig. 2.7c) in the tectonic map of the Tauern Window of *Schmid et al.* [2013, their Fig. 1]. This map is also representative of the situation some 11 Ma [*Fügenschuh et al.*, 1997], when the Brenner Normal Fault became inactive and lateral escape tectonics affected domains towards the Pannonian Basin, east of the map view. GPS studies indicate some ongoing lateral escape in response to ongoing Adria indentation [*Vrabec et al.*, 2006], but this is very slow [1-2 mm/yr, e.g., *Bada et al.*, 2007; see other references in *Scharf et al.*, 2013a; *Schmid et al.*, 2013; *Rosenberg and Garcia*, 2011].

Map for 21 Ma:

The Adriatic indenter front is presumed to have begun its fast northward movement at 23-21 Ma as constrained by two events that are kinematically linked in space and time: (1) the onset of rapid exhumation in the western Tauern Window at c. 20 Ma according to thermal modeling of cooling ages in the western Tauern Window [*Fügenschuh et al.*, 1997]; (2) the onset of northward motion of the Adriatic Indenter at 21-23 Ma based on biostratigraphic ages [*Luciani and Silvestrini*, 1996; *Luciani*, 1989] of the youngest sediments preserved in the footwall a major, SE-directed thrust in the sinistral transpressive Giudicarie Belt [*Scharf et al.*, 2013a; *Schmid et al.*, 2013]. The kinematic link of motions in (1) and (2) is a transpressive bridge system of upright folds and shear zones in the western Tauern Window (Fig. 2.7b) which transferred northward motion of the indenter to eastward lateral escape of orogenic crust between the SEMP and Periadriatic faults [*Scharf et al.*, 2013a; *Schneider et al.*, submitted]. In this system, the northwestern tip of the indenter functioned as a singularity point.

The total offset along the Giudicarie Belt that accommodated Adriatic indentation of the Eastern Alps is debated to range between 30 to 70 km [e.g. *Pieri and Groppi*, 1981; *Luciani*, 1989; *Schonborn*, 1992; *Elias*, 1998; *Prosser*, 1998; *Müller et al.*, 1998, 2001; *Viola et al.*, 2001; *Pomella et al.*, 2011, 2012]. In this reconstruction we use an estimated offset of 75 km (Fig. 2.7c) which is close to values published by previous authors [77 km, *Laubscher*, 1988; 80 km, *Frisch et al.*, 2000; *Linzer et al.*, 2002]. This estimate is based on the offset of the Periadriatic Fault, which is assumed to have been straight prior latest Oligocene time [Fig. 2.7a, *Pomella et al.*, 2012]: the total offset includes about 28 km of late Oligocene-earliest Miocene northward offset and counterclockwise rotation of the Meran-Mauls Fault (MM). Therefore, we use an offset of 47 km since 21 Ma (Fig. 2.7b).

The total sinistral offset along the SEMP in Figure 2.7a is estimated to be 65 km as obtained by restoring the tips of the grey unit on either side of this fault to their originally contiguous position (Quartzphyllite of the Silvretta-Seckau Nappe). This is within the 60-70 km range of displacements proposed by previous workers and includes 6 km of sinistral displacement on the Königsee-Lammertal-Traunsee Fault [*Decker et al.*, 1994 in *Schmid et al., 2013*; fault not shown on any figures here]. The timing of motion on the SEMP in the Tauern Window area is well constrained by widely ranging mica ages to be early Oligocene to mid-Miocene [Fig. 2.8, *Urbanek et al.*, 2002; *Glodny et al.*, 2008], whereas eastern segments of this fault (Hochschwab karst massif – Styria, Austria) may still be active [offset speleothems in caves along the fault, *Plan et al.*, 2010, U/Th dating]. In light of these broad constraints, we estimate the post-21 Ma displacement to be 32 km (Fig. 2.7b) as obtained by repositioning the Quartzphyllite unit of the Silvretta-Seckau Nappe on either side of the SEMP in the following way: (1) the block northeast of the Tauern Window and immediately south of the SEMP is restored some 43 km eastward from its present location, an amount equal to the difference of c. 54 km of east-west, orogen-parallel motion due to extension on the Brenner and Katschberg normal faults (see below) and 12 km of offset required to close the mid-Miocene Tamsweg pull-apart basin [17-14 Ma, *Zeilinger*, 1997 in *Scharf et al.*, 2013a] along the sinistral Niedertauern Fault (NF, Figs. 2.7b, c); (2) the adjacent block north of the SEMP is restored 22 km to the SE, which is taken to be equal to the minimum amount of Miocene sinistral motion on the Inntal Fault. The timing of motion on this fault is also poorly constrained, but is consistent with *Ortner et al.* [2006] that most of the maximum 40 km of sinistral displacement is post-Oligocene.

Extensional displacement on the Katschberg Normal Fault is taken to be 23 km in map view, a conservative estimate taken from the 23-29 km range of horizontal displacement provided by *Scharf et al.* [2013a]. The extensional displacement accommodated by the Brenner Normal Fault and upright folds and shear zones in its footwall is estimated to range between 2 and 42 [*Behrmann*, 1988; *Selverstone*, 1988; *Rosenberg and Garcia*, 2011; *Fügenschuh et al.*, 2012], in our reconstruction we chose an average value of 20 km.

The indenting triangular block south of the Mölltal Fault also moves toward the west along the Pustertal-Gaital segment of the Periadriatic Fault, allowing the DAV to rejoin together its eastern end, the Ragga-Teuchel Fault [RT in figure 2.7, *Hoinkes et al.*, 1999; *Scharf et al.*, 2013a] closing the 20 km offset along the Miocene sinistral strike-slip Zwischenbergen- Wöllatratten and Drautal Faults [ZWD in figure 2.7; *Exner*, 1962c; *Heinisch and Schmidt*, 1984; *Schmid et al.*, 2013]. Moving these blocks rigidly, we create a gap on the western side of the Pustertal-Gaital Fault, between the indenter and the triangular dead zone. This can be easy explained considering the fact we do not take in account the several strike-slip and inverse faults located in the triangular zone that were active at that time [e.g. *Hoke*, 1990]. Part of Sonnblick and Hochalm subdomes are already cooling down below 300°C while the western Tauern Dome is still forming and has temperatures of ~ 500 °C [*Reddy et al.*, 1993; *Luth and Willingshofer*, 2008; *Schneider et al.*, 2013; *Favaro et al.*, 2015]. Thermal modeling of the WTD indicates that the onset of rapid exhumation preceded rapid cooling at 20 Ma by some 2 Ma [*Fügenschuh et al.*, 1997] and coincided in time with this stage of orogenic indentation [*Pomella et al.*, 2011, 2012; *Schmid et al.*, 2013]. Zircon fission track ages indicate that cooling of both subdomes to below 240°C, which corresponds to the transition from ductile to brittle conditions in quartz-rich rocks [*Handy et al.*, 1999; *Stipp et al.*, 2002] occurred no later than 17-15 Ma [*Dunkl et al.*, 2003; *Wölfler et al.*, 2008; *Bertrand*, 2013].

Discussion of Austroalpine indenters

The E-W Miocene extension between the Tauern Window and the Periadriatic Fault is documented in most of the above mentioned models by dextral displacement along the NW-SE striking splay faults of the Periadriatic Fault, the Mölltal, Isental and related faults [*Linzer et al.*, 2002]. Based on the apparent offsets of stratigraphic markers in map view, previous estimates suggested a displacements ranging between 45 and 12 km for the Mölltal Fault and 20 km for the Isental and related faults [Lavanttal and Hochstuhl faults, *Linzer et al.*, 2002]. However, these displacements are overestimated: The south-eastern margin of the Tauern Window shows an apparent lateral offset of only 26 km along the dextral Mölltal Fault [*Exner*, 1962; *Kurz and Neubauer*, 1996; *Scharf et al.*, 2013a] and the marker used to estimate the offset along the Isental Fault is merely an erosional contact between basement and different covers [*Rosenberg et al.*, 2007]. Its apparent displacement in map view is of about 10 km, but the effective displacement could be much smaller [*Rosenberg et al.*, 2007; *Linner et al.*, 2013]. In our model we do not take the Isental Fault into account but we use instead the Miocene Zwischenbergen-Wöllatratten and Drautal Faults [ZWD, *Exner*, 1962c; *Heinisch and Schmidt*, 1984]. This is proposed already by *Scharf et al.*, [2013a], where is documented that the northwestern tip of the Molltal Fault does not end within the Sonnblick Subdome [*Kurz and Neubauer*, 1996] but bends into its southeastern margin and broadens into a diffuse zone of cataclasites near Obervellach, which also correspond with the northern termination of the ZWD Fault. This coincides with a sinistral shear zone found at the southeastern margin of the Sonnblick Subdome responsible of the thinning of the Sonnblick Lammelae (Fig. 2.2, domain F) and with a changing in the age pattern within the Tauern Window described in *Favaro et al.* [2015]. According to *Schmid et al.* [2013], the ZWD Fault offsets of 20 km the Defferegen-Antholz-Vals and the Ragga- Teuchel faults (DAV and RT faults, Fig. 2.1). In his work they are interpreted to be parts of the same Oligocene fault because they share same Austroalpine units on both sides and they mark the southern limit of the Late Cretaceous Eo-alpine metamorphism [SAM of *Hoinkes et al.*, 1999]. Moreover, ages on these faults show that the DAV Fault was active during the intrusion of the Riesenfernen pluton at ~ 30 Ma [*Müller et al.*, 2000; *Mancktelow et al.*, 2001; *Romer and Siegismung*, 2003; *Wagner et al.*, 2006], and the RT Fault was active between 40-30 Ma as indicated by dating on undeformed dykes that cut its fault plane [*Hoke*, 1990; *Deutsch*, 1984].

Map for 30 Ma

The ages in Figure 2.8 show that the first stage of indentation started between 30 and 25 Ma, after the emplacement of the Adamello intrusion between 42 and 30 Ma [*Brack*, 1985; *Del Moro et al.*, 1985], together with the activity of the SEMP, Meran Maules and DAV faults [*Wagner et al.*, 2006; *Frost et al.*, 2009; *Mancktelow et al.*, 2001; *Schneider et al.*, 2013].

During this incipient stage of indentation the restoration of the Adriatic Indenter is based on the horizontalization and backrotation of the Meran Mauls Fault to join the Pustertal-Gaital Fault (norther boundary of the Adriatic Indenter) with the Tonale Fault [central segment of the Periadriat Fault, *Laubscher*, 1988; *Stipp et al.*, 2004; *Pomella et al.*, 2012].

To restore the 28 km left from the previous restoration step to reach the total sinistral offset of 75 km along the Giudicarie Belt, we back-rotate the Meran Mauls Fault (MM; see Fig. 2.7b) which was already active as a transpressional restraining bend sometime between 31 Ma, according to Ar/Ar dating of pseudotachylite and of small Periadriatic intrusives arrayed along this fault, till 15 Ma [*Pomella et al.*, 2010, 2011; *Müller et al.*, 1998, 2001; *Prosser*, 1998].

The small Periadriatic intrusives arrayed along the MM Fault are called "Tonalitic Lamella". The Tonalitc Lamella is interpreted to be a sheared and rotated part of the Adamello batholith emplaced in this position during transpression and rotation along the Meran-Mules Fault, when the granitoids were still ductile [*Martin et al.*, 1993; *Morten*, 1974; *Pomella et al.*, 2011]. The Tonalitic Lamella is ~30 km long. To bring it back on the Adamello batholith we move all the blocks north of the now straight Periasdriatic Fault westward of about 30 km (30 MM label in Figure 2.7a). The Periadriatic Fault System has a total offset of 150 km [*Handy et al.*, 2015] and began its strike-slip activity at 35 Ma when a westward component between the Adriatic and European convergent plates took place [*Handy et al.*, 2005]. Unfortunately, other Oligo-Miocene displacement estimates on the Pustertal-Gaital segment of the Periadriatic Fault are still missing [*Bistacchi et al.*, 2010] but radiometric ages agrees to a continuous activity till 13 Ma [*Zwingmann and Mancktelow*, 2004].

The block south of the SEMP Fault is restored of 30 km left from the 21 Ma restoration to reach almost the total amount of 65 km. We know that the SEMP was active till 33-32 Ma [*Urbanek et al.*, 2002; *Glodny et al.*, 2008; *Schneider et al.*, 2013].

The DAV Fault reached its activity peak between 36 and 25 Ma, coheval with the emplacement of the Riesenfernen pluton [*Borsi et al.*, 1979; *Schulz*, 1990; *Müller et al.*, 2000, 2001; *Mancktelow et al.*, 2001; *Most*, 2003; *Romer and Siegesmund*, 2003; *Handy et al.*, 2005]. There are no constrain on the amount of displacement and there are controversial interpretation on the shear sense [*Mancktelow et al.*, 2001; *Handy et al.*, 2005].

This incipient indentation is well recorded within the Tauern Window, with the oldest formation ages of Sonnblick Subdome at a temperature higher than 500°C range between 31 and 24 Ma [*Cliff et al.*, 1985; *Reddy et al.*, 1993; *Inger and Cliff*, 1994; *Glodny et al.*, 2008; *Cliff et al.*, 2015; *Favaro et al.*, 2015]. The Ahorn and Tux shear zones within the Western Tauern Dome are also active, with ages on fabric forming mineral within the shear zones ranging between 32 and 10 Ma [*Urbanek*, 2002; *Peresson and Decker*, 1997; *Glodny et al.*, 2008; *Schneider et al.*, 2013].

2.8 SUPPLEMENTARY MATERIAL TO CHAPTER 2: 2

Brittle: paleostress analysis

The measures used in the paleostress analysis include the local strike and dip of the fault surfaces, the orientation of the lineations and the slip direction. With collecting data for a fault population, you privide information about the strain and orientation of the principal stress axes. To do that, we must introduce the concept of stress ratio, which ranges between 0 and 1. It can be used to express the stress tensors, which, in a defined coordinate system, are the principal axes of stress. If $\sigma = 0$ we have an ellipsoid of stress cigar, $\sigma = 1$ if the ellipsoid of stress appears flattened at the poles. The stress ratio is defined as R 1 or $1 - \sigma$. The stress tensor contains information on the orientation and shape of the stress ellipsoid. These tensors are calculated from the slip data of the fault and are very relevant for the analysis of paleostress.

In case that all three axes are known, the directions of the striae on a single fault allow the estimation of the stress ratio. For structures developed at shallow depths, sometimes it is assumed that one of the principal axes of stress is oriented normal to the surface of the soil. Instead, in case the orientations of the three axes are unknown, various methods can be developed to determine a range of possible orientations of the principal stress axes. In theory, the analysis of the relationship between stress field, fault systems and type of movement lead to the development of various methods for the reconstruction of stress tensors from fault slip data or from focal mechanisms solutions. These methods are called "paleostress methods".

The P - T - B method is based on the observation that slip vector and the normal to the fault plane define a plane that contains the principal stress axes. It is defined for each given plane a set of three perpendicular axes, P (pressure), T (tension) and B that may coincide with $\sigma 1$, $\sigma 2$ or $\sigma 3$. Subsequently, these axes, calculated for all faults, are represented in a stereo plot and the average directions are considered representative of the principal axes of stress. In an ideal situation the correspondence between the principal stresses axes and P - T - B axes is valid.

The right dihedron method is modeled on a fault plane and a second auxiliary plane perpendicular to the lineation. This method defines two pairs of quadrants, each of which corresponds to the possible orientation range of a principal stress axis. Using the slip sense of the fault is possible to decide which quadrants are "tensional" and which are "compressional".

Logically, measurement errors, possible rotation of the blocks and surface runoff may be relevant to the miscalculation of paleostress and can be minimized by statistical methods. The most widely used is the grid search. With this method, one must understand which stress tensor is more compatible with the stress field calculated. The most obvious choice is to use the deviation angle between the observed lineation and the maximum shear stress direction predicted by the tensor and to choose the tensor that produces the smallest average angle.

Win Tensor 3.0.0

The software Win Tensor 3.0.0 was used to perform paleostress analysis [*Delvaux*, 1993]. In addition to express the stress regime with the PBT method and right dihedral, Win Tensor 3.0.0 introduces a new parameter R', allowing to determine the stability of the axes and the rotation allow by the inversion on each axis [*Delvaux*, 1997; *Delvaux and Sperner*, 2003]. The regime of extensional stress can be defined when σ1 is vertical, strike-slip when σ2 is vertical and compressional when σ3 is vertical. For these three regimes, the value of stress ratio R fluctuates between 0 and 1. When it is close to 0.5, this regimes of stress are called "pure" extensional / transcurrent / compressional. R', defined as stress regime index [*Delvaux*, 1997], has been inserted to facilitate the differentiation between the three regimes and is expressed numerically as:

- R' = R when σ1 it is vertical (extensional regime)
- R' = 2 - R when σ2 it is vertical (strike-slip regime)
- R' = 2 + R when σ3 it is vertical (compressional regime)

R' varies from 0 to 3. R' has the value of 0.5 for pure extension, 1.0 for transtensional activity, 1.5 for pure strike-slip, 2.0 for transpressive activities and 2.5 for pure compression [*Delvaux and Sperner*, 2003]. The method of inversion introduced by Delvaux and coauthors [*Delvaux*, 1997; *Delvaux and Sperner*, 2003] is called Rotational Optimazion and allows, starting from an initial inversion by the method of the dihedral rectum, to minimize the errors of inversion utilizing a misfit function and an interactive process that takes in account possible slight variations of the stress differential, of R and the angles of rotations around the principal axes of the stress field. Therefore, determination of the stress tensor using the method Rotational Optimazion consists in the development of 4 Cartesian graphs, 3 concerning the possible rotation around the principal axes of stress and one relating to the stress regime index R'. The graphs show in abscissa the angle of rotation for each axis or the value of R' and in ordinate the value of the misfit function.

The plotted data are interpolated by regression curves which indicate the stability around the axes. The rotations on each axis of stress are determined through successive iterations based on minimum values of misfit function which is defined by the regression curve in the graphs. The stress tensor is then rotated accordingly. Once defined the rotation on the three main axes, is optimized the R value and therefore R'.

Table 2.1.A: values used for the paleostrain analyses in Fig. 2.6. MET - Metnitz Outcrop; MULL - Mulldorf Outcrop; TW - Outcrops in the Penninic units.

Fault-slip data			**Input row data**								
	Properties		Orientation		Orientation 1						
Id	Format	Type	OriA	OriB	Ori1A	Ori1B	Slip Sense	Conf. Level	Weight Factor	Activ. Type	Striae Intens
MET-1	11	1	79	160	21	246	N	P	2,0	2	2
MET-2	11	1	44	175	19	105	N	P	2,0	2	2
MET-3	11	1	86	159	13	248	N	P	2,0	2	2
MET-4	11	1	64	123	63	115	N	P	2,0	2	2
MET-5	11	1	78	130	26	46	N	P	2,0	2	2
MET-6	11	1	81	3	49	82	D	S	2,0	2	2
MET-7	11	1	64	3	24	80	D	S	2,0	2	2
MET-8	11	1	66	26	20	107	D	S	2,0	2	2
MET-9	11	1	85	333	44	58	D	P	2,0	2	2
MET-10	11	1	74	2	34	283	D	P	2,0	2	2
MET-11	11	1	89	100	52	11	X	X	2,0	2	2
MET-12	11	1	65	5	21	285	D	S	2,0	2	2
MET-13	11	1	89	23	18	293	S	S	2,0	2	2
MET-14	11	1	78	27	21	302	S	S	2,0	2	2
MET-15	11	1	60	132	19	53	N	S	2,0	2	2
MET-16	11	1	54	81	52	100	N	S	2,0	2	0
MET-17	11	1	56	88	54	108	N	S	2,0	2	0
MET-18	11	1	53	90	50	117	N	S	2,0	2	0
MET-19	11	1	59	105	58	122	N	S	2,0	2	0
MET-20	11	2	42	170	70	352		S	2,0	1	0
MET-21	11	2	53	127	66	312		S	2,0	1	0
MET-22	11	2	34	156	70	335		S	2,0	1	0
MET-23	22	1	141	21	117	19	N	S	2,0	2	0
MET-24	22	3	96	26	105	80		P	3,0	1	2
MET-25	22	1	154	31	120	27	N	S	2,0	2	0
MET-26	22	1	186	71	274	6	D	S	2,0	2	0
MET-27	22	1	247	54	320	22	S	S	1,0	2	0
MET-28	22	4	8	63			S	P	3,0	2	0
MET-29	22	1	52	88	322	8	S	S	1,0	2	0
MET-30	22	1	198	88	287	16	S	S	1,0	2	0
MET-31	22	1	233	79	320	15	S	S	1,0	2	0
MET-32	22	1	45	85	133	20	S	S	3,0	2	0
MET-33	22	1	165	40	163	40	N	C	3,0	2	2
MET-34	22	1	155	43	163	43	N	C	3,0	2	2
MET-35	22	4	153	53			D	S	3,0	2	0
MET-36	22	1	47	75	324	23	S	C	3,0	2	0
MET-37	22	4	75	47			N	S	3,0	2	0
MET-38	22	1	217	82	127	5	S	C	3,0	2	0
MET-39	22	1	225	74	306	28	S	C	3,0	2	0
MET-40	22	1	215	85	303	23	S	C	3,0	2	0
MET-41	22	1	188	85	100	19	S	C	3,0	2	0
MET-42	22	4	14	69			S	S	3,0	2	0
MET-43	22	1	33	67	311	19	S	C	3,0	2	0
MET-44	22	1	219	78	306	13	S	C	3,0	2	0

MET-45	22	1	180	90	90	0	S	S	3,0	2	0
MET-46	22	4	84	56			N	P	3,0	2	0
MET-47	22	1	48	78	322	19	S	C	3,0	2	0
MET-48	22	1	126	53	159	48	N	C	3,0	2	0
MET-49	22	1	228	83	318	2	S	S	3,0	2	0
MET-50	22	1	51	81	323	10	S	S	3,0	2	0
MET-51	22	1	27	76	108	32	S	S	3,0	2	0
MET-52	22	3	160	38	115	75		S	3,0	1	0
MET-53	22	1	56	85	11	83	S	C	3,0	2	2
MET-54	22	1	252	75	334	29	S	C	3,0	2	2
MET-55	22	1	20	81	292	10	N	C	3,0	2	2
MET-56	22	3	141	26	128	53		S	3,0	1	0
MET-57	22	4	3	79			S	S	3,0	2	0
MET-58	22	4	339	82			S	S	3,0	2	0
MUL-1	11	1	72	160	28	240	N	P	7,0	2	2
MUL-2	11	1	64	170	33	242	N	P	7,0	2	2
MUL-3	11	1	52	146	52	146	N	P	7,0	2	2
MUL-4	11	1	26	109	23	137	N	S	7,0	2	2
MUL-5	11	1	26	111	25	117	N	P	7,0	2	2
MUL-6	11	1	40	145	39	144	N	P	7,0	2	2
MUL-7	11	1	65	169	22	248	N	S	3,0	2	2
MUL-8	11	1	81	20	46	101	S	S	1,0	2	2
MUL-9	11	1	62	192	14	274	N	S	3,0	2	2
MUL-10	11	1	72	345	17	69	D	S	1,0	2	2
MUL-11	11	1	75	20	8	292	S	S	5,0	2	2
MUL-12	11	1	65	173	41	238	S	S	5,0	2	2
MUL-13	11	4	19	86			N	S	3,0	2	0
MUL-14	11	4	23	84			N	S	3,0	2	0
MUL-15	11	4	24	105			N	S	3,0	2	0
MUL-16	11	4	72	186			N	S	3,0	2	0
MUL-17	11	4	32	132			S	S	3,0	2	0
MUL-18	11	4	36	122			S	S	3,0	2	0
MUL-19	11	4	31	126			S	S	3,0	2	0
MUL-20	11	4	42	70			N	S	3,0	2	0
MUL-21	11	4	40	32			N	S	3,0	2	0
MUL-22	11	4	42	100			N	S	3,0	2	0
MUL-23	11	3	40	180	56	114		P	7,0	1	0
MUL-24	11	3	27	150	52	146		P	7,0	1	0
MUL-25	22	1	205	80	292	17	S	S	3,0	2	2
MUL-26	22	1	3	72	282	25	D	S	3,0	2	2
MUL-27	22	1	238	83	325	22	X	X	3,0	2	2
MUL-28	22	1	14	83	290	43	S	S	3,0	2	2
MUL-29	22	1	166	68	82	14	D	S	3,0	2	2
MUL-30	22	1	126	30	164	25	N	C	3,0	2	2
MUL-31	22	1	168	73	252	17	D	C	3,0	2	2
MUL-32	22	1	110	63	165	48	N	S	3,0	2	2
MUL-33	22	1	352	62	274	21	D	S	3,0	2	2
MUL-34	22	1	297	61	208	1	S	S	3,0	2	2
MUL-35	22	1	288	55	205	10	S	S	3,0	2	2

TW1	22	1	36	51	119	7	D	C	2,0	2	2
TW2	22	1	31	70	303	6	D	C	2,0	2	2
TW3	22	1	31	84	301	2	D	C	2,0	2	2
TW4	22	1	262	85	176	37	S	C	2,0	2	2
TW5	22	1	92	59	174	13	S	C	2,0	2	2
TW6	22	1	64	79	153	4	D	C	2,0	2	2
TW7	22	1	59	64	330	2	D	C	2,0	2	2
TW8	22	1	45	64	315	0	D	C	2,0	2	2
TW9	22	1	53	67	324	1	D	C	2,0	2	2
TW10	22	1	60	75	142	29	D	C	2,0	2	2
TW11	22	1	48	72	321	8	D	C	2,0	2	2
TW12	22	1	60	72	144	18	D	C	2,0	2	2
TW13	22	1	63	59	137	25	D	C	2,0	2	2
TW14	22	1	78	68	351	8	D	C	2,0	2	2
TW15	22	1	53	37	4	26	D	C	2,0	2	2
TW16	22	1	56	36	21	30	D	C	2,0	2	2
TW17	22	1	66	45	9	28	D	C	2,0	2	2
TW18	22	1	55	40	8	29	D	C	2,0	2	2
TW19	22	1	60	60	349	29	D	C	2,0	2	2
TW20	22	1	86	44	10	13	D	C	2,0	2	2
TW21	22	1	187	63	241	49	I	C	2,0	2	2
TW22	22	1	186	68	144	61	I	C	2,0	2	2
TW23	22	1	53	73	330	22	D	S	2,0	2	2
TW24	22	1	62	65	146	12	D	C	2,0	2	2
TW25	22	1	67	66	156	1	D	C	2,0	2	2
TW26	22	1	334	63	245	1	D	C	2,0	2	2
TW27	22	1	65	77	339	17	D	S	2,0	2	2
TW28	22	1	83	83	357	32	S	S	2,0	2	2
TW29	22	4	20	82			D	C	2,0	2	0
TW30	22	1	87	77	15	53	S	S	2,0	2	2
TW31	22	1	58	77	331	13	D	C	2,0	2	2
TW32	22	1	165	85	76	15	S	C	2,0	2	2
TW33	22	1	56	45	342	15	D	C	2,0	2	2
TW34	22	1	142	50	207	27	S	S	2,0	2	2
TW35	22	4	55	66			D	S	2,0	2	0
TW36	22	1	75	52	7	26	D	C	2,0	2	2

Chapter 3: Transition from orogen-perpendicular to orogen-parallel exhumation and cooling during crustal indentation – key constraints from ^{147}Sm/^{144}Nd and ^{87}Rb/^{87}Sr geochronology (Tauern Window, Alps)

This chapter was published on 8 December 2015 to: Tectonophysics, Volume 665, Pages 1–16
DOI: 10.1016/j.tecto.2015.08.037
Link: http://dx.doi.org/10.1016/j.tecto.2015.08.037

Silvia Favaro [1, *], Ralf Schuster [2], Mark R. Handy [1], Andreas Scharf [1, 3], Gerhard Pestal [2†]

[1] Department of Earth Sciences, Freie Universität Berlin, Malteserstrasse 74-100, 12249 Berlin, Germany

[2] Geologische Bundesanstalt, Neulinggasse 38, 1030 Wien, Austria

[3] Now at Department of Earth Science, Sultan Qaboos University, P.O. Box 36, Al-Khoudh, P.C. 123, Muscat, Sultanate of Oman

*Corresponding E-Mail: silvia.favaro@fu-berlin.de, Telephone: (+49 03) 838-70190

Short Title: Orogen-parallel tectonic unroofing and cooling of indented orogenic crust

ABSTRACT

The core of the Alpine orogen in the Eastern Alps (TauernWindow) experienced a change from orogen-normal shortening and post-nappe doming to predominantly orogen-parallel extension and tectonic unroofing during late Oligocene to Miocene northward indentation of the Adriatic Microplate. A new ^{147}Sm/^{144}Nd isochron age of 25.7±0.9 Ma on a garnet-bearing assemblage fromthe lowest nappe complex forming a dome in the eastern part of the Tauern Window indicates that high temperatures related to post-nappe Barrovian-type metamorphism overlapped in time with the onset of doming. New ^{87}Rb/^{87}Sr biotite ages from this same complex combined with previously published ^{87}Rb/^{87}Sr white mica ages suggest that doming and exhumation began no later than 28 Ma immediately in front of indenting Austroalpine crustal blocks, then migrated laterally to the ESE during rapid exhumation and orogen-parallel stretching beginning at about 23 Ma. Rapid cooling ended at approximately 17 Ma in the footwall of the Katschberg Normal Fault, which delimits the eastern margin of the Tauern Window. A similar pattern of migrating doming, orogen-parallel extension and cooling is recognized in the western part of the Tauern Window, where rapid exhumation began at about 20 Ma, some 2–3 Ma later than in the eastern part. This difference in the onset of rapid exhumation as well as the overall migration of doming from the center to the ends of the Tauern Window are attributed to fragmentation of the aforementioned Austroalpine blocks along the leading edge of the main Adriatic indenter (Southern Alps) as this indenter advanced to the north.

Keywords: Doming, indentation, exhumation, lateral escape, cooling, Tauern Window

3.1 INTRODUCTION

Orogenic crust responds to indentation by a combination of crustal thickening, erosion and orogen-parallel extension leading to lateral orogenic escape [*Royden and Burchfield*, 1989; *Ratschbacher et al.*, 1989, 1991b; *Selverstone et al.*, 2004]. The response to indentation is influenced by several factors including the shape and rigidity of the indenter as well as the thermo-mechanical state of the orogenic crust [e.g., *Tapponnier et al.*, 1986; *Rosenberg et al.*, 2007; *Luth et al.*, 2013].

The Tauern Window in the Eastern Alps (Fig. 3.1) is an excellent place to study indentation processes because it reveals an almost complete stratigraphic and tectonic record of the transition from collision to indentation. It contains part of the Alpine orogenic wedge with thrust slices of European continental crust (Subpenninic nappes) and Alpine Tethyan oceanic units (Penninic nappes) accreted to overlying Austroalpine units derived from the margin of the Adriatic microplate [e.g., *Kober*, 1920; *Staub*, 1924; *Exner*, 1971, 1982; *Tollmann*, 1977; *Thiele*, 1980; *Kurz et al.*, 1996, 1998; *Schmid et al.*, 2013]. The Tauern Window formed when the leading edge of this microplate pushed northward into the Alpine orogenic wedge [Fig. 3.1, *Ratschbacher et al.*, 1991b; *Scharf et al.*, 2013a; *Schmid et al.*, 2013]. Two amphibolite- facies metamorphic domes, the Eastern and Western Tauern Domes (ETD and WTD in Fig. 3.1), exhumed the deepest nappes of highly metamorphosed European continental crust (Venediger Nappe System). These domes are delimited by low-angle normal faults, the Brenner and Katschberg Normal Faults (BNF, KNF in Fig. 3.1) that accommodated orogen-parallel stretching in Miocene time [e.g., *Behrmann*, 1988; *Selverstone*, 1988; *Genser and Neubauer*, 1989; *Scharf et al.*, 2013a; *Schneider et al.*, submitted for publication]. Both the ETD and WTD show concentric Oligo-Miocene cooling age patterns for the ^{87}Rb/^{87}Sr white mica (500°C) and biotite (300°C) systems, but the ages in the WTD are younger than in the ETD by some 2-3 Ma [*Fügenschuh et al.*, 1997; *Frisch et al.*, 1998, 2000; *Linzer et al.*, 2002; *Handy et al.*, 2005; *Luth and Willingshofer*, 2008; *Scharf et al.*, 2013a; *Scharf et al.*, 2016]. Existing studies show that the cooling history may be heterogeneous even on the scale of the domes themselves [*Reddy et al.*, 1993]; in the ETD, ^{87}Rb/^{87}Sr white mica and biotite ages in the northwestern part are some 5 Ma older than in the southeastern part [*Cliff et al.*, 1985].

Interpreting the cooling history of deeply buried rocks in terms of exhumation is tricky because rocks are poor heat conductors and their rise to the surface in active orogens is usually faster than their ability to thermally equilibrate [e.g., *England and Thompson*, 1984]. If it is presumed that the heterogeneous cooling of the ETD obtained from existing radiometric ages is real, then this cooling can be interpreted either to indicate coeval exhumation at different exhumation rates (i.e., slower in the northwestern than in the southeastern part of the ETD) and/or diachronous exhumation that migrated from northwest to southeast across the ETD. This dilemma bears obvious implications for the response of the orogenic crust to indentation and lateral escape; in the former case, exhumation was immediate but non-uniform, whereas in the latter, exhumation migrated away from the indenting Austroalpine blocks, affecting successively more external parts of the Alpine wedge. Testing these hypotheses is one of the main goals of this paper.

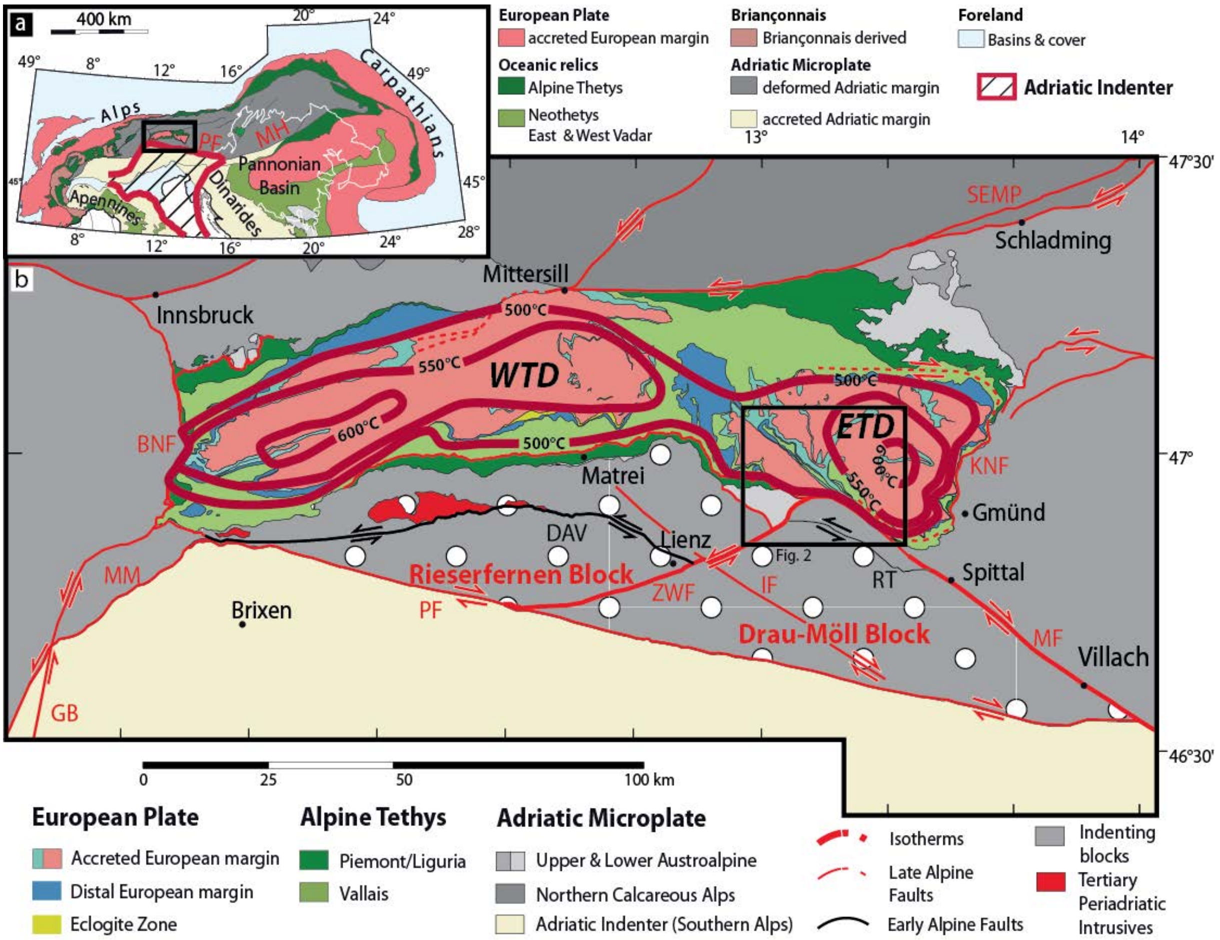

Fig. 3.1: (a) Tectonic overview of the Alps and the Carpathians [modified from *Schmid*, 2008]; (b) Tectonic map of the Tauern Window: WTD and ETD - Western and Eastern Tauern domes with isotherms for peak of Barrovian metamorphism. Major faults relevant to this study: BNF – Brenner Normal Fault; DAV – Defereggen-Antholz-Vals Fault; GB – Giudicarie Belt including sinistral strike-slip faults; IS – Iseltal Fault; KNF – Katschberg Normal Fault; MF – Mölltal Fault; MH – Mid-Hungarian Fault; MM – Meran-Mauls Fault; PF – Periadriatic Fault; RT – Ragga-Teucher Fault, SEMP – Salzach-Ennstal-Mariazell-Puchberg Fault; ZWF – Zwischenbergen-Wöllatratten. Map modified from *Schmid et al*. [2013] with isotherms for 500° and 550°C in the western and central parts of the Tauern Window taken from the compilation of *Bousquet et al*. [2012] and in the ETD from *Scharf et al*. [2013b], *Droop et al.* [1985, 2013] and own data.

The duration of orogen-parallel stretching along the Katschberg Normal Fault, as well as the effect of the indenter shape on the cooling and exhumation pattern remain enigmatic; in particular, the timing of the onset of doming and normal faulting are not yet well constrained. Previous work has suggested that rapid exhumation in the Tauern Window may have been diachronous, with ETD beginning to exhume already before the onset of rapid exhumation in the WTD at 20 Ma and prior to northward motion of the Southern Alps indenter along the Giudicarie Belt beginning at 21-23 Ma [*Scharf et al*., 2013a]. This belt comprises both oblique thrusts and a sinistral strike-slip fault that offsets the Periadriatic Fault [Fig. 3.1; e.g., *Pomella et al*., 2012]. Dating of structurally key minerals with isotopic closure temperatures in the 300-500°C range potentially enables us to determine the onset of rapid cooling and, therefore, place time limits on the beginning of rapid exhumation.

This paper integrates new ^{87}Rb/^{87}Sr and ^{147}Sm/^{144}Nd ages with microstructural studies of key mineral assemblages (garnet, white mica and biotite) to date the onset of tectonic unroofing and to show how exhumation and cooling migrated within the ETD. By relating new and existing ages to the first-order structures of indentation, a new model is proposed in which orogen-normal exhumation was transitional to orogen-parallel exhumation during fragmentation and faulting of the leading edge of the advancing Adriatic indenter. Finally, rapid cooling of the European orogenic crust in the ETD is discussed in the broader context of the evolution of the Tauern Window and the Alpine orogen. It is shown that diachronous exhumation of the Tauern Window was indeed related to this fragmentation.

3.2 GEOLOGICAL SETTING

The Tauern Window in the Eastern Alps contains an almost complete record of Alpine mountain building, from Early Mesozoic rifting and spreading, through Tethyan subduction and Adria-Europe collision, to indentation [e.g., *Trümpy*, 1973; *Dal Piaz et al.*, 1999; *Schmid et al.*, 2004]. The orogenic evolution of units in the Tauern Window is divided into five tectonometamorphic phases that were broadly continuous in Late Cretaceous to Miocene times [*Schmid et al.*, 2013]: (D1) southward subduction of Alpine Tethys represented by the Glockner Nappe System (green unit in Fig. 3.1); (D2) thrusting of the Glockner Nappe System onto the distal European margin represented by the Modereck Nappe System (blue unit in Fig. 3.1); (D3) Isoclinal folding of this nappe stack during continued thrusting onto the European margin; (D4) formation of a duplex in the accreting European margin (Venediger Nappe System, pink units in Fig. 3.1) followed by Barrow-type metamorphism [Tauernkristallisation; e.g., *Sander*, 1911; *Droop et al.*, 1985; *Hoinkes et al.*, 1999; *Dachs et al.*, 2005] and Periadriatic magmatism [e.g., *Rosenberg*, 2004]; (D5) Indentation of the Alpine orogenic crust by the Austroalpine units at the leading edge of the Adriatic indenter [*Scharf et al.*, 2013a; *Schneider et al.*, submitted for publication] represented by the Southern Alps (yellow unit in Fig. 3.1). Indentation involved coeval doming as well as E-W directed orogen-parallel normal faulting. Together, these structures accommodated orogen-normal shortening and lateral (eastward) escape of orogenic crust away from the front of the indenter [*Scharf et al.*, 2013a; see evolutionary cross sections in Fig. 13 of *Schmid et al.*, 2013].

It is important to note that by the beginning of Adria-Europe convergence in Late Cretaceous time, most of the Austroalpine units lying above and to the south of the Penninic nappe pile had already cooled to below 300°C [e.g., *Schuster et al.*, 2004]. This rendered the units between the Tauern Window and Periadriatic Fault semi-rigid blocks which were exhumed and deformed during the advanced stages of orogenesis, as described below [*Ratschbacher et al.*, 1991b; *Stöckhert et al.*, 1999; *Mancktelow et al.*, 2001; *Linzer et al.*, 2002]. Indentation of the Eastern Alps by the Southern Alps was accommodated largely by the sinistral transpressional Giudicarie Belt (GB in Fig. 3.1), which separates the eastern part of the Adriatic indenter from the somewhat older Oligo-Miocene western indenter and crustal wedge in the Central and Western Alps [e.g., *Schmid et al.*, 2004; *Handy et al.*, 2015]. The western Adriatic indenter is not regarded further as it is not relevant to indentation in the eastern Tauern Window.

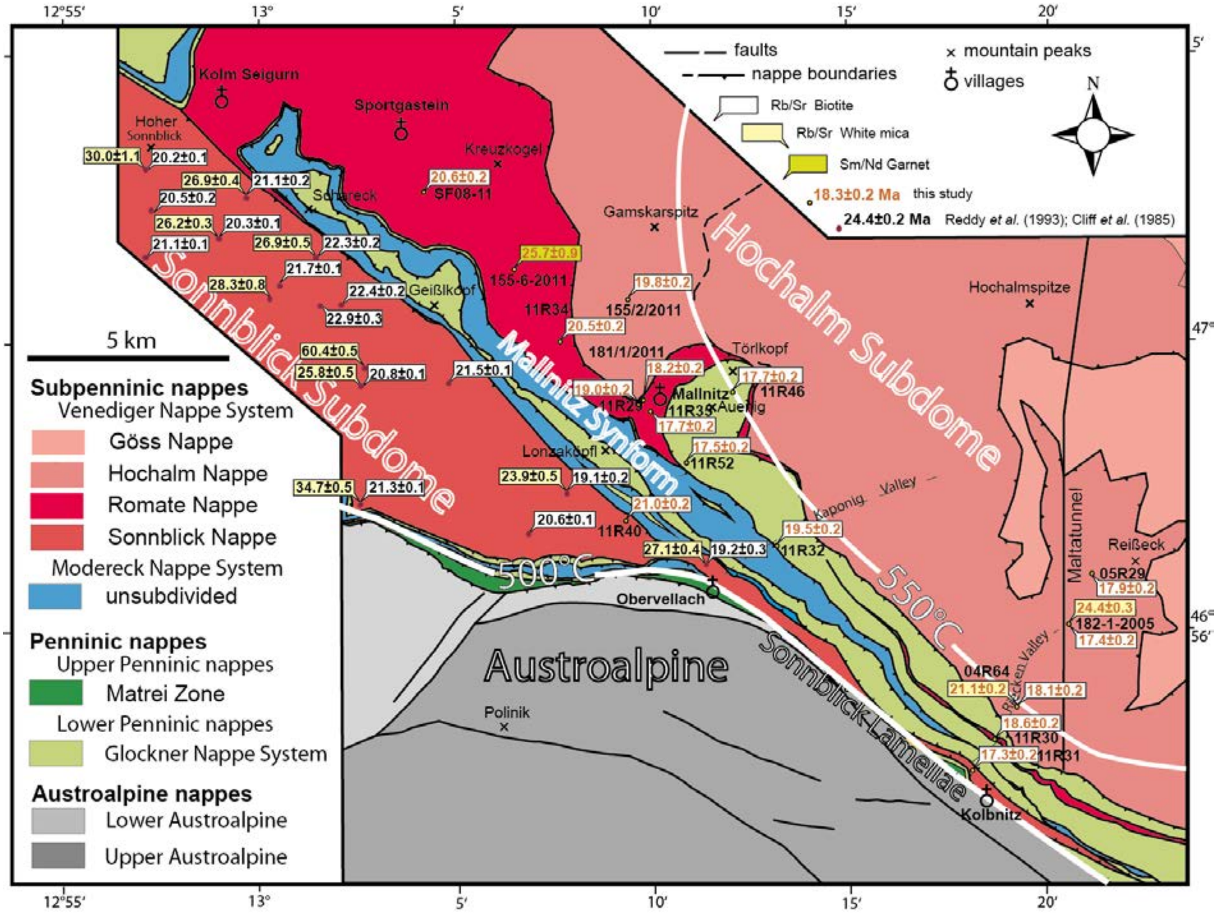

Fig. 3.2: Tectonic map of the study area delimited by the box in Fig. 3.1. The map shows sample locations and ages: Orange labels = this work, black labels indicate samples of *Cliff et al.* [1985] and *Reddy et al.* [1993]. Samples of the first study were collected along the Malta Tunnel. Ages from the latter two sources were calculated with the same constants as used for own data in this paper (see text).

The Tauern Window contains two domes: the Western Tauern Dome and the Eastern Tauern Dome (Fig. 3.1) that deform the D4 nappe stack and coincide with concentric isograds and maximum temperature lines (Fig. 3.1). The ETD is characterized by two D5 subdomes that fold the earlier D2, D3 and D4 collisional structures (Figs. 3.1 and 3.4): (1) the Hochalm Subdome, a broad box-shaped antiform that affects the D4 Göss, Hochalm and Romate nappes as well as the overlying D2 and D3 Glockner and Modereck nappe systems; and (2) a tight elongate fold with doubly plunging axes, the Sonnblick Subdome, which folds the Sonnblick Nappe as well as the Glockner and Modereck Nappe systems. The Sonnblick Lamellae [Fig. 3.2, *Exner*, 1962, 1964] is the highly sheared equivalent of the Sonnblick Subdome which runs parallel to the Mallnitz Synform [*Kober*, 1920], an acylindrical D5 fold, which tightens from NW to SE and separates the Hochalm and Sonnblick subdomes. The D5

Sonnblick Lamellae and Mallnitz Synform are progressively sheared to the SE, forming a mylonitic belt that bends into concordance with the SE-dipping, low-angle Katschberg Normal Fault [Fig. 3.2, KNF, e.g., *Genser and Neubauer*, 1989; *Becker*, 1993; *Scharf et al*., 2013a]. The WTD and ETD were kinematically linked to large, conjugate strike-slip faults, in particular for the WTD, the sinistral Salzach-Ennstal-Mariazell-Puchberg (SEMP) Fault [e.g., *Linzer et al*., 2002; *Rosenberg and Schneider*, 2008], the dextral Periadriatic Fault [PF, *Müller*, 1998; *Müller et al*., 2001; *Läufer et al*., 1997] and the Mölltal Fault [MF, e.g., *Kurz and Neubauer*, 1996; *Linzer et al*., 2002] that together accommodated lateral eastward orogenic extrusion of the Alpine orogen [*Ratschbacher et al*., 1991b] towards the Miocene Pannonian Basin [e.g., *Horvath et al*., 2006]. The contrast in D5 structural style within the Tauern Window, as well as the role of these conjugate strike-slip faults are discussed again below where the response of the Alpine collisional edifice to Adriatic indentation is considered in the light of new geochronological data.

3.3 SAMPLE DESCRIPTIONS

The samples dated in this study are listed in Table 3.1. They cover most of the ETD and also traverse the main D5 structures in the area where age data have been missing until now. Different lithologies were analyzed to determine the effect of the bulk rock composition on the age values.

Sample Nr.	Method Tc	Lithology	Lithostratigraphy	Nappe	Peak T	Locality	N	E
Penninic nappes / Glockner Nappe System								
11R32	Rb-Sr bt 300°C	Greenschist		Glockner Nappe sensu stricto	500-550°C	Kaponik valley, E' Obervellach	46° 57' 00.6"	13° 13' 06.5"
11R46	Rb-Sr bt 300°C	Prasenite		Glockner Nappe sensu stricto	500-550°C	Auenig, E' Mallnitz	46° 59' 32.9"	13° 11' 58.9"
11R52	Rb-Sr bt 300°C	Prasenite		Glockner Nappe sensu stricto	500-550°C	Auenig, E' Mallnitz	46° 58' 28.2"	13° 10' 41.4"
Subpenninic nappes / Venediger Nappe System								
11R31	Rb-Sr bt 300°C	Augengneiss	Sonnblick augengneiss	Sonnblick Nappe	500-550°C	E' Kolbnitz	46° 53' 13.7"	13° 18' 03.8"
11R40	Rb-Sr bt 300°C	Micaschist		Sonnblick Nappe	500-550°C	W' Obervellach	46° 56' 39,0"	13° 11' 23.3"
11R29	Rb-Sr bt 300°C	Syenitic orthogneiss	Romate orthogneiss	Romate Nappe	500-550°C	W' Mallnitz	46° 59' 22.8"	13° 09' 56.8"
11R30	Rb-Sr bt 300°C	Grt- mica schist		Romate Nappe	500-550°C	Riekengraben, E' Kolbnitz	46° 53' 51.2"	13° 18' 39.7"
11R34	Rb-Sr bt 300°C	Syenitic orthogneiss	Romate orthogneiss	Romate Nappe	500-550°C	NW' Mallnitz	47° 00' 09.7"	13° 07' 48.2"
11R35	Rb-Sr bt 300°C	Grt mica schist	Woiskan Schist Complex	Romate Nappe	500-550°C	W' Mallnitz	46° 59' 16.4"	13° 09' 53.7"
SF08-11	Rb-Sr bt 300°C	Syenitic orthogneiss	Romate orthogneiss	Romate Nappe	500-550°C	Sportgastein	47° 02' 23.7"	13° 04' 10.7"
155/6/2011	Sm-Nd grt 500°	Grt-chloritoid mica schist	Woiskan Schist Complex	Romate Nappe	500-550°C	NW' Mallnitz	47° 01' 29.3"	13° 06' 18.4"
181/1/2011	Rb-Sr bt 300°C	Syenitic orthogneiss	Romate orthogneiss	Romate Nappe	500-550°C	NW' Mallnitz	46° 59' 20.1"	13° 09' 52.1"
155/2/2011	Rb-Sr bt 300°C	Granitic orthogneiss		Hochalm Nappe	≥ 550°	N' Mallnitz	47° 00' 38.4"	13° 09' 27.9"
05R29	Rb-Sr bt 300°C	Grt-bearing granite		Hochalm Nappe	≥ 550°	Riekengraben, NE' Kolbnitz	46° 55' 41.7"	13° 20' 01.4"
04R64	Rb-Sr bt/wm 300, 500°C	Granitic orthogneiss		Hochalm Nappe	≥ 550°	NE' Kolbnitz	46° 54' 12.1"	13° 19' 13.9"
182/1/2005	Rb-Sr bt/wm 300, 500°C	Two-mica granitic gneiss	Schönanger orthogneiss	Hochalm Nappe	≥ 550°	Riekengraben, E' Kolbnitz	46° 56' 42.7"	13° 20' 19.9"

Table 3.1: Investigated samples and relevant information (coordinates: WGS 84)

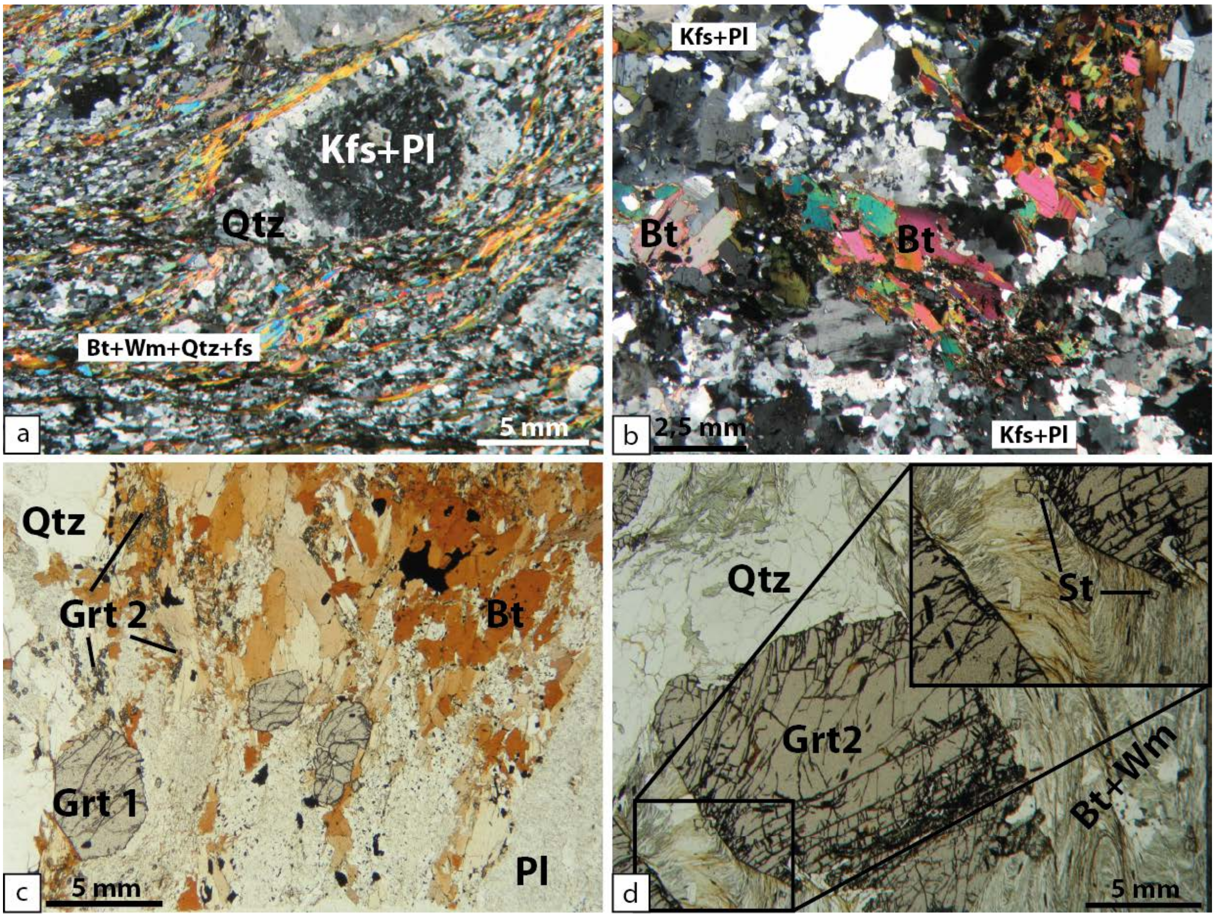

Fig. 3.3: Microstructures indicative of deformation at peak-temperature conditions in the ETD: (a) Sonnblick augengneiss (sample 11R31) with S5 is defined by biotite and white mica, interpreted to have equilibrated at or below ~ 500°C (see text). Cores of K-feldspar augen have perthitic exolutions and inclusions of euhedral plagioclase crystals, whereas rims exhibit dynamic recrystallization of feldspar intergrown with quartz in the pressure shadows; (b) Romate syenitic orthogneiss (sample SF08-11) in the northwestern part of the Hochalm Subdome shows dynamic recrystallization of feldspar and of minor amounts of quartz; dynamic recrystallization interpreted to be related to D4; (c) Granite from the Hochalm Subdome (sample 05R29) containing inclusion-free magmatic garnet (Grt1) overgrown by fine grains of metamorphic garnet (Grt2) in contact with biotite; Grt2 is interpreted to have grown at peak temperatures of ≥ 500°C; (d) Grt2 from post-Variscan cover (Woisken Schist Complex, sample 11R35) of the Romate Gneiss with F4-folded matrix comprising peak-temperature assemblage of white mica, biotite and staurolite (see inset). This assemblage is interpreted to have grown during the Tauernkristallisation.

Most samples come from the Subpenninic nappes rather than the Penninic Glockner Nappe System due to the widespread lack of biotite in the latter. The Glockner Nappe System contains ophiolitic slices and a large volume of Jurassic to Early Cretaceous calcareous metapelitic schist (so-called "Bündnerschiefer", *Pestal et al.*, 2009] with pervasive greenschist-facies fabrics. The Glockner Nappe System is generally subdivided into two imbricates (not distinguished in Fig. 3.2), a tectonically lower slice with rare relics of subduction-related metamorphism [pseudomorphs after lawsonite, *Pestal et al.*, 2009] termed the Glockner Nappe "sensu stricto" [Kolm Nappe of *Exner*, 1984], and a higher slice without such relics but containing metagabbroic dykes [Rauris Nappe, *Exner*, 1984; *Pestal and Hellerschmidt-Alber*, 2011; *Favaro and Schuster*, 2012]. The three samples collected for this paper came from the Glockner Nappe sensu stricto, which however, were void of high-pressure relics.

The samples used for ^{87}Rb/^{87}Sr dating of muscovite and biotite were collected from basement and pre-Mesozoic cover units of the Venediger Nappe System (Fig. 3.2). The basement protoliths are mostly Variscan to post-Variscan (late Paleozoic) intrusives, including granitic augengneiss from the Sonnblick Nappe (Fig. 3.3a), syenitic gneiss from the Romate Nappe (Fig. 3.3b) and other orthogneisses (Fig. 3.3c) which intruded pre-Variscan paragneisses. These pre-Variscan host rocks are locally known as the "Altes Dach" or "Old Roof" [*Kober*, 1920; *Staub*, 1924; *Exner*, 1962, 1964].

Samples of the post-Variscan, pre-Mesozoic cover of all these basement rocks (Table 3.1) are locally very aluminous and contain abundant white mica, garnet, chloritoid and locally staurolite (Figs 3.3d, 3.4). These silver to shiny greenish schists, part of the Woisken Schist Complex in the sense of *Kober* [1920], are quite striking to behold and are thought to have been deposited in Permian time because they are not intruded by Variscan dykes and are stratigraphically overlain by Mesozoic sediments [e.g., the Jurassic Hochstegen Marble and Early Cretaceous Brennkogel Schists; *Pestal et al.*, 2009; *Favaro and Schuster*, 2012]. Therefore, the amphibolite-facies assemblage in the Woisken Schist Complex must be Alpine and, indeed, overgrows the S4 foliation as shown in Figure 3.4.

3.4 ANALYTICAL METHODS: Sample preparation for ^{87}Rb/^{87}Sr and ^{147}Sm/^{144}Nd dating

The samples were mechanically prepared for ^{87}Rb/^{87}Sr and ^{147}Sm/^{144}Nd isotope analyses at the Geological Survey of Austria in Vienna. Before separating the minerals, their weathered surfaces were removed from the sample material. Minerals were separated by the standard methods of crushing, grinding, sieving and magnetic separation. Garnet and chloritoid separates were hand-picked under the binocular microscope from sieve fractions of 0.2-0.3 mm and were cleaned in distilled water and acetone. Garnet was further leached in 6n HCl at 100°C for several hours. Samples used for dissolution weighed about 100 mg for whole rock powder, ~ 200 mg for biotite and white mica and 30-45 mg for garnet and chloritoid. Chemical preparation was performed at the Geological Survey of Austria in Vienna and at the Department of Lithospheric Research at the University of Vienna. The chemical sample preparation follows the procedure described by *Sölva et al.* [2005]. Element concentrations were determined by isotope dilution using mixed ^{147}Sm/^{144}Nd and ^{87}Rb/^{87}Sr spikes. Total procedural blanks are $\leq$ 300 pg for Nd and Sm and $\leq$ 1 ng for Rb and Sr.

Rb ratios were measured at the Department of Geological Sciences, University of Vienna with a Finnigan® MAT 262, whereas Sr, Sm and Nd ratios were analyzed with a ThermoFinnigan® Triton TI TIMS. All elements were run from Re double filaments, except Rb which was evaporated from a Ta single filament. During measuring, the La Jolla standard yielded ^{143}Nd/^{144}Nd = 0.511841 ± 1 (n = 13, 2σm) on the Triton TI, whereas standard NBS987 yielded a ratio of ^{86}Sr/^{87}Sr = 0.710270 ± 3 (n = 12, 2σm) and 0.710274 ± 2 (n = 21, 2σm) respectively was determined. Errors of 1% were determined for the ^{87}Rb/^{87}Sr and ^{147}Sm/^{144}Nd ratios based on interactive sample analysis and spike recalibration. Ages were calculated with the software ISOPLOT/Ex [*Ludwig*, 2001; 2003] using the Sm- and Rb-decay constants of 6.54×10^{-12} a^{-1} and 1.42×10^{-11} a^{-1}, respectively.

3.5 RESULTS

3.5.1 ^{147}Sm/^{144}Nd garnet ages

Sample 155-6-2011 (location in Table 3.1 and Fig. 3.2) is ideally suited to place an upper age limit on the Barrow-type, amphibolite-facies metamorphism (Tauernkristallisation) because it comes from post-Variscan cover and contains both garnet and chloritoid that overgrow the folded S4 foliation formed during Duplex formation in the Venediger Nappe System (Fig. 3.4). The results of the ^{147}Sm/^{144}Nd measurements are given in Table 3.2.

Sample/Material		**^{143}Nd/^{144}Nd**	**±2σ$_m$**	**Nd [ppm]**	**Sm [ppm]**	**^{147}Sm/^{144}Nd**	**ε0 Nd$_{(Chur)}$**
Subpenninic nappes / Venediger Nappe System							
155/6/2011	WR	0,512904	±0.000003	33,52	7,806	0,1408	5,2
155/6/2011	Ctd	0,512913	±0.000003	4,005	1,149	0,1734	5,4
155/6/2011	Grt1	0,513105	±0.000020	0,439	0,982	1,3518	9,1
155/6/2011	Grt2	0,513190	±0.000009	0,401	1,216	1,8340	10,8

Table 3.2: ^{147}Sm/^{144}Nd isotopic data for a garnet-chloritoid mica schist from the post-Variscan cover in the western part of the Hochalm Subdome (Woisken Schist Complex, sample 155-6-2011).

Two fractions of garnet (Grt$_1$, Grt$_2$), chloritoid (Cld) and whole rock (WR) were analysed. The whole rock is characterized by a ε0Nd$_{(CHUR)}$ of 5.2, a ^{147}Sm/^{144}Nd ratio of ~ 0.14 and has Sm (33.5 ppm) and Nd (7.81 ppm) contents that are in the range typical for metapelites [*McCullogh and Wasserburg*, 1978]. Both garnet fractions show low concentrations of Sm (~ 1 ppm) and Nd (~ 0.4 ppm) and remarkably high ^{147}Sm/^{144}Nd ratios of > 1.3 and > 1.8, respectively (Table 3.2). The calculated isochron defines an age of 25.7 ± 0.9 Ma (Fig. 3.4).

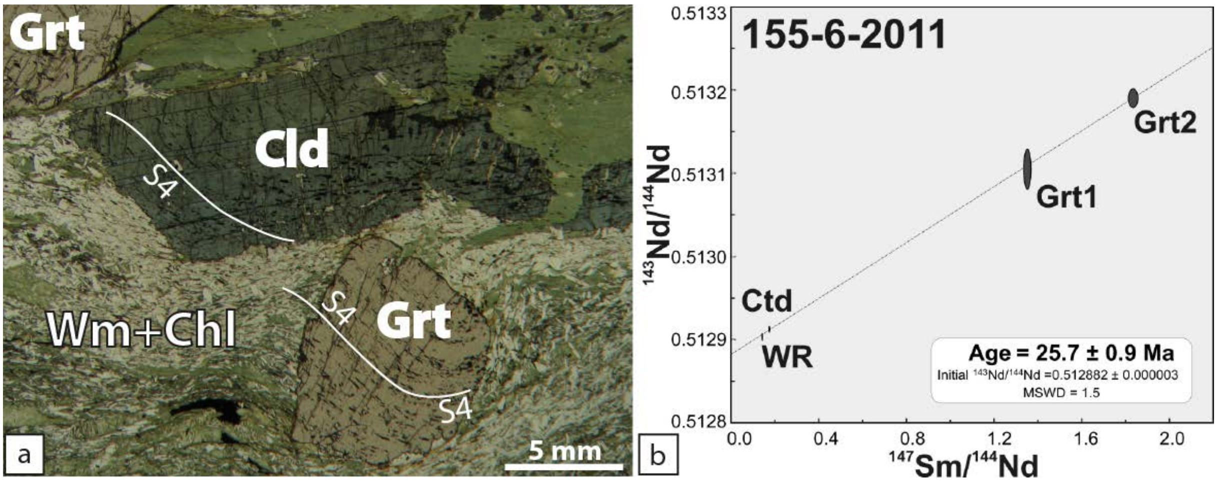

Fig. 3.4: (a) Garnet-chloritoid micaschist from the post-Variscan cover in the western part of the Hochalm Subdome (Woisken Schist Complex, sample 155-6-2011). Sample contains quartz, muscovite, biotite, garnet and minor chlorite, staurolite, chloritoid and epidote. Garnet (Grt) and chloritoid (Cld) are interpreted to overgrow the folded S4 foliation defined mainly by white mica; (b) ^{143}Nd/^{144}Nd vs ^{147}Sm/^{144}Nd plot for two garnet fractions (Grt1, Grt2), chloritoid (Ctd) and whole rock (WR).

3.5.2 ^{87}Rb/^{87}Sr micas ages

Biotite and whole rock (WR) were analyzed in a total of fifteen samples, and two of these samples were also analyzed for white mica (Table 3.1). Whole rocks, as well as the corresponding biotite separates, have a broad range of Rb- and Sr content and the biotites exhibit a wide range of ^{87}Rb/^{87}Sr ratios (50-700). The ^{87}Rb/^{87}Sr ages and analyses are listed in Table 3.3. In the following, we discuss the results with regard for the different D5 structures of the ETD.

Sample	Material	^{87}Sr/^{87}Sr±2σ$_m$	Rb [ppm]	Sr [ppm]	^{87}Rb/^{87}Sr	Age±2σ$_m$ [Ma]
Penninic nappes / Glockner Nappe System						
11R32	WR	0.707927±0.000003	322.9	379.2	2.4637	
11R32	Bt	0.778776±0.000004	380.3	4.286	258.52	**19.5±0.2**
11R46	WR	0.706317±0.000003	25.3	359.5	0.2034	
11R46	Bt	0.743767±0.000004	204.6	3.977	149.36	**17.7±0.2**
11R52	WR	0.705304±0.000003	47.7	138.4	0.9968	
11R52	Bt	0.749119±0.000003	234.7	3.855	176.92	**17.5±0.2**
Subpenninic nappes / Venediger Nappe System						
11R31	WR	0.707636±0.000004	201.4	874.7	0.6665	
11R31	Bt	0.721275±0.000004	681.1	35.12	56.198	**17.3±0.2**
11R40	WR	0.707160±0.000004	121.5	519.0	0.6774	
11R40	Bt	0.729269±0.000004	444.9	17.24	74.834	**21.0±0.2**
11R29	WR	0.712428±0.000004	250.3	580.0	1.2494	
11R29	Bt	0.879310±0.000005	538.9	5.260	301.45	**19.0±0.2**

11R30	WR	0.722992±0.000004	331.3	110.2	8.7166	
11R30	Bt	0.903758±0.000004	907.3	3.866	692.25	**18.6±0.2**
11R34	WR	0.713052±0.000004	269.1	677.2	1.1506	
11R34	Bt	0.826504±0.000004	1356	10.14	391.65	**20.5±0.2**
11R35	WR	0.714292±0.000004	204.0	157.4	3.7542	
11R35	Bt	0.738105±0.000004	605.7	17.84	98.544	**17.7±0.2**
SF08-11	WR	0.712322±0.000004	396.3	614.9	1.8657	
SF08-11	Bt	0.818404±0.000004	1560	12.54	363.78	**20.6±0.2**
181/1/2011	WR	0.712058±0.000004	374.0	978.1	1.1070	
181/1/2011	Bt	0.812299±0.000004	1483	11.15	389.03	**18.2±0.2**
155/2/2011	WR	0.709734±0.000003	145.8	561.6	0.7516	
155/2/2011	Bt	0.770631±0.000004	829.8	11.14	216.98	**19.8±0.2**
05R29	WR	0.716372±0.000004	141.1	272.2	1.5015	
05R29	Bt	0.855328±0.000005	868.4	4.651	548.17	**17.9±0.2**
04R64	WR	0.711393±0.000004	165.0	284.8	1.6775	
04R64	Bt	0.735008±0.000018	981.4	30.42	93.613	**18.1±0.2**
04R64	Ms	0.730748±0.000015	561.8	24.61	66.227	**21.1±0.2**
182/1/2005	WR	0.737378±0.000004	238.9	83.46	8.3098	
182/1/2005	Bt	1.547216±0.000702	1335	1.273	3283.2	**17.4±0.2**
182/1/2005	Ms	0.850518±0.000009	825.3	7.225	335.21	**24.4±0.3**

Table 3.3: ^{87}Rb/^{87}Sr isotopic data and ages.

3.5.2.1 Hochalm Subdome

All ten samples analyzed come from the southwestern part of the Hochalm Subdome adjacent to the Mallnitz Synform, but away from (north of) areas affected by pervasive F5 folding and S5 schistosity. The micas in these samples thus define older foliations, usually S4 which was related to nappe stacking and the formation of the Venediger Duplex. Two of these samples experienced more than 550°C (Fig. 3.2) defined by peak-temperature assemblages of the Tauernkristallisation [*Hoinkes et al.*, 1999] and by Raman microspectroscopy on carbonaceous material [*Scharf et al.*, 2013b]. The highest temperature in the area, 610°C, is measured in the core of the ETD just east of the area shown in Figure 3.2 [*Scharf et al.*, 2013b].

These two samples yield biotite ages in the narrow range of 17.9 to 17.4 ± 0.2 Ma and are the youngest biotite ages from the Hochalm Subdome. White mica from the white mica-biotite granitic gneiss (182-1-2005; Schönangergneiss, central part of the Hochalm Subdome) yields 24.4 ± 0.3 Ma, whereas another muscovite from an orthogneiss from the southwestern margin of the Hochalm Subdome near Kolbnitz (04R64) yields 21.1 ± 0.2 Ma. Both white mica ages are older than the biotite ages from the same sample.

The remaining eight samples come from areas between the 500° and 550°C isotherms and yield biotite ages between 17.7 ± 0.2 Ma and 20.6 ± 0.2 Ma. The scatter in ages is remarkably small given the different protoliths, foliations and ^{87}Rb/^{87}Sr systematics of these samples (Table 3.3). Two of these samples come from the rim of the Hochalm Nappe, one in the proximity of Kolbnitz (04R64) and one north of Mallnitz (155-2-2011, Gamskarspitz). Four samples are of relatively undeformed, biotite-rich Romate syenitic gneiss, whereas two come from the post-Variscan cover of the Romate Nappe (Permian Woisken Schist Complex). Only sample 04R64 has a composite S4-S5 foliation due to its proximity to the KNF [*Scharf et al.*, 2013a], whereas sample 155-2-2011 is located just below the contact with the Romate gneiss and preserves a strong D4 foliation. The micas in the syenitic gneiss define older, pre-D4 foliations, whereas the garnet-bearing muscovite schist (11R35, Fig. 3.3d) collected near the Venediger Duplex roof thrust has a strong S4 foliation comprising white mica, biotite and retrograde chlorite. The biotite concentrate from this schist has a high Sr content (17 ppm) resulting in a low ^{87}Rb/^{87}Sr ratio of ~ 100. This high Sr content reflects the presence of tiny Sr-rich inclusions, most probably of apatite.

Sample (11R30) from the Kolbnitz area (Fig. 3.2) contains biotite in a quartz vein. These extensional veins trend northeast-southwest and have been well studied because of their gold content [“Tauerngold”; *Feitzinger and Paar*, 1991]. The biotite is highly radiogenic (^{87}Rb/^{87}Sr ~ 700) and its orientation parallel to the KNF suggests that it formed during D5 orogen-parallel extension.

3.5.2.2 Sonnblick Subdome

A paragneiss (sample 11R40) from the Sonnblick Nappe (location north of Obervellach, Fig. 3.2) and an augengneiss from the “Sonnblick Lamellae” close to Kolbnitz (sample 11R31, Figs 3.2, 3.3a) contain biotite that defines the S5 foliation in the Katschberg Shear Zone System. The biotites from both samples have high Sr contents (17 and 34 ppm) and correspondingly low ^{87}Rb/^{87}Sr ratios (56 and 74 ppm), pointing to the presence of Sr-rich inclusions within the biotites. The calculated ages are 21.0 ± 0.2 Ma for the paragneiss near Obervellach, and 17.3 ± 0.2 Ma for the augengneiss of the Sonnblick Lamellae.

3.5.2.3 Mallnitz Synform

Sample 11R32 from the Kaponig Valley (Fig. 3.2) is a chlorite-schist with aggregates of biotite up to several millimeters long that are oriented subparallel to axial planes of F5 folds near the mylonitic belt that connects along strike to the SE with the KNF. Samples 11R46 and 11R52 from Auernig (Fig. 3.2) are prasinites (epidote, plagioclase, greenish-brown biotite, chlorite and minor quartz, tourmaline and apatite). The biotites in these samples are probably pre-D4 because they originate in the isoclinally folded (D3) Glockner Nappe System that overlies the D4 roof thrust of the Venediger Duplex. All three samples have biotites characterized by low Sr content (~ 4 ppm), relatively low Rb content (200-380 ppm) and by ^{87}Rb/^{87}Sr ratios of 150-260. The biotite age values are in the range of 17.5-19.5 ± 0.2 Ma.

3.6 DISCUSSION

3.6.1 Age of Alpine peak-temperature conditions

The age of the Barrow-type thermal event (Tauernkristallisation) in the Tauern Window is broadly constrained by cross-cutting relationships: Peak-temperature (peak-T) lines form a lopsided concentric pattern in the ETD that cuts and therefore post-dates D4 nappe contacts [Fig. 3.1, *Droop et al.*, 2013; *Scharf et al.*, 2013b]. Maximum temperatures range from ~ 612°C in the core of the EDT to only ~ 450°C along the KNF [*Scharf et al.*, 2013b]. The concentric pattern itself reflects D5 doming in the Hochalm Subdome, while the parallelism of peak-T lines to the KNF (Fig. 3.1) is attributed to shearing of isotherms into concordance with the footwall of the KNF [*Scharf et al.*, 2013b]. These overprinting relations indicate that the Tauernkristallisation occurred prior to the activity of the KNF in early Miocene time [Scharf et al., 2013a]. The Tauernkristallisation is therefore interpreted as the thermal response to crustal thickening by D4 nappe stacking and duplex formation during Adria-Europe collision [*Kurz et al.*, 2008; *Schmid et al.*, 2013].

Duplex formation must post-date subduction of the European plate and pre-date early exhumation of high-pressure metamorphic units in the Tauern Window, including the Glockner Nappe sensu stricto, the Eclogite Zone and part of the Modereck Nappe System (Fig. 3.1). However, the age of the high-pressure metamorphism in these units is controversial, with estimates ranging from 42-38 Ma [^{40}Ar/^{39}Ar phengite, *Ratschbacher et al.*, 2004; *Kurz et al.*, 2008] to 36-32 Ma [^{87}Rb/^{87}Sr white mica, *Glodny et al.*, 2005; Lu/Hf in garnet-bearing assemblage, *Nagel et al.*, 2013].

In view of this uncertainty, the best approach to dating the Tauernkristallisation employs isotopic systems with closure temperatures (T_c) higher than or near the peak temperatures recorded in the Tauern Window. Where the peak-T exceeded 500-550°C in the WTD, white micas yield 29 ± 2 Ma, 31 ± 5 Ma, [$^{87}Rb/^{87}Sr$ white mica, $T_c \sim 550°C$, *Satir*, 1975] and 32 ± 2 Ma [K/Ar white mica, $T_c \sim 420°C$, *Satir*, 1975; *Thöni*, 1980]. These ages are in good agreement with new U/Pb apatite ages mostly between 31 and 29 Ma in the core of the WTD [$T_c \sim 450°C$, *Schneider et al.*, 2015]. All of these ages can be interpreted as cooling ages that somewhat post-date the thermal peak of Tauernkristallisation because the closure temperature of the systems used was slightly less than the maximum temperature recorded in the rocks. Other studies on samples closer to the Brenner Normal Fault yield slightly younger white mica ages in the range of 30-28 Ma which are interpreted as cooling ages following the Tauernkristallisation event [e.g., *Lambert*, 1970; *Selverstone*, 1985; *Raith et al.*, 1978; *Ratschbacher*, 2004].

A detailed study of a single, 6-cm diameter synkinematic garnet [*Pollington and Baxter*, 2010] from a shear zone in the WTD indicates garnet growth at temperatures of at least 500°C from 28 to 20 Ma, with an increased growth rate at about 25 Ma. According to *Selverstone et al.* [1991] this shear zone experienced significant mass- (<50%) and volume- (<60%) loss related to fluid flow between 20 and 30 Ma [*Barnes et al.*, 2004]. These observations are in agreement with studies on steeply dipping shear zones in the WTD by *Schneider et al.* [2013].

In the southwestern part of the ETD (Sonnblick Subdome), where the peak-T of 510°C [*Droop*, 2013] is about the same as the T_c of the $^{87}Rb/^{87}Sr$ white mica system, *Reddy et al.* [1993] interpreted their ages between 30 and 24 Ma either as formation ages during the Tauernkristallisation or as cooling ages shortly thereafter. In the larger Hochalm Subdome where peak-T exceeded 550°C, the two new $^{87}Rb/^{87}Sr$ white mica ages in this study (Table 3.1, Fig. 3.2) as well as the previously published ages of *Cliff et al.* [1985; Fig. 3.2] are consistently younger (24-21 Ma). These are therefore interpreted as cooling ages after the peak of Tauernkristallisation. Note that the $^{87}Rb/^{87}Sr$ white micas ages in this study are more variable than the biotite ages from the same samples (04R64, 182-1-2005), a phenomenon also observed in the white mica ages of *Cliff et al.* [1985]. This variability most probably reflects minor and variable amounts of Sr loss during post-peak metamorphic deformation and recrystallisation of the micas.

Other systems applied to minerals of the peak-temperature assemblage in the ETD yield ages in the narrow range of 29-27 Ma [metamorphic crystallization, Th/Pb and U/Pb allanite, *Cliff et al.*, 1998; formation ages, $^{87}Rb/^{87}Sr$ white mica, U/Pb allanite and titanite, *Inger and Cliff*, 1994]. These ages lie within the broad range of the white mica ages cited above.

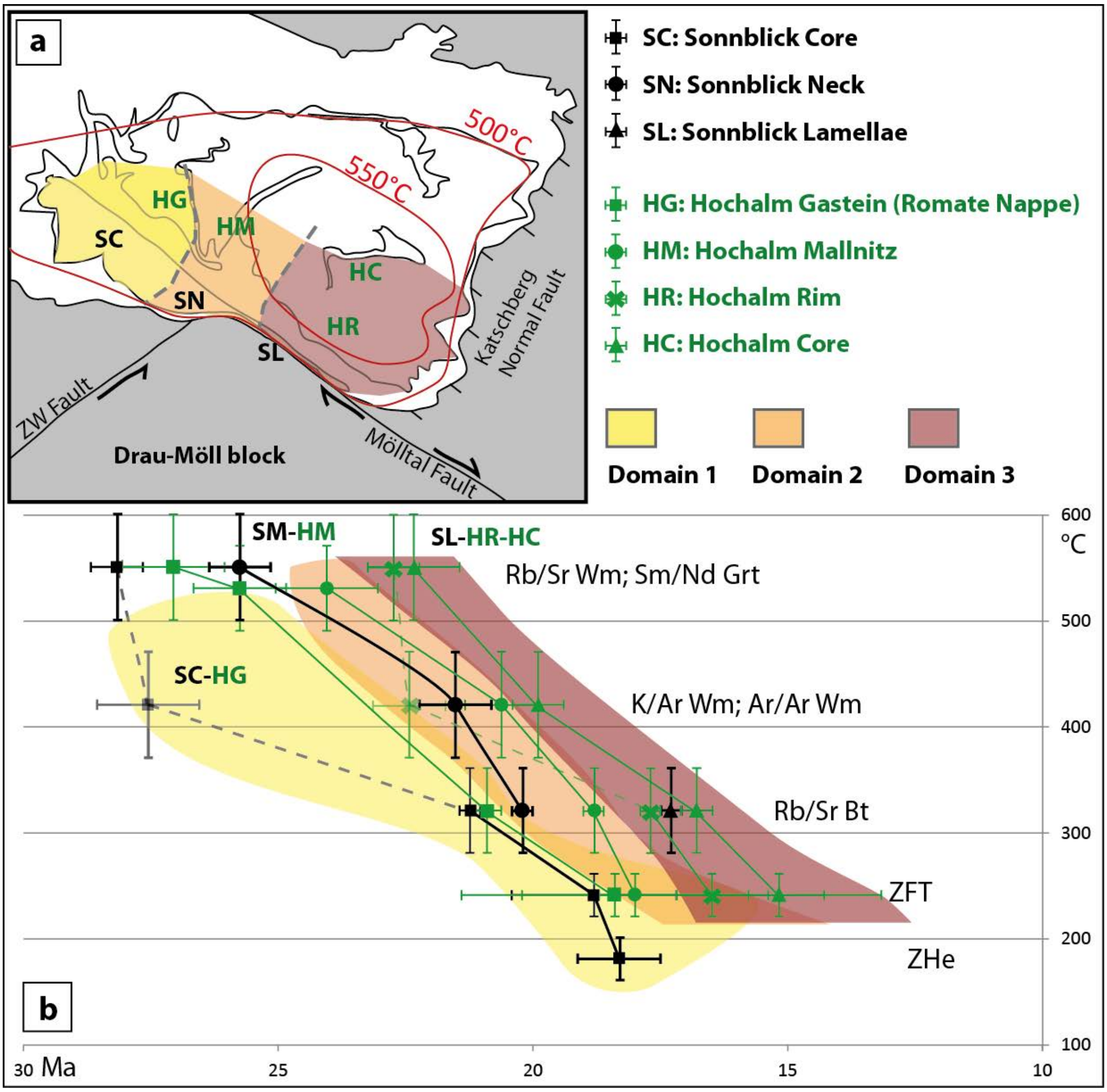

Fig. 3.5: Cooling patterns in the ETD, southeastern Tauern Window: (a) Map of the ETD showing three cooling domains (colored) that cut across D4 nappe contacts (thin black lines) and major D5 folds (Hochalm and Sonnblick Subdomes, Mallnitz Synform) and the peak-temperature lines related to the Tauernkristallisation. The cooling histories of these domains are defined by the T-t curves in (b); (b) Temperature-time (T-t) curves for the three cooling domains in (a) with crosses indicating the errors in closure temperatures (T_c) and ages for the thermochronological systems used. Dashed parts of cooling curves connecting the ages are less well constrained (few available cooling ages) than the solid parts and probably reflect an excess argon effect. Peak-temperature contours in (a) are taken from *Scharf et al*. [2013b] and sources therein. Sample locations, ages and T_c values used for this figure are listed in the table and map in the Supplementary material for chapter 3, section 3.8.

The ^{147}Sm/^{144}Nd isochron age (25.7 ± 0.9 Ma) on garnet-chloritoid-whole rock in this study (Table 3.2) is interpreted to date the growth of the peak-temperature assemblage after the formation of S4 related to shearing during duplex formation in the Venediger Nappe System. This is seen in Figure 3.4, where garnet and chloritoid overgrow a folded S4 foliation defined by fine trails of white mica.

The 25.7 Ma age supports the ages of the other high-temperature systems and predates the cooling ages in the ETD.

To summarize this section, the available isotopic ages indicate that the Barrow-type thermal event in the Tauern Window lasted for about 7 Ma, beginning no later than 32 Ma (oldest $^{87}Rb/^{87}Sr$ white micas) and lasting until about 25 Ma as indicated by the $^{147}Sm/^{144}Nd$ garnet formation ages from the WTD and ETD and the youngest $^{87}Rb/^{87}Sr$ ages on white micas. This suggests that crustal thickening during Adria-Europe collision started before 32 Ma. This fits well with geological evidence for thickening of continental crust as manifested by the transition from an underfilled trench with predominantly flysch in Eocene time, to Molasse-type sedimentation in the Alpine continental foredeep beginning in latest Eocene to early Oligocene time [see *Kurz et al*., 2008; *Handy et al*., 2010, 2015; *Schmid et al*., 2013].

3.6.2 Cooling of the Eastern Tauern Dome

All new $^{87}Rb/^{87}Sr$ biotite ages are from samples that experienced peak metamorphic temperatures of 500°C or more, well above the T_c of the $^{87}Rb/^{87}Sr$ system in biotite [300°C, *Jäger et al*., 1967; *Del Moro et al*., 1982], so these ages are clearly interpretable as cooling ages. Regarded together with existing isotopic ages in the literature, these ages define three distinct cooling domains in the study area, each with its own T-t cooling curve (color coded in Figs 3.5a, b). It is noticeable that boundaries between these cooling domains generally trend northeast-southwest, obliquely to the major D4 nappe contacts and D5 domes, as well as to the 500 and 550°C peak-T contours that outline the core of the ETD. In particular, the boundary between cooling domains 1 and 2 cuts across the Mallnitz Synform, while that between domains 2 and 3 overprints the D5 sheared contact between the Hochalm Subdome and Sonnblick Lamellae (Fig. 3.5a). The curves themselves record cooling from 500° to about 240°C and the age of this cooling is seen to become progressively younger going from the northwest (domain 1) to the southeast (domain 3) towards the footwall of the Katschberg Normal Fault (Fig. 3.5b). Judging from the average slopes of the T-t curves in Figure 3.5b, the average cooling rate was about 33°C Ma^{-1} in all domains. Constraints from lower temperature systems are sparse: zircon fission track ages show cooling of the ETD to below 240°C between 19 and 11 Ma [*Yamada et al*., 1995; *Dunkl et al*., 2003; *Wölfler et al*., 2008, 2012; *Bertrand*, 2013], and apatite fission track ages to below ~ 125°C between 27 and 3 Ma [*Staufenberg*, 1987; *Foeken et al*., 2007; *Wölfler et al*., 2008, 2012; *Bertrand*, 2013]. Cooling in this low-temperature domain to below the viscous-frictional transition in quartz-bearing rocks [~ 300°C, *Stipp et al*., 2002] is very poorly constrained [*Scharf et al*., 2013a] and sample locations are too widely spaced to resolve significant late differential cooling under subgreenschist-facies conditions within the ETD.

Deriving exhumation and exhumation rates from cooling ages is difficult in the absence of thermal modeling, which only exists for the western part of the Tauern Window [*Fügenschuh et al*., 1997]. Without such models, a number of simplifying assumptions must be made, for example, that the average heat flow and geothermal gradient did not change significantly with time and that both heat production and heat capacity of the rocks were uniform in the exhuming nappe pile. Although none of these assumptions are well constrained, they are probably realistic in light of the fact that most samples are metagranitoids with similar rock-physical properties, including heat capacity and heat production by decay of radiogenic K, Th and U. In addition, thermal modeling of exhuming basement rocks in the WTD has shown that exhumation preceded the onset of rapid cooling by only about 2 Ma [*Fügenschuh et al.*, 1997]. The time lag between the onset of rapid exhumation and rapid cooling was probably even less in the ETD, where cooling rates (33°C Ma^{-1}) were somewhat lower than in the WTD (45°C Ma^{-1}), giving the exhuming rocks more time to equilibrate with the ambient thermal state of the crust.

The trend of progressively younger cooling from NW to SE in the ETD is therefore interpreted to reflect the migration of D5 exhumation during broadly coeval post-nappe doming and top-SE orogen-parallel shearing along the southeastwardly propagating KNF [*Scharf et al.*, 2013a]. The peak pressure experienced by these units during the Tauernkristallisation was 800-1000 MPa [*Droop*, 1985; *Gipper*, 2012; *Hawemann*, 2013], consistent with 25-30 km of exhumation for an average crustal density of 2.8 g/cm^3. Doming probably started between 30 and 25 Ma in both the Sonnblick Subdome and NW part of the Hochalm Subdome (domain 1), then began to affect the rest of the Hochalm Subdome and the Sonnblick Lamellae in the SE at 25-23 Ma (domain 2) before reaching the present-day core of the Hochalm Subdome and footwall of the KNF from 23 to 17 Ma (domain 3, Fig. 3.6). The 23 Ma age for the onset of this doming in domain 3 coincides exactly with the estimated age for the beginning of top-SE mylonitic shearing in the footwall of the KNF [*Scharf et al.*, 2013a].

The obliquity of the cooling domain boundaries and the concentric peak-temperature contours in the ETD [inset to Fig. 3.5, see *Scharf et al.*, 2013b; *Cliff et al.*, 1985] indicates that these contours are not isochrons but are about 4-5 Ma older in the northwestern than in the southeastern part of the ETD. The diachronous nature of the peak-temperature contours can also be inferred on an even larger scale from cross-cutting relationships of peak-temperature contours and major D4 and D5 structures in the Tauern Window as a whole (Fig. 3.1): In the central part of the Window where somewhat lower peak temperatures (500-550°C) and oldest mica cooling ages are recorded [*Luth and Willingshofer*, 2008], the contours follow the broadly arcuate shape of the D5 fold axes around the Tauern Window [Fig. 3.1, fig. 4 of *Schmid et al.*, 2013] and clearly cut all D4 nappe contacts. There, the peak temperatures appear to have been attained during D5. In the cores of the ETD and WTD, the concentric shape of the peak-temperature contours clearly reflects later D5 doming. At both ends of the Tauern Window these contours are modified by the Brenner and Katschberg Normal Faults, as already noted by several authors [*Fügenschuh et al.*, 1997; *Frisch et al.*, 2000; *Luth and Willingshofer*, 2008; *Scharf et al.*, 2013b].

Taken together, these patterns suggest that doming in the central part of the Tauern Window occurred during the attainment of peak temperatures during the Tauernkristallisation whereas at the ends of the

Tauern Window, doming and orogen-parallel shearing clearly occurred after this thermal peak event. This map-scale pattern of orogen-parallel migration of doming and exhumation is revisited in the next section, where the exhumation pattern implied by this migration is considered as a response to changing geometric boundary conditions during indentation and fragmentation of the Adriatic indenter.

We conclude this section by noting that the cooling pattern in Figure 3.5 precludes earlier hypotheses reviewed in the Introduction in which the Sonnblick Subdome cooled from 500° to 300°C before the Hochalm Subdome [*Reddy et al.*, 1993; *Cliff et al.*, 1985]. This would imply significant vertical displacements along the intervening Mallnitz Synform, which is inconsistent with the observed subhorizontal stretching lineations and sinistral shear sense in D5 mylonites striking parallel to this synform [*Scharf et al.*, 2013a].

3.6.3 The relationship of exhumation and cooling to the structural evolution of the Adriatic Indenter – a model

Any model of exhumation must account for the 2-3 Ma difference in the onset of rapid cooling in the ETD and WTD, as well as along-strike migration in the age of D5 doming in the ETD. The schematic map in Figure 3.6 shows how the evolving pattern of cooling of orogenic crust in the Tauern Window can be related to progressive indentation and fragmentation of the Austroalpine units along the front of the Adriatic indenter.-Specifically, we propose that the migration of rapid cooling of the ETD from 500 to 300°C reflects the migration of doming and extensional exhumation in response to exhumation and fragmentation of the Austroalpine units into the two triangular blocks, the Rieserferner and Drau-Moll blocks (Fig. 3.1) along the front of the Adriatic Indenter [e.g., *Cliff et al.*, 1985; *Hoke*, 1990; *Reddy et al.*, 1993; *Inger and Cliff*, 1994; *Scharf et al.*, 2013a]. This evolution is traced schematically in Figure 3.6.

The initial configuration of the Austroalpine units proposed in Figure 3.6a was obtained by retrodeforming the Rieserferner and Drau-Moll blocks along the sinistral Zwischenbergen-Wöllatratten (ZWT) Fault, bringing them into their positions prior to the main stage of indentation. The ZWF accommodated about 20 km of sinistral displacement in map view according to offset of the late Oligocene Defferegen-Antholz-Vals and Ragga-Teuchel Faults (DAV and RT in Fig. 3.1). These are interpreted to have originally been one through-going sinistral fault that was active during intrusion of the late Oligocene Periadriatic intrusives [age criteria in *Müller et al.*, 2000; *Mancktelow et al.*, 2001; *Romer and Siegesmung*, 2003; *Wagner et al.*, 2006], prior to Miocene indentation [*Scharf et al.*, 2013a and references therein]. Other lithological markers are similarly offset along the ZWF [*Linner et al.*, 2013]. We note that both the Rieserferner and Drau-Moll blocks contain a number of shorter faults with smaller displacements [≤ a few km, *Schuster et al.*, 2015], some of which offset [e.g., Iseltal Fault; Fig. 3.1] and even reactivate [RT, e.g. *Wölfler et al.*, 2015] the larger, aforementioned faults. These smaller faults are interpreted to have allowed the Austroalpine blocks to deform compatibly during indentation, as discussed below.

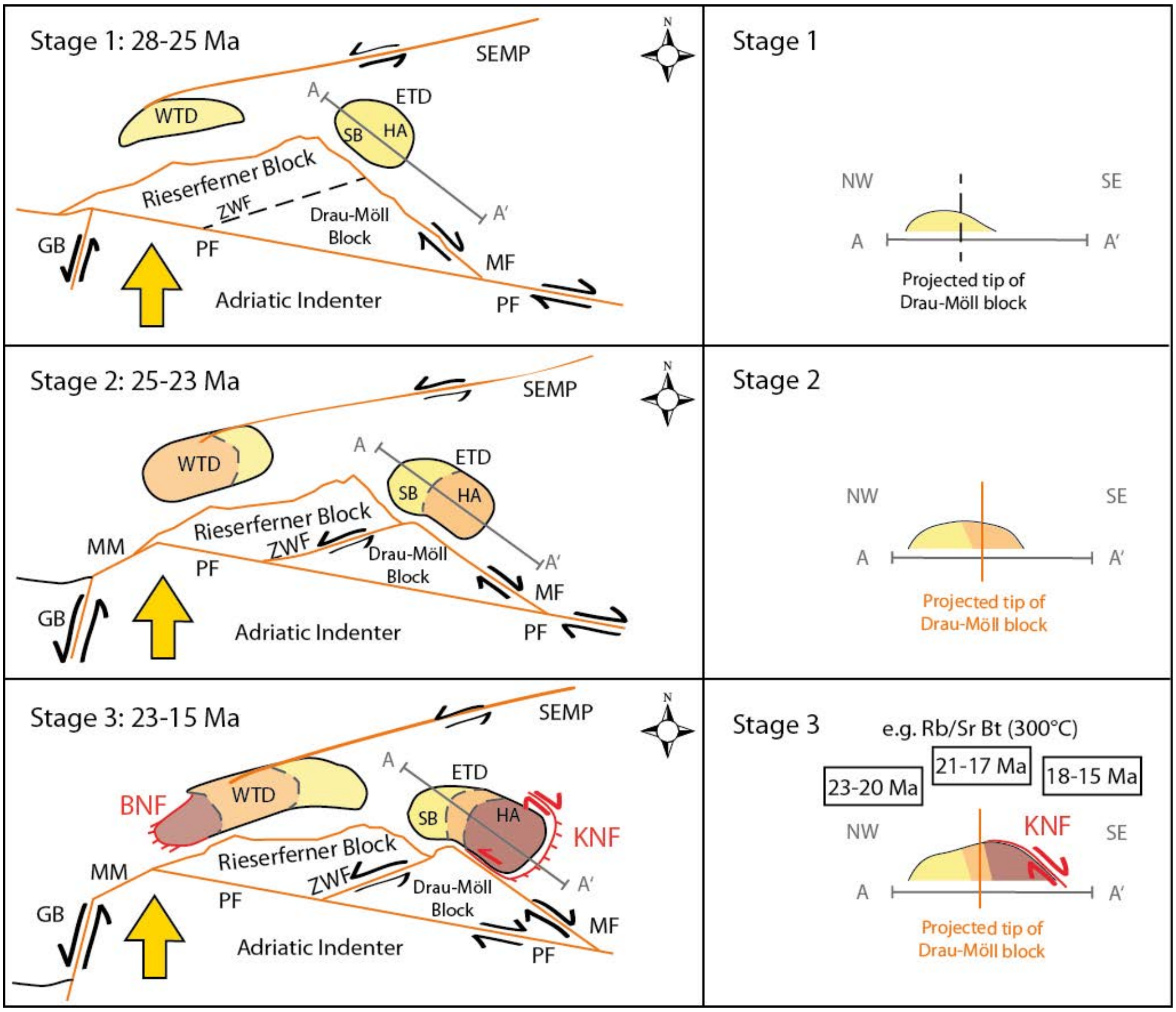

Fig. 3.6: Schematic maps (left column) and cross sections (right column) showing progressive fragmentation of indenting Austroalpine blocks and related migration of doming during exhumation of the ETD (see text for explanation). Colours marking the cooling domains previously shown in Fig. 3.5. Age intervals above the cross section for stage 3 indicate NW to SE passage of the 300°C isotherm through the ETD according to $^{87}Rb/^{87}Sr$ biotite ages in the literature (see references in Supplementary material for chapter 3, section 3.8). -Abbreviations: BNF – Brenner Normal Fault, ETD – Eastern Tauern Dome, GB – Giudicarie Belt, HA – Hochalm Subdome, KNF – Katschberg Normal Fault, MF – Mölltal Fault, MM – Meran-Mauls Fault, PF – Periadriatic Fault, SB – Sonnblick Subdome, SEMP – Salzach-Ennstal-Mariazell-Puchberg Fault, WTD – Western Tauern Dome, ZWF – Zwischenbergen-Wöllatratten Fault. Big yellow arrows indicate motion of the Adriatic indenter with respect to stable Europe. Active faults in orange (strike-slip with arrows and normal faults in red with ticks), inactive faults in black.

The occurrence of deeper Periadriatic intrusives and younger Rb-Sr mica cooling ages in the Rieserferner Block [intrusive depths of 10 km, Rensen and Rieserferner plutons, *Stöckhert et al.*, 1999;

Borsi et al., 1973, 1978] than in the Drau-Möll Block [e.g., *Rosenberg*, 2004 and references therein] suggest that the former block was exhumed from greater depths than the latter. In addition, zircon fission track ages of 30- 40 Ma [*Wölfler et al.*, 2008, 2015] in the northern parts of the Rieserfernen and Drau-Möll blocks indicate that temperatures close to 240°C prevailed during the Oligocene, whereasMesozoic sediments in the southern parts of the block near the Periadriatic Fault reached only anchizonal to diagentic conditions [*Rantitsch*, 2001; *Schuster et al.*, 2004]. The Austroalpine blocks at the time of indentation were therefore cooler and stronger than the hot and weak Paleogene nappe stack in the Tauern Window [*Genser et al.*, 1996; *Linzer et al.*, 2002; *Scharf et al.*, 2013a]. Together, the restored Rieserferner and Drau-Moll blocks formed a large triangular zone along the leading edge of the Southern Alpine crust, as depicted in Figure 3.6a. In addition, the entire Eastern Alpine orogenic edifice was restored about 50 km to the east, equivalent to the dextral displacement at that location due to eastward lateral escape accommodated by the Periadriatic Fault since late Oligocene time [30 Ma; *Pomella et al.*, 2011, 2012]. It is noted that this estimate is consistent with the overall trend of eastwardly increasing, post-20 Ma dextral displacement along the Periadriatic Fault; the displacement ranges from 0 km at its junction with the Meran-Mauls and Giudicarie Belt at the apex of the Southern Alpine indenter, to a maximum of about 260 km along the Mid-Hungarian Fault Zone [Fig. 3.1a; *Handy et al.*, 2015]. This along-strike displacement gradient is consistent with the idea that the Neogene Periadriatic Fault east of the Giudicarie Belt was a crustal stretching fault [*Means*, 1989] that accommodated lateral eastward escape of the far-travelled Austroalpine nappes [dark grey units in Fig. 3.1a, *Fodor et al.*, 1998; *Horvath et al.*, 2006].

Analogue modeling of indentation has shown that triangular zones of little or no deformation ("dead zones") form in front of rigid indenters between kinematic singularities at the corner or corners of the indenters [e.g., *Tapponnier et al.*, 1986; *Ratschbacher et al.*, 1991a; *Rosenberg et al.*, 2007]. At low strains, such dead zones are thus protected from the high differential stresses that would favour failure. However, with progressive indentation, these zones are eventually dissected by strike-slip faults and the zones fragment into smaller blocks.

In the case of the Eastern Alps, we propose that the Austroalpine crust immediately south of the Tauern Window formed such a dead zone in front of the Adriatic Indenter, which is represented by the Southern Alps east of the Giudicarie Belt (Fig. 3.1). The southeastern corner of this indenter, at the junction of the sinistral Giudicarie Belt and the dextral Periadriatic Fault (Figs 3.1, 3.6a), was the site of a kinematic singularity. Both of these faults were active throughout late Oligocene/Miocene time and delimited the indenter from the orogenic crust to the north [e.g., *Müller*, 1998; *Müller et al.*, 2001; *Läufer et al.*, 1997; *Pomella et al.*, 2011, 2012; *Handy et al.*, 2005]. The Periadriatic Fault decoupled the triangular dead zone of Austroalpine crust from this indenter and facilitated eastward lateral escape of Eastern Alps, including the exhuming Cenozoic orogenic crust in the Tauern Window [*Frisch et al.*, 1998; *Linzer et al.*, 2002]. It is important to note that this dead zone was not entirely immune to Alpine deformation and heating, as its leading edge experienced penetrative Paleogene Alpine deformation and temperature of ≥ 300°C [age maps of *Schuster et al.*, 2004; fabric map of *Scharf et al.*, 2013a, their Fig. 8]. Furthermore, as northward Adriatic indentation progressed, this zone was dissected by conjugate strike-slip faults that lead to the individuation of the semi-rigid Rieserferner and Drau-Möll blocks [Fig. 3.6b; *Scharf et al.*, 2013a, their Fig. 8]. The strike-slip faults bounding these blocks allowed the blocks to extend subparallel to the orogen, thus accommodating some of the northward Adriatic indentation [*Frisch et al.*, 1998; *Linzer et al.*, 2002].

It is proposed that the northward motion and eastward displacement of the Rieserferner and Drau-Möll blocks induced the migration of doming and KNF-related extensional exhumation in the Tauern Window away from, and to the east of, the indenter front as recorded by the cooling age pattern in this study. A key to understanding this scenario is that the tip of the Drau-Möll Block coincides approximately with the boundary between cooling domains 1 and 2 of the ETD (Fig. 3.5a). Shortening in front of the Drau-Möll Block was greatest in the vicinity of this tip, i.e. in the Sonnblick Subdome (Fig. 3.6b), where the ages in this study indicate that rapid cooling of the ETD initiated as early as 30-25 Ma. Continued indentation by the Drau-Möll Block accommodated by dextral and sinistral motion of the conjugate MF and ZWF, respectively, effected further shortening of the ETD in the Hochalm Dome and extensional exhumation in the footwall of the KNF beginning no later than 23 Ma [*Scharf et al.*, 2013a]. Final indentation of the Drau-Möll Block induced eastward extrusion and rollback of the KNF relative to the tip of this block, such that exhumation migrated laterally into what then became cooling domain 3 of the EDT. Rapid cooling ended at 17 Ma according to fission track cooling ages [Fig. 3.6c, see discussion in *Scharf et al.*, 2013a].

Northward indentation of the Southern Alps is also documented along the Giudicarie Belt along the western edge of the Southern Alps indenter [*Pomella et al.*, 2011; 2012]: Initial sinistral transpressive motion along this belt and the transpressive Meran-Mauls Fault resulted in incipient bending of the Periadriatic Fault beginning in late Oligocene time. This incipient indentation did not trigger much exhumation of the Tauern Window, but appears to have induced late Oligocene sinistral shearing in the core of the WTD [*Schneider et al.*, 2013] as well as the aforementioned early exhumation of the eastern ETD at 30-25 Ma [*Reddy et al.*, 1993; this study]. However, most of the aproximately 77 km of sinistral displacement along the Giudicarie Belt occurred in Miocene time [23-7 Ma, *Scharf et al.*, 2013a; *Schmid et al.*, 2013; *Handy et al.*, 2015; *Schneider et al.*, submitted for publication] and triggered rapid exhumation and cooling of the WTD [*Fügenschuh et al.*, 1997].

3.7 CONCLUSIONS

The cooling pattern in the Tauern Window is related to the fragmentation of an initially triangular zone of little or no ductile deformation comprising mostly Austroalpine units in front of the Adriatic Indenter (Fig. 3.6). With progressive indentation, this zone was subdivided into two, semi-rigid crustal blocks (Rieserferner and Drau-Möll blocks) along the leading edge of this indenter. Miocene doming, exhumation and cooling of the eastern part of the Tauern Window (ETD in Fig. 3.1) occurred directly in front of the Drau-Möll Block. A new ^{147}Sm/^{144}Nd isochron age of 25.7 ± 0.9 Ma on garnet that overgrows the main foliation in the ETD (Fig. 3.3) marks the age of Barrow-type, amphibolite-facies metamorphism (Tauernkristallisation) in the eastern part of the Tauern Window. This metamorphism overlapped with the onset of doming and orogen-parallel extensional shearing. The new ^{87}Rb/^{87}Sr white mica and biotite ages presented in this paper point to broadly coeval cooling of the Sonnblick and Hochalm subdomes within the ETD (Fig. 3.2) to below 500 and 300°C at about 30-21 and 23-15 Ma, respectively (Fig. 3.5). The cooling ages of these mica systems decrease from the center of the Tauern Window toward the KNF, reaching 24-21 Ma (^{87}Rb/^{87}Sr white mica) and 18-15 Ma (^{87}Rb/^{87}Sr biotite) in the KNF footwall (Fig. 3.5). Taken together, the new and existing thermochronological data show that the ETD was folded and exhumed as a single unit; doming migrated perpendicular to the indentation direction and parallel to motion of the eastward rolling footwall of the KNF during lateral orogenic escape.

The relative age of doming and Tauernkristallisation differs within the Tauern Window; in the center they are broadly coeval, whereas towards the eastern and western margins, doming was coeval with orogen-parallel extensional shearing and clearly post-dated the Tauernkristallisation. This change in the relative age of doming and peak-thermal metamorphism reflects the migration of tectonic and erosional unroofing from the center to the ends of the Tauern Window during lateral orogenic escape in latest Oligocene and Miocene time.

Regarded on the scale of the orogen, the anomalous indentation and exhumation patterns in front of the Adriatic indenter appears to have formed during a Neogene switch in subduction polarity, from south-directed European subduction to north-directed Adriatic subduction beneath the Eastern Alps [*Lippitsch et al.*, 2003; *Schmid et al.*, 2004; *Handy et al.*, 2015]. This polarity switch drove cold wedges of Austroalpine crust, which had previously formed the upper plate of the European subduction, into the warm and weak orogenic edifice of previously accreted European crust.

3.8 SUPPLEMENTARY MATERIAL TO CHAPTER 3

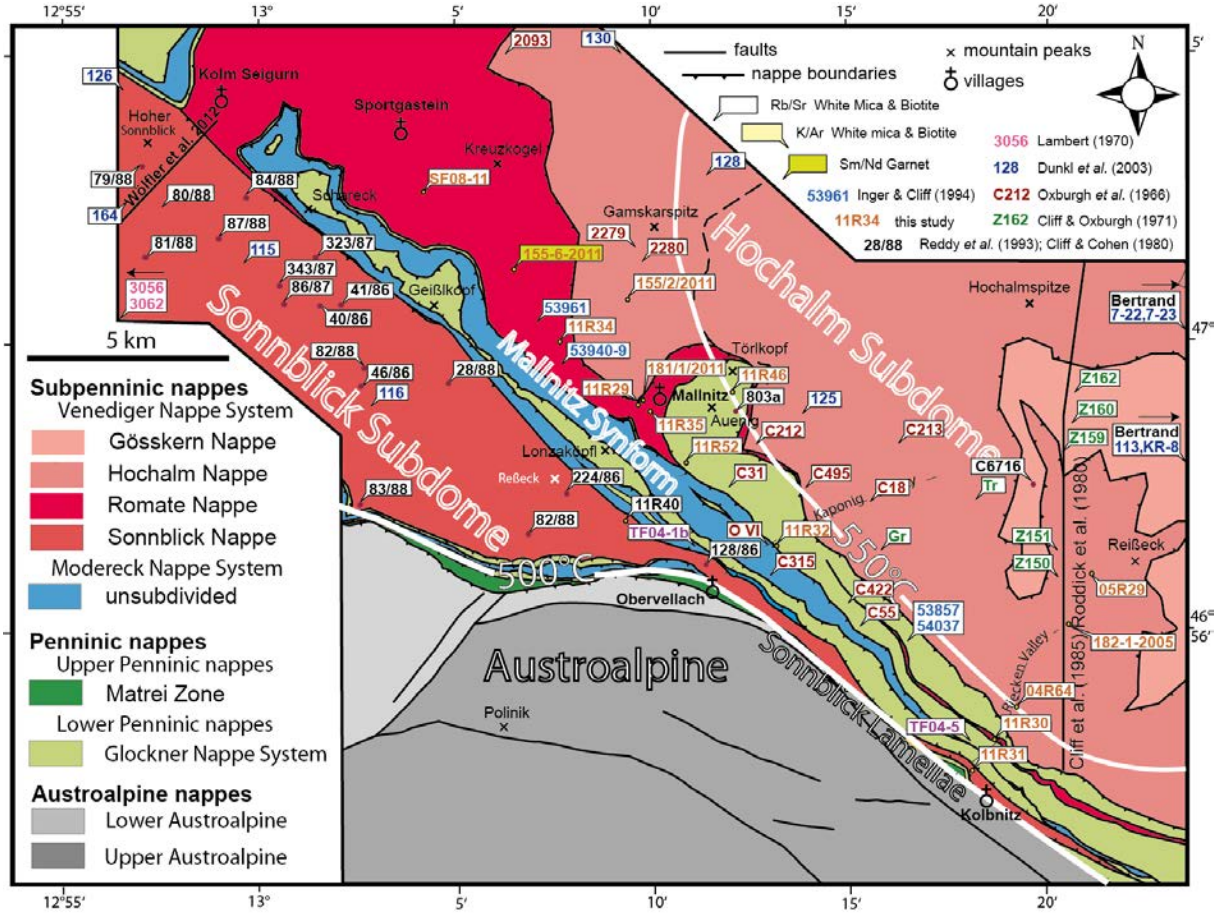

Figure 3.1.A: Sample map. Samples listed in Table 3.1A of the Supplementary material to chapter 3.

Table 3.1.A: Authors list, Sample names, ages and T_c values used for the cooling pattern in Fig. 3.5.

Method	Sonnblick Subdome West (Core)		Sonnblick Subdome Center (Mallnitz)		Sonnblick Subdome East (Lamellae)		Hochalm Subdome West (Gastein)		Hochalm Subdome Center (Mallnitz)		Hochalm Subdome East (Core)		Hochalm Subdome East (Rim)	
	Ages/ err	Sample Nr Author	Ages/ err	Sample Nr Author	Ages/ err	Sample Nr Author	Ages/ err	Sample Nr Author	Ages/ err	Sample Nr Author	Ages /err	Sample Nr Author	Ages/ err	Sample Author
Rb/Sr Wm 550±50°C Purdy and Jäger, 1976 Von Blanckenburg et al. 1989	26.9± 0.5	323/87 Reddy et al., 1993	27.1± 0.4	128/86 Reddy et al., 1993	20.7± 2.3 Deformation	TF04-5 Glodny 2008 NOT USED	24.7± 0.4	53961 Inger and Cliff, 1994			21.8± 0.5	G2038 Cliff et al., 1985	24.4± 0.3	182/1/2005 this study
	28.3± 0.8	86/87 Reddy et al., 1993	23.9± 0.5	224/86 Reddy et al., 1993			28.3± 1.4	53940 Inger and Cliff, 1994			22.6 ±0.6	G3500 Cliff et al., 1985	21.1± 0.2	04R64 This study
	26.9± 0.4	84/88 Reddy et al., 1993	25.5± 2.9	TF04-1b Glodny 2008			32.0± 1.0	53941 Inger and Cliff, 1994			27.0 ±2.0	M504 Cliff et al., 1985	21.2± 1.0	H2000 Cliff et al., 1985
	26.2± 0.4	87/88 Reddy et al., 1993					28.4± 1.2	53942 Inger and Cliff, 1994			20.5 ±1.2	M1480 Cliff et al., 1985	23.1± 0.6	H3000 Cliff et al., 1985
	30,0± 1.1	79/88 Reddy et al., 1993					29.0± 1.0	53943 Inger and Cliff, 1994			22.0 ±2.0	M2085 Cliff et al., 1985	22.6± 0.6	H1000 Cliff et al., 1985

	25.8± 0.5	46/86 Reddy et al. 1993					26.2± 0.8	53944 Inger and Cliff, 1994					23.8± 0.4	G419 Cliff et al., 1985
	34.7± 0.5	83/88 Reddy et al. 1993					31.0± 2.0	53945 Inger and Cliff, 1994					22.3± 0.8	54037 Inger and Cliff, 1994
							23.3± 1.2	53948 Inger and Cliff, 1994					24.0± 2.5	53957 Inger and Cliff, 1994
							25.0± 1.7	53949 Inger and Cliff, 1994						
mean	28.1± 0.5		25.7± 0.6				27.0± 1.0				22.3 ±0.9		22.7± 0.5	
530±40°C Ar/Ar Hbl Harrison 1981 147Sm/144Nd Grt formation							25.7± 0.9	155/6/2011This study Sm/Nd Grt	23.8± 0.8	803a Cliff et al., 1985 Ar/Ar Hbl				
									24.0± 1.0	803a Cliff et al., 1985				
									25.0± 1.3	803a Cliff et al., 1985				
mean							25.7± 0.9		24.0± 1.0					
420°C K/Ar Wm Robbins 1972	27.5± 1.0	3056 Lambert, 1970							17.5± 0.5	C31 Oxburgh et al., 1966	18.5 ±0.5	M504 Roddick et al., 1980	25 No Err	H1000 Cliff et al., 1985
									21.0± 0.5	OVI Oxburgh et al., 1966	18.0 ±0.5	M1480 Roddick et al., 1980	22.4 No Err	H2000 Cliff et al., 1985
									21.0± 1.0	C315 Oxburgh et al., 1966	22.2 ±0.5	G3500 Cliff et al., 1985	24 No Err	H3000 Cliff et al., 1985
									25.5± 1.0	2280 Oxburgh et al., 1966	20.9 ±0.5	Tr Cliff et al., 1971	21.5± 1.0	C495 Oxburgh et al., 1966
													23.5± 0.5	Gr Cliff et al., 1971
													27.9 Exc. Ar	G419 Cliff et al., 1985 NOT USED
													22.0± 1.0	C422 Oxburgh et al., 1966
													22±0.5	C55 Oxburgh et al., 1966
mean	27.5± 1.0		21.5± 0.7						20.6± 0.7		19.9 ±0.5		22.4± 0.7	
Rb/Sr Bt 320±40°C	21.7± 0.1	86/87 Reddy et al., 1993	21.0± 0.2	11R40 This study	17.3± 0.2	11R31 This study	20.6± 0.2	SF08-11 This study	20.5± 0.2	11R34 This study	16.3 ±0.2	G2085 Cliff et al., 1985	18.1± 0.2	04R64 This study
K/Ar Bt 320±40°C	20.5± 0.2	80/88 Reddy et al., 1993	19.1± 0.2	224/86 Reddy et al., 1993			21.5± 0.5	2093 Oxburgh et al.,	19.0± 0.2	11R29 This study	16.5 ±0.2	G2038 Cliff et al., 1985	17.9± 0.2	04R29 This study

Harrison et al. 1985 Del Moro et al. 1982 Jäger et al. 1967								1966						
	22.4± 0.2	41/86 Reddy et al., 1993	19.2± 0.3	128/86 Reddy et al., 1993					17.7± 0.2	11R35 This study	15.1 ±0.2	G3500 Cliff et al., 1985	17.4± 0.2	182/1/2005This study
	22.9± 0.3	40/86 Reddy et al., 1993	20.6± 0.1	82/86 Reddy et al., 1993					19.8± 0.2	155/2/2011This study	16.5 ±0.2	G4500 Cliff et al., 1985	18.6± 0.2	11R30 This study
	21.1± 0.2	84/88 Reddy et al., 1993							18.2± 0.2	181/1/2011 This study	16.2 ±0.2	G5500 Cliff et al., 1985	15.3± 0.2	H3000 Cliff et al., 1985
	20.3± 0.1	87/88 Reddy et al., 1993							17.7± 0.2	11R46 This study	16.7 ±0.4	M504 Cliff et al., 1985	16.1± 0.2	G419 Cliff et al., 1985
	21.1± 0.1	81/88 Reddy et al., 1993							17.5± 0.2	11R52 This study	17.2 ±1.3	M990 Cliff et al., 1985	17.0± 0.3	H1000 Cliff et al., 1985
	22.3± 0.2	323/87 Reddy et al., 1993							19.5± 0.2	11R32 This study	16.4 ±0.3	M1480 Cliff et al., 1985	19.5± 1.0	C18 Oxburgh et al., 1966
	20.2± 0.1	79/88 Reddy et al., 1993							18.0± 1.0	2279 Oxburgh et al., 1966	16.7 ±0.2	C6716 Cliff and Cohen, 1980	22.0± 0.5 Exc. Ar	C213 Oxburgh et al., 1966 NOT USED
	20.8± 0.1	46/86 Reddy et al., 1993							19.5± 0.5	C212 Oxburgh et al., 1966	21.9 ±0.5	Z162 Cliff et al., 1971	19.0± 0.5	Gr Cliff et al., 1971
	21.5± 0.1	28/88 Reddy et al., 1993									21.5 ±0.4	Z160 Cliff et al., 1971		
	21.3± 0.1	83/88 Reddy et al. 1993									16.0 ±0.3	Z159 Cliff et al., 1971		
	26.7 Exc. Ar	Lambert, 1970 Not used									16.1 ±0.2	Z151 Cliff et al., 1971		
											17.5 ±0.2	Z150 Cliff et al., 1971		
											25.2 ±0.5 Exc. Ar	Tr Cliff et al., 1971: NOT USED		
mean	21.2± 0.1		20.2± 0.2		17.3± 0.2		20.9± 0.3		18.8± 0.2		16.8 ±0.3		17.7± 0.2	
FTZ 240±20°C 2sigma Yamada et al., 1995	21.5± 1.4	115 Dunkl et al., 2003					18.4± 3.0	130 Dunkl et al., 2003	17.5± 2.0	128 Dunkl et al., 2003	11.8 ±3.2	Bertrand, 2013	17.5± 1.4	KR-8 Dunkl et al., 2003
	18.0± 1.6	116 Dunkl et al., 2003							18.5± 2.4	125 Dunkl et al., 2003	16.9 ±1.6	113 Dunkl et al., 2003	17.1± 2.6	7-22 Dunkl et al., 2003
	17.5± 2.0	164 Dunkl et al., 2003											16.7± 2.0	7-23 Dunkl et al., 2003
	17.5 1.6	126 Dunkl et al., 2003											10.4± 4.2	Bertrand, 2013
mean	18.8± 1.6						18.4± 3.0		18.0± 2.2		15.2 ±2.0		16.5± 2.2	
ZHE 2sigma 190±10°C Wolf et	15.4± 2.8	TW51 Wölfler et al., 2012												
	15.6± 3.4	TW111 Wölfler et al., 2012												

al., 1996	16.1± 1.2	TW110 Wölfler et al., 2012												
	19.1± 0.2	TW44 Wölfler et al., 2012												
	15.8± 6.4	TW108 Wölfler et al., 2012												
mean	18.3± 0.8													

Chapter 4: Bericht 2012 über geologische Aufnahmen auf den Blättern 154 Rauris, 155 Bad Hofgastein und 181 Obervellach

Jahrbuch der Geologische Bundesanstalt, 152/1-4, pp. 268-272.

Silvia Favaro[1] & Ralf Schuster[2]

[1] Department of Earth Sciences, Freie Universität Berlin, Malteserstrasse 74-100, 12249 Berlin, Germany

[2] Geologische Bundesanstalt, Neulinggasse 38, A-1030, Vienna, Austria

ABSTRACT

In this report results from geological mapping in the Sonnblick area near to Kolm-Saigurn (ÖK154), from the Tauerntal near to Mallnitz (ÖK 155) and from the south-western slopes of the Mölltal near to Obervellach (ÖK 181) are documented. The geological maps improve the manuscript of ÖK 154 Rauris by *Pestal & Hellerschmidt-Alber* [2011] and give additional information for the south-western part of map sheet ÖK 155 Bad Gastein. The mapping was focused on the north-western end of the Mallnitz synform and on the subdivision of pre-Mesozoic and Mesozoic rocks of the Subpenninic nappes. Additional structural investigations are reported in *Favaro*, 2012 (this volume).

4.1 TECTONIC SUBDIVISION OF THE AREA

The area is situated in the Subpenninic and Penninic nappes of the Tauern Window. From bottom to the top the following tectonic succession occurs [according to the tectonic nomenclature by *Schmid et al.*, 2004; *Pestal & Hellerschmidt-Alber*, 2011; *Schmid et al.*, 2013]:

- Hochalm Nappe (Venediger Nappe System of Subpenninic nappes).
- Romate Nappe (Venediger Nappe System of Subpenninic nappes).
- Sonnblick Nappe (Venediger Nappe System of Subpenninic nappes).
- Kolm Nappe (lower element of Glockner Nappe System of Penninic nappes).
- Modereck Nappe System (Subpenninic nappes).
- Geißel Nappe (upper element of Glockner Nappe System of Penninic nappes).

The area is characterized by a km-sized fold structure with a northwest-southeast trending fold axes. It is termed Mallnitz Synform and consists of elements of the Glockner and Modereck nappe systems infolded between Subpenninc nappes. The Mallnitz Synform is bordered to the northwest by the Hochalm Nappe with the overlying Romate Nappe and to the southwest by the Sonnblick Nappe. The nappe stack forming the Mallnitz Synform has been interpreted as a stretching fold by *Kurz & Neubauer* [1996] in the area southeast of Obervellach.

4.2 DESCRIPTION OF THE SUBPENNINIC AND PENNINIC NAPPES IN THE RAURIS AND MALLNITZ VALLEYS

In this chapter the lithostratigraphy and the lithological content of the Subpenninic and Penninic units is described.

4.2.1 Subpenninic nappes

The Subpenninic nappes, derived from the Helvetic shelf, representing the southern European margin after the opening of the Penninic Ocean in the Middle Jurassic. According to the older nomenclature [e.g. *Kober*, 1920; *Staub*, 1924; *Exner*, 1964] the "Venediger Nappe" comprises Permo-Carboniferous plutonites ("Zentralgneise"), intruding an old roof ("Altes Dach"). The old roof consists of pre-Carboniferous "Altkristallin" and Permocarboniferous schists belonging to the "Untere Schieferhülle". In 1962, Exner mentioned that due to insufficient knowledge also some Mesozoic rocks might be included in the "Untere Schieferhülle".

Maps of the area produced in the last Century are mostly lithological maps, but in the past years the lithostratigraphy of the Permomesozoic rocks of the Subpenninic nappes has been improved significantly [e.g. *Pestal et al*., 2009]. The newly established lithostratigraphy constrained specifying quartzites or blackish schists in different stratigraphic positions.

This leads to a better understanding of the tectonic style of the area. Equally important for the definition of individual nappes are different orthogneisses and the old roof lithologies.

A problematic lithological unit in the eastern part of the Tauern Window comprises the Permocarboniferous schists of the "Untere Schieferhülle". In the area between Mallnitz and Gastein *Kober* [1920] summarized them as "Woisgenschiefer" based on their occurrence in the Woisgen valley. For the same rocks association *Exner* [1957] uses the term basal and central schist series ("Basale und Zentrale Schieferserie") and in the maps of the Sonnblick area by *Exner* [1956; 1962] they are shown as bright micaschist ("Heller Glimmerschiefer") and aplitic bright and black micaschist ("Aplitisch inizierter heller und schwarzer Glimmerschiefer").

However, investigations of the last years allow subdividing these schists in at least two genetic types: The first is mostly composed of dark colored schists rich in biotite and intruded locally by granitic dykes. For these lithologies the term biotite-porphyroblast schist ("Biotitporphyroblastenschiefer"), "Furtschagelschiefer" or "Kleinelendschiefer" is in use. Detrital zircons from these schists yielded ages as young as 339 Ma [*Kebede et al*., 2005; *Lärchbaumer et al*., 2010]. For this reason the protolite age of these rocks is Carboniferous or younger.

The second type is a garnet, chloritoid-bearing chlorite-muscovite schist. No granitic dykes have been found in these schists until now. They are expected to be younger than the dark variety and therefore maybe more pelitic equivalents to the Permian Wustkogel Formation. For this reasons they are quoted as a post-Variscan cover. This very typical rock type can be found to the northeast of the Mallnitz synform from the area of Kolm-Saigurn, along the eastern slopes of the Schareck (3.123 m), in the

Tauern valley and further until Mallnitz. However, they do not appear in the Woisgen valley. Further occurrences of similar schists are present as thin slices below the Glockner Nappe System at Törlkopf (2.446 m) and within the Mallnitz Synform until Göriach in the lowermost part of the Möll valley (ÖK 182 Spittal a. d. Drau).

From Kolm-Saigurn until Mallnitz the schists are bright, shining, and silvery to greenish colored and often sprinkled with red garnets up to 5 mm in diameter. Chloritoid appears in the rock matrix as tiny black dots 0.1–0.3 mm in size, but may form flakes up to 5 mm in diameter. Often chloritoid is also present as inclusions within the garnet. In thin section a layering of chlorite and mica-rich and quartz-rich lamellae and often also a folding and crenulation is visible. The micas show waving extinction, but in some cases they are recrystallized during the deformation. Chlorite is green colored, Fe-rich and forms larger patches. New white mica is overgrowing and cuts the older foliation. In associations with the mica also some crystals of plagioclase are visible. Quartz and mica are up to 0.5 mm in size, whereas the plagioclase is more fine-grained. Tourmaline is a frequent accessory mineral. It forms tiny bluish-green crystals with idiomorphic shape and up to 0.3 mm in length. In the area around Mallnitz, chlorite is less frequent and some biotite is inter-grown with the white mica. Chloritoid is still present as inclusions within the garnet, but in the matrix instead of chloritoid tiny idioblastic staurolite crystals appear.

Southeast of Mallnitz the schists are pinched between elements of the Glockner and Modereck nappe systems of the Mallnitz Synform. They form several hundred meters long and up to 50 m thick slices. Staurolite was described by *Exner* [1984] from a locality in the Odengraben near Göriach. It appears in a 10 m thick layer of staurolite-garnet-muscovite-chlorite-quartz schist which occurs in the gorge at 1.200 m altitude. Garnets are 3 mm in diameter and staurolite forms 2 mm long prismatic crystals. In other localities no staurolite, but epidote is present forming often idioblastic and up to several millimeters big crystals. We guess that the epidote developed during the breakdown of chloritoid when calcium from the surrounding calcareous micaschist of the Glockner Nappe System was available.

In our maps the subdivision of the Subpenninic nappes follows the suggestion by *Pestal & Hellerschmidt-Alber* [2011], *Favaro et al.* [EGU Abstract 2012] and *Schmid et al.* [2013].

The Subpenninic nappes are split into the Venediger Nappe System, representing thick basement and cover nappes, and the Modereck Nappe System forming thin slices mostly consisting of metasedimentary rocks. The metasedimentary rocks are subdivided into pre-Variscan metasediments and metavolcanics, syn-Variscan Upper Devonian to early Carboniferous metasediments, post-Variscan late Carboniferous and Permian metasediments and Mesozoic metasediments.

4.2.1.1 Venediger Nappe System

In the investigated area three nappes of the Venediger Nappe System occur. From bottom to the top are the Hochalm, Romate and Sonnblick nappes.

4.2.1.1.1. Hochalm Nappe

This nappe is built up by different orthogneisses intruding an old roof consisting of pre-Variscan migmatic paragneisses, paragneisses, micaschists and amphibolites andsyn-Variscan metasediments belonging to the "Kleinelendschiefer". Locally and with variable thickness a Permomesozoic transgressional sequence is preserved.

Orthogneisses ("Zentralgneis")

In the Hochalm Nappe several types of orthogneisses are present [*Holub & MarschallinGer*, 1989; *Schuster et al.*, 2006]. In general an increase of deformation from the central parts of the Reiseck Mountains towards the margins and the top of the nappe respectively can be recognized. In the investigated area orthogneisses of the Hochalm Nappe appear north of Mallnitz around the Hindenburg Höhe (2.315 m). The most frequent lithologys are mediumgrained augengneisses and fine- to medium-grained leucocratic granitgneisses with garnets (Figs. 4.1a, b). The latter also appear as up to several meters thick dykes within the old roof.

Old roof ("Altes Dach")

The pre-Variscan metasediments comprise paragneisses (Fig. 4.1c) to micaschists and amphibolites (Fig. 4.1d). The paragneisses and micaschists of the old roof are monotonous with a pronounced schistosity. White mica, biotite and a few tiny garnets are visible with the naked eye. Sometimes the rocks are dark greyish, because of a small amount of graphitic pigment. Amphibolites form up to 100 m thick layers and bodies. They are mostly fine-grained, dark green and strongly foliated. Locally, a larger amount of feldspar is present and in some layers garnet up to 2 mm in diameter occurs. Further intercalations of metagabbroic amphibolites, with hornblende crystals up to 1 cm in a finegrained plagioclase-rich matrix as well as bright colored hornblende gneisses appear.

Syn-Variscan cover

While they are missing in the southern part of the Hochalm Nappe, north of the Törlkopf (2.446 m) an up to several hundred meters thick sequence of "Biotitpor- phyroblastenschiefer" is present. They can be nicely studied on the northern slopes of the Seebachtal close to the Stappitzersee and in the Woisgen valley. They comprise bright colored, quartz-rich gneisses with biotite porphyroblasts, paragneisses and dark, sometimes graphitic, biotite dominated schists. Also layers of garnet-bearing muscovite-chlorite schists with some biotite are present. The biotite porphyroblasts reach up to 2 mm in size.

Permomesozoic cover

The lithologies and lithostratigraphic units on top of the Hochalm Nappe are the same as in the Modereck Nappe System and described there. Remarkable is the occurrence of garnet in the dark schists and graphitic quartzites of the Brennkogel Formation at Dösner Schönberg east of Mallnitz.

As mentioned above a Permomesozoic cover is only locally preserved: At the ridge to the Groneck (2.691 m) near to Obervellach a sequence of Wustkogel, Seidelwinkel and Pfiffkar formations is several hundred meters thick. Further to the northwest at the Dösner Schönberg more than hundred meters of Brennkogel Formation are present. In contrast on the slopes on both sides of the Seebachtal no remnants of Permomesozoic cover have been found.

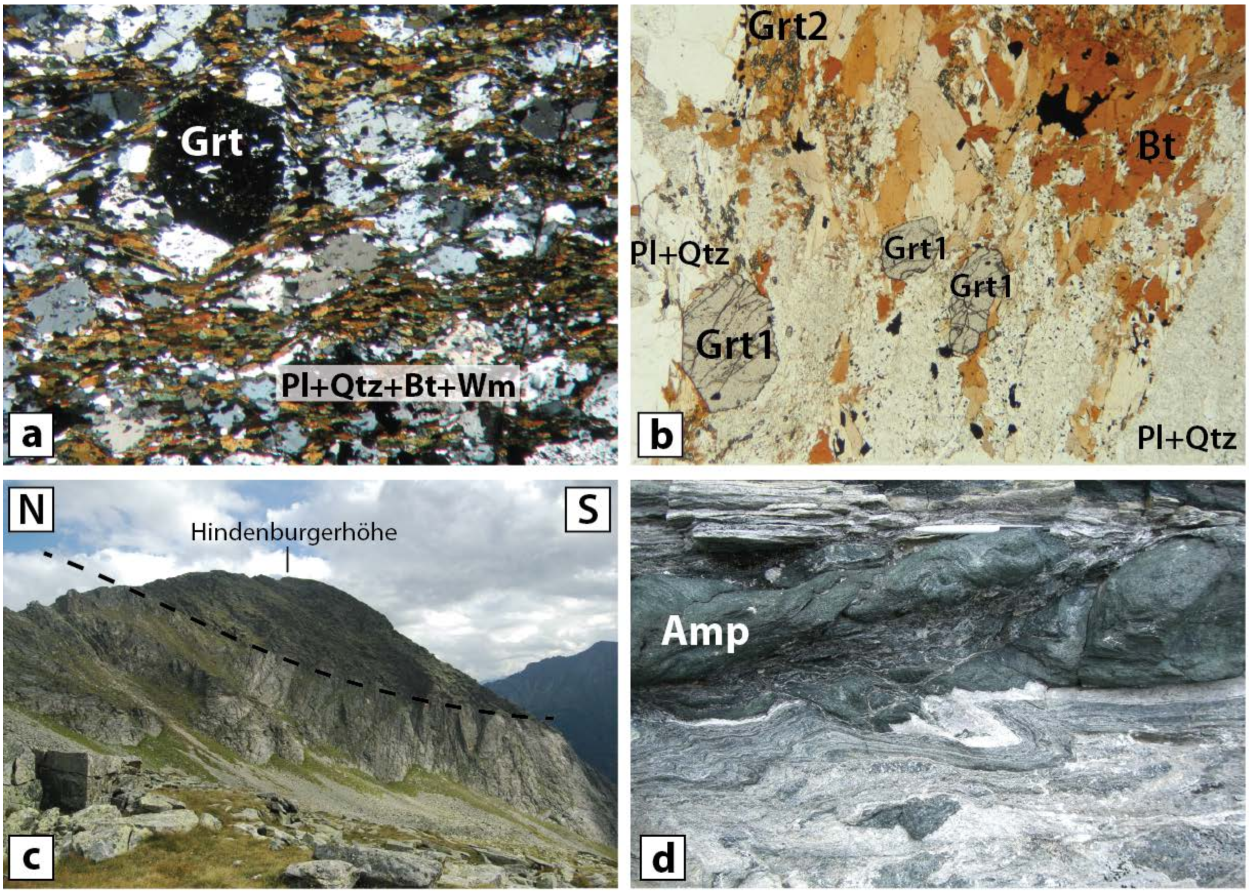

Figure 4.1: Hochalm Nappe (a,b) granitoids of the Hochalm Nappe, Mineral content: Plagioclase, Biotite, Muscovite, Quartz, Garnet. Accessory: Kyanite, Garnet, Apatite, ore mineral; (b) contact between Old Roof ("Altes Dach") above and granitoids below; (c) Amphibolites of the Old Roof of the Hochalm Nappe.

4.2.1.1.2. Romate Nappe

The Romate Nappe is termed after the Romatespitze (2.696 m, Rameterspitz in the most recent map) between Gastein and Tauern valley. It is a basement and cover nappe with a thickness up to several kilometers, built up by the following lithostratigraphic units: Carboniferous orthogneisses ("Zentralgneiss") are present in two varieties, the Romate monzosyenitegneiss (Fig. 4.2b) and the Siglitz granitgneiss. These are overlain by garnet and chloritoid-bearing chlorite-muscovite schist (Fig. 4.2a, c). The Permian Wustkogel Formation is overlying in the Hüttwinkel valley outside the investigated area [*Pestal & Hellerschmidt-alber*, 2011]. Marbles of the Silbereck Group [Fig. 4.2d; *Pestal et al.*, 2009] which are the continuation of the "Angertal marble" in the Gastein valley follow. They have been deposited in Jurassic to Lower Cretaceous time. The uppermost lithostratigraphic unit present is the Brennkogel Formation.

Romate monzosyenite gneiss ("Zentralgneis")

The Romate syenitegneis was mapped for the first time by *Angel and Staber* [1952]. It is a medium to coarse-grained, white and black spotted orthogneiss (Fig. 4.2b). Less deformed types show rectangular dark green patches with biotite, whitish K-feldspat phenocrysts up to 3 cm in diameter, whitish plagioclase and minor greyish quartz. With increasing deformation a flaser texture develops.

Siglitz granitegneiss ("Zentralgneis")

According to *Exner* [1949; 1957] the Siglitz orthogneiss is a leucocratic and fine to medium-grained Augen gneiss. It is rich in plagioclase and on the schistosity planes muscovite and minor flakes of biotite and chlorite occur. The feldspar augen are a few millimeters in size and consist of twinned albite, which developed from K-feldspar. The Siglitz granitgneiss does not appear in the investigated area.

Post-Variscan cover

In the mapped area the Siglitz and Romate orthogneiss are covered everywhere by silvery to greenish garnet and chloritoid-bearing chlorite-muscovite schist attributed as a Permian and therefore post-Variscan cover (Fig. 4.2a, c). When there is a stratigraphic contact the garnet and chloritoid-bearing chlorite-muscovite schist are overlain by Mesozoic rocks. This is the case between Mallnitz in the southeast and the Niedersachsenhaus in the northwest. In the area of Kolm-Saigurn a variegated rock series with garnet-bearing micaschists, dark grey micaschists, micaschists with biotite-porphyroblasts, greenschists, quartzitic gneisses is overlying. This rock series is interpreted as a shear zone including lithologies from the post-Variscan cover of the Romate Nappe, but also pre- and syn-Variscan metasediments of the Sonnblick Nappe which is following next in the succession.

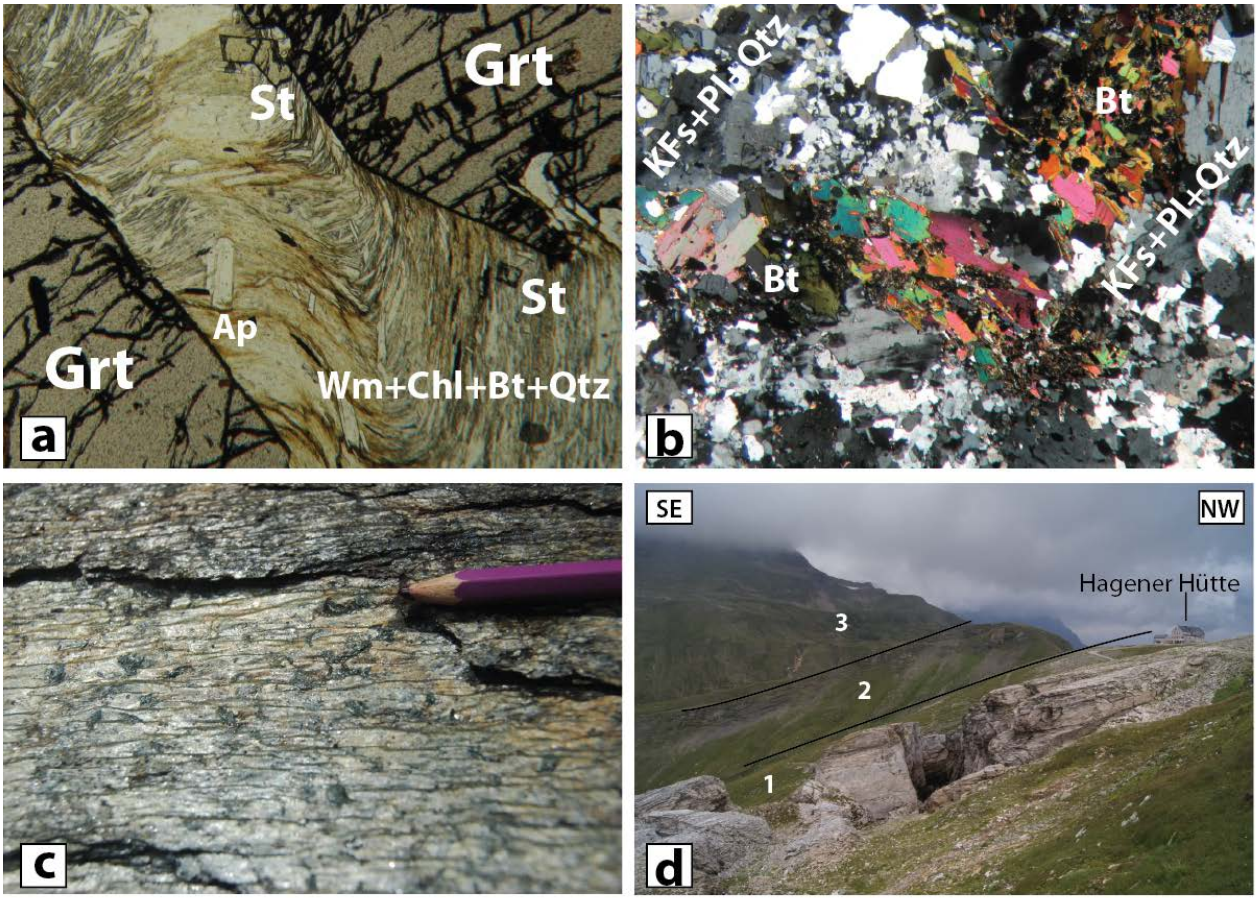

Figure 4.2: Romate unit (a) chloritoid-bearing chlorite-muscovite schist from the post-Variscan cover; (b) Romate monzosyenite gneiss; (c) Chloritoid-bearing chlorite-muscovite schist from the post-Variscan cover; (d) 1-Marble from the post-Variscan cover of the Romate Nappe, 2-Lower Glockner Nappe System, 3-Brennkogel Formation.

Marble (Silbereck Group, "Angertal Marble"; Upper Jurassic to early Cretaceous)

In the Tauerntal and east of Mallnitz a rock series dominated by marbles is folded together with the post-Variscan cover of the Romate Nappe. At its base it comprises bright colored siliziclastic schists, impure quartzites and carbonatic schists. This series is just a few meters thick, except in the area around the Greilkopf (2.581 m) where it reaches up to 100 m in thickness. In the uppermost part, close to the Hagener hut marble layers several decimeters in thickness are intercalated and form the transition to the overlying massive marbles (Fig. 4.2d). The latter are usually whitish to greyish and thick-bedded (up to 1 meter). They contain white mica in a variable amount, but also pure whitish marble with a thickness of several meters are present. In some places deformed layers and boudins of grey and yellowish weathering dolomite have been recognized. Further, at the cliff 200 m northwest of the Laschghütte in the Tauerntal kyanite-bearing grayish quartzites have been found as loose blocks. These quartzites may represent the Schwarzkopf Formation. A Sr-isotopic ratio of a pure whitish marble from an outcrop on the road up to the Jamnig hut yielded an 87Sr/86Sr ratio of 0.707721±3 (sample 11R33). Plotted on the Sr-seawater curve from *Mc Arthur et al*. [2001], it indicates a stratigraphic age in the Ladinian to Carnian or in the Upper Jurassic to early Cretaceous. Based on regional considerations the second possibility is supported (Fig. 4.3).

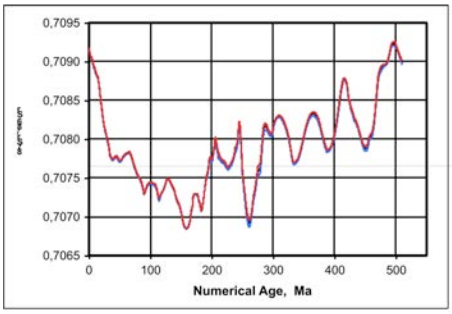

Figure 4.3: Sr-isotopic ratio of a pure whitish marble from an outcrop on the road near Jamnig hut yielded an 87Sr/86Sr ratio of 0.707721±3 (sample 11R33). Plotted on the Sr-seawater curve from *Mc Arthur et al.* [2001], it indicates a stratigraphic age Ladinian to Carnian or Upper Jurassic to early Cretaceous.

4.2.1.1.3. Sonnblick Nappe

The Sonnblick Nappe forms a NW–SE orientated domal structure, about 25 km long and 5 km broad, with a 25 km long and just about 100 m thick continuation towards SE.

This elongated part is the Sonnblick Lamellae. The Sonnblick Nappe is built up mostly by orthogneisses, covered by an old roof. The latter consists of paragneisses with intercalated amphibolites and overlying graphitic micaschists (Fig. 4.4a). Whereas the paragneisses and amphibolites (Fig. 4.4b) occur everywhere on top of the orthogneisses, the graphitic micaschists appear just locally, for example on the southern side of the Schareck. The top of the Sonnblick Nappe is marked by a shear zone composed of variegated lithologies including Permomesozoic metasediments. However, no Permomesozoic metasediments with a transgressive contact to the old roof have been found until now.

Sonnblick Augengneiss

Three different types of orthogneisses with crosscutting relationships can be distinguished macroscopically in the Sonnblick Nappe: The oldest is fine-grained, greyish, because of a larger amount of biotite and contains rare and up to 2 cm large K-feldspar phenocrysts. The main type, forming more than 95 % of the whole body is a leucocratic granitic augengneiss (Fig. 4.4a, c). Both are cut by aplitic dykes. Outcrops with cross-cutting relationships can be studied to the south of the Schareck and northeast of the Sonnblick peaks.

Old roof (“Altes Dach” – “Neubau Nappe”)

In general the pre-Variscan metasediments of the old roof comprise paragneisses, micaschists, amphibolites and quartzites. However, in detail within the Sonnblick Nappe lots of different and heterogeneous lithologies can be subdivided based on the structural imprint and various retrograde overprints. On the north-western side of the Sonnblick Dome, near Himmelbauer homogeneous fine-grained to very finegrained, dark grey and brownish paragneisses are present. Sometimes they contain larger amounts of chlorite. This lithology breaks in thin slices. On the exposed surface thin discontinuous layer of iron oxides occur. In contact with these paragneisses, an amphibole-bearing schist with 20–30 % of amphibole in a matrix composed by muscovite, biotite and quartz has been found. The amphiboles are up to 3 mm in size (Fig. 4.4b). In several places white to greyish, muscovite-rich quartzites breaking in coarse tabular slices are present.

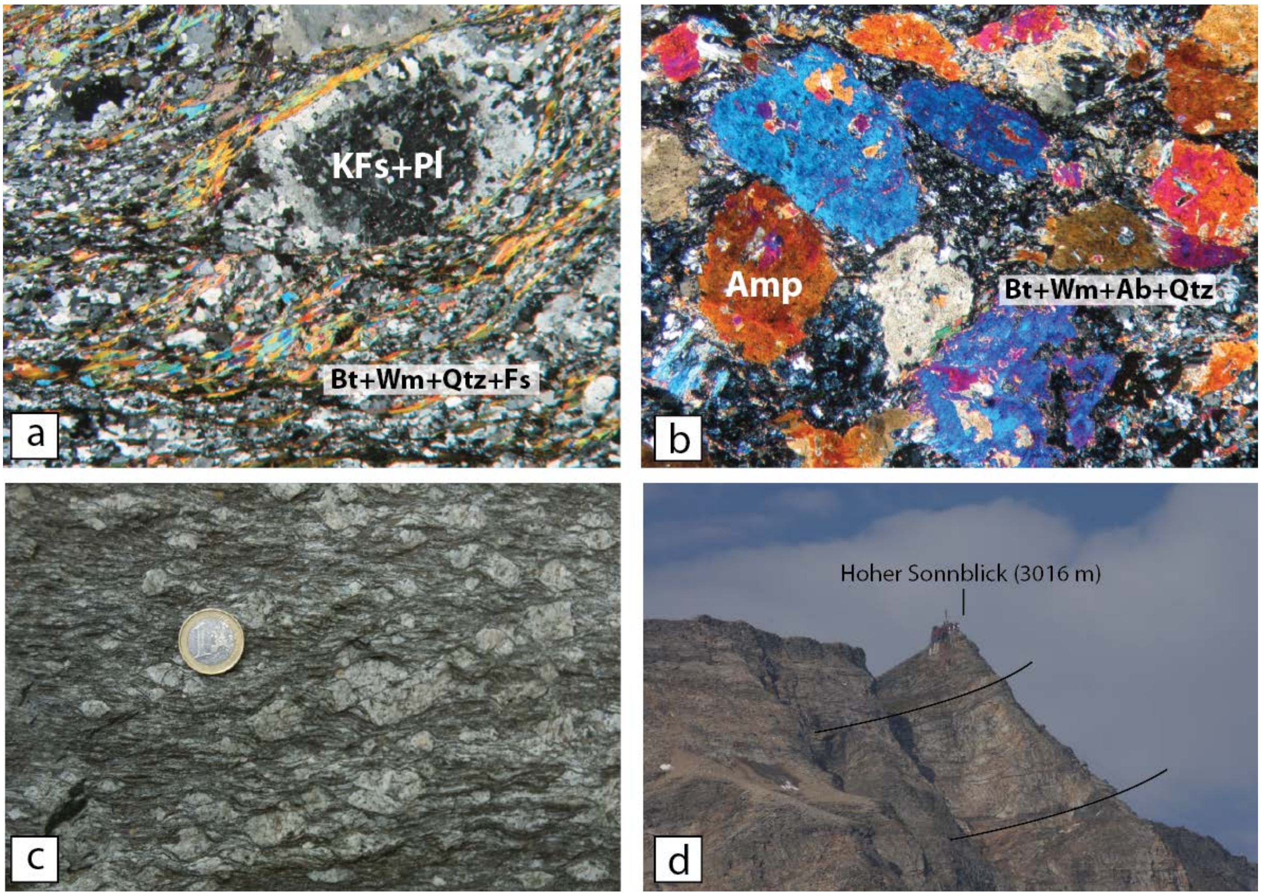

Figure 4.4: Sonnblick Subdome (a) Sonnblick augengneiss; (b) Amphibolite from the Sonnblick Old Roof; (c) Sonnblick Lamellae; (d) Overturned limb, nortern rim of the Sonnblick Subdome: augengneiss lies above the Old Roof paragneisses.

Further to the northwest, close to the Zedelnig (2.330 m) and the Biwak hut at Feldseescharte (2.714 m) paragneisses with amphibolite lenses are frequent. Characteristic is a layered series of quartzitic gneisses, quartzites and partly boudinaged amphibolites). The individual layers are several centimeters up to a few meters thick. South of the Schareck (3.123 m) close to Eisseehaus an old roof similar to Feldseescharte (2.714 m) is overlain by dark grey graphitic micaschists crosscut by some granitic dikes (Fig. 4.4d).

4.2.1.2 Modereck Nappe System

The Modereck Nappe System in the area southwest of the Sonnblick Dome is subdivided in several nappes and slices: Trogereck Lamelle, Rotewand-Seidlwinkl Nappe and Schuppen Zone [*Pestal & Hellerschmidt-Alber*, 2011]. In the Mallnitz Synform an element of this nappe system is present between two elements of the Glockner Nappe System, but its correlation to the tectonic elements in the southwest is not totally clear. In the following paragraphs the lithological content of the Modereck Nappe System in the Mallnitz Synform is described.

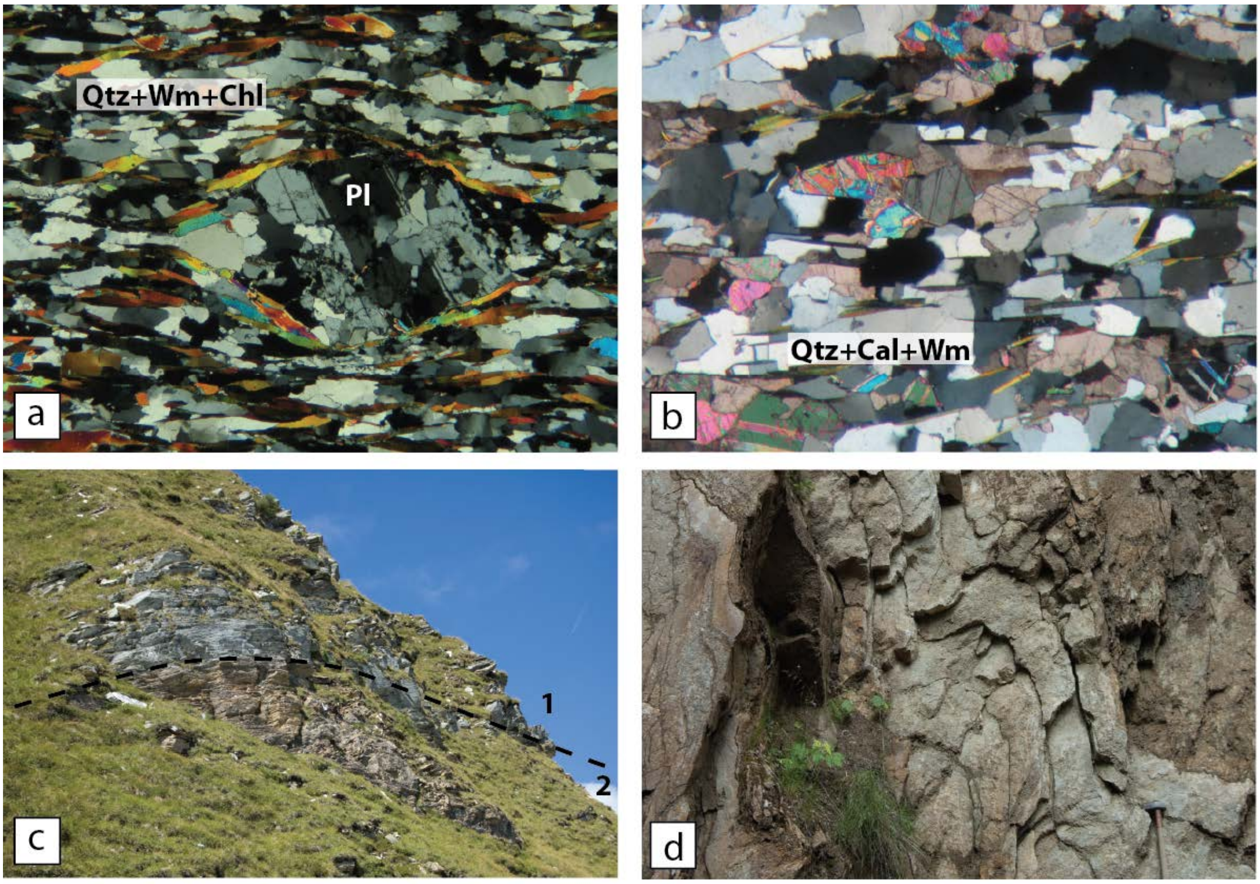

Figure 4.5: Modereck Nappe System (a) Wustkogel Formation; (b) layers of metabreccies with components of yellowish or greyish marbles occuring inside the Piffkar Quartzite; (c) Boundary between Seidelwinkel (2) and Piffkar (1) formations; (d) folded Brennkogel Quartzite.

Wustkogel Formation (Permian–Lower Triassic)

The Wustkogel Formation mainly consists of greyish to greenish paragneisses with whitish albite porphyroclasts, which developed from arkoses (Fig. 4.5a). The rocks show a layering with greenish phengite-rich and greyish quartz-rich layers. When highly deformed, the albite porphyroclasts form ribbons. In contact with these lithologies, white mica-rich schist with small pyrites, leaving yellowish dots on the weathered surfaces have been found. The uppermost part consists of thin bedded, greenish quartzites (Lantschfeld quartzite). In the investigated area these rocks were found only in the gorge 500 m south of the Häusleralm near to Mallnitz. In thin section sometimes grains of detrital magmatic biotite are visible. Mostly, they are transformed in chlorite, whereby rutile exolutions developed.

Quartz shows a shape preferred orientation. Mineral content is: quartz, albite-plagioclase, phengite and chlorite. Accessory minerals are opaque ore and epidote.

Seidelwinkel Formation (Middle Triassic)

At the type locality in the Seidelwinkel valley, the Seidelwinkel Formation consists of dark grey calcitic marbles, turning into bright colored dolomites and yellowish rauhwacke. In contrast, within the investigated area these carbonatic rocks occur just as dissected slices. Homogeneous mica-free marble is present in different colours: Often it is whitish, but sometimes it can be pinkish or greyish. Usually, it is without mica, but it also has been found micarich when it is highly deformed and sheared together with mica-bearing rocks. Further, there are whitish dolomites with a typical yellowish weathering colour and coarse cellular, yellowish “cargneules”. The largest outcrops of marbles occur on the crest between Häusleralm and Lonzaköpfl (2.317 m, Fig. 4.5c). Sheared marbles together with quartzites of the Piffkar Formation and other lithologies are present in the southwestern limb of the Mallnitz Synform, e.g., at the crest between Törlkopf (2.517 m) and Reßeck (2.498 m).

Piffkar Formation (Upper Triassic)

Whitish, thick-bedded quartzite (called also Keuper quartzites) with some muscovite is the most frequent lithology of the Pfiffkar Formation occurring in the mapped area. The quartzite breaks in decimeter to centimeter sized blocks or tabular sheets. Often they are intercalated with silvery mica- and quartz-rich schist and dark, carbonatefree schist. Frequently, these schists contain dark spots of chloritoid. On the south-easter slopes of the Kaponig some layers of metabreccies with components of yellowish or greyish marbles occur (Fig. 4.5b). The layers are up to 1 m thick and the size of the components is up to 10 cm. The sequence of the Piffkar Formation reaches locally up to hundred meters. However, most probable this thickness is due to isoclinal folding. In thin sections the rocks exhibit a foliation and a crenulation. Grain-size of the minerals is up to 1 mm. Quartz is undulous and shows dynamic recrystallization by subgrain rotation and grain boundary migration. There is just one generation of slightly undulous white mica present. The following minerals can be recognized: quartz muscovite and minor plagioclase. Accessory opaque ore is present and as alterations carbonate and iron hydroxides can be found.

Schwarzkopf Formation (Lower Jurassic, “Lias”)

Black, thin laminated phyllite intercalated with dark grey quartzite in beds with 5–6 cm thickness. Within these quartzites needles of kyanite up to 2 cm long may occur. In the Mallnitz area this lithologies have been found only 200 m south of the Häusleralm. In the Tauerntal kyanite-bearing, greyish quartzites occur as loose blocks at the cliff (1.900 m) 200 m northwest of Laschghütte.

Brennkogel Formation (Upper Jurassic to Cretaceous)

The Brennkogel Formation comprises dark greyishbrownish schist with layers of flyschoid quartzites (Fig. 4.5d). The schists are rich in fine-grained white mica with a greyish colour due to a larger amount of graphitic pigment. A low amount of carbonate varies in the individual layers. Typical are reddish-brown iron-oxide dots. Locally, black chloritoid or albite porphyroblasts are present. In thin sections the following minerals occur within the Brennkogel schist: quartz, muscovite, plagioclase; accessory: calcite, iron-oxide, apatite and chloritoid. Garnet is present in some places, e.g. in the basal part of the Brennkogel Formation between Neubau hut and Niedersachsenhaus. The quartzites are usually porous due to dissolution of calcite components, reddish, yellowish or whitish depending on the amount of oxides and thin-bedded (from 3 to 30 cm). They form layers up to a few meters in thickness. In general, the amount and thickness of the quartzite layers increases upwards within the rock column. In the Kaponig valley and along the old Railroad trail track not more than one meter thick zones of actinolite and talc-bearing schists occur within the Brennkogel Formation. They are interpreted as shear zones including material of the nearby ophiolites from the Penninic nappes.

4.2.2 Penninic nappes

The Penninic nappes derived from the Penninic Ocean (Alpine Tethys Ocean) which opened in the Middle Jurassic and was closed in the Paleogene. According to *Schmid et al*. [2004] the Penninic nappes can be subdivided into Lower, Middle and Upper Penninic nappes. In the investigated area the Matrei Zone is part of the Upper Penninic nappes. It just forms highly sheared slices which cannot be separated exactly from the underlying Glockner Nappe System. The Glockner Nappe System is attributed to the Lower Penninic nappes.

4.2.2.1. Glockner Nappe System

The Glockner Nappe System mainly consists of calcareous micaschist of the Jurassic to Cretaceous Bundeschiefer Group and ophiolite slices including amphibolite, prasinite and serpentinite. Its peleogeographic position is attributed to the Valais Ocean [*Schmid et al*., 2004]. In the area of the Mallnitz synform we subdivided the Glockner Nappe System in two nappes: the tectonically lower Kolm Nappe and the upper Geißel Nappe. West and north of the Sonnblick Dome at least three elements of the Glockner Nappe System are present according to the manuscript of ÖK 154 Rauris [*Pestal & Hellerschmidt-Alber*, 2011]. The most important are the Glockner Nappe and the tectonically higher Rauris Nappe. These nappes exhibit typical rock associations: The Glockner Nappe is characterized by the “Glockner facies” with larger ophiolite bodies, including serpentinites, prasenites and greenschists. In some places, pseudomorphs after lawsonite and eclogites indicate a high pressure imprint. In the Rauris Nappe with the “Fuscher facies” dykes of metagabbroic rocks are typical whereas large ophioloite bodies and indications for a high pressure imprint are missing.

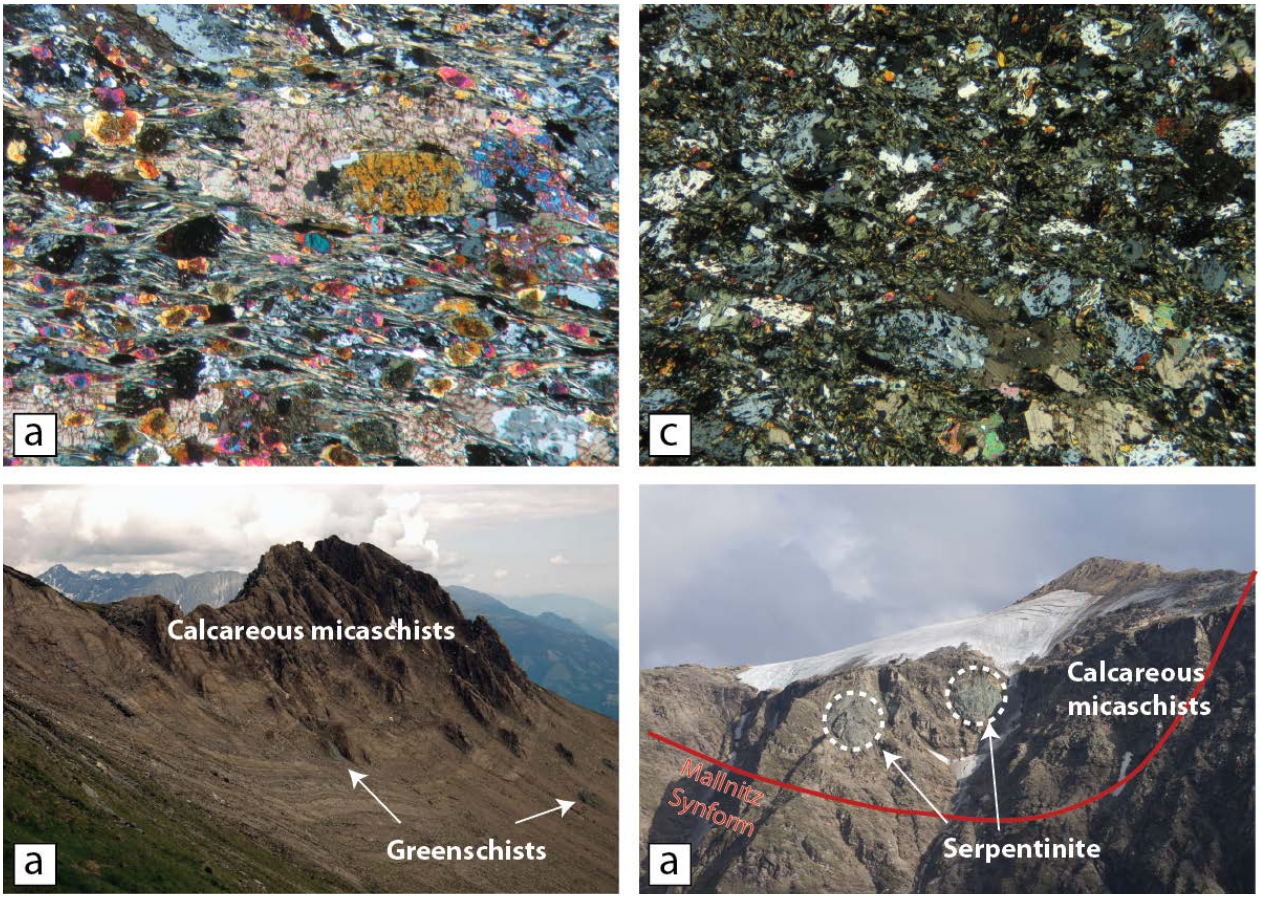

Figure 4.6: Glockner Nappe System (a) Amphibolite from the Kolm Nappe; (b) Greenschist from the Geißel Nappe; (c) Geißel Nappe looking toward the east at the Lönzakopfl (2.317 m); (d) Geißel Nappe looking toward the east at Schareck (3100 m).

Kolm Nappe

Typical lithologies of the Bundnerschiefer Group in the Kolm Nappe are grayish-bluish, thick-bedded, micabearing marbles intercalated with dark greyish to brownish calcareous micaschists. Large ophiolite bodies with prasenites, amphibolites and serpentinites occur at the Auernig (2.130 m) and all along the southwest dipping slopes of the Möll valley. For this reason the Kolm Nappe is characterized by the “Glockner facies”. Prasenites are massive greenish rocks with a high, but variable content of epidote together with amphibole, chlorite and albite. They are frequent at Auernig and built up the rock walls at the Törlkopf (2.446 m). The amphibolites are strongly foliated, fine-grained and greenish to blackish colored (Fig. 4.6a). They form blocks and tabular pieces. In thin section they look fresh, without evidences of a retrograde overprint and the mineral assemblage reflects peak metamorphic condition. The matrix consists of amphibole needles, plagioclase and minor quartz and titanite. Around epidote crystals Mg-rich chlorite with greyish interference colours and some amphiboles appear in pressure shadows. Bodies of dark green to blackish serpentinites occur between

Auernig and Törlkopf. A layer of schists with biotite and muscovite can be followed from the Törlkopf to the southern slopes of the Auernig. Chlorite-biotite schists occur as a more or less continuous layer with up to 15 m thickness between Kaponigwiesen and Hartlberg. Mainly, they consist of chlorite whereas biotite is present as individual black flakes or as elongated aggregates up to 2 cm in length.

Geißel Nappe

The Bündnerschiefer Group of the Geißel Nappe consists of calcareous micaschists with intercalated greenish chlorite-schist (Figs. 4.6b, c). Serpentinites are present as tiny bodies (Fig. 4.6d). The Geißel Nappe can be attributed to the "Fuscher Facies".The calcareous micaschists are rich in white mica and characterized by a yellowish to brownish weathering colour. Grey mica-bearing marbles are intercalated. During weathering fine-grained pieces are split of and forming brownish sand. The left rock walls are rounded, e.g., at the south-western slopes between Törlkopf (2.517 m) and Lonzaköpfl (2.317 m). The chlorite schists show nodules of albite porphyroblasts 1–3 mm in diameter. In thin sections a mineral assemblage with chlorite, albite and minor epidote, titanite and biotite is visible. Serpentinites are characterized by a grass-green weathering colour. Often they contain talc and up to 1 cm large ancerite crystals. They have been found south of Vorderer Geißelkopf (2.974 m), close to the old railway station of Obervellach and at Hartlberg.

Chapter 5: Bericht 2012 über geologische Aufnahmen auf den Blättern 154 Rauris und 181 Obervellach

Jahrbuch der Geologische Bundesanstalt, 152/1-4, pp. 265-268.

Silvia Favaro[1]

[1]Department of Earth Sciences, Freie Universität Berlin, Malteserstrasse 74-100, 12249 Berlin, Germany

ABSTRACT

The Mallnitz Synform is a structure affecting the Subpenninicand Penninic nappes in the eastern part of the Tauern Window (Salzburg/Carinthia, Austria, Fig. 5.1). This report describes the structure of the Malnitz synform along three sections. Two are located in the Sonnblick area close to Kolm-Saigurn (sheet 154 Rauris) and the third is situated close to Obervellach (sheet 181 Obervellach). The sections are based on structural investigations in combination with geological mapping of a larger area in scale 1:10.000 which is reported in *Favaro and Schuster* [2012].

The Tauern Window is the most prominent tectonic window of the Eastern Alps. Within Subpenninic derived from the European continental margin and Penninic nappes derived from the Alpine Tethys Ocean are exposed under the Austroalpine nappes. In the investigated area from bottom to the top the following tectonic is present [according to the tectonic nomenclature by *Schmid et al.*, 2004; *Pestal & Hellerschmidt-Alber*, 2011; *Schmid et al.*, 2013]:

- Hochalm Nappe (Venediger Nappe System of Subpenninic nappes).
- Romate Nappe (Venediger Nappe System of Subpenninic nappes).
- Sonnblick Nappe (Venediger Nappe System of Subpenninic nappes).
- Kolm Nappe (lower element of Glockner Nappe System of Penninic nappes).
- Modereck Nappe System (Subpenninic nappes).
- Geißel Nappe (upper element of Glockner Nappe System of Penninic nappes).

The Mallnitz Synform is a km-sized fold structure with a northwest-southeast trending fold axis. It affects mainly elements of the Glockner and Modereck nappe systems and has been interpreted as being the continuation of a stretching fault by *Kurz & Neubauer* [1996]. To the southwest of the Mallnitz Synform the Sonnblick Nappe is located, whereas to the northeast a nappe stack including the Hochalm and Romate nappes appears.

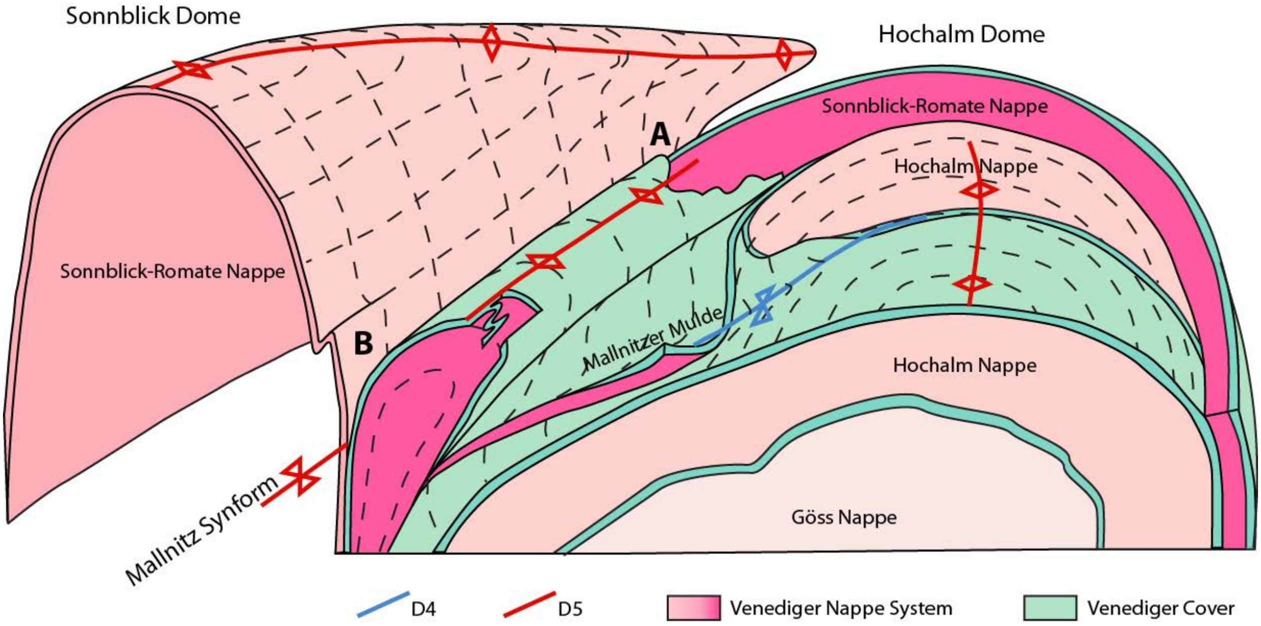

Figure 5.1: 3D model of the studied area. (A) location of the Rauris section; (B) location of the Obervellach-Kaponig Graben section.

According to *Favaro et al*. [EGU Abstracts, 2012] simplified deformation history within Tauern Window units starts with nappe stacking in the Penninic (D1 – D2) and Subpenninic nappes (D3), followed by duplex formation (D4), doming (D5 ductile) and brittle exhumation (D5 brittle). In this nomenclature the Mallnitz Synform is a D5 structure showing different structural domains along strike. In the northwest it is an open fold dominated by S2 – S3 foliations. Further to the south S2 –S3 dips to the northeast and it is cut by a SW dipping axial plane foliation S5. Intensity of S5 increases southeastward until it becomes the main foliation. In the lower nappes of the northeastern limb (Kolm and Romate nappes) SW–NE directed structures D4 are overprinted by D5. From Obervellach until Pusaritz, still within the Tauern Window, the synform is rotated and the southwestern limb dips to the northeast. In this area a sinistral shear bands pattern related to the ductile Katschberg Shear Zone System (D5) is present [*Scharf et al*., 2013a].

5.1 DESCRIPTION OF THE SECTIONS

In the following the structures and the lithostratigraphic succession of the two sections in the Rauris valley and the one close to Obervellach are described.

5.1.1 Sections in the Rauris valley

Along the profiles, between Niedersachsen Haus, Neuerkogel, Bockhartscharte and Neubau respectively, the Mallnitz Synform is highly asymmetric. From bottom to the top three different nappes built up the Mallnitz Synform:

- lower nappe of the Glockner Nappe System (Penninic nappes).

- element of the Modereck nappe System (Subpenninic nappes).
- upper nappe of the Glockner Nappe System that forms the core of the synform (Penninic nappes).

There are two possible interpretations of the tectonostratigraphy of the Mallnitz Synform in this area: there might be only one element of the Glockner Nappe System whereby the lower element is the inverted limb of the upper one, or there might be two nappes of the Glockner Nappe System. Accepting the first solution, this nappe could be connected with the crustal-scale, N-facing, sheath fold to the west of the Sonnblick Dome. This fold displays an isoclinals folding of the Modereck Nappe System and Glockner Nappe System and it brings the Glockner Nappe System into the inverted limb of an antiform whose core comprises the normal and inverse stratigraphic sequences of the Modereck Nappe System [*Kurz & Neubauer*, 1996]. The second solution connects the lower element of the Glockner Nappe System with the Kolm Nappe and the upper one with the Geißel Nappe, both outcropping in the Mallnitz area. Several arguments argue for the second possibility: directly at Mallnitz, the Kolm Nappe gets very thin, but can be traced as slices below the element of the Modereck Nappe System until the Hagener hut and further to the northwest. Also the lower nappe of the Glockner Nappe System in the Rauris valley is not more than few meters thick and highly sheared.
It consists of calcareous micaschists, mica bearing marbles and prasenites. Remarkably garnet is present in this unit, which is missing in the upper nappe. This indicates as lightly higher metamorphic grade in the lower element of the Glockner Nappe System than in the upper one. This reflects the situation in the Mallnitz area where also the Kolm Nappe shows a slightly higher metamorphic grade than the Geißel Nappe.

The element of the Modereck Nappe System consists mainly of the Brennkogel Formation. Additionally in the southwestern limb of the synform arkoses and whitish Brennkogel quartzites are intercalated. Further slices of whitish to grayish marble occur. These marbles might be interpreted as equivalents to the “Angertal marble” [*Pestal,* pers. com.], but the age and the tectonic position is still unclear.

At the base of the lower Glockner Nappe element, a layer with a mix of highly sheared lithologies is present. It consists of retrogressed amphibolites, calcareous micaschist, black schist and quartzites. This layer is interpreted as the roof thrust of the Venediger Nappe Duplex.

The structures within the Mallnitz Synform can be described as follows: In the northeastern limb only a single, almost horizontal or slightly southwest dipping foliation is present. In the core of the synform, where the upper element of the Glockner Nappe System occurs, an overprinting foliation can be identified. Both foliations diverge slightly in angle and create an intersection lineation striking approximately N130E. Further towards southwest an axial plane foliation appear and becomes more frequent until the southwestern limb is ending. This axial plane foliation dips approximately 200/25. The older foliation will have formed during nappe stacking event (D2 – D3), whereas the axial plane foliation is due to the doming event of the Sonnblick Nappe (D5).

Underneath the roof thrust a distinct lithological association occurs: a mix of bright colored, Qtz-rich gneisses intercalated with carbonate-bearing chlorite-schists, biotite- porphyroblasts schists and dark graphitic schist with albite-porphyroblasts crops out for several meters. This sequence is interpreted as the shear zone that developed between two horses during the duplex formation in the Venediger Nappe System (D4). In our case it divides the Sonnblick and the Romate nappes. The lithological association and the style of deformation support this interpretation: the lithological association reminds to highly hydrated lithologies of the old roof (paragneisses, amphibolites and dark micaschists) of the Venediger Nappe System. For what concerns the structures, in this shear zone two folding events can be recognized. The younger one, affecting the overall area, is the folding event due to the doming (D4). F4 fold axis always strikes approximately N140E, the folds are NE-verging and the orientation of the axial surfaces is orientated from recumbent to horizontal inclined. Features of an older deformational event are upright folds, with fold axis that turned from strike values of approximately N100E into the doming fold axis direction of N140E. The older fold axis and lineation formed during the duplex formation event (D4). They were re-aligned during the doming event (D5). The shear zone described above rests on the cover of the Romate Nappe below the northeastern limb of the Mallnitz Synform and on the old roof of the Sonnblick Dome below its southwestern limb. The post-Variscan cover of the Romate Nappe is very typical and can be found on top of the Romate orthogneiss in the whole area. It is greenish, bright colored garnet and chloritoid-bearing muscovite-chlorite schist. As the deformation event leading to the doming of the Sonnblick Nappe does not affect strongly the Romate Nappe several pre-doming structures are still preserved in the post-Variscan cover of the Romate Nappe. The strike of stretching and mineral lineation is scattering from N110E to N150E. The crenulation is mostly due to the doming event (D4) (strike around N140E), but sometimes also a N–S oriented crenulation has been found. It is associated with N–S oriented fold axis of kink bands. Shear bands are oriented N290E with a dip between 30 and 50 degrees.

Normal to the direction of the Mallnitz Synform a set of fractures filled by quartz occurs in the whole area. These veins are well known as they are gold-bearing (Golden Tauern).

5.1.2 Section Obervellach – Kaponig Graben

In the section close to Obervellach the Mallnitz Synform is much broader and shows a much more complicated internal structure than in the Rauris valley. According to mapping more than one synform and antiform is present and the whole structure is highly sheared. However, the internal part of the synform is again built up by three nappes:

- Kolm Nappe of the Glockner Nappe System (Penninic nappes).
- Element of the Modereck Nappe System (Subpenninic nappes).
- Geißel Nappe of the Glockner Nappe System that forms the core of the synform (Penninic nappes).

The Kolm Nappe is interpreted to be the lower nappe of the Glockner Nappe System. Typical lithologies are greyish- bluish, thick bedded, mica-bearing marble intercalated with dark, greyish, brownish calcareous mica schist of the Bündnerschiefer Group. Further large ophiolite bodies with prasenites, amphibolites and serpentinites occur. For this reason the Kolm Nappe is characterized by the "Glockner Facies". This lithological association is similar to that of the Glockner Nappe sensu stricto [*Pestal & Hellerschmidt-Alber*, 2011], but in contrast to the Glockner Nappe sensu stricto of the Glockner area, no relics of a high pressure imprint have been reported from the Kolm Nappe until now. The Geißel Nappe is interpreted to be the upper nappe of the Glockner Nappe System. It is different because of different primary lithologies and a weaker metamorphic imprint: The Bündnerschiefer Group of the Geißel Nappe consists of brownish calcareous micaschists with intercalated greenish chlorite schist with albite-porphyroblasts. Serpentinites are present just as tiny bodies. Therefore the Geißel Nappe can be attributed to the "Fuscher Facies" [*Pestal & Hellerschmidt-Alber*, 2011].

The Modereck Nappe System in between the Kolm and Geißel nappes shows the following units along the ridge between Häusleralm and Lonzaköpfl: Its lowermost part is built up by the Brennkogel Formation. Above some slices of Schwarzkopf Formation, Piffkar Formation and Wustkogel Formation occur. After a thick pile of Brennkogel Formation a sequence starting with Lower-Triassic quartzites (Lantschfeld quartzite), Seidelwinkel Formation, Piffkar Formation, Schwarzkopf Formation and Brennkogel Formation continues. It is not totally clear, but this succession can be interpreted as an isoclinally folded and contemporaneously sheared nappe. The lower part up to the Wustkogel Formation might be the inverted limb, whereas the succession starting with the Lower Triassic quartzites represents the upright limb. The Brennkogel Formation interval in between can be interpreted as an intercalated sheared slice.

Based on mapping the hinge of the synform coming from the Rauris valley continues within the Geißel Nappe to Lonzaköpfl and Lassacher Höhe. Here the synform is tight and the axial plane is dipping steeply towards southwest. Close to Mallnitz, at Auernig a second synform develops. It is open, the hinge is located in the Kolm Nappe and the axial plane is dipping parallel to that of the other synform.

Towards the south, this synform gets also narrower and intensely sheared. In this synform the Kolm Nappe is underlain by a thin tectonic zone including highly sheared lithologies of the Kolm Nappe, garnet and chloritoidbearing schists of the Romate Nappe and schists of the Brennkogel Formation from the underlying Hochalm Nappe. This zone represents the roof thrust on top of the Venediger Nappe System.

The antiform located between the two synformes is situated directly west of Mallnitz. On the path up to the Häusleralm (at 1.800 m altitude) amphibolites and calcareous micaschist of the Kolm Nappe are dipping below the element of the Modereck Nappe System. Further to the south the Kolm Nappe disappears, because the fold axis of the anticline is dipping towards southeast and it is truncated by a shear zone. Therefore the anticline affecting the Kolm and Romate nappes is visible only in the subsurface. The southwestern limb of the Mallnitz Synform shows different features: The Kolm Nappe is not present and the stratigraphy doesn´t follow a clear succession, because it is more sheared and folded. The southwestern limb is overturned and the Sonnblick Nappe is therefore overlying. The contact between the elements of the Glockner and Modereck Nappe systems with the Sonnblick Nappe is in most cases a shear zone dipping steeply toward the southwest and subparallel to the fault planes of the Mallnitz Synform. This shear zone is several meters wide and formed by mixed up lithologies of the bordering units. The Sonnblick Nappe forms an antiform with a southwest dipping axial plane, which gets narrower towards the southeast.

Also the structural inventory across the Mallnitz Synform is changing: In the northeastern limb of the synform at Auernig the foliation of the nappe stacking event (D2 – D3) is always visible. The foliation formed during the doming event (D5) occurs as an incipient axial plane foliation that infolds the nappe stacking foliation. The orientation of the axial plane foliation is approximately 220/40. A crenulation due to the doming event (D5) with southeast dipping fold axis is also present. As in the Rauris valley, the post-Variscan cover of the Romate Nappe is folded by axis perpendicular to those of the Mallnitz Synform. These folds are related to the D3 event.

In contrast, in the main part of the synform and on the southwestern limb the main foliation is a composed foliation formed during the nappe stacking event (D2 – D3) and the doming event (D5). In the more competent lithologies (e.g. quartzites of the Piffkar Formation) the nappe stacking foliation is still visible, but isoclinally folded. Both foliations are steep, almost vertical and parallel to each other (dipping of foliation c. 210/70-80).

Towards the southwest, south of Obervellach the Mallnitz Synform is rotated and the axial plane is dipping to the northeast (c. 040/30). Also the Sonnblick Nappe, forming a narrow lamella is rotated and dipping towards northeast. This rotation is pre-brittle deformation (D5) as brittle planes measured in the rotated and un-rotated part are fitting perfectly to the strike of the brittle Mölltal Fault. Along the slopes of the Möll valley an intense pattern of transpressive sinistral shear bands occurs within the nappes of the Glockner and Modereck Nappe System. This pattern is interpreted as the continuation of the Katschberg Shear Zone System that swings around the gneisses of the Hochalm dome in the southeastern corner of the Tauern Window [*Scharf et al.*, 2013a]. In contrast, the Sonnblick Lamellae disappears below the Austroalpine nappes.

Chapter 6: Grain-size effects on the closure temperature of white mica in a crustal-scale extensional shear zone – implications of in-situ $^{40}Ar/^{39}Ar$ laser-ablation of white mica for dating shearing and cooling (Tauern Window, Eastern Alps)

This chapter was published on 2 April 2016 to: **Tectonophysics, Volume 674, Pages 210–226**
DOI: 10.1016/j.tecto.2016.02.014;
Link: http://www.sciencedirect.com/science/article/pii/S0040195116001116

Andreas Scharf[1, 2, *], Mark R. Handy[1], Stefan M. Schmid[1, 3], Silvia Favaro[1], Masafumi Sudo[4], Ralf Schuster[5], Konrad Hammerschmidt[1]

[1] Department of Earth Sciences, Freie Universität Berlin, Malteserstrasse 74-100, 12249 Berlin, Germany

[2] Department of Earth Science, Sultan Qaboos University, P.O. Box 36, Al-Khoudh, P.C. 123, Muscat, Sultanate of Oman

[3] Institute of Geophysics, Eidgenössische Technische Hochschule (ETH), Sonneggstrasse 5, 8092 Zürich, Switzerland

[4] Institute of Earth and Environmental Science, Universität Potsdam, Karl-Liebknecht-Strasse 24-25, 14476 Potsdam-Golm, Germany

[5] Geologische Bundesanstalt, Neulinggasse 38, 1030 Wien, Austria

*Corresponding E-Mail: andreas.scharf@fu-berlin.de; Telephone: (+968) 2414 6846

Short title: Thermal evolution of a normal fault

ABSTRACT

In-situ $^{40}Ar/^{39}Ar$ laser ablation dating of white-mica grains was performed on samples from the footwall of a crustal-scale extensional fault (Katschberg Normal Fault; KNF) that accommodated eastward orogen-parallel displacement of Alpine orogenic crust in the eastern part of the Tauern Window. This dating yields predominantly cooling ages ranging from 31 to 13 Myr, with most ages clustering between 21 and 17 Myr. Folded white micas that predate the main Katschberg foliation yield, within error, the same ages as white-mica grains that overgrow this foliation. However, the absolute ages of both generations are older at the base (20 Myr) where their grain size is larger (300-500 µm), than at the top and adjacent to the hangingwall (17 Myr) of this shear zone where grain size is smaller (< 100-300 µm). This fining-upward trend of white-mica grain size within the KNF is associated with a reduction of the closure temperature from the base (~445°C) to the top (< 400°C) and explains the counter-intuitive trend of downward-increasing age of cooling in the footwall. The new data show that rapid cooling within the KNF of the eastern Tauern Window started sometime before 21 Myr according to the $^{40}Ar/^{39}Ar$ white-mica cooling ages and between 25-21 Myr according to the new Rb/Sr white-mica ages, i.e., shortly after the attainment of the thermal peak in the Tauern Window at ~25 Myr ago. These new data, combined with literature data, support earlier cooling in the eastern part of then Tauern Window than in the western part by some 3-5 Myr.

Keywords

Eastern Alps; ^{40}Ar/^{39}Ar laser ablation; closure temperature; orogen-parallel lateral extrusion; rapid exhumation/cooling

6.1 INTRODUCTION

Determining the timing of cooling of deeply buried basement rocks is crucial for evaluating the age and rates of exhumation in orogens and for understanding the mechanisms of exhumation, e.g., the relative importance of tectonic unroofing and erosional denudation [e.g., *Ring et al.*, 1999; *Reiners and Brandon*, 2006]. In the Alps, two Oligo-Miocene thermal domes (Lepontine Dome, Tauern Window; "L" and "T" in inset of Fig. 6.1) overprint an early Cenozoic nappe stack whose units derive from the accreted European lower plate of the Alpine orogen. Conventional thermochronology paired with petrological studies over the past four decades have shown that exhumation of both domes largely occurred in Miocene time [e.g., *Clark and Jäger*, 1969; *Wagner and Reimer*, 1972; *Selverstone*, 1988; *Grasemann and Mancktelow*, 1993; *Fügenschuh et al.*, 1997; *Neubauer et al.*, 1999; *Luth and Willingshofer*, 2008; *Campani et al.*, 2010; *Fox*, 2012]. However, recent in-situ dating reveals that cooling in the Tauern Window was heterogeneous and related to a combination of folding, extensional faulting and erosion [*Scharf et al.*, 2013a].

The Tauern Window comprises two main structural and metamorphic domes: the Western and Eastern Tauern domes (WTD, ETD; Fig. 6.1a). These expose post-nappe amphibolite-facies metamorphism in their cores and are flanked at either end by low-angle normal faults: the Brenner and Katschberg normal faults [BNF, KNF; *Selverstone*, 1988; *Behrmann*, 1988; *Genser and Neubauer*, 1989]. Most authors relate the exhumation of the basement nappes contained in these domes to the northward indentation of that part of the Adriatic Microplate located south of the Tauern Window and east of the Giudicarie Belt [*Scharf et al.*, 2013a and references cited therein]. This late-stage deformation in front of the indenter involved a combination of broadly coeval post-nappe folding, orogen-parallel extension and erosion [e.g., *Ratschbacher et al.*, 1991; *Fügenschuh et al.*, 1997; *Rosenberg et al.*, 2007; *Schmid et al.*, 2013]. However, distinguishing the relative contribution of these mechanisms has proved elusive. Compilations of the available thermochronometric data indicate that rapid exhumation (~1 mm/yr) and cooling [≤ 40°C/Myr; *Foeken et al.*, 2007] began and ended earlier in the eastern part of the Tauern Window than in the western part [e.g., *Luth and Willingshofer*, 2008; *Scharf et al.*, 2013a]. At first sight this is at odds with analogue models of Adriatic Microplate indentation in the Eastern Alps that predict synchronous exhumation of units in the entire Tauern Window [*Ratschbacher et al.*, 1991; *Rosenberg et al.*, 2007].

The amount and quality of data in the Tauern Window are not uniform. Exhumation and cooling of the western Tauern Window are fairly well constrained by thermochronometry and thermal modelling [e.g., *von Blanckenburg et al.*, 1989; *Genser et al.*, 1996; *Fügenschuh et al.*, 1997]. In contrast there is a relative dearth of such work in the east where past efforts [e.g., *Cliff et al.*, 1985; *Droop*, 1985; *Dunkl et al.*, 2003] have not been complemented by thermal modelling.

This paper presents new $^{40}Ar/^{39}Ar$ laser-ablation ages from white-mica aggregates and new Rb/Sr white-mica ages from the footwall of the KNF. After a brief introduction to the geological setting and methods, the in-situ age data are presented in their microstructural and metamorphic context. It is shown that the ages obtained do not vary with growth generation in the same sample, but with average size of the grains in the KNF. This pronounced grain-size dependence of the new $^{40}Ar/^{39}Ar$ laser-ablation ages is used to track the cooling history of the eastern Tauern Window during activity of the KNF. It is argued that cooling migrates from the base of a low-angle normal fault (445°C) towards the top, near the hangingwall (< 400°C). This cooling trend is best explained with the smaller grain-size of the white mica and, therefore lower closure temperature towards the top of the normal fault. Finally, a comparison of the cooling histories of the eastern and western parts of the Tauern Window discusses the implications for determining whether large-scale exhumation and cooling of orogenic crust was triggered during collision or later, during indentation of the Adriatic Microplate.

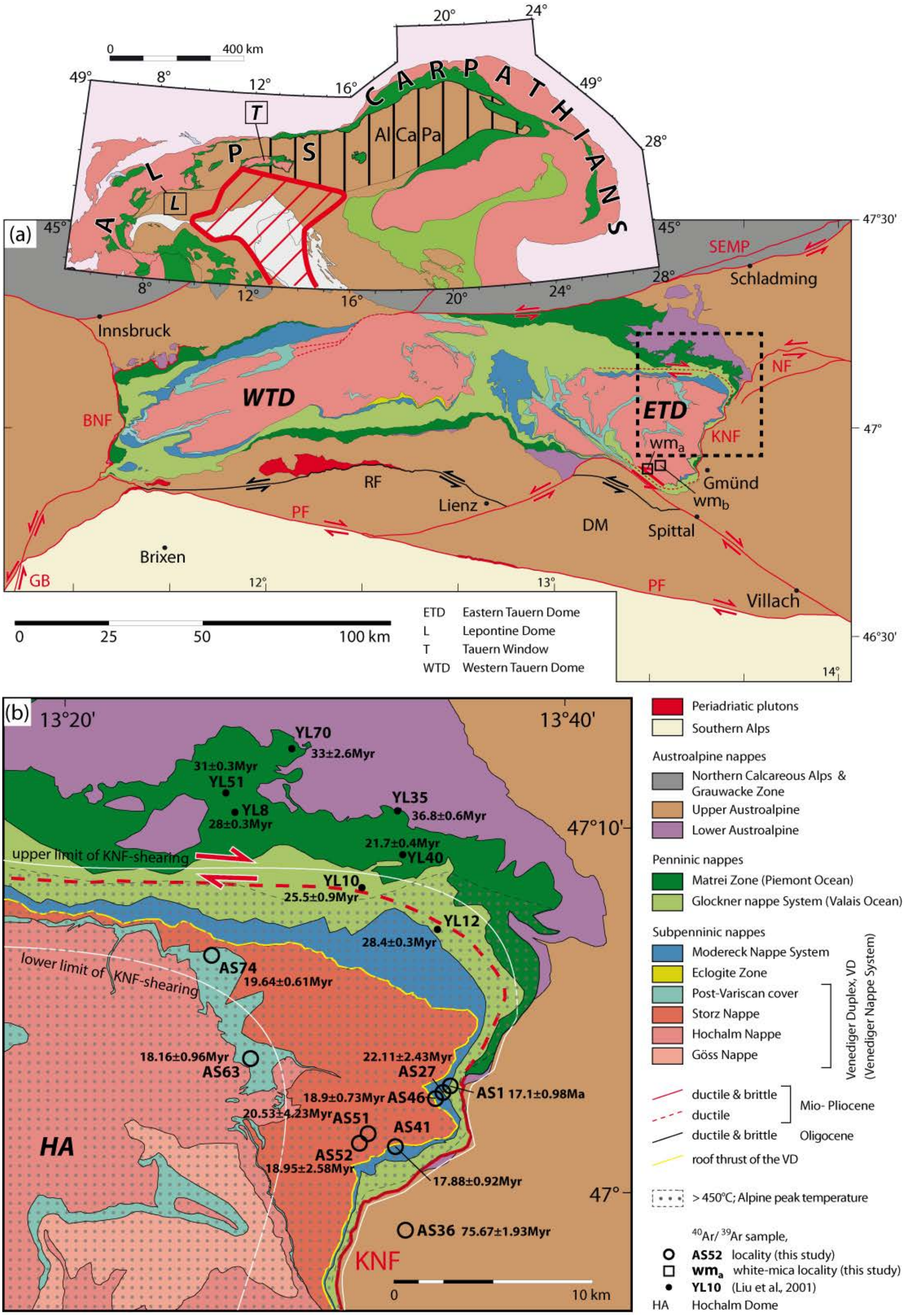

Figure 6.1: (a) Tectonic map of the Tauern Window with investigated area (box within dotted lines). BNF - Brenner Normal Fault; DM – Drau-Möll Block; GB - Giudicarie Belt; KNF - Katschberg Normal Fault; NF - Niedere Tauern Southern Fault; PF - Periadriatic Fault; RF – Rieserferner Block; SEMP - Salzach-Ennstal-Mariazell-Puchberg Fault. Inset map shows the Lepontine Dome (L) and the Tauern Window (T) within the

Alps-Carpathians Orogen with its major tectonic units derived from accreted and undeformed parts of the European continent (dark and bright red), Alpine Tethys and Neotethys (dark and light green) and accreted and autochthonous Adriatic continent (brown and light grey). The Adriatic indenter is framed by the red-striped area; AlCaPa – Alps-Carpathian-Pannonian part of accreted Adria that experienced lateral escape (vertical stripes); The sample names of the two white-mica samples wm_a and wm_b are 4R64 and 182/1/2005, respectively; (b) Tectonic map of the north-eastern margin of the Tauern Window showing the location and mean age with standard deviation of the nine samples collected for $^{40}Ar/^{39}Ar$ laser ablation of white mica. Yellow line - roof thrust of the Venediger Duplex with Alpine-peak temperatures > 450°C [*Scharf et al.*, 2013b]. White lines delimit upper and lower limits of KNF shearing. Maps modified from *Schmid et al.* [2004, 2008 & 2013].

6.2 GEOLOGICAL SETTING

6.2.1 Tectonic overview

The nappe stack exposed in the Tauern Window formed during convergence and collision of the Adriatic and European plates in late Cretaceous to Cenozoic time [e.g., *Trümpy*, 1960; *Frisch*, 1979; *Stampfli et al.*, 2001; *Schmid et al.*, 2004; *Handy et al.*, 2010]. From top to bottom, this nappe stack comprises oceanic (Penninic units: Matreier Zone and Glockner Nappe System) and Europe-derived (Subpenninic units: Modereck and Venediger nappe systems) crustal units, some of which experienced high-pressure subduction metamorphism prior to nappe stacking [*Kurz et al.*, 2008]. These units were refolded, imbricated and partly exhumed in Oligo-Miocene time before undergoing final exhumation during coeval doming and orogen-parallel extrusion of the entire orogenic edifice towards the Pannonian Basin [e.g., *Ratschbacher et al.*, 1991; *Royden*, 1993; *Decker et al.*, 1994; *Peresson and Decker*, 1997; *Frisch et al.*, 1998; *Scharf et al.*, 2013a; *Schmid et al.*, 2013]. The Austroalpine units surrounding and overlying this nappe stack represent an earlier orogenic wedge that formed in late Cretaceous time [Eo-Alpine Orogeny *Frank*, 1987; *Froitzheim et al.*, 1994, 2008; *Handy et al.*, 2010]. The base of this wedge that directly overlies the Penninic nappes shows latest Cretaceous to Cenozoic Rb/Sr and $^{40}Ar/^{39}Ar$ ages [*Brewer*, 1969; *Hawkesworth*, 1976; *Liu et al.*, 2001] and is highly retrogressed. The ETD and WTD (Fig. 6.1a) expose Subpenninic basement units that experienced upper greenschist- to amphibolite-facies Barrovian-type thermal overprinting [the so-called “Tauernkristallisation”; *Sander*, 1911] at 30-28 Myr [*Inger and Cliff*, 1994; *Thöni*, 1999; *Kurz et al.*, 2008]. This thermal event may have lasted until 25 Myr according to new Sm/Nd ages of garnets from the WTD [*Pollington and Baxter*, 2010] and ETD [*Favaro et al.*, 2015], and it overprinted a duplex system within the Europe-derived basement rocks [Venediger Duplex; *Lammerer and Weger*, 1998; *Scharf et al.*, 2013a; *Schmid et al.*, 2013].

Subsequent to this thermal overprint both Tauern domes were sheared, especially near their margins, i.e., adjacent to the overlying Austroalpine units, during final unroofing and exhumation in latest Oligocene to early Miocene time [e.g., *Fügenschuh et al.*, 1997; *Scharf et al.*, 2013a; *Schmid et al.*, 2013]. The Southern Alps, located south of the Periadriatic Fault and east of the Giudicarie Belt (PF and GB; Fig. 6.1a), were unaffected by Alpine metamorphism and represent the Adriatic Microplate

Indenter in map view [*Rosenberg et al.*, 2007]. The leading edge of this indenter also included Austroalpine units north of the Periadriatic Fault and south of the Tauern Window that show little or no ductile overprint and behaved as rigid blocks during indentation [*Scharf et al.*, 2013a].

The KNF as first described by *Genser and Neubauer* [1989] is a 5 to 10 km thick mylonite belt which is overprinted by cataclasites developed towards the hangingwall [Fig. 6.1b; see *Scharf et al.*, 2013a and *Schmid et al.*, 2013 for further details]. The lower limit of this mylonite belt is defined by the transition from gneisses of the Venediger Nappe Complex below to a pervasive mylonitic fabric carrying a E to ESE-plunging stretching lineation within the KNF. The top of the KNF comprises 100-200 meters of greenschist facies mylonite capped by cataclasites that also affect basal Austroalpine units along the eastern margin of the KNF [Fig. 6.1b; *Scharf et al.*, 2013a].

6.2.2 Samples and their locations

Seven samples were collected from the KNF along the north-eastern margin of the Tauern Window (see Fig. 6.1b, Table 6.1 & Supplementary material 6.1.A for exact locations, lithologies and tectonic units). The main foliation in these samples is oriented parallel to the macroscopic shearing plane of the KNF and is therefore assumed to have been active during orogen-parallel extensional exhumation. The protoliths of these samples comprise basement gneiss of the Venediger Nappe System and its cover, basement gneiss of the Modereck Nappe System, as well as calc-schists and metapelites of the Glockner Nappe System. Two additional samples, AS36 and AS63, are from above (hangingwall) and below (footwall) the KNF, respectively. The sample from below is a paragneiss of the post-Variscan cover from the Venediger Nappe System, whereas the sample from above is a paragneiss of the Radenthein Complex belonging to the Koralpe-Wölz Nappe System of the Upper Austroalpine Unit. The ages of the white-mica grains from the seven KNF samples are expected either to date cooling to below a grain-size dependent closure temperature, or alternatively, to date white-mica formation [see review of *Villa*, 2010].

6.3 METHODS

6.3.1 Sample preparation for ^{40}Ar/^{39}Ar and Rb/Sr dating

The ^{40}Ar/^{39}Ar in-situ laser ablation technique [e.g., *Kelley et al.*, 1994] was combined with micro-structural investigations of grain aggregates and single grains to constrain the tectono-thermal history of the eastern Tauern Window. Microprobe-quality polished samples 1 mm thick and with a diameter of 7 mm were drilled from the samples oriented parallel to the stretching lineation and perpendicular to the main foliation of the KNF.

Prior to laser ablation, samples were investigated with an electron microprobe (JEOL JXA-8200 at the Freie Universität Berlin) to determine the relationship, if any, of mineral chemistry to microstructural position. After electron microprobe analysis, carbon-coating of the sample surface was removed by polishing. The nine samples were wrapped in commercial grade Al foil, loaded into the 99.999% pure

Al container, then sent for neutron activation to the *Nuclear Research and consultancy Group* (NRG) reactor in Petten, Netherlands. There, the Al container was wrapped in a 0.5 mm thick Cd foil. Irradiation with fast neutrons (neutron flux of ~1.1×10^{13} n cm^{-2} s) was performed for 10 h. Fish Canyon Tuff sanidine [27.5 Myr; *Uto et al.*, 1997; *Ishizuka*, 1998] was the neutron flux-monitoring mineral used for calculating J-values.

Two months later, the samples were returned and analysed at the ^{40}Ar/^{39}Ar laboratory of the Universität Potsdam using the same system and conditions as described in *Wiederkehr et al.* [2009], *Schneider et al.* [2013] and *Halama et al.* [2014]. The Nd-YAG UV pulse laser (New Wave © Gantry Dual Wave laser ablation systems) with a maximal energy of 6 mJ and a wavelength of 266 nm was used for extracting Ar gas from the samples. Sample gas was cleaned with SAES © getters and cold trap (≤ -114°C) in the ultrahigh-vacuum purification line. After 10 min of purification by the getters and the trap, the sample gas was released on-line to the noble gas mass spectrometer (Micromass © 5400). Ages and errors were calculated according to *Uto et al.* [1997].

A total of 87 spot measurements were made on white micas from nine samples. Each measurement involved the following procedure: (1) analysis of a blank (b_1), (2) three measurements of a sample; (3) measurement of a second blank (b_2). In this way, the first sample was corrected by the first blank (b_1), the third sample by the second blank (b_2) and the second sample by a mean value of the two blanks ($[b_1 + b_2]/2$). Typical blanks for 84% of all unknown analyses of this time were 0.0001 to 0.0002 Volts for ^{40}Ar which roughly corresponds to 2-4x10^{-12} cm^3 STP (standard temperature and pressure) with our typical sensitivity (2x10^{-8} cm^3/Volts). For ^{39}Ar, ^{38}Ar and ^{37}Ar, < 2x10^{-7} Volts, thus < 4x10^{-15} cm^3 STP, and for ^{36}Ar, < 5x10^{-7} Volts, thus < 1x10^{-15} cm^3 STP, respectively. Total ^{40}Ar intensities at unknown analysis ranged from 0.0004 to 0.005 Volts were mostly ~0.001 Volts. Therefore, the ratios of total intensity/blank of 5 to 10 were kept through the analyses.

The laser-beam size used was 75 µm. The length of laser ablation on the sample surface depended on the size and orientation of the grain (parallel or perpendicular to main foliation, shear bands); for one big grain, the total length of the laser ablation was 1000-1500 µm, whereas for smaller grains the laser ablation was divided into several (up to six) segments.

Mechanical preparations for Rb/Sr isotope analyses were performed at the Geological Survey of Austria in Vienna. Before starting the separation procedure weathered surfaces were removed from the sample material. Minerals were separated by standard methods of crushing, grinding, sieving and magnetic separations. Mass of samples used for dissolution were ~100 mg for whole-rock powder, ~200 mg for white mica. Chemical preparations were performed at the Geological Survey of Austria in Vienna and at the Department of Lithospheric Research at the University of Vienna following the procedure described by *Sölva et al.* [2005]. Element concentrations were determined by isotope dilution using mixed Rb/Sr spikes. Total procedural blanks are ≤ 1ng for Rb and Sr.

Isotopic measurements were made at the Department of Geological Sciences at the University of Vienna. Rb ratios were measured at a Finnigan® MAT 262, whereas Sr ratios were analyzed with a

ThermoFinnigan® Triton MC-TIMS. Sr was run from Re double filaments, whereas Rb was evaporated from Ta single filaments. During measurements, the NBS987 standard yielded $^{86}Sr/^{87}Sr$ = 0.710253 ± 4 2Sd(m) (n = 15) on the Triton TI. Errors for the $^{87}Rb/^{86}Sr$ ratios are ± 1% based on iterative sample analysis and spike recalibration. Ages were calculated using the ISOPLOT/Ex software [*Ludwig*, 2001, 2003] and a Rb-decay constant of 1.42 x 10^{11}/yr.

6.4 MICROSTRUCTURES, METAMORPHISM and GEOCHEMISTRY

6.4.1 Microstructures

All seven samples from the KNF (sample AS1, AS27, AS41, AS46, AS51, AS52 and AS74; Fig. 6.1b) have matrix minerals that underwent dynamic recrystallization (white mica, quartz ± albite ± calcite ± chlorite). Samples near the top of the KNF, i.e., near the hangingwall, preserve quartz grains with arcuate and lobate grain boundaries that are diagnostic of fast grain-boundary-migration recrystallization (parts of AS1, AS27 and AS46). Samples near the base of the KNF show late-stage static recrystallization of quartz and albite aggregates, and fast migration in quartz aggregates (parts of AS1, AS41, AS52, AS52 and AS74). The two samples from below the footwall (AS63) and above the hangingwall of the KNF (AS36) show annealed quartz (120° grain boundaries), albite and white mica [*Scharf et al.*, 2013a].
A combination of optical microscopy and Scanning Electron Microscope (SEM) mapping allows five different types of white-mica grains to be distinguished (Figs. 6.2, 6.3 & Table 6.1).

(1) Folded white micas (Wm_1) occur between domains of white micas that define the main foliation (Wm_2) and are interpreted to have formed prior to or during the activity of the KNF (see central parts of Figs. 6.2a, 6.3a &Table 6.1). In Fig. 6.2a, the trace of the folded Wm_1 grains defining the S_1 foliation is indicated by the yellow line.

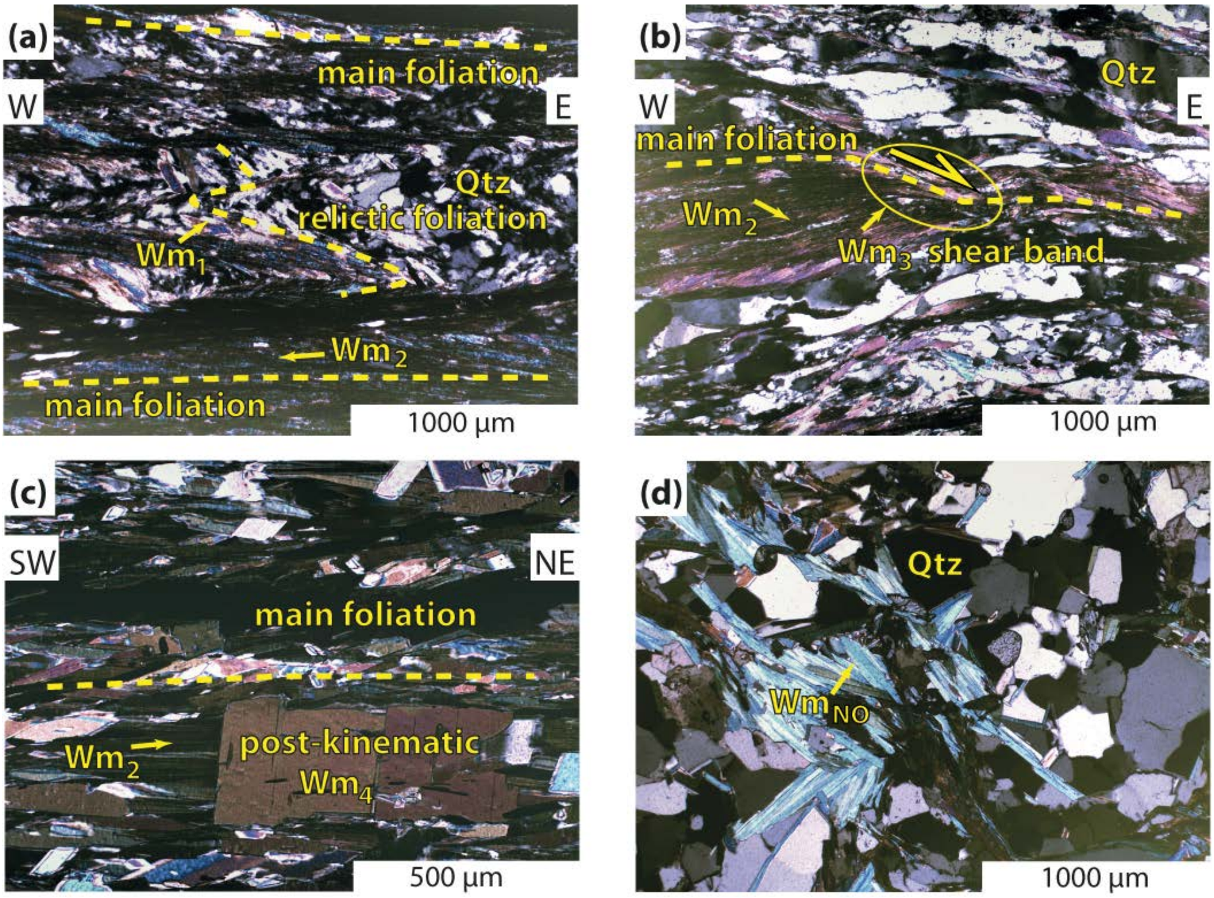

Figure 6.2: Typical optical microstructures of white mica. (a) Wm$_2$ grains define the KNF main foliation while folded Wm$_1$ grains in the central part of the micrograph are relicts of an earlier schistosity (sample AS1); (b) Post-kinematic Wm$_4$ overgrows Wm$_2$ defining the main KNF foliation (sample AS74); (c) Wm$_3$ shear bands deform Wm$_2$ (sample AS41); (d) Wm$_{NO}$ lacks a preferred orientation in a fabric domain unaffected by KNF shearing (sample AS63). All photos taken with crossed nichols.

(2) White-mica grains (Wm$_2$) define the main mylonitic foliation (S$_2$) of the KNF, and are not folded. They are interpreted to have grown during activity of the KNF, although we cannot rule out the possibility that some of them grew prior to the KNF and were subsequently rotated into the macroscopic shearing plane of this normal fault (Figs. 6.2a-c, 6.3a-c and 6.3e-f & Table 6.1). Note that the axial planes of the folds affecting S$_1$ are parallel to the main foliation (S$_2$), suggesting that these are F$_2$ folds. These microstructural relations show clearly that Wm$_1$ and Wm$_2$ grains belong to different growth generations and deformation phases. Although samples AS27 and AS52 contain one domain of white mica only (Wm$_2$), a significant difference in individual white-mica ages can be discerned (see section 6.6.3 for further discussion).

(3) Wm$_3$ grains are oriented parallel to, and indeed define, the shear bands associated with the main foliation (S$_2$) of the KNF. Near the ends of these shear bands, the Wm$_3$ grains bend into concordance with the main foliation (S$_2$). Based on these microstructural criteria [e.g., *Simpson and Schmid*, 1983; *Lister and Snoke*, 1984], the Wm$_3$ grains are therefore interpreted to have formed coevally with the

Wm_2 grains and thus with KNF shearing (Figs. 6.2c, 6.3c & Table 6.1). In contrast to Wm_1 grains, the Wm_2 and Wm_3 grains formed during a single, progressive shearing event. It is very unlikely that S_1 and S_2 formed during one progressive deformational event: first, S_1 does not bend into the S_2 shearing plane as would be expected if the white-mica growth was continuous during progressive non-coaxial shearing and second, the vergence of F_2 folds is not consistent with the top-E to –SE sense of S_2 shear for the KNF.

(4) Wm_4 grains are isometric and oriented with their cleavage oblique to all structures, as seen by the sharp and large angle of discordance between the cleavage surfaces of Wm_2 and Wm_4 grains (Figs. 6.2b & 6.3b). In addition, the Wm_4 grains are not oriented parallel to any macroscopic structures, including the KNF. The Wm_4 grains are therefore interpreted to have grown post-kinematically (Wm_4; Figs. 6.2b, 6.3b & Table 6.1).

(5) White micas with no preferred orientation (Wm_{NO}) are found in samples from above (sample AS36) and below the KNF (sample AS63). Associated quartz microstructures are characterized by 120° grain boundaries, indicative of annealing (Figs. 6.2d, 6.3d & Table 6.1). The age of the Wm_{NO} grains with respect to the Wm_1 to Wm_4 grains is unknown; white micas in the hangingwall of the KNF are probably older and related to late Cretaceous post-kinematic cooling of Austroalpine nappe units [*Schuster et al.*, 2004, 2006; *Schmid et al.*, 2013]. In contrast, the random orientation of Wm_{NO} grains in the footwall of the KNF does not indicate whether they grew before, during or even after activity of the KNF. This point is discussed below in the light of the age data.

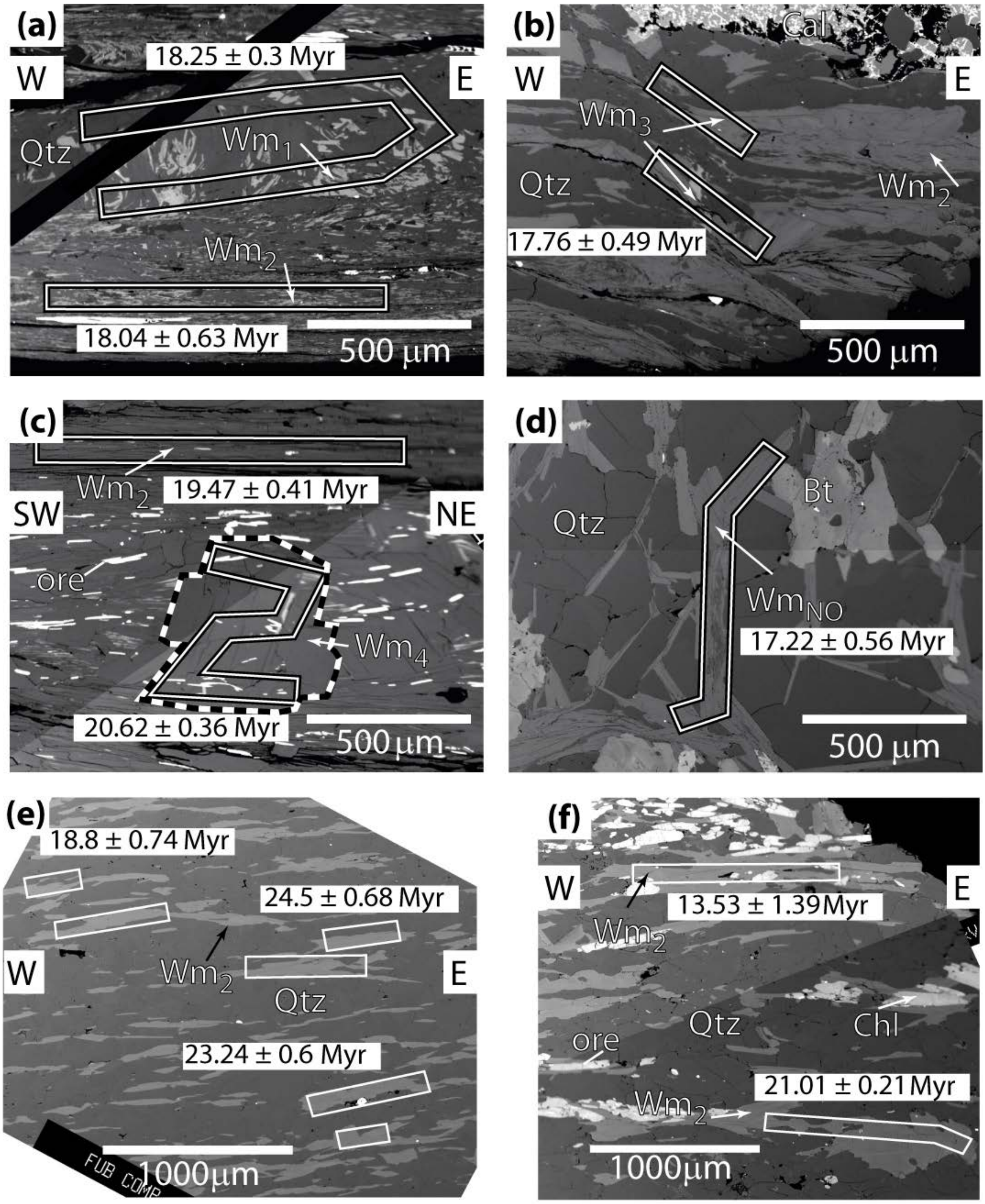

Figure 6.3: Scanning electron microscope (SEM) back-scatter photomicrographs of white micas. White boxes outline laser-ablated areas with corresponding age and 1σ error. (a) Wm_2 grains along the upper and lower margins define the main foliation of the KNF, whereas folded Wm_1 grains in the centre are older mica that became reoriented during folding related to KNF shearing (sample AS1); (b) Wm_4 post-kinematic cross white mica outlined by the black/white dashed line, and main foliation (Wm_2) of the KNF (sample AS74); (c) Wm_3 grains define shear bands indicating top-E shearing within the KNF (sample AS41); (d) Wm_{NO} annealed white mica and quartz microstructures in an unfoliated sample (A63); Wm_2 defines the main foliation. Although the ages of the white mica in sample AS27 (e) and sample AS52 (f) differ significantly, no differences in the composition of the mica could be discerned. Note that in microstructural domains with grain size < 75 μm, some

ages represent a composite of the ages of several white micas (e.g., samples AS1 in 'a' and AS27 in 'e').

6.4.2 Metamorphism

The Alpine peak-metamorphic temperature in the study area was inferred from Raman microspectroscopy on carbonaceous material (RSCM) and varies from ~525°C below the footwall of the KNF to 450°C at the top of the KNF [*Scharf et al.*, 2013b]. Thus, the peak temperature is always higher than or equal to the closure temperature of the $^{40}Ar/^{39}Ar$ white-mica system [~445-400°C according to *Harrison et al.*, 2009] and can vary with cooling rate and/or grain size [e.g., *Dodson*, 1973; *Mulch et al.*, 2002; *Harrison et al.*, 2009].

There is no evidence that any of the samples from the Penninic units at the eastern margin of the Tauern Window ever underwent blueschist- or eclogite-facies metamorphism. The highest pressure recorded in the Venediger Nappe System less than 10 km south of the study area (0.76 ± 0.12 GPa at ~620°C) was reached in Oligocene time [*Cliff et al.*, 1985; *Droop*, 1985; *Scharf et al.*, 2013b]. The only sample from the Upper Austroalpine unit in the hangingwall of the KNF (sample AS36; Fig. 6.1b) experienced late Cretaceous amphibolite-facies metamorphism and was not overprinted by Cenozoic metamorphism [*Schuster et al.*, 2004, 2006].

6.4.3 Geochemistry

Microprobe analyses of the white micas at 258 single spots in all nine samples are listed in the "Supplementary material" section in Table 6.1.A. Most white micas have similar major-element compositions, irrespective of their microstructural setting (Fig. 6.4). Exceptions are sample AS27 (qtz-rich metapelite of the Modereck Nappe System, Al-ce: 0.32; Fe-Al-ce: 0.23 of analysis 2 in Fig. 6.4a) and sample AS36 (Upper Austroalpine paragneiss, Al-ce: 0.38; Fe-Al-ce: 0.38, analysis 3 in Fig. 6.4a) which both have higher Al-celadonite and Fe-Al-celadonite components than the other samples of the KNF (Al-ce: 0.15-0.25; Fe-Al-ce 0.18-0.22 in Fig. 6.4a).

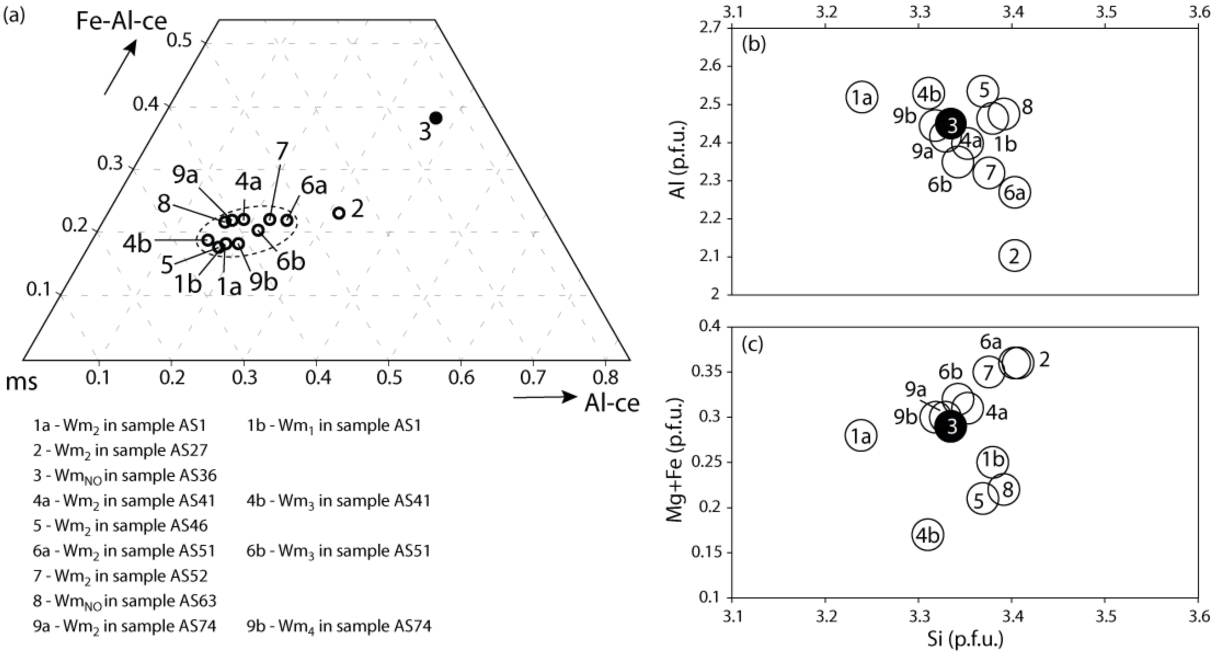

Figure 6.4: Compositional range of white micas belonging to the various microstructural types measured within the nine samples analysed (Table 6.1). (a) Fe-Al-ce (celadonite), ms (muscovite) and Al-ce (celadonite); (b) Al (p.f.u.) versus Si (p.f.u.); (c) Fe + Mg (p.f.u.) versus Si (p.f.u.). Abbreviations: Wm$_1$ - refolded grains; Wm$_2$ - grains parallel to the main foliation; Wm$_3$ - white mica aligned parallel to shear bands formed during KNF shearing; Wm$_4$ - post-kinematic grains; Wm$_{NO}$ - grains with no preferred orientation. The black circle refers to white mica in AS36 from the hangingwall of the KNF; open circles are white mica from within or below the KNF.

6.5 ^{40}Ar/^{39}Ar and Rb/Sr AGE RESULTS

White micas ranging in length from 100 to 500 µm were ablated parallel to their long axes with a UV laser. Because single grains shorter than 75 µm could not be measured, the in-situ ^{40}Ar/^{39}Ar ages of such small grains were estimated by ablating grain aggregates. Such aggregate ages are less reliable because it cannot be ruled out that ablation affected other interstitial minerals during gas extraction (e.g., quartz and chlorite) and/or that argon was trapped along the grain boundaries. The absolute analytical errors (1σ) of single grain ages are mostly < 1 Myr, which is less than 5% relative error. Only 13 of 87 ablation measurements have an error of > 1 Myr (Table 6.1). In the case of sample AS36, the errors are < 0.7 Myr; this corresponds to an error of < 1% for the absolute age (~76 Myr) in this sample.

Table 6.1: Isotopic analyses for ^{40}Ar/^{39}Ar dating of different types of white-mica grains: Wm_1 - foliation predating the KNF; Wm_2 - main foliation of the KNF; Wm_3 - shear bands during KNF shearing; Wm_4 - grains overgrowing KNF foliation; $\mathrm{Wm}_{\mathrm{NO}}$ - no preferred orientation. Note that only the smallest length of the grain dimension (divided by two = radius) was used for the closure temperature estimates as discussed in the text.

Age[Myr]	±1σ	^{40}Ar*/^{39}ArK	±1σ	^{40}Ar/^{39}Ar	±1σ	^{38}Ar/^{39}Ar	±1σ	^{37}Ar/^{39}Ar	±1σ	^{36}Ar/^{39}Ar	±1σ	%40$\mathrm{Ar}_{\mathrm{atm}}$	grain dimension [μm]	Microstructure
Sample AS1; J = 0.002393; metapelite; Glockner Nappe System; N 47°03′14.2″ E 13°35′11.6″, 1965 m														
16.54	0.83	3.888	0.194	4.727	0.037	0.012	<0.001	<0.001	<0.001	0.003	0.001	17.8	~100 x <100	Wm_1
17.06	0.47	4.011	0.110	4.463	0.011	0.013	<0.001	<0.001	<0.001	0.002	<0.001	10.1	~100 x <100	Wm_2
16.18	0.75	3.802	0.178	5.187	0.033	0.015	<0.001	<0.001	<0.001	0.005	0.001	26.7	~100 x <100	Wm_2
18.30	0.58	4.305	0.136	4.869	0.022	0.013	<0.001	<0.001	<0.001	0.002	<0.001	11.6	~100 x <100	Wm_1
17.43	0.75	4.099	0.177	4.641	0.020	0.015	<0.001	<0.001	<0.001	0.002	0.001	11.7	~100 x <100	Wm_1
16.02	0.60	3.761	0.140	5.421	0.039	0.013	<0.001	<0.001	<0.001	0.006	<0.001	30.6	~100 x <100	Wm_2
15.36	0.50	3.610	0.118	4.757	0.037	0.014	<0.001	<0.001	<0.001	0.004	<0.001	24.1	~100 x <100	Wm_2
18.06	0.30	4.248	0.068	4.592	0.030	0.012	<0.001	<0.001	<0.001	0.001	<0.001	07.1	~100 x <100	Wm_1
18.19	0.49	4.278	0.114	4.466	0.017	0.012	<0.001	<0.001	<0.001	0.001	<0.001	04.2	~100 x <100	Wm_1
17.85	0.62	4.199	0.146	4.786	0.027	0.011	<0.001	<0.001	<0.001	0.002	<0.001	12.3	~100 x <100	Wm_2
Sample AS27; J = 0.002391; metapelite; Modereck Nappe System; N 47°03′07″ E 13°34′50.2″, 2059 m														
22.85	1.53	5.331	0.359	9.666	0.070	0.014	<0.001	<0.001	<0.001	0.015	0.001	44.8	~1000 x 200	Wm_2
17.35	1.57	4.042	0.368	110.75	0.060	0.076	0.001	<0.001	<0.001	0.366	0.001	96.4	~1000 x 100	Wm_2
23.18	0.55	5.409	0.128	6.619	0.038	0.012	<0.001	<0.001	<0.001	0.004	<0.001	18.2	~1000 x 100	Wm_2
23.24	0.60	5.422	0.140	6.434	0.028	0.012	<0.001	<0.001	<0.001	0.003	<0.001	15.7	~1000 x 150	Wm_2
24.32	0.55	5.676	0.128	7.394	0.036	0.011	<0.001	<0.001	<0.001	0.006	<0.001	23.2	~1000 x 100	Wm_2
22.63	0.69	5.279	0.160	6.823	0.030	0.012	<0.001	<0.001	<0.001	0.005	<0.001	22.6	~1000 x 150	Wm_2
24.50	0.68	5.717	0.158	6.722	0.019	0.010	<0.001	<0.001	<0.001	0.003	<0.001	14.9	~1000 x 100	Wm_2
18.80	0.74	4.382	0.172	14.737	0.040	0.019	<0.001	<0.001	<0.001	0.036	<0.001	70.3	~1000 x 100	Wm_2
Sample AS 36; J = 0.002388; paragneiss; Upper Austroalpine, Koralpe-Wölz Nappe System; N 46° 59′23.8″ E 13°33′20.1″, 2162 m														
77.33	0.50	18.530	0.096	19.578	0.069	0.014	<0.001	<0.001	<0.001	0.004	<0.001	05.4	~1000 x 500	$\mathrm{Wm}_{\mathrm{NO}}$
77.89	0.47	18.667	0.086	19.487	0.054	0.012	<0.001	<0.001	<0.001	0.003	<0.001	04.2	~1000 x 500	$\mathrm{Wm}_{\mathrm{NO}}$
76.95	0.60	18.436	0.126	20.157	0.072	0.015	<0.001	<0.001	<0.001	0.006	<0.001	08.5	~1000 x 200	$\mathrm{Wm}_{\mathrm{NO}}$
78.68	0.49	18.860	0.093	20.190	0.044	0.013	<0.001	<0.001	<0.001	0.005	<0.001	06.6	~1000 x 500	$\mathrm{Wm}_{\mathrm{NO}}$
71.90	0.62	17.203	0.134	18.963	0.081	0.014	<0.001	<0.001	<0.001	0.006	<0.001	09.3	~1000 x 500	$\mathrm{Wm}_{\mathrm{NO}}$
74.45	0.61	17.825	0.131	18.953	0.091	0.013	<0.001	<0.001	<0.001	0.004	<0.001	06.0	~1000 x 300	$\mathrm{Wm}_{\mathrm{NO}}$
75.56	0.62	18.096	0.134	19.489	0.124	0.013	<0.001	<0.001	<0.001	0.005	<0.001	07.1	~1000 x 500	$\mathrm{Wm}_{\mathrm{NO}}$
74.41	0.66	17.793	0.144	19.271	0.093	0.012	<0.001	<0.001	<0.001	0.005	<0.001	07.7	~1000 x 500	$\mathrm{Wm}_{\mathrm{NO}}$
74.56	0.53	17.851	0.108	19.549	0.080	0.013	<0.001	<0.001	<0.001	0.006	<0.001	08.7	~1000 x 500	$\mathrm{Wm}_{\mathrm{NO}}$
75.02	0.63	17.949	0.136	18.718	0.077	0.014	<0.001	<0.001	<0.001	0.003	<0.001	04.1	~1000 x 500	$\mathrm{Wm}_{\mathrm{NO}}$
Sample AS41; J = 0.002385; metapelite; Modereck Nappe System; N 47°01′29.8″ E 13°32′49.4″, 2148 m														
17.61	0.48	4.148	0.114	6.025	0.023	0.013	<0.001	<0.001	<0.001	0.006	<0.001	31.2	~1000 x 100	Wm_3
19.10	0.39	4.510	0.092	4.790	0.025	0.012	<0.001	<0.001	<0.001	0.001	<0.001	05.8	~1000 x 300	Wm_2
18.14	0.48	4.281	0.114	5.220	0.023	0.015	<0.001	<0.001	<0.001	0.003	<0.001	18.0	~1000 x 200	Wm_2
17.56	0.50	4.142	0.117	5.170	0.024	0.014	<0.001	<0.001	<0.001	0.003	<0.001	19.9	~1000 x 100	Wm_2
18.73	0.27	4.421	0.063	5.079	0.024	0.013	<0.001	<0.001	<0.001	0.002	<0.001	13.0	~1000 x 200	Wm_2
15.65	0.23	3.690	0.055	4.284	0.019	0.013	<0.001	<0.001	<0.001	0.002	<0.001	13.9	~1000 x 200	Wm_2
18.06	0.44	4.261	0.104	5.125	0.030	0.014	<0.001	<0.001	<0.001	0.003	<0.001	16.9	~1000 x 100	Wm_3
17.17	0.33	4.051	0.078	4.242	0.008	0.013	<0.001	<0.001	<0.001	0.001	<0.001	04.5	~1000 x 200	Wm_2
18.31	0.31	4.321	0.073	4.949	0.026	0.014	<0.001	<0.001	<0.001	0.002	<0.001	12.7	~1000 x 200	Wm_2
18.43	0.50	4.349	0.118	4.705	0.029	0.012	<0.001	<0.001	<0.001	0.001	<0.001	07.6	~1000 x 200	Wm_2
Sample AS46; J = 0.002383; metapelite; Modereck Nappe System; N 47°02′55.1″ E 13°34′44.2″, 2018 m														
17.69	0.49	4.177	0.116	4.924	0.011	0.013	<0.001	<0.001	<0.001	0.003	<0.001	15.2	~1000 x 100	Wm_2
18.73	0.74	4.424	0.175	5.110	0.045	0.014	<0.001	<0.001	<0.001	0.002	0.001	13.4	~1000 x 200	Wm_2
18.89	0.30	4.463	0.072	5.462	0.040	0.012	<0.001	<0.001	<0.001	0.003	<0.001	18.3	~1000 x 100	Wm_2
19.80	0.61	4.679	0.145	5.539	0.036	0.012	<0.001	<0.001	<0.001	0.003	<0.001	15.5	~1000 x 100	Wm_2
19.55	0.46	4.618	0.109	5.003	0.029	0.013	<0.001	<0.001	<0.001	0.001	<0.001	07.7	~1000 x 200	Wm_2

Sample AS51; J = 0.00238; paragneiss; Storz Nappe; 47°01′54.1″ E 13°31′45.4″, 1757 m														
12.22	5.14	2.883	1.213	8.696	0.440	0.018	<0.001	<0.001	<0.001	0.020	0.004	66.9	~1000 x 400	Wm$_2$
21.46	1.66	5.081	0.393	11.331	0.204	0.013	<0.001	<0.001	<0.001	0.021	0.001	55.2	~1000 x 300	Wm$_2$
14.51	2.13	3.428	0.503	8.675	0.221	0.017	<0.001	<0.001	<0.001	0.018	0.002	60.5	~1000 x 500	Wm$_2$
21.25	2.06	5.031	0.488	9.613	0.308	0.017	<0.001	<0.001	<0.001	0.016	0.001	47.7	~1000 x 500	Wm$_2$
18.62	1.52	4.396	0.359	14.017	0.221	0.015	<0.001	<0.001	<0.001	0.033	0.001	68.6	~1000 x 300	Wm$_2$
24.31	2.95	5.760	0.700	10.862	0.218	0.012	<0.001	<0.001	<0.001	0.017	0.002	47.0	~1000 x 300	Wm$_2$
19.84	0.28	4.695	0.065	5.707	0.016	0.012	<0.001	<0.001	<0.001	0.003	<0.001	17.7	~1000 x 300	Wm$_2$
21.17	0.75	5.012	0.178	7.350	0.033	0.014	<0.001	<0.001	<0.001	0.008	0.001	31.8	~1000 x 300	Wm$_2$
19.63	0.41	4.640	0.097	7.265	0.050	0.016	<0.001	<0.001	<0.001	0.009	<0.001	36.1	~1000 x 500	Wm$_2$
21.70	1.57	5.136	0.373	11.185	0.091	0.018	<0.001	<0.001	<0.001	0.020	0.001	54.1	~1000 x 300	Wm$_2$
22.66	1.22	5.367	0.290	10.641	0.092	0.017	<0.001	<0.001	<0.001	0.018	0.001	49.6	~1000 x 300	Wm$_3$
19.28	0.63	4.515	0.148	6.424	0.044	0.011	<0.001	<0.001	<0.001	0.006	<0.001	29.7	~1000 x 300	Wm$_3$
30.44	2.95	7.223	0.701	16.115	0.198	0.012	<0.001	<0.001	<0.001	0.030	0.002	55.2	~1000 x 300	Wm$_2$
Sample AS52; J = 0.002377; paragneiss; Storz Nappe; N 47°01′47.9″ E 13°31′35.3″, 1815 m														
16.64	1.11	3.808	0.264	8.492	0.041	0.012	<0.001	<0.001	<0.001	0.016	0.001	55.2	~1000 x 200	Wm$_2$
13.53	1.39	3.170	0.328	5.352	0.067	0.015	<0.001	<0.001	<0.001	0.007	0.001	40.8	~1000 x 300	Wm$_2$
19.57	0.58	4.578	0.137	6.417	0.032	0.012	<0.001	<0.001	<0.001	0.006	<0.001	28.7	~1000 x 200	Wm$_2$
21.01	0.21	4.973	0.051	5.929	0.011	0.012	<0.001	<0.001	<0.001	0.003	<0.001	16.1	~1000 x 300	Wm$_2$
21.70	0.82	5.092	0.195	5.457	0.022	0.013	<0.001	<0.001	<0.001	0.001	0.001	06.7	~1000 x 200	Wm$_2$
15.13	0.82	3.487	0.194	5.096	0.023	0.015	<0.001	<0.001	<0.001	0.005	0.001	31.6	~1000 x 200	Wm$_2$
19.68	0.74	4.587	0.175	5.488	0.024	0.014	<0.001	<0.001	<0.001	0.003	0.001	16.4	~1000 x 200	Wm$_2$
19.49	0.56	4.601	0.133	5.728	0.016	0.013	<0.001	<0.001	<0.001	0.004	<0.001	19.7	~1000 x 300	Wm$_2$
19.51	0.77	4.617	0.181	6.131	0.026	0.012	<0.001	<0.001	<0.001	0.005	0.001	24.7	~1000 x 300	Wm$_2$
21.87	0.54	5.184	0.129	6.699	0.014	0.015	<0.001	<0.001	<0.001	0.005	<0.001	22.6	~1000 x 300	Wm$_2$
20.33	0.98	4.782	0.232	11.247	0.049	0.018	<0.001	<0.001	<0.001	0.022	0.001	57.5	~1000 x 300	Wm$_2$
Sample AS63; J = 0.002374; metapelite; Permo-mesozoic cover of Hochalm Nappe; N 47° 04′04.5″ E 13°27′21.7″, 1905 m														
17.80	0.49	4.210	0.117	4.955	0.025	0.011	<0.001	<0.001	<0.001	0.003	<0.001	15.0	~1000 x 200	Wm$_{NO}$
16.49	0.72	3.864	0.171	5.781	0.027	0.014	<0.001	<0.001	<0.001	0.006	0.001	33.2	~1000 x 400	Wm$_{NO}$
18.91	0.39	4.477	0.093	5.510	0.028	0.013	<0.001	<0.001	<0.001	0.003	<0.001	18.7	~1000 x 200	Wm$_{NO}$
17.81	0.45	4.207	0.106	5.063	0.011	0.013	<0.001	<0.001	<0.001	0.003	<0.001	16.9	~1000 x 300	Wm$_{NO}$
18.64	0.76	4.418	0.180	4.817	0.016	0.013	<0.001	<0.001	<0.001	0.001	0.001	08.3	~1000 x 300	Wm$_{NO}$
17.06	0.55	4.040	0.130	4.695	0.020	0.012	<0.001	<0.001	<0.001	0.002	<0.001	13.9	~1000 x 200	Wm$_{NO}$
17.54	0.41	4.134	0.097	4.975	0.019	0.014	<0.001	<0.001	<0.001	0.003	<0.001	16.9	~1000 x 200	Wm$_{NO}$
19.67	0.78	4.657	0.185	6.246	0.013	0.014	<0.001	<0.001	<0.001	0.005	0.001	25.4	~1000 x 200	Wm$_{NO}$
18.27	0.22	4.319	0.052	5.486	0.031	0.014	<0.001	<0.001	<0.001	0.004	<0.001	21.3	~1000 x 200	Wm$_{NO}$
19.37	0.47	4.578	0.113	5.096	0.014	0.016	<0.001	<0.001	<0.001	0.002	<0.001	10.2	~1000 x 300	Wm$_{NO}$
Sample AS74; J = 0.00237; metapelite; Permo-mesozoic cover of Hochalm Nappe; N 47°06′51.2″ E 13°25′42.8″, 1363 m														
20.41	0.35	4.849	0.083	5.236	0.018	0.013	<0.001	<0.001	<0.001	0.001	<0.001	07.4	500 x 500	Wm$_4$
19.27	0.40	4.578	0.094	4.908	0.009	0.012	<0.001	<0.001	<0.001	0.001	<0.001	06.7	~1000 x 100	Wm$_2$
19.28	0.42	4.580	0.100	5.255	0.021	0.014	<0.001	<0.001	<0.001	0.002	<0.001	12.8	300 x 300	Wm$_4$
20.19	0.30	4.796	0.072	5.224	0.029	0.013	<0.001	<0.001	<0.001	0.001	<0.001	08.2	~1000 x 100	Wm$_2$
19.54	0.64	4.641	0.152	5.316	0.015	0.014	<0.001	<0.001	<0.001	0.002	0.001	12.7	400 x 400	Wm$_4$
20.56	0.40	4.886	0.096	4.984	0.017	0.012	<0.001	<0.001	<0.001	<0.001	<0.001	02.0	400 x 400	Wm$_4$
19.62	0.35	4.661	0.082	5.508	0.020	0.013	<0.001	<0.001	<0.001	0.003	<0.001	15.4	~1000 x 200	Wm$_2$
18.59	0.50	4.416	0.119	4.909	0.019	0.014	<0.001	<0.001	<0.001	0.002	<0.001	10.1	~1000 x 200	Wm$_2$
18.93	0.41	4.498	0.098	4.723	0.016	0.011	<0.001	<0.001	<0.001	0.001	<0.001	04.8	~1000 x 200	Wm$_2$
19.99	0.44	4.748	0.105	5.030	0.016	0.012	<0.001	<0.001	<0.001	0.001	<0.001	06.6	400 x 400	Wm$_4$

6.5.1 Estimates of closure temperature

Any potential attempt to interpret the age data in terms of cooling ages rather than formation ages (discussed in section 6.6) needs to take into account the fact that closure temperatures of white mica will differ amongst the samples. These expected closure temperatures were calculated using the Arrhenius parameters (E = 267.8 kJ/mol, D_o = 20 cm^2/s) of *Harrison et al*. [2009] and the equations of *Dodson* [1973]. In order to apply these equations, it is necessary to make some assumptions: First, it is assumed that micas are spheres, in agreement with the diffusive geometry of grains adopted by *Dodson* [1973]. Since the white micas are generally elongate, only the half of the shortest dimension of the grains, corresponding to the radius of a sphere, was used to calculate the closure temperature. Half of the shortest dimension of the white mica grains is therefore referred to as the radius in the rest of the text and varies from < 50 to ~225 µm, corresponding to a closure temperature in the range of < 403 to 446°C, respectively (Table 6.2). Second, a pressure of 0.5 GPa during growth of the mica is assumed. This assumed pressure of white-mica growth during exhumation in the footwall of the KNF is a very approximate value taken to be less than the peak pressure of 0.76 ± 0.12 GPa [*Droop*, 1985]. Third, a cooling rate of 40°C/Myr is assumed for all rocks within and below the KNF. This cooling rate is obtained from the temperature drop of 500 to 300°C over the 22 to 17 Myr time period constrained by the Rb/Sr white mica and biotite systems in the ETD [see Fig. 6.7 of *Scharf et al.*, 2013a and references therein]. A lower cooling rate of 10°C/Myr was used for sample AS36 from the hangingwall of the KNF because cooling of these Austroalpine units from peak metamorphism at ~550 to 300°C must have started some 100 to 75 Myr ago [*Schuster and Frank*, 2000].

6.5.2 Samples from top and bottom of the KNF

Samples AS1 (Fig. 6.5a) and AS74 (Fig. 6.5h) yield remarkably similar ages despite the different types of grains that they contain. Wm_1 and Wm_2 grains from sample AS1 at the top of the KNF, e.g., near the hangingwall (Figs. 6.1b, 6.2a & 6.3a), scatter over a narrow range. Their average ages differ slightly but overlap within their standard deviations (17.70 ± 0.66 Myr for Wm_1 grains and 16.49 ± 0.87 Myr for Wm_2 grains; Fig. 6.5a & Table 6.1). The slightly older average ages of folded Wm_1 grains compared to the well-oriented Wm_2 grains is consistent with the microstructural evidence that Wm_1 grains are relics preserved between the Wm_2 grains defining the main foliation of the KNF (Figs. 6.2a & 6.3a). The average age of all grains in sample AS1 is 17.10 ± 0.98 Myr. The white-mica grain radius in this sample (< 50 µm) is the smallest of all samples, hence, the expected closure temperature is < 403°C.

In sample AS74 (Figs. 6.2b & 6.3b) from the base of the KNF, Wm_2 grains and post-kinematic Wm_4 grains yield slightly different average ages, although they agree within 1 sigma error (respectively, 19.32 ± 0.55 and 19.95 ± 0.49 Myr). The average age of its entire population of Wm_2 and Wm_4 grains is one of the oldest of all analysed samples (19.64 ± 0.61 Myr), even though this specimen is located at the base of the KNF where rocks are expected to have cooled later than in structurally higher positions closer to the top of the KNF. The radii of the Wm_2 (~100 µm), and Wm_4 grains (~225 µm, Tables 6.1 & 6.2) yield closure temperatures of ~420 and ~445°C, respectively (Figs. 6.6 & 6.7).

Table 6.2: Samples, their location with respect to the KNF, white-mica radius, estimated closure temperature based on the white-mica radius and the cooling rate (40°C/Myr for all samples expect sample AS36 with 10°C/Myr; see Fig. 6.6 and discussion in the text), and average age with standard deviation (SD). The radius is defined as the shortest dimension of the white mica divided by two. The stars at samples AS51 and AS52 indicates the apparent cooling ages without anomalous ages, as discussed in the text. AA - Austroalpine Units; GL - Glockner Nappe System; MO - Modereck Nappe System; ST - Storz Nappe; PVC - Post-Variscan cover; a - refolded Wm$_1$ grains; b - grains parallel to the main foliation Wm$_2$; c - post-kinematic Wm$_4$ grains. Sample locations shown in Fig. 6.1b.

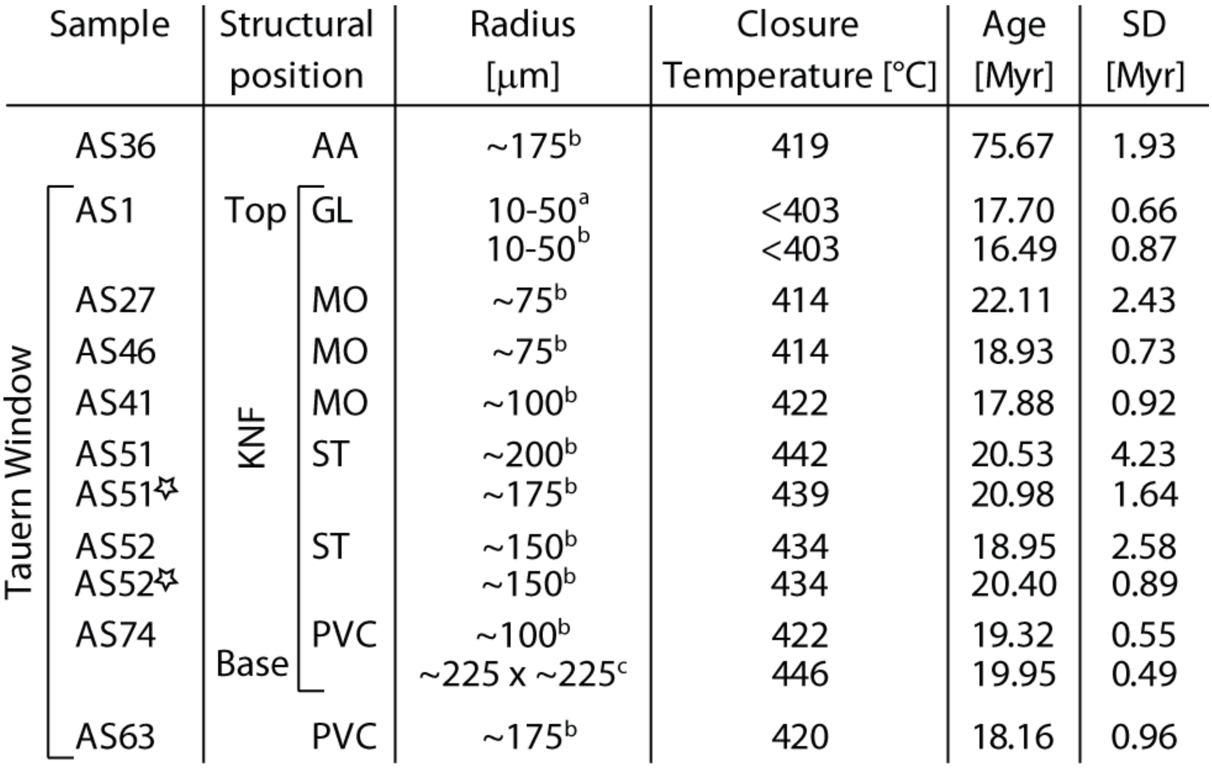

	Sample	Structural position		Radius [µm]	Closure Temperature [°C]	Age [Myr]	SD [Myr]
	AS36		AA	~175[b]	419	75.67	1.93
Tauern Window	AS1	Top	GL	10-50[a]	<403	17.70	0.66
				10-50[b]	<403	16.49	0.87
	AS27		MO	~75[b]	414	22.11	2.43
	AS46		MO	~75[b]	414	18.93	0.73
	AS41	KNF	MO	~100[b]	422	17.88	0.92
	AS51		ST	~200[b]	442	20.53	4.23
	AS51✩			~175[b]	439	20.98	1.64
	AS52		ST	~150[b]	434	18.95	2.58
	AS52✩			~150[b]	434	20.40	0.89
	AS74		PVC	~100[b]	422	19.32	0.55
		Base		~225 x ~225[c]	446	19.95	0.49
	AS63		PVC	~175[b]	420	18.16	0.96

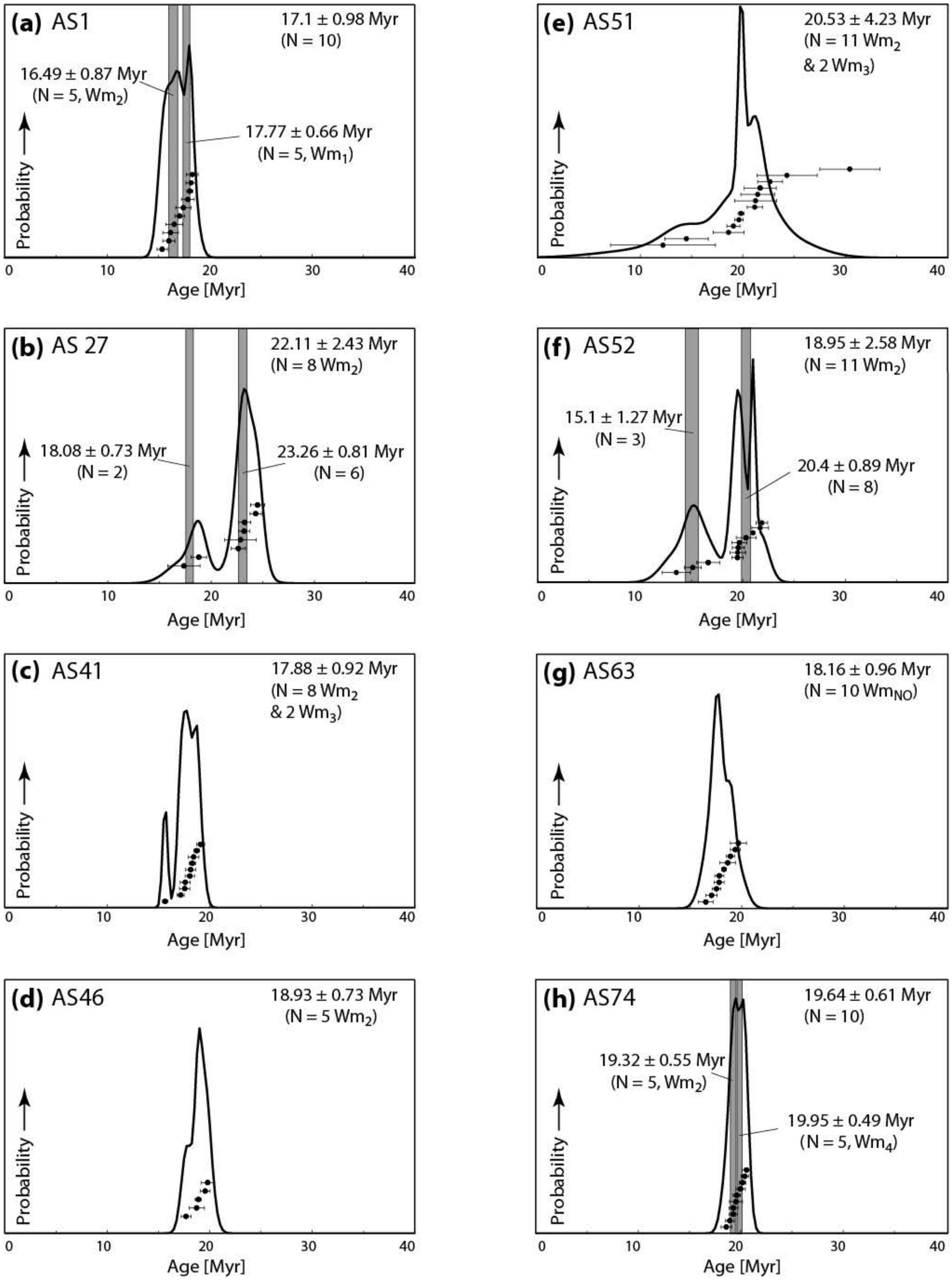

Figure 6.5: Probability of grain ages of white micas versus age from the KNF and, in the case of sample AS63, from below the KNF: (a) folded Wm$_1$ and Wm$_2$ defining the KNF main foliation; (b) Wm$_2$ with bimodal age distribution; (c) predominantly Wm$_2$; (d) only Wm$_2$; (e) predominantly Wm$_2$ grains; (f) only Wm$_2$ grains with a bimodal age distribution; (g) post-kinematic Wm$_4$; (h) Wm$_2$ and Wm$_4$. Ages in upper right corner are average ages with standard deviation, N - number of grain ages used for age calculation. Black curves defining the age

peaks indicate the probability of a given single grain age; black dots with 1σ error bar are the single grain data listed in Table 6.1; grey stripes visualize the average ages and SD's of grain sub-populations with similar average ages, Wm_1 - foliation predating the KNF; Wm_2 - main foliation of the KNF; Wm_3 - shear bands during KNF shearing; Wm_4 - grains overgrowing KNF foliation; Wm_{NO} - no preferred orientation. Note that specimens AS27 (b) and AS52 (f) preserve two distinct age populations even though only Wm_2 grains were measured. On the other hand, differences in ages obtained for different categories of white micas are negligible in samples AS1 (a) and AS74 (h).

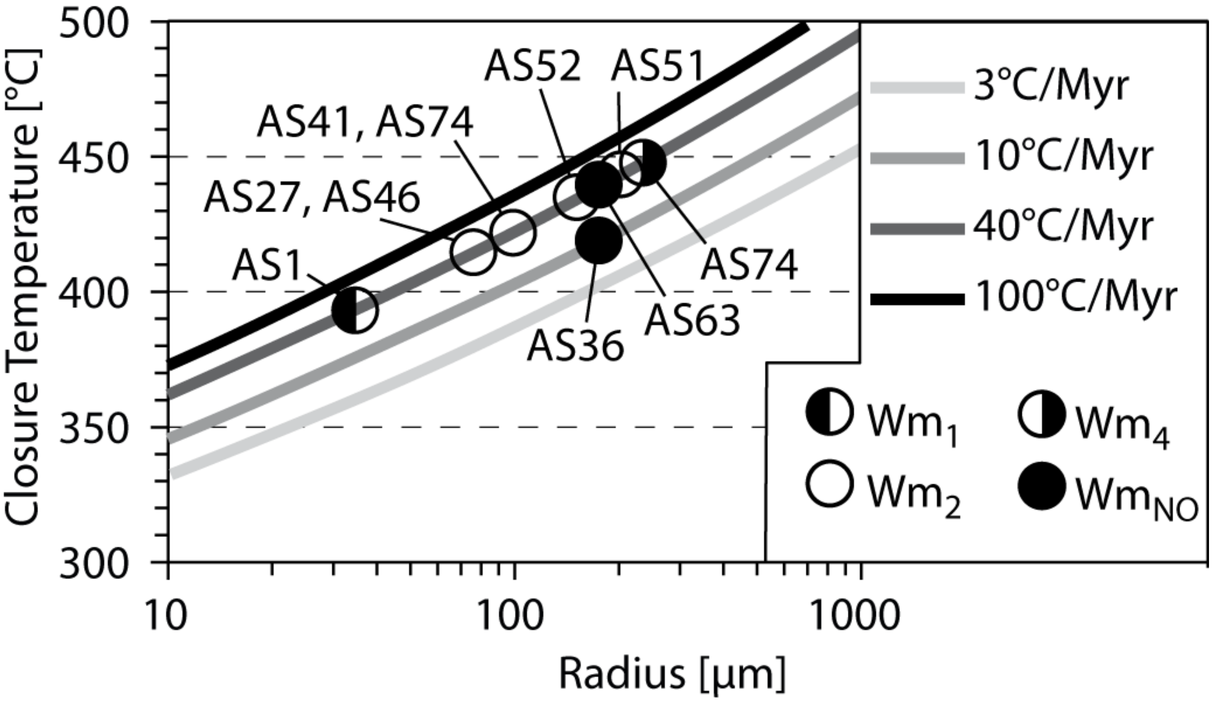

Figure 6.6: Closure temperature versus radius for the white-mica grains (circles) listed in Tables 6.1 and 6.2. The radius is defined as the shortest dimension of the white mica divided by two. Lines are based on the equations of *Dodson* [1973] and *Harrison et al*. [2009] for an assumed cooling rate of 3, 10, 40 and 100°C/Myr. Parameters used are the activation energy = 267.8 kJ/mol, the diffusional probability D_0 = 20 cm^2/s [*Hames and Bowring*, 1994], and are adjusted to 0.5 GPa, the diffusion geometry is spherical. Shortest grain length is treated as the radius of isometric grains or the shortest distance across elongate lath-like grains (Table 6.2). Sample locations are shown in Fig. 6.1b. Abbreviations: Wm_1 - refolded grains; Wm_2 - grains parallel to the main foliation; Wm_4 - post-kinematic grains; Wm_{NO} - grains with no preferred orientation.

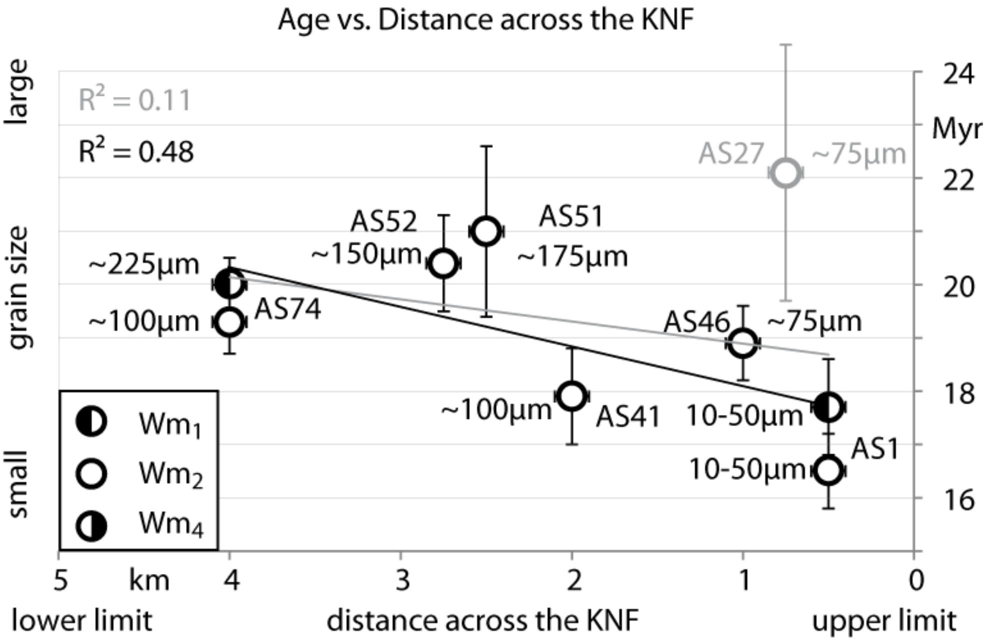

Figure 6.7: Radius and age versus distance across the KNF for white-mica grains analysed in this study according to Fig. 6.6 and the equations of *Dodson* [1973] and *Harrison et al.* [2009]. The radius is defined as the shortest dimension of the white mica divided by two. The black line shows the linear regression with the correlation coefficient (R^2). Sample AS27 was excluded for the calculation of the black regression line, since white mica of this sample consist of an anomalous composition (see section 6.6.2). The regression line including sample AS27 is shown in grey. Ages and grain size radius of the white mica as listed in Table 6.2. Lower and upper limit marks the KNF mylonite belt (Fig. 6.1b). The distance across the 5 km-wide KNF mylonite belt is estimated by projecting the sample localities from map view into the cross-section 10 of *Schmid et al.* [2013], their Fig. 3. Wm_1 - refolded grains; Wm_2 - grains parallel to the main foliation; Wm_4 - post-kinematic grains. Sample location shown in Fig. 6.1b.

6.5.3 Samples with shear bands

Two specimens (AS41 and AS51) contain Wm_2 grains defining the main KNF foliation (S_2) as well as Wm_3 grains oriented parallel to shear bands (Figs. 6.2c, 6.3c & Table 6.1). Hence, both white-mica generations are syn-kinematic with respect to top-E orogen-parallel extension. In sample AS41, the two measured Wm_3 grains yield ages of 18.06 ± 0.44 and 17.61 ± 0.47 Myr and are within the age range of the Wm_2 grains between 19.10 ± 0.39 and 15.65 ± 0.23 Myr. The average age of all grains in sample AS41 is 17.88 ± 0.92 Myr. The radius of white-mica grains in sample AS41 is ~100 µm, yielding a closure temperature of ~420°C.

In sample AS51, Wm_3 grains yield ages of 22.66 ± 1.22 and 19.28 ± 0.63 Myr, whereas the Wm_2 grain ages scatter widely between 30.44 ± 2.95 to 12.22 ± 5.14 Myr (Fig. 6.5e & Table 6.1). In this sample the average age is 20.53 ± 4.23 Myr. The radius of the measured mica in specimen AS51 is ~200 µm, indicating a closure temperature of ~440°C (Figs. 6.6, 6.7, Tables 6.1 & 6.2).

6.5.4 Samples with the main KNF foliation and containing only Wm_2 grains

Samples AS27, AS46 and AS52 contain only Wm_2 grains that formed during KNF shearing. Their ages vary widely (24.5-13.53 Myr) and two age subpopulations can be discerned in samples AS27 and AS52 (Fig. 6.5b, f & Table 6.1). Sample AS27 has a bimodal age distribution with peaks at 18.08 ± 0.73 and 23.26 ± 0.81 Myr (Fig. 6.5b). The bimodal age distribution of sample AS52 has a younger group (three of eleven individual grains) with a mean age of 15.10 ± 1.27 Myr and an older group (eight of eleven individual grains) with a mean age of 20.40 ± 0.89 Myr (Fig. 6.5f). As will be discussed below, the subpopulations in both samples may reflect the anomalous white-mica chemistry (AS27), and possibly also inherited Variscan $^{40}Ar/^{39}Ar$ white mica ages (AS52). The average ages of AS27 and AS52 are 22.11 ± 2.43 and 18.95 ± 2.58 Myr, respectively. The average age of this sample is (18.90 ± 0.21 Myr; Fig. 6.5d & Table 6.1). The white-mica radii for samples AS27 and AS46 are ~75 μm and for sample AS52 the radius is ~150 μm. Hence, the calculated closure temperatures for samples AS27 and AS46 are ~415°C, and that for sample AS52 is ~435°C (Figs. 6.6, 6.7, Tables 6.1 & 6.2).

6.5.5 Samples from below and above the KNF

Sample AS63 is from below the lower fabric boundary of the KNF in the Venediger Nappe System (Fig. 6.1b), contains annealed quartz and only randomly oriented Wm_{NO} white-mica grains yielding an average age of 18.16 ± 0.96 Myr. Interestingly, this is within the age range obtained for the seven specimens collected from the KNF (Fig. 6.5g, Tables 6.1 & 6.2). Given the radius of these white-mica grains (~175 μm), the closure temperature is calculated to be ~440°C (Figs. 6.6 & 6.7). Sample AS36, from the Upper Austroalpine units in the hangingwall of the KNF, has an average age of 75.67 ± 1.93 Myr (Fig. 6.8 & Table 6.1). This confirms the late Cretaceous white-mica cooling ages commonly obtained for the Upper Austroalpine units above the KNF [*Brewer*, 1969; *Schuster and Frank*, 2000]. Therefore, the $^{40}Ar/^{39}Ar$ system in white mica was quite obviously not reset by Cenozoic metamorphic events in the Tauern Window. For the radius ~175 μm of these white-mica grains, the closure temperature is calculated to be ~420°C. Note that the assumed cooling rate for this sample is slower than for the other samples (10°C /Myr; Figs. 6.6, 6.7, Tables 6.1 & 6.2).

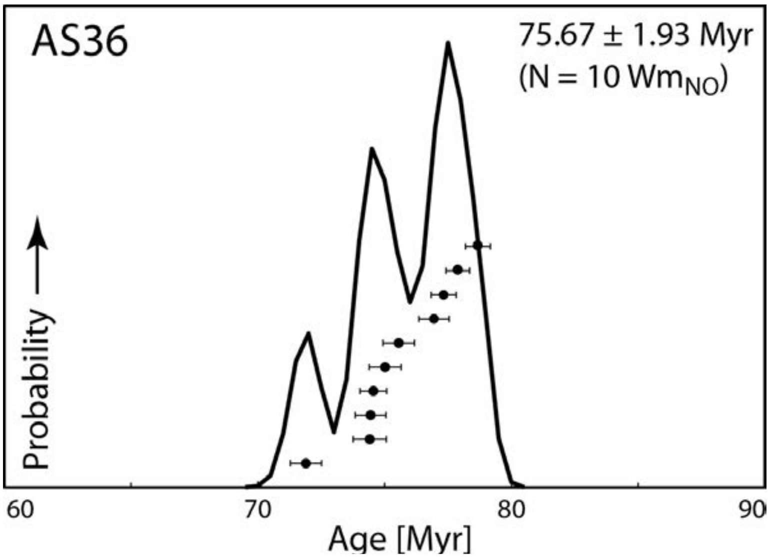

Figure 6.8: Probability of grain ages of white micas versus age of sample AS36 from the Austroalpine Unit in the hangingwall of the KNF. Age in upper right corner is the average age with standard deviation, N - number of grain ages used for age calculation. Black curve indicates the probability of a given single grain age; black dots with 1σ-error bar are the single grain data listed in Table 6.1, Wm$_{NO}$ - grains with no preferred orientation.

6.5.6 Summary of Ar-age results

In summary, 65% (50 out of 77) of the white-mica single grain ages measured from within and immediately below the KNF in the eastern part of the Tauern Window fall within the range of 21 to 17 Myr, irrespective of the microstructural characteristics of the individual grains. Only in the cases of paragneiss samples from the Storz Nappe (AS51 and AS52) and a metapelite from the Modereck Nappe System (AS27) does the majority of single grains ages scatter on either side of the 21-17 Myr interval (Table 6.1). The single sample from the hangingwall of the KNF yields late Cretaceous ages. Ages in the hangingwall that pre-date cooling of the footwall are indeed expected for a major low-angle normal fault, where heating of the hangingwall by the warm, exhuming footwall is usually very limited [e.g., *ter Voorde and Bertotti*, 1994].

6.5.7 Rb/Sr white-mica ages

The Rb/Sr white-mica ages are from two samples in the Hochalm and Göss nappes making up the core of the ETD, (Fig. 6.1b). Table 6.3 lists the amount of Rb and Sr, the whole-rock analysis, the ^{87}Rb/^{86}Sr ratio, and the errors (2σ) for these samples. The 24.4-21.1 Myr ages of the white micas in these samples are included in the discussion of the T-t path (section 6.6.3) because the micas define the main foliation of the KNF [sample locations in Fig. 6.1a and further details in *Favaro et al.*, 2015].

Table 6.3: Results for the two Rb/Sr white-mica analyses. Sample location is shown in Fig. 6.1a. wm – white mica; wr – whole rock.

Sample		Rock type	$^{87}Sr/^{86}Sr$	+/-2s$_m$	Rb [ppm]	Sr [ppm]	$^{87}Rb/^{86}Sr$	Age [Myr]	+/-
04R64	wm	Granitic orthogneiss	0.730748	0.000015	561.84	24.61	66.227	21.1	0.2
04R64	wr		0.711393	0.000004	165.04	284.8	1.6775		
182/1/2005	wm	Bt-wm granitic gneiss	0.850518	0.000009	825.31	7.225	335.21	24.4	0.3
182/1/2005	wr		0.737378	0.000004	238.94	83.46	8.3098		

6.6 DISCUSSION

6.6.1 Do the ^{40}Ar/^{39}Ar ages represent formational or cooling ages?

Within any given sample containing two microstructurally distinct generations of white mica, the differences in ^{40}Ar/^{39}Ar white-mica ages are statistically indistinguishable. For example, in sample AS1, the ages of the Wm$_1$ and Wm$_2$ grains differ by 1.28 Myr (Wm$_1$ = 17.77 ± 0.66 Myr, Wm$_2$ = 16.49 ± 0.87 Myr). In sample AS74, the difference is 0.63 Myr (Wm$_4$ = 19.95 ± 0.49 Myr; Wm$_2$ =19.32 ± 0.55 Myr) and in samples AS41 and AS52, the Wm$_3$ ages fall within the range of Wm$_2$ ages.

There are two possible interpretations of these data: either all four types of white mica (Wm$_1$-Wm$_4$) grew within the same time span and yield formational ages, or alternatively, they all cooled below their closure temperatures at about the same time, i.e., they represent cooling ages. The second interpretation (cooling ages) is preferred for the following reasons:

(1) The microstructures described in section 6.4.1 show that there were three distinct phases of white-mica growth that were kinematically unrelated to each other (Wm$_1$ pre-KNF, Wm$_{2-3}$ syn-KNF and Wm$_4$ post-KNF). It is extremely unlikely that geometrically and kinematically unrelated white micas would grow at the same time;

(2) Sample AS74 yields slightly older ^{40}Ar/^{39}Ar ages for Wm$_4$ grains than for Wm$_2$ grains although they agree within 1-sigma error. This is inconsistent with the microstructural evidence that Wm$_2$ grains grew before Wm$_4$ grains. Therefore, the ages cannot possibly be formational ages. The discrepancy in the ages of Wm$_2$ and Wm$_4$ grains is best explained as due to their different grain-sizes; Wm$_2$ grains are smaller than Wm$_4$ grains and therefore have lower closure temperatures and yield correspondingly younger ages.

The fact that the maximum metamorphic temperature in the KNF and its footwall was > 450-525°C [*Scharf et al.*, 2013b], i.e., above the expected closure temperature of 400-445°C, lends additional support to the interpretation of these ^{40}Ar/^{39}Ar white-mica ages as cooling ages. This makes it unlikely that the white-mica ages are formational ages or that deformation-induced argon loss led to younger ages in some of the grains. Stated positively, the general similarity of white-mica ages within the same sample, irrespective of microstructural orientation, indicates that the ages date cooling of the samples to below the grain-size dependent closure temperatures of the ^{40}Ar/^{39}Ar white-mica system.

Several authors have argued that diffusion in rocks and minerals strongly depends on fluids [*Villa*, 2010; *Warren et al*., 2012; *Halama et al*., 2014] and that, without fluids, a much higher closure temperature should be assumed than if a fluid was present. Moreover, *Warren et al*. [2012] and *Halama et al*. [2014] confirm earlier studies showing that Ar-loss must be taken into account when interpreting ^{40}Ar/^{39}Ar ages in high-pressure rocks. In our case, however, it is important to note that none of the rocks and samples in our study area contain traces of high-pressure metamorphism, nor is there any reason to suspect that they ever experienced such metamorphism; subduction-related metamorphism is restricted to other nappe units in the central part of the Tauern Window [see reviews in *Schuster et al*., 2004; *Schmid et al*., 2013 and references therein]. Furthermore, fluid must have been present during shearing because the KNF mylonites contain syn-tectonically nucleated hydrous phases, including the white micas investigated here (e.g., samples AS41 & AS51). The temperature of mylonitisation, and therefore also of the fluid, was in the same range as that for intragranular Ar-diffusion in white mica (~300-500°C). Finally, the study area contains many veins and joints filled with hydrous secondary minerals (e.g., epidote, stable at ~300-650°C). Taken together, this indicates that excess water was present during the cooling of white mica, and therefore, that the closure temperatures for white mica were probably not any higher than assumed here.

6.6.2 Pattern of cooling along the KNF

In contrast to the general homogeneity of ^{40}Ar/^{39}Ar cooling ages within individual samples, the samples considered as a group reveal an overall trend of younger ages from the bottom to the top of the KNF (Fig. 6.7 & Table 6.2). The only exception is specimen AS27, as discussed below. This upwardly younging trend in cooling ages is opposite to the downward younging trend expected for a large normal fault [e.g., *Grasemann and Mancktelow*, 1993; *Seward et al*., 2009] where the top of the hot footwall close to the cool hangingwall would normally be thought to cool below the closure temperature earlier than the hotter, structurally lower parts of the footwall.

An explanation for this unexpected age pattern is provided by the observation that white mica tends to decrease in size from the bottom to the top of the KNF (Fig. 6.7, Tables 6.1 & 6.2). Specifically, white-mica grains in samples AS1, AS27 and AS46 from the top of the KNF vary in size (radius) from < 50 to 100 μm, whereas in samples AS51, AS52 and AS74 from the base of the KNF, the size of white-mica grains varies from 100 to 250 μm. Smaller grains have smaller effective diffusional radii, yielding lower closure temperatures for a given cooling rate [Fig. 6.6; *Mulch et al*., 2002; *Harrison et al*., 2009]. For white-mica grains in the KNF, the closure temperature decreased from 445 to 420°C in initially hotter, coarser-grained samples at the base of the KNF to 420 to 400°C in the cooler, fine-grained samples near the top.

A schematic cross section of a generic normal fault in Figure 6.9 serves to illustrate the effect of grain-size on the pattern of cooling ages in the exhumed footwall exposed at the surface today. Note that the bending of isotherms across a normal fault depends strongly on the temperature contrast between hanging- and footwalls and the exhumation rate, as well as on the thermal properties of the fault rock (e.g., thermal conductivity, density, heat capacity); generally, stronger bending reflects faster exhumation rates and/or lower rates of thermal equilibration, as modelled by *Grasemann and Mancktelow* [1993], *Ketcham* [1996], and *Ehlers and Chapman* [1999]. However, as discussed below, the curvature of the isotherms is not the only factor influencing the age pattern in the footwall of the KNF.

An idealized normal fault with constant grain size and closure temperature across the shear zone will produce the expected pattern of progressively younger cooling ages away from the cold hangingwall because a rock from the base of the shear zone exposed at the Earth's surface today has passed through a given isotherm (marking the closure temperature) later than a rock from the top that is now also at the surface (blue exhumation paths in Fig. 6.9). This pattern can also result from the gradual relaxation and downward motion of isotherms after faulting has stopped.

In contrast, a normal fault like the KNF with decreasing grain size towards the cooler hangingwall will record younger ages near the top of the shear zone because a fine-grained rock exposed there at the Earth's surface has passed through a lower-temperature isotherm (corresponding to the reduced closure temperature) at a later time than a coarser-grained rock from the base of this shear zone (red exhumation paths in Fig. 6.9). Stated otherwise, the time since closure of a given isotopic system will be shorter for rocks with lower closure temperatures and therefore these systems will record younger ages than coarser grained rocks with higher closure temperatures. In the case of the KNF, the five-fold decrease in grain radii (50-225 μm) from the bottom to the top of the shear zone corresponds to a reduction in closure temperature of 50 to 100°C (Fig. 6.6). In such cases, cooling ages reflect the grain-size dependence of closure temperature rather than the exhumation history of the shear zone. The contrast in white-mica grain size across shear zones is augmented if grains continue to grow at or below the base of the shear zone; this is the case below the KNF, where static grain growth (the "Tauernkristallisation" in the Venediger Nappe Complex) continued during and after the onset of KNF shearing [*Scharf et al.*, 2013; *Favaro et al.*, 2015].

Despite the strong dependence of closure temperature on grain size, cooling ages from the ^{40}Ar-^{39}Ar system in white mica are a reliable way of dating the main activity of the KNF because the closure temperatures for this system fall in the same general range (445-400°C) as the temperatures estimated from dynamically recrystallized quartz microstructures in the KNF; the occurrence of subgrain-rotation recrystallization and fast-grain-boundary migration recrystallization [*Scharf et al.*, 2013a] yields a temperature range of 440 to 510 ± 30°C for geological strain rates, according to the calibration of *Stipp et al*. [2002].

Finally, it is important to note that the grain-size effect on the cooling-age pattern in the footwall of a normal fault is actually dependent on the relative rates of shearing (affecting the displacement and exhumation rates of the rocks) and thermal equilibration of the footwall. These factors affect the exhumation paths and the curvature of the isotherms in the shear zone. This is not shown in Figure 6.9

and would require thermomechanical modelling beyond the scope of this paper. In general, higher shearing rates are expected to increase the curvature of the isotherms near the hangingwall, somewhat counteracting the grain-size effect on the age pattern discussed above and illustrated in Figure 6.9.

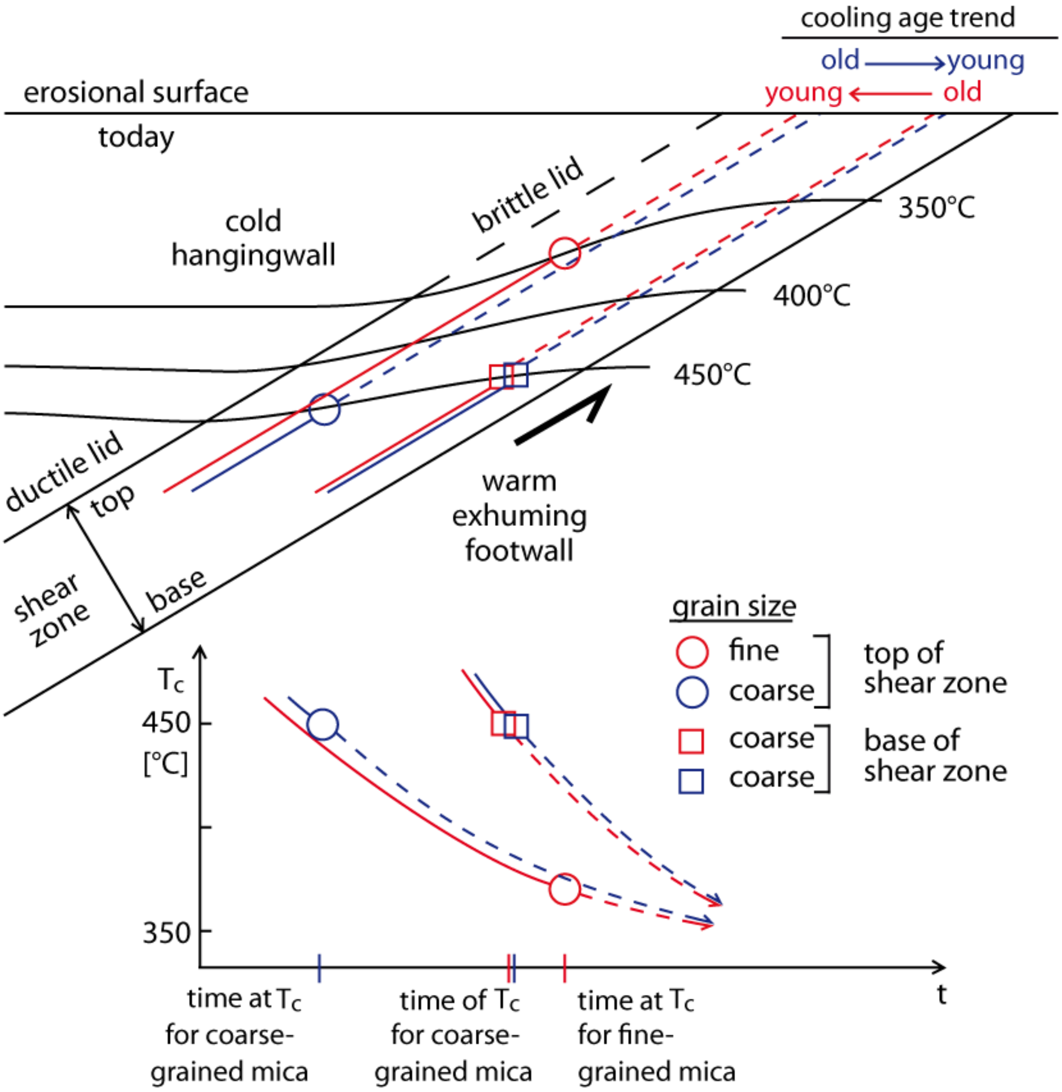

Figure 6.9: Cross section of a low-angle normal fault showing exhumation paths of rocks from the base (squares) and near the top (circles) of the shear zone. Blue paths for rock with constant white-mica grain size across and along shear zone, red paths for rock with smaller white-mica grain size near the lid than at the base of the shear zone. Grain size at base of shear zone assumed to be identical in both cases. Dashed paths indicate part of exhumation after closure of the isotopic system to diffusion. Temperature (T) versus time (t) plot shows that for a rock with constant grain size, the cooling ages young towards the base of the shear zone, whereas for rock with smaller grain size, cooling ages young towards the top because the isotherm corresponding to the lower closure temperature (T_c) is reached later (see text). Isotherms are drawn schematically based on previous thermal modeling [e.g., *Grasemann & Mancktelow*, 1993; *Ketcham*, 1996].

6.6.3 Anomalous ages of individual white-mica grains

Some 35% of the analysed grains in the samples fall outside of the 21-17 Myr age range, and in some cases the deviations are substantial (e.g., samples AS51 and AS52). Sample AS27 with the oldest average age (22.11 ± 2.43 Myr) and an estimated closure temperature of ~415°C (Figs. 6.5b, 6.6, 6.7, Tables 6.1 & 6.2) is located near the top of the KNF, close to sample AS1 which has substantially younger cooling ages (~18-16 Myr) and a lower closure temperature (< 403°C, Figs. 6.5a, 6.6, 6.7, Tables 6.1 & 6.2). However, Wm_2 grains in sample AS27 have slightly higher Al-ce and Fe-Al-ce components (Al-ce: 0.32; Fe-Al-ce: 0.23) than other white micas in the study area (Al-ce: 0.15-0.25; Fe-Al-ce 0.18-0.22; section 6.4.3 and Fig. 6.4a; except sample AS36 from the hangingwall of the KNF).

Sample AS51, a paragneisses from the structurally highest Storz Nappe of the Venediger Nappe System (Fig. 6.1b), has an anomalously wide range of Wm_2 ages (30.44-12.22 Myr and an expected closure temperature of ~440°C (Figs. 6.5e, 6.6, 6.7, Tables 6.1 & 6.2) even though all measured grains are similarly sized. This precludes a simple interpretation of this broad age distribution in terms of cooling ages. The oldest grain (30.44 ± 2.95 Myr) may preserve an isotopic signature related to the "Tauernkristallisation", which previous studies have dated in the range of 25-30 Myr [*Inger and Cliff*, 1994; *Thöni*, 1999; *Liu et al.*, 2001; *Kurz et al.*, 2008; *Pollington and Baxter*, 2010; *Favaro et al.*, 2015]. The two youngest ages from this sample have a large error (14.51 ± 2.13 Myr and 12.22 ± 5.14 Myr). Taking the upper values of their individual errors, their age would be ~17 Myr. Alternatively, these two samples may have been affected by late-stage shearing after 17 Myr ago that led to argon-loss. However, no white-mica subgrains were observed in thin section of these samples. Excluding these three anomalous ages, the average age of sample AS52 is 20.98 ± 1.64 Myr (Table 6.2).

Sample AS52, a paragneiss from the structurally highest Storz Nappe of the Venediger Nappe System, also has an anomalously wide, bimodal range of ages for Wm_2 grains: an older group with an average age of 20.40 ± 0.89 Myr and a younger group at 15.10 ± 1.27 Myr (Fig. 6.5f). Again, a simple interpretation in terms of cooling ages is not possible. The younger age group may indicate that shearing and/or fluid-influx and argon-loss lasted until ~15 Myr. However, continued shearing after 17 Myr is considered unlikely given the regional constraints on the end of shearing at ~17 Myr [see next section below and *Scharf et al.*, 2013a].

It is interesting to note that the two samples with the broadest age distributions (AS51 and AS52) are both pre-Variscan basement rocks that experienced Variscan metamorphism and thus are likeliest to have retained old, 'excess' argon. A tentative interpretation is that these earlier events preconditioned the white micas to preserve older Argon ages in some instances, while opening them to resetting in others.

6.6.4 T-t paths and a comparison of new and existing Rb/Sr and $^{40}Ar/^{39}Ar$ mica ages for the Eastern Tauern Dome

Figure 6.10 shows the cooling paths of the Brenner- and Katschberg normal faults (BNF, KNF), including the new $^{40}Ar/^{39}Ar$ laser-ablation data on white-mica from this study (solid red bars and brackets). As discussed above, these new data define the cooling interval of 445-400°C, depending on grain-size, and hence record relatively early cooling of the footwall of the KNF. Both cooling trends are interpreted to reflect exhumation related to upright folding and extensional exhumation of the basement nappe complex in the footwalls of the BNF and KNF [*Scharf et al.*, 2013a]. There is a small but consistent difference of some 3 Myr in the age of cooling beneath the BNF compared to the KNF, as discussed below. The samples used to constrain the T-t paths in Figure 6.10 all came from mylonites in the footwalls of the BNF and KNF [see Fig. 6.12 and Table 6.1 in *Scharf et al.*, 2013a for locations of samples used in this compilation] and are located within about 6 km of these normal faults.

The steep part of the cooling curve for the KNF in Figure 6.10 is constrained by the white mica $^{40}Ar/^{39}Ar$ single-grain data and the Rb/Sr systems in white mica and biotite, covering a wide range of closure temperatures from 550 ± 50°C [Rb/Sr white mica; *Purdy and Jäger*, 1976], 445-400°C [$^{40}Ar/^{39}Ar$ white mica; this study] and 350 ± 50°C [Rb/Sr biotite; *Jäger et al.*, 1967]. The much larger 27-19.6 Myr range in the samples of Cliff et al., 1985 (excluding two samples with 214 ± 8 and 226 ± 8 Myr ages) from the core of the ETD is geologically ambiguous because the measured white micas are microstructurally unconstrained. In addition, *Cliff et al.* [1985] noticed that the Rb/Sr white-mica ages are very sensitive to uncertainties in initial isotopic composition. Their samples with the smallest analytical error (< 1 Myr) cluster between 24 and 21 Myr, i.e., within the same age range of our two Rb/Sr on white-mica samples. In all samples, the closure temperature of 550 ± 50°C for the Rb/Sr white-mica system is less than the peak temperature of ~620°C in the core of the ETD [*Droop*, 1985; *Scharf et al.*, 2013b]. Two facts indicate that the Rb/Sr white-mica ages can indeed be interpreted as cooling ages (i) the peak temperature exceeds the closure temperature of the Rb/Sr white-mica system, and (ii) that the Wm_2 grains define the main KNF foliation. Likewise, the 17.0 ± 0.3 Myr Rb/Sr biotite age of *Cliff et al.* [1985] from the south-eastern margin of the ETD, affected by the KNF, is interpreted as a cooling age because the closure temperature of 350 ± 50°C for this system is much less than the peak temperature of ~500°C in this area [*Scharf et al.*, 2013b].

Liu et al. [2001] published $^{40}Ar/^{39}Ar$ white-mica plateau ages in the range of 37-22 Myr for samples from ophiolites and metasediments of the Penninic nappes (Glockner Nappe System, Matrei Zone) mostly located in the periphery and hangingwall of the KNF (sample locations and ages in Fig. 6.1b). Their ages generally decrease from outside the Tauern Window towards the KNF. The authors interpreted their ages as dating cooling after the attainment of greenschist-facies metamorphism during the stacking of the Penninic nappes in Eocene time or earlier. This suggests that cooling of the peripheral parts of the eastern Tauern Window started well before the KNF became active. Such cooling started sometime after 25-28 Myr, the age of thermal peak metamorphism, but no later than 21.1-24.1 Myr (the Rb/Sr white-mica ages). The youngest age (~22 Myr) of *Liu et al.* [2001] located near the KNF is interpreted to date cooling after Penninic nappe stacking in Eocene time and may mark the onset of rapid exhumation in the footwall of the KNF. Unfortunately, the white-mica ages of *Liu et al.* [2001] are of limited use because they are microstructurally unconstrained and represent bulk ages of all microstructural domains in one and the same sample.

To conclude, rapid cooling of rocks within and below the KNF began after the "Tauernkristallisation" which ended no earlier than 28 Myr [*Inger and Cliff*, 1994; *Thöni*, 1999; *Kurz et al.*, 2008], probably at 25 Myr [*Pollington and Baxter*, 2010; *Favaro et al.*, 2015]. The cooling within the KNF started sometime before 21 Myr according to the new ^{40}Ar/^{39}Ar white-mica cooling ages in this study and sometime before 24-21 Myr according to the new Rb/Sr white mica ages. The closure temperature of ^{40}Ar/^{39}Ar white-mica in the basal part of the KNF fell below 445°C at ~20 Myr and at the top part near the hangingwall to ~400°C at ~17 Myr.

The Rb/Sr biotite age of *Cliff et al.* [1985] and zircon fission-track ages of *Dunkl et al.* [2003] indicate that a temperature of ~300°C corresponding to the viscous-frictional transition in quartz-rich rocks [*Handy et al.*, 1999; *Stöckhert et al.*, 1999; *Stipp et al.*, 2002] was reached at 17 Myr in the footwall of the KNF. The similar ages obtained by other geochronometers with different closure temperatures suggest that the footwall of the KNF cooled very rapidly from ~400 to 270°C at about 17 Myr (Fig. 6.10). It is important to note that the ^{40}Ar/^{39}Ar white-mica cooling ages cannot significantly post-date the end of mylonitic deformation in the KNF, because peak temperatures in the rocks affected by this deformation were only ~50°C higher than the closure temperatures of the ^{40}Ar/^{39}Ar white-mica system [*Scharf et al.*, 2013b]. Substantially younger ^{40}Ar/^{39}Ar ages of individual white-mica grains in some samples (~15 Myr) may indicate Ar-loss during shearing after 17 Myr or reduced closure temperature due to grain-size reduction. The difference of the weighted mean zircon fission-track ages of *Dunkl et al.* [2003; 17 Myr] and *Bertrand* [2013; 12.8 Myr] is attributed to the long time the rocks spent within the partial annealing zone after rapid cooling [*Bertrand*, 2013]. As discussed in *Scharf et al.* [2013a], the attainment of the viscous-frictional transition along the KNF at ~17 Myr coincides with the opening of intramontane Miocene pull-apart basins in the hangingwall of the KNF [e.g., the Tamsweg and Seetal basins along the Niedere Tauern Southern Fault in Figs. 6.1 & 6.10 of *Scharf et al.*, 2013a and discussed in their text].

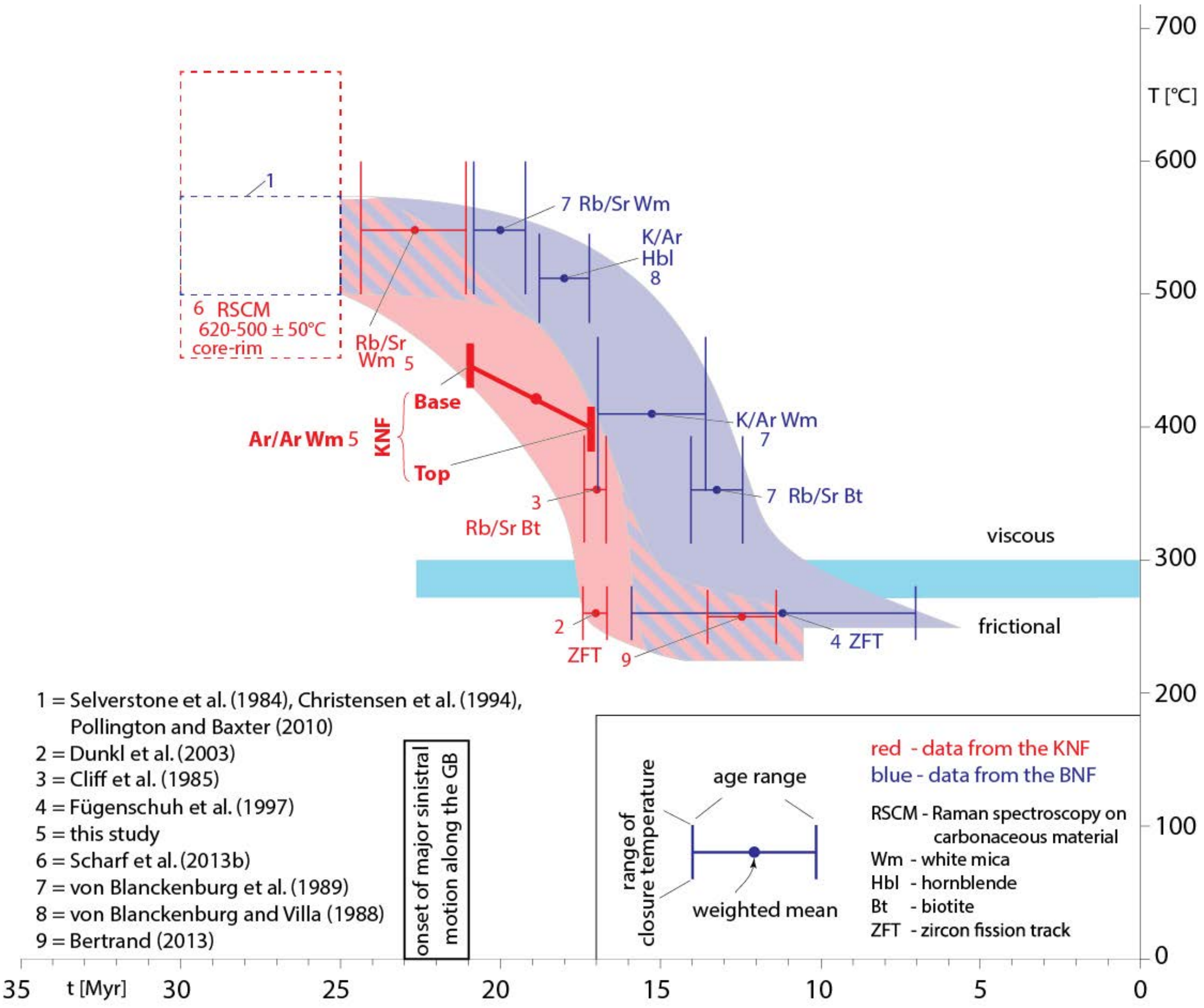

Figure 6.10: Temperature-time paths of the footwall of the Brenner and Katschberg normal faults (BNF - blue, KNF - red) including the ^{40}Ar/^{39}Ar data of this study for the base and top of the KNF (bold red). All samples, systems and localities are listed in the "Supplementaru material 6.8" section of *Scharf et al.* [2013a; their Fig. 6.12 & Table 6.1]. Temperature interval of frictional-viscous transition in quartz-rich rocks taken from *Handy et al.* [1999] and *Stipp et al.* [2002]. Dashed boxes at upper left indicate peak temperature of the "Tauernkristallisation" [in the east after *Scharf et al.*, 2013b; in the west after *von Blanckenburg et al.*, 1989] at 25-30 Myr. ^{40}Ar/^{39}Ar single grain ages outside the 21-17 Myr age range obtained in this study are not included in this figure (see text for discussion "anomalous ages"). Closure temperatures used: Rb/Sr white mica 500 ± 50°C [*Purdy and Jäger*,1976]; K/Ar hornblende 530 +33/-40°C [*Harris*, 1981]; ^{40}Ar/^{39}Ar white mica 445-400°C depending on grain radius and cooling rate (this study; Fig. 6.6); K/Ar white mica 410°C [*von Blanckenburg et al.*, 1989]; Rb/Sr biotite 350 ± 50°C [*Jäger et al.*, 1967 used in *von Blanckenburg et al.*, 1989]; Zircon Fission Track 260 ± 20°C [*Foster et al.*, 1996 used in *Fügenschuh et al.*, 1997; *Dunkl et al.*, 2003; *Bertrand*, 2013]. Note that the closure temperature assumed for the Rb/Sr white-mica system is 500 ± 50°C, which is somewhat below the 550 ± 50°C used by *von Blanckenburg et al.* [1989]. Data of samples from the BNF are within 6 km of the BNF [samples labelled 'LH' and 'PJ' in fig. 1 of *von Blanckenburg et al.*, 1989]. The vertical bar along the time axes at 23-21 Myr indicates the probable onset of the main stage of Adriatic Microplate indentation, as discussed in the text.

6.6.5 Diachronous versus contemporaneous onset of rapid exhumation in the eastern and western Tauern Window

The separate T-t paths for the footwalls of the BNF and KNF in Figure 6.10 indicate that the onset of rapid cooling in the eastern Tauern Window may have predated the onset in the western Tauern Window by ~2-3 Myr. Thermal modelling of cooling ages in the exhumed units beneath the BNF [*Fügenschuh et al.*, 1997] indicates that rapid exhumation there began at ~20 Myr, some 2 Myr before the onset of rapid cooling. This fits well with biostratigraphic evidence for the onset of indentation accommodated by the Giudicarie Belt [Fig. 6.1a, *Luciani and Silvestrini*, 1996] and its lateral continuation to the west [Mt. Orfano area, *Scuinnach et al.*, 2010] some 23 to 21 Myr ago [Fig. 6.10, discussion in *Scharf et al.*, 2013a]. Unfortunately, the onset of rapid exhumation in the footwall of the KNF is not constrained by thermal modelling, making a comparison of the exhumation histories of the BNF and KNF somewhat speculative. Therefore, within the limits of error for the cooling ages, the onset of rapid exhumation in the WTD and ETD may be regarded as either roughly contemporaneous at 20-21 Myr, or diachronous by some 2-3 Myr. We favor the latter interpretation in light of the consistency with which the various of isotopic systems (Fig. 6.10; Rb/Sr wm and bt, K-Ar hbl, ZFT) yield earlier cooling ages in the east than in the west. Even if one assumes a shorter delay time (< 2 Myr) between rapid exhumation and cooling in the eastern Tauern Window, the onset of rapid exhumation in the eastern must have begun before 25-21 Myr ago, the age range of the new Rb/Sr white mica ages and the oldest ^{40}Ar/^{39}Ar white mica cooling ages in this study. This is earlier than indicated by the biostratigraphic constraints on the onset of indentation cited above (23-21 Myr). In fact, *Pomella et al.* [2011, 2012] set the onset of indentation of the Adriatic Microplate east of the Giudicarie Belt in late Oligocene to earliest Miocene time based on isotopic age constraints on transpression and bending of the Periadriatic Fault at its junction with the Giudicarie Fault. However, they do not specify absolute ages for this beyond the kinematic necessity that this bending related to indentation must have post-dated Paleogene dextral motion on the Periadriatic fault [*Pomella et al.*, 2011; Fig. 6.11].

The possibility that exhumation and cooling of the Tauern Window was diachronous raises the question of how. Analogue models of Eastern Alpine indentation using a rigid indenter with a straight front produce upright folds and thrusts that exhume orogenic crust directly in front of the indenter; however [e.g., *Ratschbacher et al.*, 1991; *Rosenberg et al.*, 2007], they produce little or no orogen-parallel extensional exhumation and do not hint at possible diachronous exhumation of deeply buried orogenic crust. We suspect, however, that the indenter front was not straight, but rather comprised two blocks of semi-rigid Austro-alpine crust north of the Periadriatic Fault [marked RF and DM in Fig. 6.1; *Scharf et al.*, 2013a] that individuated during N-S convergence and indented the orogenic crust [*Frisch et al.*, 1998; *Linzer et al.*, 2002] earlier in the eastern part of the Tauern Window than in the west [*Favaro et al.*, 2015]. A full test of this model awaits thermal modelling of cooling ages in the eastern Tauern Window, as well as analogue modelling of indentation with irregular indenter fronts.

6.7 CONCLUSIONS

This study shows that the majority (65%) of white-mica aggregates ages obtained by ^{40}Ar/^{39}Ar laser ablation date cooling below closure temperatures ranging from 445 to < 400°C, depending on grain size, during top-SE extensional shearing at the eastern margin of the Tauern Window. When combined with new Rb/Sr white-mica cooling ages and existing thermochronological ages, the ^{40}Ar/^{39}Ar laser ablation ages constrain rapid cooling in the Eastern Tauern Dome (ETD) to have started in the latest Oligocene – earliest Miocene, i.e., sometime between 25 and 21 Myr, and the rapid cooling have ended no later than 17 Myr. Moreover, the new ^{40}Ar/^{39}Ar white-mica ages indicate that cooling in the KNF reached 445°C at ~20 Myr and subsequently migrated upwards within the KNF towards the already-cool Austroalpine units in the hangingwall. Near the hangingwall, where the grain-size of white mica within the KNF is smaller, temperatures reached the ~400°C closure temperature of the ^{40}Ar/^{39}Ar white-mica system at ~17 Myr. The almost identical ages provided by Rb/Sr on biotite, zircon fission track and ^{40}Ar/^{39}Ar white-mica systems in samples from the top of the KNF indicate that this part of the shear zone cooled very rapidly from ~400 to 270°C. The ^{40}Ar/^{39}Ar white-mica thermochronomter is well suited to date the early-stage rapid cooling history of the KNF because the interval of grain-size dependent closure temperatures (445-400°C) overlaps with the range of temperatures obtained from dynamically recrystallized quartz microstructures [440-510° ± 30°C; *Stipp et al.*, 2002]. A transition from viscous to cataclastic flow at the top of the KNF at ~17 Myr coincides temporally with the opening of intramontane pull-apart basins immediately east of and in the hangingwall of the KNF [*Scharf et al.*, 2013a].

6.8 SUPPLEMENTARY MATERIAL TO CHAPTER 6

Table 6.1.A shows the summary of the white-mica compositions of the nine samples, including their different microfabrics used in this study. Note that the values are average values.

Table 6.1.A: Summary of microprobe results of all nine samples with sample name, lithology, tectonic unit, mineral, microfabrics and number of measurements (# analyses). AA, Austroalpine Unit; GL, Glockner Nappe System; MO, Modereck Nappe System; PVC, Post-Variscan cover; ST, Storz Nappe; see Fig. 6.1 and *Schmid et al.* [2013] for further details; ms, muscovite; pg, paragonite; Wm_1 - refolded grains; Wm_2 - grains parallel to the main foliation; Wm_3 - white mica aligned parallel to shear bands formed during KNF shearing; Wm_4 - post-kinematic grains; Wm_{NO} - grains with no preferred orientation.

sample	AS1		AS27	AS36	AS41		AS46	AS51		AS52	AS63	AS74	
lithology	mica schist		mica schist	paragneiss	mica schist		mica schist	mica schist		mica schist	para gneiss	mica schist	
tectonic unit	GL		GL	AA	MO		MO	ST		ST	PVC	PVC	
mineral	ms	ms	ms	ms	ms	ms	ms	ms	pg	ms	ms	ms	ms
microfabric	Wm_2	Wm_1	Wm_2	Wm_{NO}	Wm_2	Wm_3	Wm_2	Wm_2	Wm_3	Wm_2	Wm_{NO}	Wm_4	Wm_2
# analyses	32	17	13	38	3	2	25	23	3	15	56	17	14
SiO_2	49.46	49.32	52.81	49.63	49.82	49.78	49.66	48.11	47.37	50.54	49.92	49.44	49.64
TiO	0.11	0.12	0.14	0.19	0.13	0.14	0.15	0.22	0.25	0.21	0.18	0.12	0.12
Al_2O_3	31.77	30.50	26.95	31.07	30.22	32.22	31.64	27.21	28.27	29.47	30.94	30.87	30.58
FeO	2.60	2.17	1.35	2.53	3.39	2.80	1.68	2.37	2.45	3.00	1.52	3.64	3.56
MgO	1.37	1.18	2.85	1.51	1.19	0.91	1.01	2.06	1.72	1.85	1.34	0.92	1.00
CaO	0.01	<0.01	<0.01	<0.01	<0.01	0.01	<0.01	<0.01	<0.01	<0.01	0.27	0.01	0.01
Na_2O	0.37	0.33	0.02	0.30	0.38	0.53	0.37	0.23	0.23	0.29	0.34	0.39	0.31
K_2O	9.35	9.86	12.19	10.34	10.29	9.90	9.74	10.26	10.41	10.60	9.75	10.34	10.60
Total	95.05	93.49	96.31	95.58	95.43	96.30	94.26	90.46	90.69	95.97	94.26	95.73	95.82
Si	3.33	3.38	3.50	3.32	3.35	3.31	3.37	3.40	3.34	3.38	3.39	3.32	3.33
Ti	0.01	0.01	0.01	0.01	0.01	0.01	0.01	0.01	0.01	0.01	0.01	0.01	0.01
Al	2.52	2.46	2.10	2.45	2.40	2.53	2.53	2.27	2.35	2.32	2.47	2.44	2.42
Fe^{3+}	0.15	0.12	0.07	0.14	0.19	0.16	0.10	0.14	0.14	0.17	0.09	0.20	0.20
Mg	0.14	0.12	0.28	0.15	0.12	0.09	0.10	0.22	0.18	0.18	0.14	0.09	0.10
Ca	<0.01	<0.01	<0.01	<0.01	<0.01	<0.01	<0.01	<0.01	<0.01	<0.01	0.02	<0.01	<0.01
Na	0.05	0.04	<0.01	0.04	0.05	0.07	0.05	0.03	0.03	0.04	0.04	0.05	0.04
K	0.80	0.86	1.03	0.88	0.88	0.84	0.84	0.93	0.94	0.90	0.84	0.89	0.91
H	2.00	2.00	2.00	2.00	2.00	2.00	2.00	2.00	2.00	2.00	2.00	2.00	2.00
Total	7.00	7.00	7.00	7.00	7.00	7.00	7.00	7.00	7.00	7.00	7.00	7.00	7.00

Tectonic history

The Neogene north-south shortening in the Eastern Alps was contemporaneous with orogen-parallel extension and eastward extrusion of a wedge-shaped piece of crust in map view, as delimited to the north and south, respectively, by the Salzach-Ennstal-Mariazell-Puchberg (SEMP) Fault and the Periadriatic (PF) Fault [*Ratschbacher et al.*, 1991; *Rosenberg et al.*, 2007; *Scharf et al.*, 2013; *Schmid et al.*, 2013]. Indentation induced rapid exhumation (≤ 1 mm/yr) and cooling (≤ 40°C/Myr) of the Subpenninic- and Penninic units of the Tauern Window [e.g., *Fügenschuh et al.*, 1997; *Luth and Willingshofer*, 2008; *Scharf et al.*, 2013]. Orogen-parallel extension was facilitated by the opening of the Pannonian Basin at 20 Myr [*Fodor et al.*, 1999]. The eastward extension caused by the extension beneath the Pannonian Basin, only affected the Austroalpine units immediately east of the eastern Tauern Window during the final stage of rapid exhumation 17 Myr [*Scharf et al.*, 2013]. The tectonic units of the Tauern Window and the Austroalpine frame and their Cenozoic evolution, including faults and folds, are presented and discussed in greater detail in *Scharf et al.* [2013] and *Schmid et al.* [2013].

Detailed sample information

Two of the samples (AS63 and AS74) are metapelites from the Post-Variscan cover of the Subpenninic units. These metasediments, mostly marbles and mica-schists [Silbereck Unit; *Exner*, 1939], experienced Alpine metamorphism and are sandwiched between the Hochalm- and Storz nappes of the Venediger Duplex (Fig. 6.1b). Sample AS63 contains mostly quartz, white mica, albite, biotite and opaque minerals. Sample AS74 contains quartz, white mica, calcite and opaque minerals. Two samples (AS51 and AS52) are derived from pre-Variscan paragneisses ["Storz Komplex"; *Exner*, 1971] that are part of the Storz Nappe (Fig. 6.1b). This nappe represents the structurally highest unit of the Venediger Duplex [*Schmid et al.*, 2013]. Those two samples contain quartz, white mica, chlorite, albite and opaque minerals. Another three samples [AS27, AS41 and AS46 all from the "Brennkogel Formation"; see *Pestal et al.*, 2009 and *Schmid et al.*, 2013 for further details] are quartz- and albite-rich metapelites taken from the Modereck Nappe System located above the roof thrust of the Venediger Duplex and detached from the distal-most European continental margin [Fig. 6.1b; *Schmid et al.*, 2013]. Sample AS27 contains quartz, white mica and opaque minerals, whereas the other two samples AS41 and AS46 contain in addition albite and AS46 garnet. Sample AS1 is a metapelite from the Glockner Nappe System, derived from the Valais branch of the Alpine Tethys (Fig. 6.1b). This sample AS1 contains quartz, white mica, chlorite, albite, garnet and opaque minerals. Sample AS36 is an amphibolite-facies paragneiss belonging to the Radenthein Complex of the Upper Austroalpine Unit (Koralpe Nappe System) in the hangingwall of the Katschberg Normal Fault (KNF; Fig. 6.1b). This sample contains quartz, feldspar, white mica, biotite and opaque minerals.

^{40}Ar/^{39}Ar age distributions in the samples

The smallest scatter in the grain ages is found in sample AS74, yielding an average age of 19.64 ± 0.61 Myr (Fig. 6.5h & Table 6.1). AS74 is from the northern dextral strike-slip branch of the KNF (Fig. 6.1) and contains two categories of mica grains (Wm_2 and Wm_4). The average ages only insignificantly differ from each other (Fig. 6.5h). A small scatter is also found in the annealed sample AS63 giving a mean age of 18.16 ± 0.96 Myr (Fig. 6.5g & Table 6.1). The scatter in Sample AS46 with a mean age of 18.93 ± 0.74 Myr (weighted average age: 18.90 ± 0.21 Myr; Fig. 6.5d) is also small, but the number of grains measured is also little (N = 5). A somewhat greater scatter is seen in specimen AS41 with a mean age of 17.88 ± 0.92 Myr (Fig. 6.5c & Table 6.1). The average ages for these four samples only vary little and are between 17.88 Myr (AS41) and 19.64 Myr (AS74) in spite of the fact that the four samples substantially vary in terms of location (AS63 is outside the area affected by the shearing within the KNF, while AS41 and AS46 are within an intensely sheared part of the KNF near the margin of the ETD; Fig. 6.1b).

Sample AS1 with a mean age of 17.11 ± 0.98 Myr (Fig. 6.5a & Table 6.1) has a small scatter although it contains two categories of grains (Wm_1 and Wm_2) whose average means do not significantly differ. The scatter of grain ages is significantly greater in the following two samples (Table 6.1): AS27 (22.11 ± 2.43 Myr); AS51 (20.53 ± 4.23 Myr). Sub-populations in these two samples exhibit rather old average ages (23.26 ± 0.81 Myr) in the case of specimen AS27 (Fig. 6.5b) or rather young average ages (15.10 ± 1.27 Myr) for sample AS52 (Fig. 6.5f).

Sample AS36 (Fig. 6.8 & Table 6.1), originating from the Upper Austroalpine units in the hangingwall of the KNF, reveals a mean age of 75.67 ± 1.93 Myr. This is expected since the degree of Cenozoic-age metamorphism in the Upper Austroalpine units above the KNF did not allow for resetting the $^{40}Ar/^{39}Ar$ system that, hence, reflects Cretaceous-age metamorphism.

Closure temperature versus grain radius

The closure temperature depends on the cooling rate and the diffusion radius (smallest grain length of the elongated white mica divided by two) of the mica [Figs. 6.6 & 6.7; *Harrison et al.*, 2009]. It is assumed that the cooling rate in all eight samples from within the KNF or in its immediate footwall experienced the same constant cooling rate of ≤ 40°C/Myr. Therefore, grain size is expected to control the closure temperature of the white micas. Moreover the $^{40}Ar/^{39}Ar$ diffusion curves from the experiments of *Harrison et al.* [2009] are calculated under the assumption of radial diffusion in the micas. Only the smallest diffusion radius (grain radius) of a individual white mica was used for determining the grain-size dependent cooling temperature. The radiuses of the individual white micas are listed in Table 6.1 and averaged for each sample in Table 6.2. The closure temperature varies from ~400 to ~445°C for diffusion radiuses of < 50 to ~250 μm, respectively (Fig. 6.7).

It must be kept in mind that the large spread of single grain ages in some of the samples from the KNF makes it difficult to assign all ages to the same closure temperature during cooling. Therefore, single grain ages reflect several factors that are not directly related to the history of exhumation.

Sample AS1 lends itself particularly well for applying the closure-temperature concept. The average age of all grains (17.10 ± 0.98 Myr) is interpreted to represent the time when the temperature dropped below the closure temperature in the upper part of the KNF, just below the hangingwall. The closure temperature for this particular specimen is expected to have been ~400°C given the small grain size of this specimen (radius of < 50 μm; Figs. 6.2a & 6.3a) and an assumed constant cooling rate of ≤ 40°C/Myr in the exhuming footwall of a low-angle normal fault.

In sample AS74, another sample with two microstructurally distinct grain populations (Wm_2 and Wm_4) but from the base of the KNF, the $^{40}Ar/^{39}Ar$ white-mica ages are identical within error (Fig. 6.5h). Some of the post-kinematic grains (Wm_4) are slightly older, probably due to their larger size (~250 by 250 μm; Figs. 6.2b, 6.3b, 6.6, 6.7, Tables 6.1 & 6.2) and, hence, somewhat higher closure temperature (~445°C) than that of the Wm_2 micas defining the main mylonitic foliation (~420°C). Thus, applying the same logic as above for sample AS1, the average age of all grains in sample AS74

(19.64 ± 0.61 Myr; Table 6.1) is interpreted to date the time when temperature dropped to below ~445°C [*Harrison et al*., 2009]. Because Wm_4 is post-kinematic, this closure temperature must have been reached after the shearing ended along the base of the KNF. Thus, shearing along the warm base of the KNF ended no later than ~20 Myr, i.e., at least 3 Myr earlier than at the cooler top of the KNF. The estimated closure temperature of Wm_4 in sample AS74 (~445°C) is slightly below the peak temperature reached along the base of the KNF [500-525°C; *Scharf et al*., 2013b]. Thus, the KNF-related shearing at the base of the KNF is likely to have occurred at a temperature slightly below the peak-metamorphic temperature attained during the "Tauernkristallisation" event in late Oligocene time.

Sample AS46 containing the main KNF mylonitic foliation (Wm_2) and located between the two aforementioned samples, has an average age distribution of ~19 Myr (Figs. 6.1b, 6.5d, 6.6, Tables 6.1 & 6.2) for grains with a radius of ~75 µm, which can likewise be interpreted to date cooling below ~415°C.

Wm_3 grains from shear bands in samples AS41 (~18 Myr) and AS51 (~20.5 Myr) yield the same ages within error as most Wm_2 grains in the same sample (Table 6.1). This is an additional indication that almost all white-mica ages in these samples are either cooling or formational ages (see minor exceptions below). Based on the grain size of the micas the closure temperature is expected to be ~420 and ~440°C, respectively (Figs. 6.6, 6.7, Tables 6.1 & 6.2).

The annealed sample, AS63 with randomly oriented white-mica laths (Wm_{NO}), comes from the domain of statically recrystallized "Tauernkristallisation" fabrics beneath the KNF (Figs. 6.1b, 6.2d & 6.3d). The average age of these white micas (~18 Myr with a closure temperature of ~440°C, Figs. 6.5g, 6.6, 6.7, Tables 6.1 & 6.2) indicates that exhumation by KNF-related shearing must have started > 18 Myr ago, regardless of whether the ages are interpreted as formation or cooling ages. This is consistent with arguments regarding sample AS74, from the base of the KNF, that shearing at the base of the KNF ended no later than > 20 Myr when temperatures fell below an assumed closure temperature of ~445°C at the base of the KNF.

Chapter 7: Conclusion and future work

7.1 CONCLUSIONS

Accretion of units exposed in the Tauern Window began with Late Cretaceous thrusting of the Adriatic margin onto oceanic units of Alpine Tethys. This continued throughout the early Cenozoic with the subduction (D1) and early exhumation (D2-D3) of imbricated oceanic and distal European units, as recorded by Eocene high-pressure metamorphic assemblages [e.g., *Kurz et al.*, 2008 and refs.]. The onset of collision between the Eupean and Adriatic plates at c. 35 Ma is marked by nappes and duplex formation (D4, Venediger Nappe System) in the European basement units forming the core of the Tauern Window. Rapid exhumation began no later than 20-23 Ma and lasted until about 15 Ma in the Tauern Window area. This shortening, due to indentation of the Adriatic Microplate, was accommodated by a combination of km-scale upright-folding, doming and low-angle normal faulting (D5) at both eastern and western ends of the Tauern Window.

The structure evolution of fault-bounded blocks of Austroalpine crust arrayed along the front of the Adriatic Indenter had a first-order effect on the pattern of shortening and lateral escape of the orogenic crust in the Tauern Window. In the eastern part of the window, initial indentation at c. 23 Ma involved post-nappe upright folding that propagated away from the indenter front as indicated by the northeastward younging of mica cooling ages in the Venediger Nappe System [*Favaro et al.*, 2015]. According to our cooling model in chapter 3, rapid exhumation initiated near the Giudicarie Belt where north-south shortening was greatest and after jumped to the Eastern Tauern Dome and latest to the Brenner and Katschberg Normal faults. The cooling pattern of the Tauern Window, described in chapter 3, reflect this migration and we relate it to the fragmentation of an initially triangular zone of little or no ductile deformation comprising mostly Austroalpine units in front of the Adriatic Indenter. With progressive indentation, this zone was subdivided into two, semi-rigid crustal blocks (Rieserferner and Drau-Möll blocks) along the leading edge of this indenter. Miocene doming, exhumation and cooling of the eastern part of the Tauern Window (ETD) occurred directly in front of the Drau-Möll Block as is demonstrated by our new ^{147}Sm/^{144}Nd isochron age of 25.7 ± 0.9 Ma on garnet and ^{87}Rb/^{87}Sr white mica and biotite ages which show coeval cooling of the Sonnblick and Hochalm subdomes within the ETD to below 500 and 300°C at about 30-21 and 23-15 Ma, respectively. The cooling ages of these mica systems decrease from the center of the Tauern Window toward the KNF, reaching 24-21 Ma (^{87}Rb/^{87}Sr white mica) and 18-15 Ma (^{87}Rb/^{87}Sr biotite) in the KNF footwall. Taken together, the new and existing thermochronological data show that the ETD was folded and exhumed as a single unit; doming migrated perpendicular to the indentation direction and parallel to motion of the eastward rolling footwall of the KNF during lateral orogenic escape. This change in the relative age of doming and peak-thermal metamorphism reflects the migration of tectonic and erosional unroofing from the center to the ends of the Tauern Window during lateral orogenic escape in latest Oligocene and Miocene time.

The contrast in rheology of the cold indenting block and hot orogenic crust is expressed by opposite shear senses in cataclasite along the indenter front (Mölltal Fault, dextral type 1 cataclasites, see chapter 2) and in mylonite along the adjacent margin of the eastwardly stretching and exhuming Eastern Tauern Dome [sinistral southern branch of the Katschberg Normal Fault, see also *Scharf et al.*, 2013]. By 17 Ma, the orogenic crust had cooled to below 300°C [*Dunkl et al.*, 2003; *Bertrand et al.*, 2013], resulting in brittle top-SE extension as recorded by shear surfaces in both the Austroalpine and Penninic units (cataclasites of the KNF and type 2 cataclasites of the Mölltal Fault, see chapter 2).

Similar patterns of indentation, folding and orogen-parallel stretching are also observed in the Western Tauern Window where, however, shortening was much greater and kinematically linked to lateral escape along the sinistral SEMP Fault via a transpressional bridge structure [*Scharf et al.*, 2013]. This bridge structure, which after 21 Ma included the Brenner Normal Fault [*Fügenschuh et al.*, 1997], accommodated some 70 km of E-W extension.

Retrodeforming the post-nappe fold and fault systems of the entire Tauern Window in map view yields a reconstruction of the orogenic crust reaching back to 30 Ma, including the onset of indentation at c. 23 Ma (Fig. 2.7 of chapter 2). This 2-D model supports the notion that indentation lead to roughly equal amounts of north-south shortening (75 km) and east-west orogen-parallel stretching (71 km) of the orogenic crust in the Tauern Window. Estimates of the areas of denudation prior to and after the onset of indentation indicate that erosion associated with upright folding and thickening was the primary agent of denudation, whereas extensional unroofing accounted for only about a third of the total denudation and affected only the eastern and western ends of the Tauern Window.

Previous models of lateral escape and denudation in the Eastern Alps have tended either to emphasize the role of post-nappe, upright folding in the Tauern Window with only a modest contribution of orogen-parallel extension [*Laubscher*, 1988; *Lammerer*, 1988; *Behrmann*, 1988; *Rosenberg et al.*, 2004, 2007; *Rosenberg and Garcia*, 2011, 2012] or, on the contrary, to assume orogen-parallel extension and unroofing to the virtual exclusion of upright folding [*Genser and Neubauer*, 1989; *Frisch et al.*, 2000; *Linzer et al.*, 2002]. We follow *Fügenschuh et al.* [1997] in proposing a mix of coeval folding and orogen-parallel stretching of the Tauern Window in Miocene time, but emphasize that the eastern and western parts of this window experienced different patterns of shortening and orogen-parallel stretching: in the east, doming initiated before stretching and migrated from SW to NE away from the indenter front, whereas in the west, strike-slip shearing preceded upright folding and this folding progressed from NW to SE towards the indenter [*Schneider et al.*, 2013].

These contrasting strain patterns may reflect varied structure of the interface between indenting and indented crust along strike of the Tauern Window. Gravimetry reveals a robust mass deficit in the vicinity of the western Tauern Window [*Ebbing e al.*, 2006], suggesting the existence of an anomalously dense body (c. 2.9 g/cm) in the underlying crust. A recent Moho study based on inverting the results of four independent geophysical methods (controlled-source seismology, ambient noise and local earthquake tomographies, receiver functions) indicates that the Moho beneath the eastern half of the Tauern Window is poorly defined or even absent [*Spada et al.*, 2013]. Solving this problem is contingent on higher resolution studies of the substructure along the front of the Adriatic Indenter.

7.2 FUTURE WORK

7.2.1 Ar/Ar dating

In Chapter 6 we show Ar-Ar spot dating on white mica from orthogneises and shear zones of the Katschberg Normal Fault, at the eastern end of the Tauern Window. Usually, while for biotites scattering age values, due to different amounts of excess Argon, are often documented [western Tauern Window, *Schneider et al.*, 2013], white micas yield excellent indications for the activity of shear zones. Summarizing the results from the eastern Tauern Window [*Scharf et al.*, 2013] and the western Tauern Window [*Schneider et al.*, 2013], the coarser muscovite flakes shows regional cooling below 400±50 °C before phengitic white mica from the same shear zones. Phengitic mica develops at lower greenshist facies conditions and by the expense of biotite. Rb/Sr biotite ages from the same areas displays younger ages then the phengitic white micas [*Borsi et al.*, 1973, 1978; *Satir*, 1975; *Luth & Willingshofer*, 2008] and they indicate cooling below 300±50 °C, the end of greenschist facies metamorphism. These ages are confirmed by zircon fission track ages of *Most* [2003].

This implies that the knowledge of the Ar/Ar muscovite ages and corresponding Rb-Sr biotite ages of orthogneisses gives a range for the phengitic white mica which grew during greenshist facies deformation. In the eastern part of the Tauern Window we find also deformed orthogneisses with two mica generations. The Rb/Sr biotite ages of these samples are measured and described in chapter 3 and the Ar/Ar muscovite ages with the coarser grains would allow defining the age range of the phengitic muscovite grown during the late ductile greenschist facies deformation (in analogy to the western part of the Tauern Window). Further with Ar/Ar muscovite, Rb/Sr biotite and Apatite-fission track it would be possible to define better cooling curves of the individual gneiss domes in the eastern part of the Tauern Window. Differences in the cooling history imply relative movements of the domes and the ages give time constrains on the related deformation.

Samples for Ar/Ar dating

Eight samples were already selected for Ar/Ar multigrain dating. These samples are described in the following. Based on textural relations and grains size some of these samples contain more than one mica generations. However, due to the used separation technique only the coarse grained generation, and in all cases the oldest generation was separated.

According to geological maps [*Exner*, 1959; *Schmid et al.*, 2013], the Venediger Nappe System in the eastern Tauern Window consists of at least three basement nappes. These nappes are the Sonnblick, Romate and Hochalm nappes. For the Sonnblick Nappe Rb/Sr muscovite ages > 27 Ma and Rb/Sr biotite ages of 19-23 Ma are reported [*Reddy et al.*, 1993; *Cliff et al.*, 1985]. The youngest biotite ages are found around Obervellach, where the so-called “Sonnblick Lamelle” develops from the main part of the dome. Further to the southeast new Rb/Sr data are now available from the "Sonnblick Lamelle" [*Favaro et al.*, 2015]. Fission track data show the same trend [*Staufenberg*, 1987; *Wölfler et al.*, 2008]. From the Hochalm Nappe Rb/Sr muscovite ages between 20-25 Ma and Rb/Sr biotite ages of 16-18 Ma were measured [*Reddy et al.*, 1993; *Favaro et al.*, 2015]. The Rb/Sr biotite ages of more than 20 Ma from the Sonnblick Nappe were measured northwest of Obervellach, whereas those from the Hochalm nappe come from the southeast. To enlarge the data set we sampled three syenitic orthogneisses (11R29, 11R32) of the Romate Nappe (Romate orthogneiss) to compare Rb-Sr biotite ages of those with those from the other basement nappes. Further one sample of the Sonnblick orthogneiss in the "Sonnblick Lamelle" near to Kolbnitz was collected (11R30) to prove if the trend to younger ages in the lamella continues to the southeast.

Few data are available for the Modereck Nappe System and the Glockner Nappe System, which form the core of the Mallnitz Synform and the northeastern slopes of the Möll valley. One Ar/Ar amphibol age of the Kolm nappe [*Cliff et al.*, 1985] of the Glockner Nappe System at Auernig yielded c. 23 Ma [*Cliff et al.*, 1985]. This hornblende age suggests that this nappe exhumed together with the underlying Hochalm- and Romate nappes.

The nappes in the Mallnitz Synform may have been exhumed together with the Sonnblick or with the joint Hochalm (05R29, 04R64) and Romate nappes (11R29, 11R34), or at a different time. So far not enough data to answer this question is available. For this reason we collected samples for Ar/Ar muscovite dating. One from micaschist (Woisken Schiefer) from the "Alte Dach" of the Romate Nappe (SF1-11 = 11R35), a paragneiss from the "Alte Dach" of the Sonnblick Nappe (11R40), and several samples across the tectonic units forming the Mallnitz Synform (11R50). Moreover, one chlorite-biotite schist from the Kolm Nappe in the Kaponig valley (11R31, 11R32) and a sample of garnet-bearing micaschist (Woiskenschists 11R30) were collected in the Rieken Graben.

7.2.2 Exhumation structures in the Tauern Window and their relation to present-day crust-mantle structure in the Eastern Alps.

The MOHO attains a maximum depth of 50-52 km at the western end of the Tauern Window, where it appears to be sinistrally offset by the Guidicarie Line. To the east, this thickness gradually decreases to about 44 km at the eastern end of the Tauern Window, and to as little as 38-40 km towards the Pannonian Basin. The Tauern Window also coincides broadly with a positive Vp mantle anomaly, which in tomographic studies is variously interpreted as a lithospheric slab dipping steeply to the N [*Lippitsch et al.*, 2003] or to the S [*Mitterbauer et al.*, 2011]. We attribute the formation of the MOHO root beneath the Tauern Window to a combination of Oligocene nappes stacking and Miocene late-orogenic doming. Doming coincided broadly with two kinematically related events: (1) sinistral Guidicarie faulting which reaches down to the base of the thickened crust and deforms the MOHO; (2) E-W stretching of the orogenic crust in the footwall of the normal faults bounding the Tauern Window. This would supports the notion that pronounced exhumation and lateral escape were triggered by indentation of the eastern part of the rigid Adriatric microplate. This indentation may be related to the high Vp mantle anomaly beneath the Eastern Alps. However, too relate the kinematics of crustal thickening and exhumation in the Tauern Window to these first-order geophysical anomalies would require additional investigation.

REFERENCES

Ahrendt, H. **1980**. Die Bedeutung der Insubrischen Linie für den tektonischen Bau der Alpen. *N. Jb. Geol. Paläont. Abh.* **160**, 336-362.

Angel, F. and Staber, R., 1952. Gestainswelt und bauder Hochalm-Ankigel-Gruppe (mit 1 Geol. Karte 1:50000). *Wiss. Alpenvereinshefte*, **13**, Innsbruck, Universitaetsverl. Wagner.

Argand, E., 1924. Des Alpes et de l'Afrique. *Bull. Soc. Vaudoise Sci. Nat.*, **55**, 233-236.

Bada, G., Horvath, F. , Dövényi, P., Szafian, P., Windhoffer, G., Cloetingh, S., 2007**.** Present-day stress field and tectonic inversion in the Pannonian basin. *Global and Planetary Changes*, **58**, 165-180.

Barnes, J.D., Selverstone, J., Sharp, Z.D., 2004. Interactions between serpentinite devolatilization, metasomatism and strike-slip strain localization during deepcrustal shearing in the Eastern Alps. *Journal of metamorphic Geology,* **22**, 283–300.

Beaumont, C., Jamieson, R.A., Nguyen, M.H. and Lee, B., 2001. Himalayan tectonics explained by extrusion of a low-viscosity crustal channel coupled to focused surface denudation. *Nature*, **414**, 738-742, doi: 10.1038/414738a.

Becker, B., 1993. The structural evolution of the Radstadt Thrust System, Eastern Alps, Austria — kinematics, thrust geometries, strain analysis. *Tübinger Geowissenschaftliche Arbeiten*,**14**, 92.

Behrmann, J.H., 1988. Crustal-scale extension in a convergent orogen: the Sterzing–Steinach mylonite zone in the Eastern Alps. *Geodinamica Acta,* **2 (2)**, 63–73.

Bertrand, A., 2013. Exhuming the core of collisional orogens, the Tauern Window (Eastern- Alps) - A geochronological, modelling and structural study. PhD thesis. Freie Universität Berlin, Berlin, Germany.

Bertrand, A., Rosenberg, C., and Garcia, S., 2015. Fault slip analysis and late exhumation of the Tauern Window, Eastern Alps. *Tectonophysics*, **649**, 1-17. doi:10.1016/j.tecto.2015.01.002.

Bistacchi, A., Massironi, M., Menegon, L., 2010. Three-dimensional characterization of a crustal-scale fault zone: The Pusteria and Sprechenstein fault system (Eastern Alps). *Journal of Structural Geology*, **32**, 2022-2041.

Borsi, S., Del Moro, A., Sassi, F.P., Zirpoli, G., 1973. Metamorphic evolution of the Austric rocks to the south of the Tauern Window (eastern Alps): radiometric and geopetrologic data. *Memorie della Società Geologica Italiana*, **12**, 549–571.

Borsi, S., Del Moro, A., Sassi, F.P., Zanferrari, A., Zirpoli, G., 1978. New geopetrologic and radiometric data on the Alpine history of the Austridic continental margin south of the Tauern

Window (Eastern Alps). *Memorie degli Instituti di Geologia e Mineralogia dell'Università di Padova*. **32,** 1–17.

Borsi, S., Del Moro, A., Sassi, F.P., and Zirpoli, G., 1979. On the age of the Vedrette di Ries (Rieserferner) massif and its geodynamic significance. *Geologische Rundschau*, **68(1)**, 41-60.

Bousquet, R., Oberhänsli, R., Schmid, S.M., Berger, A.,Wiederkehr,M., Robert, C., Möller, A., Rosenberg, C., Zeilinger, G., Molli, G., Koller, F., 2012. Metamorphic framework of the Alps. *Commission for the Geological Map of the World* (CCGM/CGMW).

Bögel, H.,1975. Zur Literatur über die "Periadriatische Naht". *Verh. Geol. B.-A.*, **2-3**, 163-199.

Brack, P.B., 1985. Multiple intrusions – examples from the Adamello batholith (Italy) and their significance on the mechanism of intrusion, *Memorie della Società Geologica Italy*, **26**, 145–157.

Brewer, M.S., 1969. Excess radiogenic argon in metamorphic micas from the Eastern Alps, Austria. *Earth and Planetary Science Letters*, **6**, 321-331.

Campani, M., Herman, F. and Mancktelow, N.S., 2010. Two- and three-dimensional thermal modelling of a low-angle detachment: Exhumation history of the Simplon Fault Zone, central Alps. *Journal of Geophysical Research*, **115**, B10420, doi: 10.1029/2009JB007036.

Castellarin, A., Vai, G.B., Cantelli L., 2006. The Alpine evolution of the Southern Alps around the Giudicarie faults: A Late Cretaceous to Early Eocene transfer zone. *Tectonophysics*, **414**, 203-223.

Christensen, J.N., Selverstone, J., Rosenfeld, J. L. and De Paolo, D. J., 1994. Correlation by Rb-Sr geochronology of garnet growth histories from different structural levels within the Tauern Window, Eastern Alps. *Contributions to Mineralogy and Petrology*, **118**, 1–12.

Clark, S.P. and Jäger, E., 1969. Denudation rate in the Alps from geochronologic and heat flow data. *American Journal of Sciences*, **267(10)**, 1143-1160.

Clark, M.K., J.W.M. Bush, and Royden L.H., 2005. Dynamic topography produced by lower crustal flow against rheological strength heterogeneities bordering the Tibetean Plateau, *Geophys. J. Int.*, **162**, 575-590, doi: 10.1111/j.1365-246X.2005.02580.x.

Cliff, R.A. and Cohen, A., 1980. Uranium–lead isotope systematics in a regionally metamorphosed tonalite from the Eastern Alps. *Earth and Planetary Science Letters*, **50**, 211–218.

Cliff, R.A., Droop, G.T.R., Rex, D.C., 1985. Alpine metamorphism in the south-east Tauern Window, Austria: 2. Rates of heating, cooling and uplift. *Journal of Metamorphic Geology*, **3**, 403–415.

Cliff, R.A. and Meffan-Main, S., 2003. Evidence from Rb-Sr microsampling geochronology for the timing of Alpine deformation in the Sonnblick Dome, SE Tauern Window, Austria. In: Vance, D., Müller, W., and Villa, I.M. (eds) 2003. Geochronology: Linking the Isotopic Record with Petrology and Textures. *Geological Society, London, Special Publications,* **220**, 159-172.

Cliff, R.A., Norris, R.J., Oxburgh, E.R.,Wright, R.C., 1971. Structural, metamorphic and geochronological studies in the Reisseck and southern Ankogel Groups, the Eastern Alps. *Jahrbuch der Geologischen Bundesanstalt Wien,* **144 (2)**, 121–279.

Cliff, R.A., Oberli, O., Droop, G.T.R., 1998. Achieving geological precision in metamorphic geochronology: a Th-Pb age for the syn-metamorphic formation of the Mallnitzermulde Synform, Tauern Window, from individual allanite porphyroblasts. *J. Conf. Abstr. V.M. Goldschmidt Conf.* **62A**, 337-338.

Cliff, R.A., Oberli, F., Meier, M., Droop, G.T.R. and Kelly, M., 2015. Syn-metamorphic folding in the Tauern Window, Austria dated by Th-Pb ages from individual allanite porphyroblasts. *Journal of metamorphic Geology*, **33**, 427-435.

Dachs, E., 1990. Ceothermobarometry in metasediments of the southern Grossvenediger area (Tauern Window, Austria). *Journal of Metamorphic Geology*, **8**, 217-230.

Dachs, E., Kurz, W. and Proyer, A., 2005. Alpine eclogites in the Tauern Window. *Mitteilungen der Österreichischen Mineralogischen Gesellschaft*, **150**, 199-226.

Dal Piaz, G.V., 1999. The Austroalpine-Piedmont nappe stack and the puzzle of Alpine Tethys. *Memorie di Scienze Geologiche*, **51(1)**, 155-176.

Davies, J. H., and von Blanckenburg, F., 1995. Slab breakoff: a model of lithosphere detachment and its test in the magmatism and deformation of collisional orogens. *Earth and Planetary Science Letters*, ***129*****(1)**, 85-102.

Decker, K., Peresson, H. and Faupl. P., 1994. Die miozäne Tektonik der östlichen Kalkalpen: Kinematik, Paläospannung und Deformationsaufteilung während der „lateralen Extrusion" der Zentralalpen. *Jahrbuch der Geologischen Bundesanstalt, Wien*, **137**, 5-18.

Del Moro, A., Puxeddu, M., Radicati di Brozolo, F. and Villa, I.M., 1982. Rb/Sr and K-Ar ages on minerals at temperatures of 300°–400° C from deep wells in the Larderello geothermal field (Italy). *Contributions to Mineralogy and Petrology*, **81(4)**, 340-349.

Del Moro, A., G. Pardini, C. Quercioli, I.M. Villa and E. Callegari, 1985. Rb/Sr and K/Ar chronology of adamello granitoids, southern Alps, *Memorie della Società Geologica,* Italy, **26**, 285–299.

Delvaux, D. (1997). Present-day intraplate stress field in the Varican Front and Rhenish Massif: Influence of rifting and reactivation of pre-existing structures. *Aardkundige Mededelingen*, **8**, 57-60.

Delvaux, D. and Sperner, B., 2003. Stress tensor inversion from fault kinematic indicators and focal mechanism data: the TENSOR program. *New insights into structural interpretation and modelling*, **212**, 75-100.

Deutsch, A., 1984. Young Alpine dykes south of the Tauern Window (Austria): A K-Ar and Sr isotope study, *Contrib. Mineral. Petrol.,* **85**, 45- 57.

Dodson, H., 1973. Closure temperature in cooling geochronological and petrological systems. *Contributions to Mineralogy and Petrology*, **40**, 259-274.

Droop, G.T.R., 1985. Alpine metamorphism in the south-east Tauern Window, Austria: 1. P-T variations in space and time. *Journal of metamorphic Geology*, **3**, 371-402.

Droop, G.T.R., 2013. Paragonite in marbles from the Tauern Window, Austria: Compositional and thermobaric controls. *Lithos*, **162-163**, 1-13.

Dunkl, I., Frisch, W. and Grundmann, G., 2003. Zircon fission track thermochronolgy of the southeastern part of the Tauern Window and adjacent Austroalpine margin, Eastern Alps. *Eclogae Geologicae Helveticae*, **96**, 209-217.

Ebbing, J., Braitenberg, C., Götze, H.-J., 2006. The lithospheric density structure of the Eastern Alps. *Tectonophysics*, **414**, 145-155.

Ehlers, T.A. and Chapman D.S., 1999, Normal fault thermal regimes: conductive and hydrothermal heat transfer surrounding the Wasatch fault, Utah. *Tectonophysics*, **312**, 217-234.

Elias, J., 1998. The thermal history of the Ötztal–Stubai complex (Tyrol, Austria/Italy) in the light of the lateral extrusion model. *Tübinger Geowiss. Arb., Reihe A*, **42**, 1–172.

England, P., and Molnar, P., 1990. Surface uplift, uplift of rocks, and exhumation of rocks. *Geology*. **18**, 1173-1177.

England, P.C. and Thompson, A.B., 1984. Pressure-temperature-time paths of regional metamorphism, I. Heat transfer during the evolution of regions of thickened continental crust. *Journal of Petrology*, **25**, 894-928.

Exner, C., 1939. Das Ostende der Hohen Tauern zwischen Mur- und Maltatal (I. Teil). *Jahrbuch Zweigstelle, Wien, Reichsstation der Bodenforschung. Jahrbuch der Geologischen Bundesanstalt*, **89**, 285-314.

Exner, C., 1948. Mallnitzer Rollfalte und Sirnfront des Sonnblick-Gneiskerns. *Jahrbuch der Geologischen Bundesanstalt, Wien*, 57-81.

Exner, C., 1949. Tektonik, Feldspatausbildungen und deren gegenseitige Beziehungen in den östlichen Hohen Tauern. Beiträge zur Kenntnis der Zentralgneisfazies. I. Teil. TMPM, sere 3, **1**, 197–284.

Exner, C., 1956. Geologische Karte der Umgebung von Gastein. *Geologische Bundesanstalt Wien.*

Exner, C., 1957. Erläuterungen zur geologischen Karte der Umgebung von Gastein. – Umgebung Gastein. *Geologische Bundesanstalt Wien.*

Exner, C., 1962. Geologische Karte der Sonnblickgruppe, M 1:50000. *Geologische Bundesanstalt Wien.*

Exner, C., 1964. Erläuterungen zur Geologischen Karte der Sonnblickgruppe. *Geologische Bundesanstalt Wien,* 130 p.

Exner, C., 1971. Geologie der peripheren Hafnergruppe (Hohe Tauern). *Jahrbuch der Geologischen Bundesanstalt, Wien*, **114**, 1-119.

Exner, C., 1971. Aufnahmen 1970 auf Blatt Muhr (156) und Vergleichsbegehungen auf Blatt Spittal a.d. Drau (182). *Verhandlungen der Geologischen Bundesanstalt Wien*, **1971(4)**, 28-30.

Exner, C., 1982. Geologie der zentralen Hafnergruppe (Hohe Tauern). *Jahrbuch der Geologischen Bundesanstalt, Wien*, **125(1-2)**, 51-154.

Exner, C., 1984. Der Südrand des Tauernfensters bei Spittal an der Drau. *Jahrbuch der Geologischen Bundesanstalt, Wien*, **127(3)**, 349-367.

Favaro et al., 2012. The Mallnitz synform and its relation to the Mölltal Fault (Tauern Window, Eastern Alps/Austria). *Geophysical Research Abstracts. EGU General Assembly 2012*, **14**, EGU2012-10371.

Favaro, S. and Schuster, R., 2012. Bericht 2012 über geologische Aufnahmen auf den Blättern 154 Rauris, 155 Bad Hofgastein und 181 Obervellach. *Jahrbuch der Geologischen Bundesanstalt Wien*, **152(1-4)**, 268-272.

Favaro, S., Schuster, R., Handy, M. R., Scharf, A., and Pestal, G, 2015. Transition from orogen-perpendicular to orogen-parallel exhumation and cooling during crustal indentation – key constraints from ^{147}Sm/^{144}Nd and ^{87}Rb/^{87}Sr geochronology (Tauern Window, Alps). *Tectonophysics*, ***665***, 1-16.

Feitzinger, G., and Paar, W.H., 1991. Gangförmige Gold–Silber–Vererzungen in der Sonnblickgruppe (Hohe Tauern, Kärnten). *Archiv Lagerstättenforschung Geologischen Bundesanstalt*, **13**, 17-50.

Fodor, L., B. Jelen, E. Márton, D. Skaberne, J. Čar, and M. Vrabec, 1998. Miocene-Pliocene tectonic evolution of the Slovenian Periadriatic fault: Implications for Alpine-Carpathian extrusion models. *Tectonics*, **17(5)**, 690-709.

Fodor, L., Csontos, L., Bada, G., Györfi, I. and Benkovics, L., 1999. Tertiary evolution of the Pannonian Basin system and neighboring orogens: a new synthesis of palaostress data. In: Durand, B., Jolivet, L., Horvath, F. and Seranne, M. (Eds.) The Mediterranean Basins: Tertiary Extension within the Alpine Orogen. *Geological Society Special Publication*, **156**, 295-334.

Foeken, J.P.T., Persano, C., Stuart, F.M. and ter Voorde, M., 2007. Role of topography in isotherm perturbation: Apatite (U-Th)/He and fission track results from the Malta tunnel, Tauern Window, Austria. *Tectonics*, **26**, doi:10.10129/2006TC002049.

Foster, D.A., Gleadow, A.J.W. and Noble, W.P., 1996. Sphene and zircon fission track closure temperature revisited: Empirical calibration from ^{40}Ar/^{39}Ar diffusion studies of K-feldspar and biotite. *International Workshop on Fission-Track Dating*, Gent, Abstracts 37.

Fox, M., 2012. The Inversion of Low-Temperature thermochronometry to extract spatially and temporally varying exhumation rates within the Alps. PhD thesis, ETH Zürich, Switzerland, No. 20851, 283 p.

Frank, W., 1987. Evolution of the Austroalpine elements in the Cretaceous. In: H.W. Flügel and P. Faupl (Eds.), Geodynamics of the Eastern Alps. *Deuticke, Wien*, 379-406.

Franz, G., Mosbrugger, V., and Menge, R., 1991. Carbo-Permian pteridophyll leaf fragments from an amphibolite facies basement, Tauern Window, Austria. *Terra Nova*, **3 (2)**, 137-141.

Frisch, W., 1979. Tectonic progradation and plate tectonic evolution of the Alps. *Tectonophysics*, **60**, 121–139.

Frisch, W., Kuhlemann, J., Dunkl, I. and Brügel, A., 1998. Palinspastic reconstruction and topographic evolution of the Eastern Alps during late Cenozoic tectonic extrusion. *Tectonophysics*, **297**, 1-15.

Frisch, W., Dunkl, I. and Kuhlemann, J., 2000. Post-collisional orgogen-parallel large-scale extension in the Eastern Alps. *Tectonophysics*, **327**, 239-265.

Frisch, W., Kuhlemann, J., Dunkl, I., Szkely, B., 2001. The Dachstein paleosurface and the Augenstein formation in the Northern Calcareous Alps—a mosaic stone in the geomorphological evolution of the Eastern Alps. *Int. J. Earth Sci.,* **90**, 500–518.

Froitzheim, N., Schmid, S.M. and Conti, P., 1994. Repeated change from crustal shortening to orogen-parallel extension in the Austroalpine units of Graubünden. *Eclogae geologicae Helvetiae*, **87**, 559-612.

Froitzheim, N., Plašienka, D. and Schuster, R., 2008. Alpine tectonics of the Alps and Western Carpathians. In: McCann. T (Ed.) The geology of Central Europe. Volume 2: Mesozoic and Cenozoic. *Geological Society of London*, 1141-1232.

Frost, E., Dolan, J., Sammis, C., Hacker, B., Cole, J., and Ratschbacher, L., 2009. Progressive strain localization in a major strike-slip fault exhumed from midseismogenic depths: Structural observations from the Salzach-EnnstalMariazel Puchberg fault system, Austria. *Journal of Geophysical Research*, **114**, B04406, doi: 10.1029/2008JB005763.

Fügenschuh, B., Seward, D. and Mantckelow, N.S., 1997. Exhumation in a convergent orogen: the western Tauern Window. *Terra Nova*, **9**, 213-217.

Fügenschuh, B., Mancktelow, N. S., Schmid, S. S., 2012. Comment on Rosenberg and Garcia (2011) : Estimating displacement along the Brenner Fault and orogen-parallel extension in the Eastern Alps, International Journal of Earth Sciences, 100, 1129–1145. *International Journal of Earth Sciences*, **101**, 1451–1455, doi:10.1007/s00531-011-0725-4

Genser, J. and Neubauer, F., 1989. Low angle normal faults at the eastern margin of the Tauern window (Eastern Alps). *Mitteilungen der Österreichischen Geologischen Gesellschaft*, **81**, 233-243.

Genser, J., van Wees, J.D., Cloething, S., Neubauer, F., 1996. Eastern Alpine tectonometamorphic evolution: constraints from two-dimensional P–T–t modeling. *Tectonics*, **15**, 584-604.

Gipper, P., 2012. Crustal imbrication and nappe folding in the southeastern Tauern Window. *MSc thesis*, Freie Universität Berlin, Berlin, Germany.

Glodny, J., Ring, U., and Kühn, A., 2008. Coeval high-pressure metamorphism, thrusting, strike-slip, and extensional shearing in the Tauern Window, Eastern Alps. *Tectonics*, **27**, TC4004, doi:10.1029/2007TC002193.

Glodny, J., Ring, U., Kühn, A., Gleissner, P. and Franz, G., 2005. Crystallization and very rapid exhumation of the youngest Alpine eclogites (Tauern Window, Eastern Alps) from ^{87}Rb/^{87}Sr mineral assemblage analysis. *Contributions to Mineralogy and Petrology*, **149**, 699-712, doi: 10.1007/s00410-005-0676-5.

Grasemann, A. and Mancktelow, N.S., 1993. Two-dimensional thermal modelling of normal faulting: the Simplon Fault Zone, Central Alps, Switzerland. *Tectonophysics*, **225**, 155-165.

Hames, W.E. and Bowring, S.A., 1994. An empirical evaluation of the argon diffusion geometry in muscovite. *Earth and Planetary Science Letters*, **124(1-4)**, 161-169.

Halama, R., Konrad-Schmolke, M., Sudo, M., Marschall, H. and Wiedenbeck, M., 2014. Effects of fluid-rock interaction on ^{40}Ar/^{39}Ar geochronology in high-pressure rocks (Sesia-Lanzo Zone, Western Alps). *Geochimica et Cosmochimica Acta*, **126**, 475-494, doi: 10.1016/j.gca.2013.10.023.

Handy, M. R., and Oberhänsli, R., 2004. Metamorphic structure of the Alps, age map of the metamorphic structure of the Alps—tectonic interpretation and outstanding problems. *Mitteilungen der Österreichischen Mineralogischen Gesellschaft*, **149**, 201-226.

Handy, M. R., Wissing, S. B., and Streit, L. E., 1999. Strength and structure of mylonite with combined frictional-viscous rheology and varied bimineralic composition. *Tectonophysics*, **303(1)**, 175-192.

Handy, M.R., Babist, J., Rosenberg, C.L., Wagner, R. and Konrad, M., 2005. Decoupling and is relation to strain partitioning in continental lithosphere – Insight from the Periadriatic fault system (European Alps). In: Deformation Mechanism, Rheology and Tectonics, edited by Gapais, D., Brun, J.P. and Cobbold, P.R., *Geological Society of London, Special Publication*, **243**, 249-276.

Handy, M.R., Schmid, S.M., Bousquet, R., Kissling, E. and Bernoulli, D., 2010. Reconciling plate-tectonic reconstructions of Alpine Tethys with the geological-geophysical record of spreading and subduction in the Alps. *Earth-Sciences Reviews*, **102**, 121-158, doi:10.1016/j.earscirev.2010.06.002.

Handy, M.R., Ustaszewski, K. and Kissling, E., 2015. Reconstructing the Alps–Carpathians–Dinarides as a key to understanding switches in subduction polarity, slab gaps and surface motion. *International Journal of Earth Sciences*. **104**, 1, 1-26, doi: 10.1007/s00531-014-1060-3.

Harrison, T.M., 1981. Diffusion of ^{40}Ar in hornblende. *Contribution to Mineralogy Petrology*, **78**, 324-331.

Harrison, T.M., Duncan, I. and McDougall, I., 1985. Diffusion of ^{40}Ar in biotite: temperature, pressure and compositional effects. *Geochimica Cosmochimica Acta*, **49**, 2461-2468.

Harrison, M.T., Célérier, J., Aikman, A.B., Hermann, J. and Heizler, M.T., 2009. Diffusion of ^{40}Ar in muscovite. *Geochemica et Cosmochimica Acta*, **73**, 1039-1051.

Hawemann, F., 2013. Metamorphic conditions during crustal imbrication and nappe stacking in the southeastern Tauern Window. M.Sc. thesis, Freie Universität Berlin, Berlin, Germany.

Hawkesworth, C.J., 1976. Rb/Sr Geochronology in the Eastern Alps. *Contributions to Mineralogy and Petrology*, **54**, 225-244.

Heinisch, H. and Schmidt, K., 1984. Zur Geologie des Thurntaler Quarzphyllits und des Altkristallins südlich des Tauernfensters (Ostalpen, Südtirol). *Geologische Rundschau,* **73**, 113-129, Stuttgart.

Holub, B., and Marschallinger, R., 1989. Die Zentralgneise im Hochalm-Ankogel-Massiv (östliches Tauernfenster). Teil I: petrographische Gliederung und Intrusionsfolge. *Mitteilungen der Österreichischen Geologischen Gesellschaft,* **81**, 5–31.

Hoinkes, G., Koller, F., Rantitsch, G., Dachs, E., Hock, V., Neubauer, F. and Schuster, R., 1999. Alpine metamorphism of the Eastern Alps. *Schweizerische Mineralogische und petrographische Mitteilungen*, **79**, 155-181.

Hoke, L., 1990. The Altkristallin of the Kreuzeck Mountains, SE Tauern Window, Eastern Alps-basement crust in a convergent plate boundary zone. *Jahrbuch der Geologischen Bundesanstalt, Wien*, **133**, 5–87.

Horvath, F., Bada, G., Szafián, P., Tari, G., Ádám, A. and Cloetingh, S., 2006. Formation and deformation of the Pannonian basin: constraints from observational data, in: D.G. Gee, R.A. Stephenson (Eds.), European Lithosphere Dynamics, Memoirs, *Geological Society of London*, **32**, 191–206.

Hurford, A., 1986. Cooling and uplift patterns in the Lepontine Alps South Central Switzerland and an age of vertical movement on the Insubric fault line. *Contributions to Mineralogy and Petrology.* **92(4)**, 413-427.

Inger, S. and Cliff, R.A., 1994. Timing of metamorphism in the Tauern Window, Eastern Alps: Rb/Sr ages and fabric formation. *Journal of metamorphic Geology*, **12**, 695–707.

Ishizuka, O., 1998. Vertical and horizontal variations of the fast neutron flux in a single irradiation capsule and their significance in the laser-heating ^{40}Ar/^{39}Ar analysis: Case study for the hydraulic rabbit facility of the JMTR reactor, Japan. *Geochemical Journal*, **32**, 243-252.

Jäger, E., Niggli, E. and Wenk, E., 1967. Rb/Sr Attersbestimmungen an Glimmern der Zentralalpen. Beiträge zur geologische Karte der Schweiz, NF 1344, Bern: 67.

Johnson, M.R.E., 2002. Shortening budgets and the role of continental subduction during the India-Asia collision. *Earth-Science Review*, **59**, 101-123.

Kebede, T., Klötzli, U., Kosler, J., and Skiöld, T., 2005. Understanding the pre-Variscan and Variscan basement components of the central Tauern Window, Eastern Alps (Austria): constraints from single zircon U-Pb geochronology. *International Journal of Earth Sciences*, **94(3)**, 336-353.

Kelley, S.P., Arnaud, N.O. and Turner, S.P., 1994. High spatial resolution ^{40}Ar/^{39}Ar investigations using an ultra-violet laser probe extraction technique. *Geochemica et Cosmochimica Acta*, **58**, 3519-3525.

Ketcham, R.A., 1996. Thermal model of core-complex evolution in Arizona and New Guinea: Implications for ancient cooling paths and present-day heat flow. *Tectonics*, **15(5)**, 933-951.

Kober, L., 1920. Das Östliche Tauernfenster. *Denkschrift der Akademie der Wissenschaften Wien*, Mathematisch-Naturwissenschaftliche Klasse, Abt I, 98 pp., 201-243.

Kitzig, M.C., 2010. Structural analyses and dating of deformation of the Ahrntal Fault. M.Sc. thesis, Freie Universität Berlin, Berlin, Germany.

Kuhlemann, J., Frisch, W., Dunkl, I., Székely, B., 2001. Quantifying tectonic versus erosive denudation by the sediment budget: the Miocene core complexes of the Alps. *Tectonophysics*, **330**, 1–23

Kurz, W. and Neubauer, F., 1996. Deformation partitioning during updoming of the Sonnblick area in the Tauern Window (Eastern Alps, Austria). *Journal of Structural Geology*, **18(11)**, 1327-1343.

Kurz, W., Neubauer, F. and Genser, J., 1996. Kinematics of Penninic nappes (Glockner Nappe and basement-cover nappes) in the Tauern Window (Eastern Alps, Austria) during subduction and Penninic-Austroalpine collision. *Eclogae Geologicae Helveticae*, **89(1)**, 573-605.

Kurz, W., Neubauer, F. and Dachs, E., 1998. Eclogite meso- and microfabrics: implications for the burial and exhumation history of eclogites in the Tauern Window (Eastern Alps) from P–T–d paths. *Tectonophysics*, **285**, 183–209.

Kurz, W., Handler, R. and Bertoldi, C., 2008. Tracing the exhumation of the Eclogite Zone (Tauern Window, Eastern Alps) by 40Ar/39Ar dating of white mica in eclogites. *Swiss Journal of Geoscience*, **101(1)**, 191-206, doi: 10.1007/s00015-008-1281-1.

Lambert, R.S.t.J., 1970. A potassium - argon study of the margin of the Tauernfenster at Döllach, Austria. *Eclogae Geologicae Helveticae*, **63**, 197- 205.

Lammerer, B., 1988. Thrust-regime and transpression-regime tectonics in the Tauern Window (Eastern Alps). *Geologische Rundschau*, **77(1)**, I43-156.

Lammerer, B. and Weger, M., 1998. Footwall uplift in an orogenic wedge: the Tauern Window in the Eastern Alps of Europe. *Tectonophysics*, **285**, 213-230.

Laubscher, H. P., 1988. The arcs of the Western Alps and the Northern Apennines: an updated view. *Tectonophysics*, **146**, 61-18.

Lärchbaumer, L., Klötzli, U., and Pestal, G., 2010. Schists and amphibolites of the Kleinelendtal (Ankogel-Hochalm-Gruppe/Hohe Tauern, Austria)/New insights on the Variscan basement in the Eastern Tauern Window. *Austrian Journal of Earth Scineces, **103***(**2**), 138–152.

Läufer A.L., Frisch, W., Steinitz, G., Loeschke, J., 1997. Exhumed fault-bounded blocks along the Periadriatic lineament. *Geologische Rundschau*, **86**, 612–626.

Linner, M., Reitner, J.M. and Pavlik, W., 2013. Geologische Karte der Republik Österreich 1:50000 Blatt 179 Lienz. *Geologische Bundesanstalt*, Wien.

Linzer, H.G., Decker, K., Peresson, H., Dell'Mour, R. and Frisch, W., 2002. Balancing lateral orogenic float of the Eastern Alps. *Tectonophysics*, **54**, 211-237.

Lippitsch, R., Kissling, E. and Ansorge, J., 2003. Upper mantle structure beneath the Alpine orogen from high-resolution teleseismic tomography. *Journal of Geophysical Research*, **108(B8)**, 2376. doi:10.1029/2002JB002016

Lister, G.S. and Snoke, A.W., 1984. S-C Mylonites. *Journal of Structural Geology*, **6(6)**, 617-638.

Liu, Y., Genser, J., Handler, R., Friedl, G. and Neubauer F., 2001. ^{40}Ar/^{39}Ar muscovite ages from the Penninic-Austroalpine plate boundary, Eastern Alps. *Tectonics*, **20**, 526-547.

Luciani, V., 1989. Stratigrafia Sequenziale del Terziaro Nelle Catena del Monte Baldo (Provincie di Verona a Trento). *Memorie di Scienze Geologiche*, **41**, 263–351.

Luciani, V. and Silvestrini, A., 1996. Planktonic foraminiferal biostratigraphy and paleoclimatology of the Oligocene/Miocene transition from the Monte Brione Formation (Northern Italy, Lake Garda). *Memorie di Scienze Geologiche*, **48**, 155-169.

Ludwig, K.R., 2001. Isoplot/Ex version 2.49. A Geochronological toolkit for Microsoft Excel. *Berkeley Geochronology Center Special Publication*, 1a.

Ludwig, K.R., 2003. Isoplot/Ex version 3.0. A geochronological toolkit for Microsoft Excel. *Berkeley Geochronological Centre Special Publication*, 70 p.

Luth, S.W. and Willingshofer, E., 2008. Mapping of the post-collisional cooling history of the Eastern Apls. *Swiss Journal of Geoscience*, **101**, 207-223, doi: 10.1007/s00015-008-1294-9.

Luth, S., Willingshofer, E., ter Borgh, M., Sokoutis, D., van Otterloo, J. and Versteeg, A., 2013. Kinematic analysis and analogue modeling of the Passeier- and Jaufen faults: implications for crustal indentation in the Eastern Alps. *International Journal of Earth Science*, **102**, 1071-1090, doi:10.1007/s00531-012-0846-4.

Mancktelow, N.S., Stöckli, D.F., Grollimund, B., Müller, W., Fügenschuh, B., Viola, G., Seward, D. and Villa, I.M., 2001. The DAV and Periadriatic fault systems in the Eastern Alps south of the Tauern window. *International Journal of Earth Science*, **90**, 593–622.

Marrett, R., and R. W. Allmendinger, 1990. Kinematic analysis of fault-slip data, *Journal of Structural Geology*, **12**, 973 – 986

Martin, S., Prosser, G., Morten L., 1993. Tectono-magmatic evolution of sheeted plutonic bodies along the North Giudicarie line (northern Italy), *Geol. Rundsch.*, **82**, 51–66, 1993.

McArthur, J. M., R. J. Howarth, and T. R. Bailey. 2001. Strontium Isotope Stratigraphy: LOWESS Version 3: Best Fit to the Marine Sr-isotope Curve for 0–509 Ma and Accompanying Look-up Table for Deriving Numerical Age. *The Journal of Geology,* 109 (2). University of Chicago Press: 155–70. doi:10.1086/319243.

McCullogh, M.T. and Wasserburg, G.J., 1978. Sm-Nd and Rb/Sr chronology of continental crust formation. *Science*, **200**, 1003-1011.

Means, W.D., 1989. Stretching faults. *Geology*, **17**, 893–896.

Morten, L., 1974. La tonalite della Valle dei Rivi (Rumo). *Mineralogica e Petrografica Acta*, **20**, 79–90.

Most, P., Dunkl, I., Frisch, W., 2003. Fission track tomography of the Tauern window along the TRANSALP profile. In: Nicolich, R., Polizzi, D., Furlani, S. (Eds.), TRANSALP Conference, Extended Abstracts, *Mem. Sci. Geol. Padova*, **54**, 225 – 226

Mitterbauer, U., Behm, M., Brückl, E., Lippitsch, R., Guterch, A., Keller, G. R., ... & Šumanovac, F., 2011. Shape and origin of the East-Alpine slab constrained by the ALPASS teleseismic model. *Tectonophysics*, **510(1)**, 195-206.

Müller, W., 1998. Isotopic dating of deformation using microsampling techniques: the evolution of the Periadriatic Fault System (Alps). Ph.D. thesis, ETH Zürich, 135 p.

Müller, W., Mancktelow, N. S., and Meier, M., 2000. Rb-Sr microchrones of synkinematic mica in mylonites: an example from the DAV fault of the Eastern Alps. *Earth and Planetary Science Letter*, **180**, 385-397.

Müller, W., Prosser, G., Mancktelow, N. S., Villa, I. M., Kelley, S. P., Viola, G. and Oberli F., 2001. Geochronological constraints on the evolution of the Periadriatic Fault System (Alps), *International Journal of Earth Science*, **90**, 623-653.

Mulch, A., Cosca, M.A. and Handy, M.R., 2002. In-situ UV-laser ^{40}Ar/^{39}Ar geochronology of a micaceous mylonite : an example of defect-enhanced argon loss. *Contributions to Mineralogy and Petrology*, **142**, 738-752, doi: 10.1007/s00410-001-0325-6.

Nagel, T.J., Herwartz, D., Rexroth, S., Münker, C., Froitzheim, N. and Kurz, W., 2013. Lu–Hf dating, petrography, and tectonic implications of the youngest Alpine eclogites (Tauern Window, Austria). *Lithos*, **170 (171)**, 179-190, doi: 10.1016/j.lithos.2013.02.008.

Neubauer, F., Genser, J., Kurz, W. and Wang, X., 1999. Exhumation of the Tauern Window, Eastern Alps. *Physics and Chemistry of the Earth (A)*, **24(8)**, 675-680.

Oberhänsli R., Bousquet, R., Engi, M., Goffé, B., Gosso, G., Handy, M., 2004. Metamorphic structure of the Alps 1: 1000000. Paris: *Commission for the Geological Map of the World.*

Ortner, H., and R. Sachsenhofer, 1996. Evolution of the Lower Inn Valley Tertiary and constraints on the development of the source area. G. Wessely, W. Liebl (Eds.), Oil and Gas in Alpidic Thrustbelts and Basins of Central and Eastern Europe EAGE Special Publication, Geological Society, Londons, **5**, 237–248.

Ortner, H., 2003b. Local and far field stress-analysis of brittle deformation in the western part of the Northern Calcareous Alps, Austria. *Geol.-Paläontol. Mitt. Univ. Innsbruck,* **26**, 109 – 131.

Ortner, H., Reiter, F., and Brandner, R., 2006. Kinematics of the Inntal shear zone–sub-Tauern ramp fault system and the interpretation of the TRANSALP seismic section, Eastern Alps, Austria. *Tectonophysics*, **414**, 241-258.

Oxburgh, E.R., Lambert, R.S.t.J., Baadsgaard, H. and Simons, J.G., 1966. Potassium-argon age studies across the southeast margin of the Tauern Window, the Eastern Alps. *Verhandlungen der Geologischen Bundesanstalt, Wien*, 17-33.

Peresson, H., and K. Decker, 1997a. Far-field effects of Late Miocene subduction in the Eastern Carpathians: E–W compression and inversion of structures in the Alpine-Carpathian–Pannonian region. *Tectonics*, **16**, 38–56.

Peresson, H., and K. Decker, 1997b. The Tertiary dynamics of the northern Eastern Alps (Austria): changing paleostresses in a collisional plate boundary. *Tectonophysics,* **272**, 125–157.

Pestal, G. and Hellerschmidt-Alber, J., 2011. Bericht 2009 und 2010 über geologische Aufnahmen auf Blatt 154 Rauris. *Jahrbuch der Geologischen Bundesanstalt, Wien*, **151(1-2)**, 142-148.

Pestal, G., Hejl, E., Braunstingl, R. and Schuster, R., 2009. Erläuterungen Geologische Karte von Salzburg 1 : 200.000. *Land Salzburg und Geologische Bundesanstalt Wien*, 1-162.

Petit, J.P., 1987. Criteria for sense of movement on fault surfaces in brittle rocks. *Journal of Structural Geology*, **9 (5/6)**, 597-608.

Picotti, V., Prosser, G., Castellarin, A., 1995. Structures and kinematics of the Giudicarie - Val Trompia fold and thrust belt (Central Southern Alps Northern Italy). *Mem. Sc. Geol*, **47**, 95-109.

Pieri, M., and Groppi, G., 1981. Subsurface geological structures of the Po Plain. CNR-PF Geodinamica, Sottoprog. Modello Strutturale contr. 414.

Plan, L., Grasemann, B., Spötl, C., Decker, K., Boch, R., and Kramers, J., 2010. Neotectonic extrusion of the Eastern Alps: Constraints from U/Th dating of tectonically damaged speleothems. *Geology*, **38(6)**, 483-486.

Pollington, A.D. and Baxter, E., 2010. High resolution Sm-Nd garnet geochronology reveals the uneven pace of tectonometamorphic processes. *Earth and Planetary Science Letter*, **293**, 63-71.

Pomella, H., 2010. The Cenozoic evolution of the Giudicarie fault system (Eastern/Southern Alps, northern Italy). A geochronological, structural and paleomagnetic study. University of Innsbruck, Innsbruck.

Pomella, H., Klötzli, U., Scholger, R., Stipp, M. and Fügenschuh, B., 2011. The Northern Giudicarie and the Meran-Mauls fault (Alps, Northern Italy) in the light of new paleomagnetic and geochronological data from boudinaged Eo-/Oligocene tonalites. *International Journal of Earth Science*, **100**, 1827-1850, doi:10.1007/s00531-010-0612-4.

Pomella, H., Stipp, M. and Fügenschuh, B., 2012. Thermochronological record of thrusting and strike-slip faulting along the Giudicarie fault system (Alps, Northern Italy). *Tectonophysics*, **579**, 118-130, doi:10.1016/j.tecto.2012.04.015.

Prosser, G., 1998. Strike-slip movements and thrusting along a transpressive fault zone: The North Giudicarie line (Insubric line, northern Italy). *Tectonics*, ***17*****(6)**, 921-937.

Prosser, G., 2000. The development of the North Giudicarie fault zone (Insubric line, Northern Italy). *Journal of Geodynamics*, **30 (1-2)**, 229-250.

Purdy, J.W. and Jäger, E., 1976. K-Ar ages on rock-forming minerals from the Central Alps. *Memorie degli Istituti di Geologia e Mineralogia dell'Università de Padova*, 30.

Raith, M., Raase, P., Kreuzer, H., and Moller, 1978. The age of the Alpidic metamorphism in the Western Tauern Window, Austrian Alps, according to radiometric dating. In: Cless, H., Roeder, D. and Schmid, K. (eds.): Alps, Appenines and Hellenides, Inter-Union Commission on Geodynamics, Scientific Report No. **38**, 140-149.

Rantitsch, G., 2001. Thermal history of the Drau Range (Eastern Alps). *Schweizerische Mineralogische und petrographische Mitteilungen*, **81**, 181-196.

Ratschbacher, L., Frisch, W., Neubauer, F., Schmid, S.M. and Neugebauer, J., 1989. Extension in compressional orogenic belts: The Eastern Alps. *Geology*, **17**, 404-407.

Ratschbacher, L., Merle, O., Davy, P. and Cobbold, P, 1991a. Lateral extrusion in the eastern Alps, Part1: Boundary conditions and experiments scaled for gravity. *Tectonics*, **10**, 245-256.

Ratschbacher, L., Frisch, W., Linzer, H. G. and Merle, O., 1991b. Lateral extrusion in the Eastern Alps, Part2: Structural analysis. *Tectonics*, **10**, 257-271.

Ratschbacher, L., Dingeldey, Ch., Miller Ch., Hacker, B.R. and McWilliams, M.O., 2004. Formation, subduction, and exhumation of Penninic oceanic crust in the Eastern Alps: time constraints from ^{40}Ar/^{39}Ar geochronology. *Tectonophysics*, **394**, 155-170.

Reddy, S. M., 1990. The structural, metamorphic and thermal history of the Sonnblick Dome, southeast Tauern Window, Austria (Doctoral dissertation, University of Leeds).

Reddy, S.M., Cliff, R.A. and East, R., 1993. Thermal history of the Sonnblick Subdome, south-east Tauern Window, Austria: Implications for Heterogeneous Uplift within the Pennine Basement. *Geologische Rundschau*, **82**, 667-675.

Reicherter, K., Fimmel, R. and Frisch, W., 1993. Sinistral strike-slip faults in the central Tauern window (Eastern Alps, Austria). *Jahrbuch der Geologische Bundesanstalt*, **136**, 495–502.

Reiners, P.W. and Brandon, M.T., 2006. Using Thermochronology to Understand Orogenic Erosion. *Annual Review of Earth Planet Sciences*, **34**, 419-466.

Ring, U., Brandon, M., Willet, S. and Lister, G., 1999. Exhumation processes. *Geological Society, London, Special Publication*, **154(1)**, 1-27.

Robbins, G.A., 1972. Radiogenic argon diffusion in muscovite under hydrothermal conditions. *M.Sc. Thesis*, Brown University, Rhode Island.

Roddick, J. C., Cliff, R. A. and Rex. D. C., 1980. The evolution of excess argon in Alpine biotite - a ^{39}Ar/^{40}Ar analysis. *Earth and Planetary Science Letters*, **48**, 185-208.

Romer, R. L. and Siegesmund, S., 2003. Why allanite may swindle about its true age, *Contribution to Mineralogy and Petrology*, **146**, 297–307.

Rosenberg, C.L. 2004. Shear zones and magma ascent: a model based on a review of the Tertiary magmatism in the Alps. *Tectonics*, **23**, 1-21.

Rosenberg, C. L., and Berger, A., 2009. On the causes and modes of exhumation and lateral growth of the Alps. *Tectonics*, ***28*****(6)**.

Rosenberg, C.L., Garcia, S., 2011. Estimating displacement along the Brenner Fault and orogen-parallel extension in the Eastern Alps. *International Journal of Earth Sciences*, **100**, 1129–1145.

Rosenberg, C.L., and Garcia, S., 2012, Reply to the comment of Fűgenschuh et al. on the paper 'Estimating displacement along the Brenner Fault and orogen-parallel extension in the Eastern Alps' by Rosenberg and Garcia, Int J Earth Sci (2011) 100:1129–1145. *International Journal of Earth Sciences*, doi :10.1007/s00531-011-0726-3.

Rosenberg, C.L., and Schneider, S., 2008. The western termination of the SEMP Fault (eastern Alps) and is bearing on the exhumation of the Tauern Window. *Geological Society of London, Special Publication*, **298**, 197–218.

Rosenberg, C.L., and E. Kissling, 2013. Three-dimensional insight into Central-Alpine collision: Lower-plate or upper-plate indentation? *Geology*, **41**, 1219-1222, doi: 10.1130/G34584.1.

Rosenberg, C.L., Brun, J.P., Cagnard, F. and Gapais, D., 2007. Oblique indentation in the Eastern Alps: Insights from laboratory experiments. *Tectonics*, **26**, TC2003. doi:10.1029/2006TC 001960.

Royden, L.H., 1993. Evolution of retreating subduction boundaries formed during continental collision. *Tectonics*, **12(3)**, 629-638.

Royden, L.H. and Burchfield, B.C., 1989. Are systematic variations in thrust belt style related to plate boundary processes? (The western Alps versus the Carparthians). *Tectonics*, **8**, 51-61.

Royden, L.H., B.C. Burchfield, R. W. King, E. Wang, Z. Chen, F. Sheng, and Y. Liu, 1997. Surface Deformation and Lower Crustal Flow in Eastern Tibet. *Science*, **276**, 788-790.

Sander, B., 1911. Geologische Studien am Westende der hohen Tauern. Bericht—Denkschrift d. kais. *Akademie der Wissenschaften, Wien*, **83**, 257–319.

Satir, M., 1975. Die Entwicklungsgeschichte der westlichen Hohen Tauern und der südlichen Ötztalmasse auf Grund radiometrischer Altersbestimmungen. Ph.D. thesis, Società cooperativa tipografica, Padova, 1-84.

Scharbart, S. 1975. Radiometrische Altersdaten von Intrusivgesteinen im Raum Eisenkappel (Karawanken, K~irnten). *Verhandlungen der Geologischen Bundesanstalt, Wien,* **4**, 301-304.

Scharf, A., Handy, M.R., Favaro, S., Schmid, S.M. and Bertrand, A., 2013a. Modes of orogen-parallel stretching and extensional exhumation of thickening orogenic crust in response to microplate indentation and slab roll-back (Tauern Window, Eastern Alps). *International Journal of Earth Sciences*, **102(6)**, 1627-1654, doi:10.1007/s00531-013-0894-4.

Scharf, A., Handy, M.R., Ziemann, M.A. and Schmid, S.M., 2013b. Peak-temperature patterns of polyphase metamorphism resulting from accretion, subduction and collision (eastern Tauern Window, European Alps) – A study with Raman microspectroscopy on carbonaceous material (RSCM). *Journal of metamorphic Geology*, **31(8)**, 863-880, doi:10.1111/jmg.12048.

Scharf, A., Handy, M.R., Schmid, S.M., Favaro, S., Sudo, M., Schuster, R. and Hammerschmidt, K., (submitted). Grain-size effects on the closure temperature of white mica in a crustal-scale extensional shear zone – implications for dating shearing and cooling from in-situ ^{40}Ar/^{39}Ar laser-ablation ages of white mica (Tauern Window, Eastern Alps). *Accepted to Tectonophysics*.

Schmid, S. M., Zingg, A. and Handy, M. R. 1987. The kinematics of movements along the Insubric Line and the emplacement of the Ivrea Zone. *Tectonophysics*, **135**, 47-66.

Schmid, S. M., Aebli, H. R., Heller, F. & Zingg, A. 1989. The role of the Periadriatic Line in the tectonic evolution of the Alps. In: COWARD, M. P., DIETRICH, D. & PARK, R. (Eds) Alpine Tectonics. *Geological Society, London, Special Publications*, **45**, 153-171.

Schmid, S.M., Fügenschuh, B., Kissling, E. and Schuster, R., 2004. Tectonic map and overall architecture of the Alpine orogen. *Eclogae Geologicae Helveticae*, 97, 93-117, doi: 10.1007/s00015-004-1113-x.

Schmid, S.M., Bernoulli, D., Fügenschuh, B., Matenco, L., Schefer, S., Schuster, R., Tischler, M. and Ustaszewsky, K., 2008. The Alpine-Carpathian-Dinaridic system: correlation and evolution of tectonic units. *Swiss Journal of Geosciences*, **101(1)**, 139-183.

Schmid, S.M., Scharf, A., Handy, M.R. and Rosenberg, C.L., 2013. The Tauern Window (Eastern Alps, Austria) – A new tectonic map, cross-sections and tectonometamorphic synthesis. *Swiss Journal of Geosciences*, **106**, 1-32, doi:10.1007/s00015-013-0123-y.

Schneider, S. and Hammerschmidt, K. 2009. K-Ar dating of sinistral deformation in the upper Schieferhülle, south-western Tauern Window (Eastern Alps). *EGU General Assembly Conference Abstracts*, **11**, 13813.

Schneider, S., Hammerschmidt, K. and Rosenberg, C.L., 2013. Dating the longevity of ductile shear zones: Insight from ^{40}Ar/^{39}Ar in situ analyses. *Earth and Planetary Science Letters*, **369-370**, 43-58, doi:10.1016/j.epsl.2013.03.002.

Schneider, S., Hammerschmidt, K., Rosenberg, C.L., Gerdes, A., Frei, D. and Bertrand, A., 2015. U-Pb ages of apatite in the western Tauern Window (Eastern Alps): Tracing the onset of collision-related exhumation in the European plate, *Earth and Planetary Science Letter*, **418**, 53-65.

Schneider, S., Rosenberg, C.L., Scharf, A. and Hammerschmidt, K., (submitted). Translation of indentation into lateral extrusion across a restraining bend: The western Tauern Window, Eastern Alp*s. Submitted to Tectonics.*

Schönborn, G., 1992. Alpine tectonics and kinematic models of the central Southern Alps.

Schönborn, G., 1999. Balancing cross sections with kinematic constraints: the Dolomites (northern Italy). *Tectonics*, ***18*(3)**, 527-545.

Schulz, B., 1990. Prograde-retrograde P-T-t-deformation path of Austroalpine micaschists during Variscan continental collision (Eastern Alps). *Journal of metamorphic Geology*, **8**, 629-443.

Schuster, R. and Frank, W., 2000. Metamorphic evolution of the Austroalpine units east of the Tauern Window: indications for Jurassic strike slip tectonics. *Mitteilungen der Gesellschaft der Geologie- und Bergbaustudenten in Österreich*, **42**, 37-58

Schuster, R., Koller, F., Hoeck, V., Hoinkes, G. and Bousquet, R., 2004. Explanatory notes to the map: Metamorphic structure of the Alps - Metamorphic evolution of the Eastern Alps. *Mitteilungen der Österreichischen Mineralogischen Gesellschaft*, **149**, 175-199.

Schuster, R., Pestal, G. and Reitner, J.M., 2006. Geologische Karte der Republik Österreich: Erläuterungen Geol. Karte 1:50.000 zu Blatt 182 Spittal a.d. Drau. *Geologischen Bundesanstalt*, (in Vorbereitung), Wien.

Schuster, R., Tropper, P., Krenn, E., Finger, F., Frank, W. and Philippisch, R., 2015. Prograde Permo-Triassic metamorphic HT/LP assemblages from the Austroalpine Jenig Complex (Carinthia, Austria). *Austrian Journal of Earth Sciences*, **108(1)**, 73-90.

Sciunnach, D., Scardia, G., Tremolada, F., and Silva, I. P. (2010). The Monte Orfano Conglomerate revisited: stratigraphic constraints on Cenozoic tectonic uplift of the Southern Alps (Lombardy, northern Italy). *International Journal of Earth Sciences*, ***99*****(6)**, 1335-1355.

Selverstone, J., 1985. Petrologic constraints on imbrication, metamorphism, and uplift in the SW Tauern Window, Eastern Alps. *Tectonics*, **4**, 687-704.

Selverstone, J., 1988. Evidence for east-west crustal extension in the Eastern Alps: implications for the unroofing history of the Tauern Window. *Tectonics*, **7**, 87-105.

Selverstone, J., 2004. Are the Alps collapsing? *Annual Review of Earth and Planetary Sciences*, **33(1)**, 113-132, doi: 10.1146/annurev.earth.33.092203.122535.

Selverstone, J., Spear, F.S., Franz, G. and Morteani, G., 1984. High-pressure metamorphism in the SW Tauern Window, Austria: P-T Paths from Hornblende-Kyanite-Staurolite Schists. *Journal of Petrology*, **25**, 501-531.

Selverstone, J., Morteani, G., Staude, J.M., 1991. Fluid channeling during ductile shearing - transformation of granodiorite into aluminous schist in the Tauern Window, Eastern Alps. *Journal of metamorphic Geology*, **9**, 419–431.

Selverstone, J., 2004. Are the Alps collapsing? *Annual Review of Earth and Planetary Sciences,* **33**, 113-132, doi: 10.1146/annurev.earth.33.092203.122535

Seward, D., Vanderhaeghe, O., Siebenaller, L., Thomson, S., Hibsch, C., Zingg, A., Holzner, P., Ring, U. and Duchêne, S., 2009. Cenozoic tectonic evolution of Naxos Island through a multi-faceted approach of fission-track analysis. In: Ring, U. and Wernicke, B. (Eds.) Extending a Continent: Architecture, Rheology and Heat Budget. *Geological Society, London, Special Publication*, **321**, 179-196. doi: 10.1144/SP321.9.

Simpson, C. and Schmid, S.M., 1983. An evaluation of criteria to deduce the sense of movement in sheared rocks. *Geological Society of American Bulletin*, **94(11)**, 1281-1288.

Sölva, H., Grasemann, B., Thöni, M., Thiede, R. and Habler, G., 2005. The Schneeberg Normal Fault Zone: Normal faulting associated with Cretaceous SE-directed extrusion in the Eastern Alps (Italy/ Austria). *Tectonophysics*, **401**, 143-166.

Spada, M. Bianchi, I., Kissling, E., Piana Agostinetti, N., Wiemers, S., 2013. Combining controlled-source seismology and receiver function information to derive 3-D Moho topography for Italy. *Geophysical Journal International*, **194 (2)**, 1050-1068, doi: 10.1093/gji/ggt148.

Stampfli, G., Mosar, J., Favre, P., Pillevuit, A. and Vannay, J.-C., 2001. Permo-Mesozoic evolution of the western Tethys realm: the Neo-Tethys East Mediterranean Basin connection. In: Ziegler, P.A., et al. (Eds.) Peri-Tethys Memoir 6: Peri-Tethyan Rift/Wrench Basins and Passive Margins. *Mémoires du Muséum Natnional d'histoire Naturelle Paris*, **186**, 51-108.

Staub, R., 1924. Der Bau der Alpen. *Betrieb Geologische Karte Schweiz (N.F.)*, **52**, 272.

Staufenberg, H., 1987. Apatite Fission-Track Evidence for Postmetamorphic Uplift and Cooling History of the Eastern Tauern Window and the Surrounding Austroalpine (Central Eastern Alps, Austria). *Jahrbuch der Geologischen Bundesanstalt, Wien*, **130**, 571–586.

Steffen, K., Selverstone, J., and Brearley, A., 2001. Episodic weakening and strengthening during synmetamorphic deformation in a deep crustal shear zone in the Alps. *Special Publication-Geological Society Of London*, ***186***, 141-156.

Stipp, M., Stünitz, H., Heilbronner, R. and Schmid, S.M., 2002. The eastern Tonale fault zone: a natural laboratory for crystal plastic deformation of quartz over a temperature range from 250 to 700°C. *Journal of Structural Geology*, **24**, 1861-1884.

Stipp, M., Fügenschuh, B., Gromet, L. P., Stünitz, H., and Schmid, S. M., 2004. Contemporaneous plutonism and strike-slip faulting: A case study from the Tonale fault zone north of the Adamello pluton (Italian Alps). *Tectonics*, *23*(3).

Stöckhert, B., Brix, M.R., Kleinschrodt, R., Huford, A.J. and Wirth, R., 1999. Thermochronometry and microstructures of quartz—a comparison with experimental flow laws and predictions on the temperature of the brittle-plastic-transition. *Journal of Structural Geology*, **21**, 351–369.

Tapponnier, P., Peltzer, G. and Armijo, R., 1986. On the mechanics of the collision between India and Asia, in Collision Tectonics, edited by M.P. Coward and A. C. Ries, *Geological Society of London, Special Publication*, **19**, 113-157.

ter Voorde, M. and Bertotti, G., 1994. Thermal effects of normal faulting during rifted basin formation, 1. A finite difference model. *Tectonophysics*, **240**, 133-144.

Thiele, O., 1980. Das Tauernfenster. In R. Oberhauser (Ed.): *Der Geologische Aufbau Österreichs*, 300-314). Wien: Springer.

Thöni, M., 1980. Distribution of pre-Alpine and Alpine metamorphism of the southern Ötztal Mass and the Scarl Unit based on K/Ar age determinations. *Mitteilungen der österreichischen geologischen Gesellschaft, Wien*, **71**, 139-165.

Thöni, M., 1999. A review of geochronological data from the Eastern Alps. *Schweizerische Mineralogische und Petrographische Mitteilungen*, **79**, 209-230.

Tollmann, A., 1977. Geologic von Oesterreich, I, Die Zentralalpen. *Franz Deuticke*, Vienna.

Trümpy, R., 1960. Paleotectonic evolution of the Central and Western Alps. *Geological Society of America Bulletin*, **71**, 843-908.

Trümpy, R., 1973. The timing of orogenic events in the Central Alps. *K.A. De Jong and R. Scholten: Gravity and tectonics*, 229-251, J. Wiley and Sons.

Urbanek, C., Frank, W., Grasemann, B. & Decker, K., 2002. Eoalpine versus Tertiary deformation: Dating of heterogeneously partitioned strain (Tauern Window, Austria). Pangeo Austria: Erdwissenschaften in Österreich 28.-30.6.2002 (Program and abstract), Institute for geology and paleontology University of Salzburg.

Uto, K., Ishizuka, O., Matsumoto, A., Kamioka, H. and Togashi, S., 1997. Laser-heating ^{40}Ar/^{39}Ar dating system of the Geological Survey of Japan: system outlines and preliminary results. *Bulletin of the Geological Survey of Japan*, **48**, 23-48.

Villa, I.M., 2010. Disequilibrium Textures vs Equilibrium Modelling: Geochronology at the Crossroads. In: Spalla, M.I., Marotta, A.M. and Gosso, G. (Eds.) Advances in interpretation of geological processes. *Geological Society, London, Special Publications*, **332**, 1-15.

Viola, G., 2000. Kinematics and Timing of the Periadriatic Fault System in the Giudicarie Region (Central-Eastern Alps). PhD thesis, University of Zurich.

Viola, G., Mancktelow, N. S., and Seward, D., 2001. Late Oligocene-Neogene evolution of Europe-Adria collision: New structural and geochronological evidence from the Giudicarie fault system (Italian Eastern Alps). *Tectonics*, ***20*(6)**, 999-1020.

von Blanckenburg, F. and Villa, I.M., 1988. Argon retentively and argon excess in amphiboles from the garbenschists of the Western Tauern Window, Eastern Alps *Contribution to Mineralogy and Petrology*, **100**, 1-11.

von Blanckenburg, F., Villa, I.M., Baur, H., Morteani, G. and Steiger, R.H., 1989. Time calibration of a PT-path from the Western Tauern Window, Eastern Alps: the problem of closure temperatures. *Contribution to Mineralogy and Petrology*, **101**, 1-11.

Vrabec, M., Preseren, P.P., Stopar, B., 2006. GPS study (1996–2002) of active deformation along the Periadriatic fault system in northeastern Slovenia: tectonic model. *Geol Carpath,* **57**, 57–65

Wagner, G.A. and Reimer, G.M., 1972. Fission track tectonics: the tectonic interpretation of fission track apatite ages. *Earth and Planetary Science Letters*, **14(2)**, 263-268.

Wagner, R., Rosenberg, C.L., Handy, M.R., Möbus, C. and Abertz, M., 2006. Fracture-driven intrusion and upwelling of a mid-crust pluton fed from a transpressive shear zone – The Rieserferner Pluton (Eastern Alps). *The Geological Society of America Bulletin*, **118 (1-2)**, 219-237. doi: 10.1130/B25841.1

Warren, C.J., Smye, A.J., Kelley, S.P. and Sherlock, S.C., 2012. Using white mica ^{40}Ar/^{39}Ar data as a tracer for fluid flow and permeability under high-P conditions: Tauern Window, Eastern Alps. *Journal of Metamorphic Geology*, **30**, 63-80, doi: 10.1111/j.1525-1314.2011.00956.x.

Werling, E.,1992. Tonale-, Pejo- und Judicarien-Linie: Kinematik, Mikrostrukturen und Metamorphose von Tektoniten aus räumlich interferierenden aber verschiedenaltrigen Verwerfungszonen. PhD thesis, ETH Zurich.

Wiederkehr, M., Sudo, M., Bousquet, R., Berger, A. and Schmid, S.M., 2009. Alpine orogenic evolution from subduction to collisional thermal overprint: The ^{40}Ar/^{39}Ar age constraints from the Valaisan Ocean, Central Alps. *Tectonics*, **28(6)**, TC6009, doi: 10.1029/2009TC002496.

Wolf, R.A., Farley, K.A. and Silver, L.T., 1996. Helium diffusion and low temperature thermochronometry of apatite. *Geochimical Cosmochim. Acta*, **60**, 4231-4240.

Wölfler, A., Dekant, C., Danisík, M., Kurz, W., Dunkl, I., Putis, M. and Frisch, W., 2008. Late stage differential exhumation of crustal blocks in the central Eastern Alps: evidence from fission track and (U–Th)⁄He thermochronology. *Terra Nova*, **20**, 378–384.

Wölfler, A., Stüwe, K., Danišik, M. and Evans, N.J., 2012. Low temperature thermochronology in the Eastern Alps: implications for structural and topographic evolution. *Tectonophysics*, **541-543**, 1-18. doi: 10.1016/j.tecto.2012.03.016

Wölfler, A., Dekant, Ch., Frisch, W., Danišik, M. and Frank, W., 2015. Cretaceous to Miocene cooling of Austroalpine units southeast of the Tauern Window (Eastern Alps) contrained by multi-system thermochronometry. *Austrian Journal of Earth Sciences*, **108/1**, 16-33.

Yamada, R., Tagami, T., Nishimura, S. and Ito, H., 1995. Annealing kinetics of fission tracks in zircon; an experimental study. *Chemical Geology,* **122,** 249-258.

Zeilinger, G., 1997. Das Tamsweger Tertia¨r: Fazies und Deformation eines intramontanen Beckens und seine regionale geodynamische Bedeutung. Diploma Thesis at University Tübingen.

Zwingmann, H., and Mancktelow, N., 2004. Timing of Alpine fault gouges. *Earth Planet. Sci. Lett*. **223**, 415–425.

ACKNOWLEDGEMENTS

I am indebted to my supervisors Mark Handy and to many colleagues for discussions, especially Audrey Bertrand, Andreas Scharf, Susanne Schneider, Sebastian Garcia, Friedrich Hawemann, Peter Gipper, Jorg Giese, Eline Le Breton, Jan Pleuger, Claudio Rosenberg and Konrad Hammerschmidt all from the Freie Universität Berlin, as well as my second supervisor Ralf Schuster and Gerhard Pestal, Manfred Linner, Manfred Rockenschaub from the Austrian Geological Survey, Vienna. Lazslo Fodor and Matteo Massironi are thanked for their tips on P-T-B analysis. I also thank Stanislaw Grabala from the Geological Survey of Austria for mechanical preparation of the samples and Monika Horschinegg from the Department of Lithospheric Research, Vienna, Austria, for her help with the isotopic analyses. I greatly acknowledge Hugo Ortner, Bernhard Fügenschuh, Stefan Schmid, Giorgio Pennacchioni, Andrea Marzoli for their tips and the critical and helpful reviews of M. Calderon, Christian Teyssier, Uwe Ring, Doug Robinson, Neil Mancktelow, Jean-Philippe Avouac and anonymous reviewer. R. Oberhänsli and M.J. Timmermann are thanked especially for supporting the work in the Ar/Ar lab at the Universität Potsdam. Anna Giribaldi and Sandra Wollnik are thanked for preparing thin-sections and Martina Grundmann for solving all my computer problems. I acknowledge the support of the National Park Services Hohe Tauern, in particular of Katharina Aichhorn and the staff of the Bios Zentrum in Mallnitz.

Finally, I thank all my colleagues and friends from the FU Berlin, Martin Homann, Xiaojuan Sun, Sami Nabhan, Nico Schmedemann, Fabian Hecht, Sascha Zertani and Alessandro Airo; all my family members and cousins for the great support; my friends in Berlin (expecially Peter, Audrey, Marilisa, Claudia, Julia, Laura, Andrea, Gianluca, Michele, Alessandro, Francesca/o, Luca, Massimo, Franzy, Enrico, Davide and Flavio) and all the great people I met during conferences and fieldwork.

My work was financed in part by the German Science Foundation (DFG-project Ha 2403/10), the German unemployment fund, the Geological Survey of Australia for the summer job and the Geological Survey of Austria for financial support for additional fieldwork.

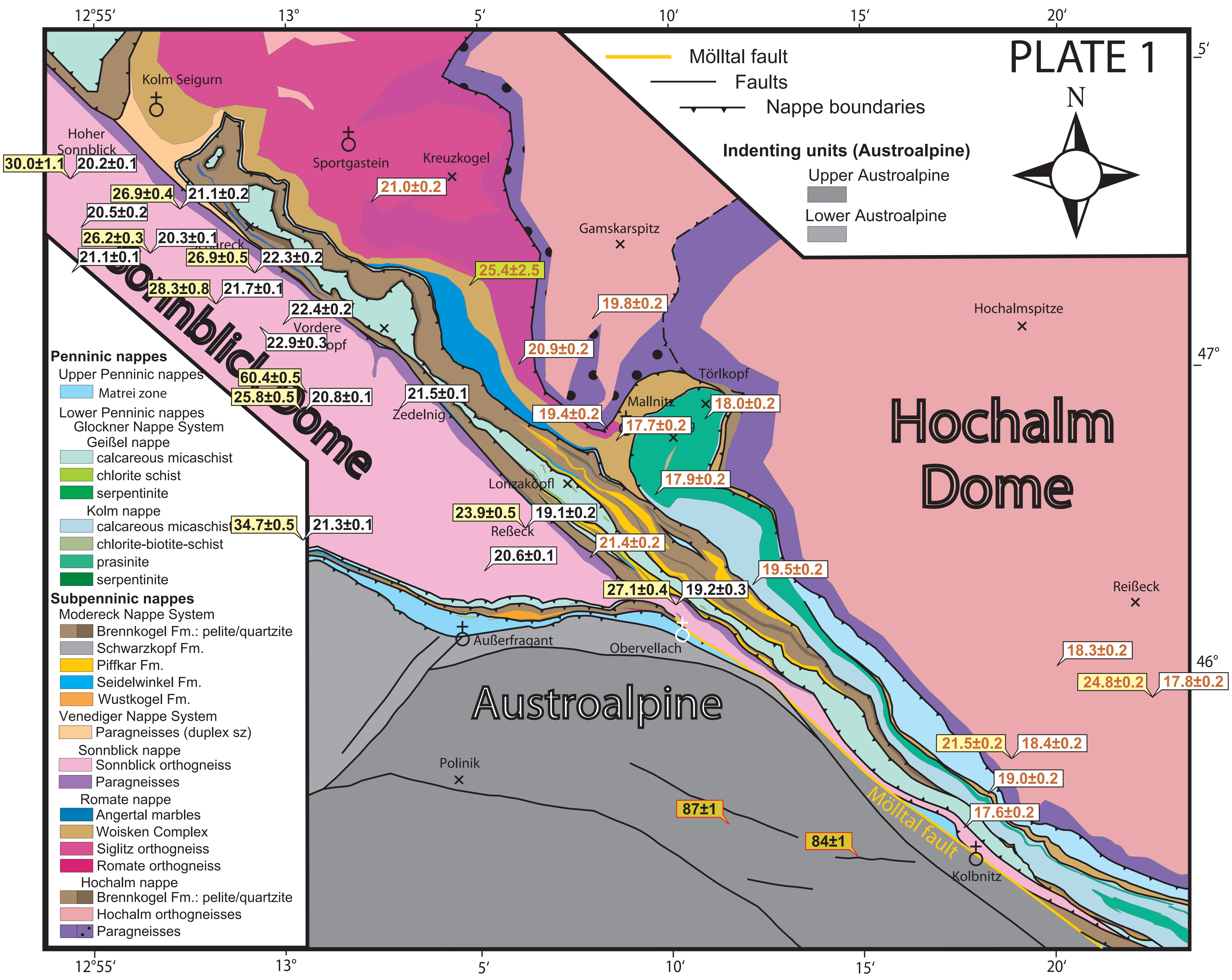
PLATE 1
Mölltal fault
Faults
Nappe boundaries
Indenting units (Austroalpine)
Upper Austroalpine
Lower Austroalpine
N
12°55′
13°
5′
10′
15′
20′
5′
47°
46°
Kolm Seigurn
Sportgastein
Kreuzkogel
Hoher Sonnblick
Gamskarspitz
Hochalmspitze
Vordere
opf
Zedelnig
Mallnitz
Törlkopf
Lonzaköpfl
Reßeck
Außerfragant
Obervellach
Polinik
Kolbnitz
Reißeck
Sonnblick Dome
Hochalm Dome
Austroalpine
Mölltal fault
30.0±1.1
20.2±0.1
26.9±0.4
21.1±0.2
20.5±0.2
26.2±0.3
20.3±0.1
21.1±0.1
26.9±0.5
22.3±0.2
28.3±0.8
21.7±0.1
22.4±0.2
22.9±0.3
60.4±0.5
25.8±0.5
20.8±0.1
21.5±0.1
21.0±0.2
25.4±2.5
19.8±0.2
20.9±0.2
19.4±0.2
17.7±0.2
18.0±0.2
17.9±0.2
23.9±0.5
19.1±0.2
34.7±0.5
21.3±0.1
21.4±0.2
20.6±0.1
19.5±0.2
27.1±0.4
19.2±0.3
18.3±0.2
24.8±0.2
17.8±0.2
21.5±0.2
18.4±0.2
19.0±0.2
17.6±0.2
87±1
84±1
Penninic nappes
Upper Penninic nappes
Matrei zone
Lower Penninic nappes
Glockner Nappe System
Geißel nappe
calcareous micaschist
chlorite schist
serpentinite
Kolm nappe
calcareous micaschist
chlorite-biotite-schist
prasinite
serpentinite
Subpenninic nappes
Modereck Nappe System
Brennkogel Fm.: pelite/quartzite
Schwarzkopf Fm.
Piffkar Fm.
Seidelwinkel Fm.
Wustkogel Fm.
Venediger Nappe System
Paragneisses (duplex sz)
Sonnblick nappe
Sonnblick orthogneiss
Paragneisses
Romate nappe
Angertal marbles
Woisken Complex
Siglitz orthogneiss
Romate orthogneiss
Hochalm nappe
Brennkogel Fm.: pelite/quartzite
Hochalm orthogneisses
Paragneisses

PLATE 2

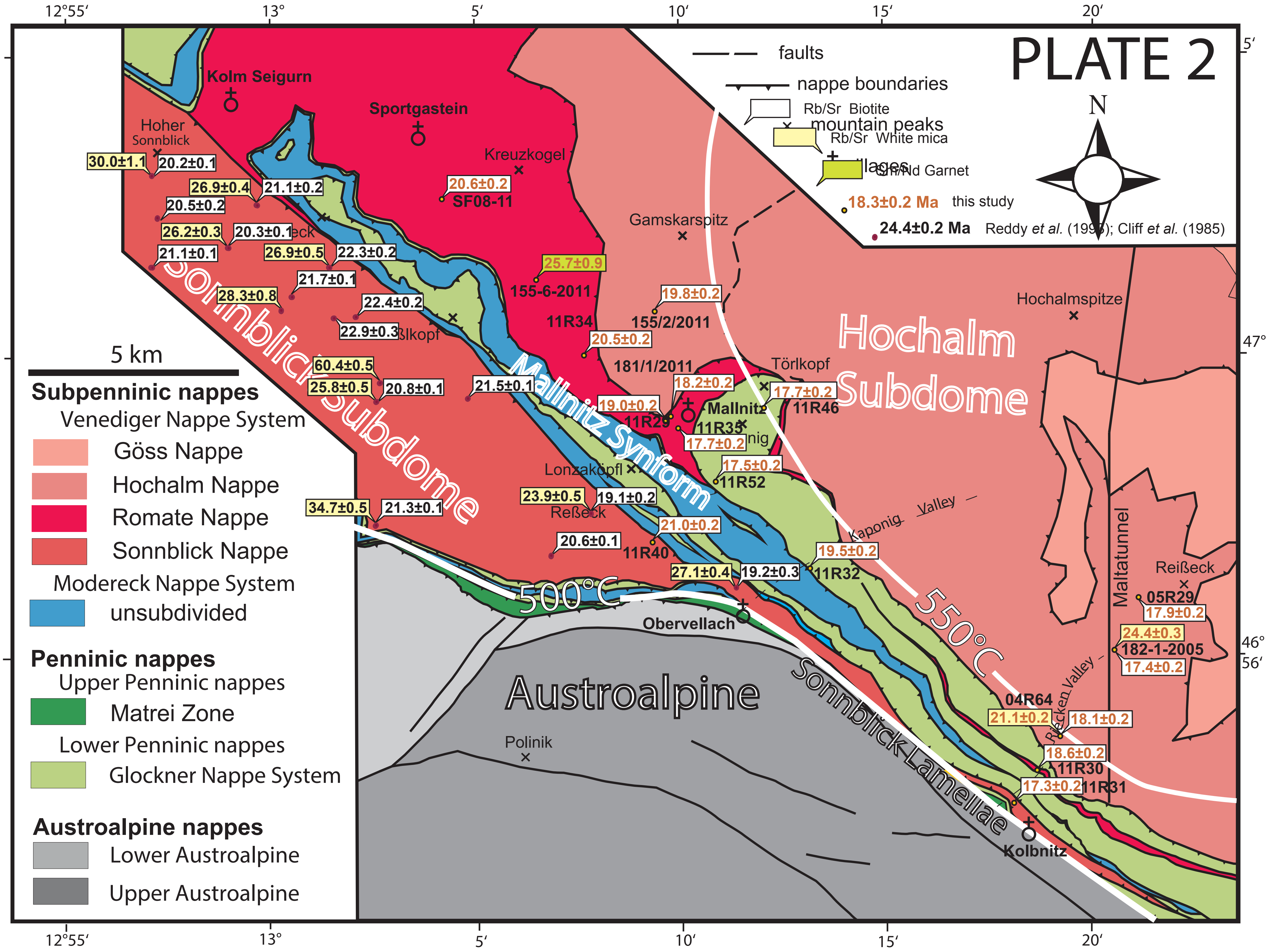

12°55′
13°
5′
10′
15′
20′
5′
47°
46°
56′
faults
nappe boundaries
Rb/Sr Biotite
mountain peaks
Rb/Sr White mica
villages
Sm/Nd Garnet
18.3±0.2 Ma this study
24.4±0.2 Ma Reddy et al. (1993); Cliff et al. (1985)
N
5 km
Subpenninic nappes
Venediger Nappe System
Göss Nappe
Hochalm Nappe
Romate Nappe
Sonnblick Nappe
Modereck Nappe System
unsubdivided
Penninic nappes
Upper Penninic nappes
Matrei Zone
Lower Penninic nappes
Glockner Nappe System
Austroalpine nappes
Lower Austroalpine
Upper Austroalpine
Kolm Seigurn
Sportgastein
Hoher Sonnblick
Kreuzkogel
Gamskarspitz
Hochalmspitze
Törlkopf
Mallnitz
Lonzaköpfl
Reißeck
Obervellach
Polinik
Kolbnitz
Maltatunnel
Kaponig Valley
Riecken Valley
Sonnblick Subdome
Hochalm Subdome
Mallnitz Synform
Sonnblick Lamellae
Austroalpine
500°C
550°C
30.0±1.1
20.2±0.1
26.9±0.4
21.1±0.2
20.5±0.2
26.2±0.3
20.3±0.1
21.1±0.1
26.9±0.5
22.3±0.2
21.7±0.1
28.3±0.8
22.4±0.2
22.9±0.3
60.4±0.5
25.8±0.5
20.8±0.1
21.5±0.1
34.7±0.5
21.3±0.1
23.9±0.5
19.1±0.2
20.6±0.1
20.6±0.2
SF08-11
25.7±0.9
155-6-2011
11R34
19.8±0.2
155/2/2011
20.5±0.2
181/1/2011
18.2±0.2
19.0±0.2
11R29
17.7±0.2
11R46
11R35
17.7±0.2
17.5±0.2
11R52
21.0±0.2
11R40
19.5±0.2
11R32
27.1±0.4
19.2±0.3
05R29
17.9±0.2
24.4±0.3
182-1-2005
17.4±0.2
04R64
21.1±0.2
18.1±0.2
18.6±0.2
11R30
17.3±0.2
11R31

PLATE 3

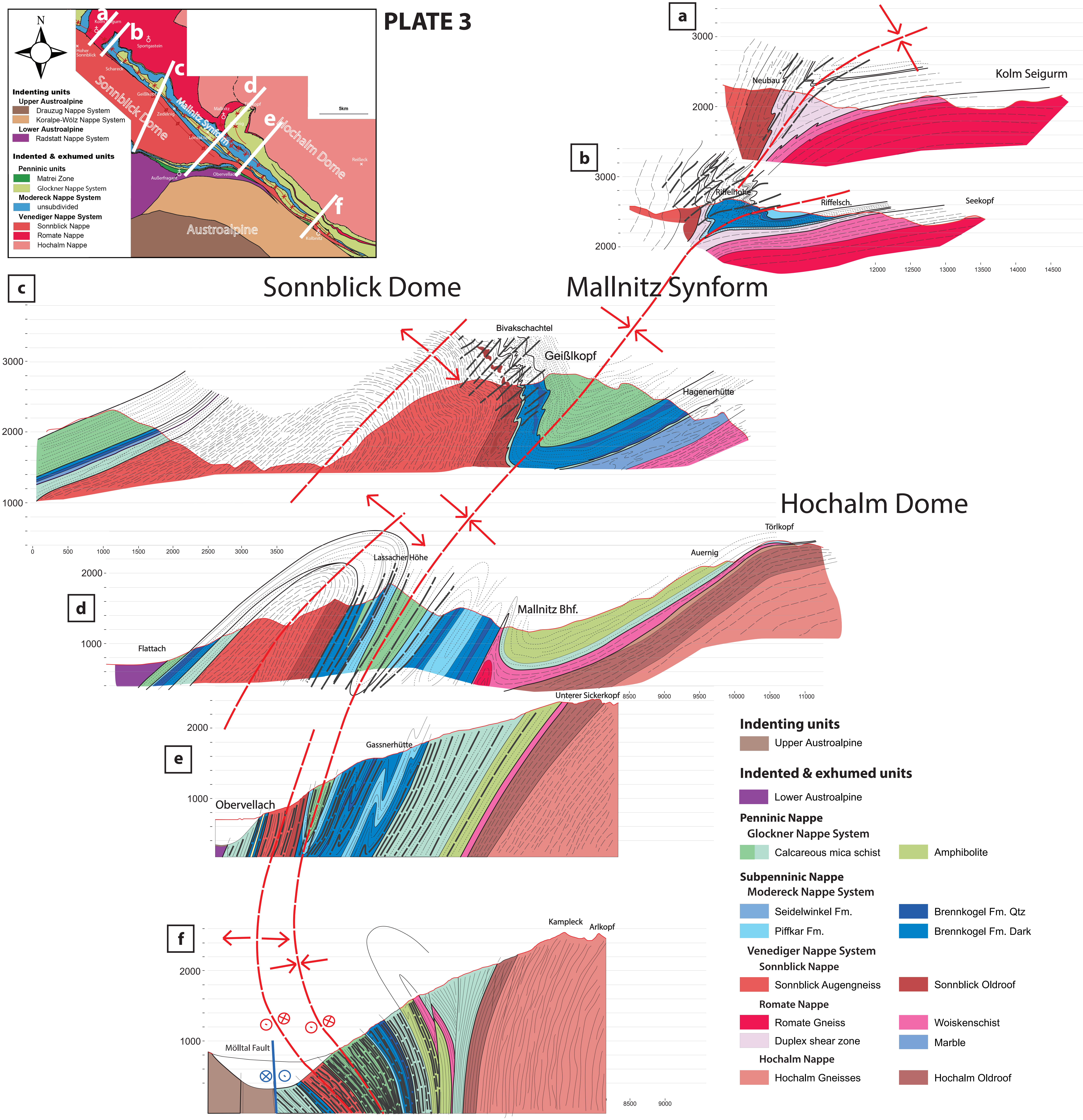
N
Indenting units
Upper Austroalpine
Drauzug Nappe System
Koralpe-Wölz Nappe System
Lower Austroalpine
Radstatt Nappe System
Indented & exhumed units
Penninic units
Matrei Zone
Glockner Nappe System
Modereck Nappe System
unsubdivided
Venediger Nappe System
Sonnblick Nappe
Romate Nappe
Hochalm Nappe
a
b
c
d
e
f
Kolm Seigurn
Sportgastein
Hoher Sonnblick
Schareck
Geißlkopf
Zedelnig
Lonzaköpfl
Mallnitz
Törlkopf
Auernig
Außerfragant
Obervellach
Reißeck
Kolbnitz
Sonnblick Dome
Mallnitz Synform
Hochalm Dome
Austroalpine
5km
3000
2000
Neubau
Kolm Seigurm
Riffelhöhe
Riffelsch.
Seekopf
12000
12500
13000
13500
14000
14500
Sonnblick Dome
Mallnitz Synform
Bivakschachtel
Geißlkopf
Hagenerhütte
1000
0
500
1000
1500
2000
2500
3000
3500
Hochalm Dome
Törlkopf
Auernig
Lassacher Höhe
Mallnitz Bhf.
Flattach
8500
9000
9500
10000
10500
11000
Unterer Sickerkopf
Gassnerhütte
Obervellach
Kampleck
Arlkopf
Mölltal Fault
8500
9000
Indenting units
Upper Austroalpine
Indented & exhumed units
Lower Austroalpine
Penninic Nappe
Glockner Nappe System
Calcareous mica schist
Amphibolite
Subpenninic Nappe
Modereck Nappe System
Seidelwinkel Fm.
Brennkogel Fm. Qtz
Piffkar Fm.
Brennkogel Fm. Dark
Venediger Nappe System
Sonnblick Nappe
Sonnblick Augengneiss
Sonnblick Oldroof
Romate Nappe
Romate Gneiss
Woiskenschist
Duplex shear zone
Marble
Hochalm Nappe
Hochalm Gneisses
Hochalm Oldroof